This thesis has been accepted for the award of the degree in the Faculty of Engineering

TEMPCORE REINFORCING STEEL:

MICROSTRUCTURE AND MECHANICAL PROPERTIES

by

Hang ZHENG

A thesis submitted in fulfillment of the
requirements for the Degree of
Doctor of Philosophy

Department of Civil Engineering
The University of Sydney

March 1998

SYNOPOSIS

TEMPCORE reinforcing steel is a product of a patented process in which the hot rolled bar is intensively surface quenched, by water spraying, immediately as the bar emerges from the last hot rolling strand and during the subsequent air cooling the quenched outer layer is tempered by the dissipation of retained heat from the core. The final result consist of a bar with a composite metallurgical structure containing tempered martensitic hardened outer layer and ferrite-pearlite core with a mixture of bainite and ferrite as an intermediate hardened layer in the transition area between the core and the outside layer. The mechanical properties were investigated with particular attention to the roles played by the peculiar metallurgical microstructure, the patterns of surface geometry and the residual stresses associated with TEMPCORE bars.

Reinforcing steel bars with seven diameters were tested and metallurgical investigations revealed that the cores of different bars do not have identical microstructures. The majority of the bars possess normal fine ferrite-pearlite crystals, while Widmanstätten ferrite and pseudo-eutectoid structure was found in others. These differences in microstructure significantly affect the yield behaviour of the bars as the latter type exhibit preyield microstrain during tensile loading, i.e., some microplasticity takes place before the attainment of macro-scale yielding which however shows similar characteristics for all the bars. Analytical work based on the theory of microplasticity has been applied to elucidate this phenomenon. It has been concluded that the grain size is the most important influencing factor relating to preyield.

In zero to tension and zero to compression loadings cyclic hardening was observed but with fully reversed loading, below the yield strength, cyclic softening took place. The hardening and softening are related to the interaction between the yielding core and elastic case.

Axial fatigue test results are presented in the form of S-N curves and in comparison with other types of reinforcing steel bars. It was found that the TEMPCORE reinforcing steels have significantly better fatigue properties than the "conventional" bars although the stress concentration factors associated with the surface geometry are approximately the same. Explanations are offered for this behaviour using the peculiar metallurgical microstructure and residual stresses in reasoning.

PREFACE

This thesis is submitted for the degree of Doctor of Philosophy to the University of Sydney. The work described in the thesis was carried out in the Department of Civil Engineering at the University of Sydney under the supervision of Associate Professor A. Abel.

In accordance with the Bye-Laws of the University of Sydney governing the requirement for the degree of Doctor of Philosophy, the author submits that the work in this thesis is original unless otherwise specified in the text.

The following papers were derived from the work presented in this thesis:

1. Zheng, H., Abel, A. "Fatigue properties of reinforcing steels produced by TEMPCORE process." Journal of Materials in Civil Engineering, American Society of Civil Engineering (accepted).

2. Zheng, H., Abel, A. (1997) "Residual stress effects on the fatigue properties of TEMPCORE reinforcing steels." International conference on analysis of residual stresses from materials to bio-materials. Mat-Tec 97, edited by Lodini, A., Reims, France, 177-182.

3. Zheng, H., Abel, A. (1998). "Mechanical properties of TEMPCORE reinforcing steels." The 8th International Offshore and Polar Engineering Conference, Montreal, Canada (accepted).

4. Zheng, H., Abel, A. (1998). "Elasto-plastic transition in TEMPCORE reinforcing steel." The Fourth International Conference on Low Cycle Fatigue and Elasto-Plastic behavior of Materials, Garmisch-Partenkirchen, Germany (accepted).

5. Zheng, H., Abel, A. "Stress concentration and fatigue of deformed reinforcing steels." International Journal of Fatigue (submitted).

ACKNOWLEDGEMENT

Special thanks are due to Associate Professor A. Abel, for his guidance, encouragement, suggestions and criticism throughout the course of this thesis work.

The reinforcing steel bars were generously supplied by BHP and this is gratefully acknowledged.

Thanks are also due to the staff of the Materials and Structures Laboratory of the Department of Civil Engineering for the assistance with the experimental work. Mr. Ian Hoggart deserves special mention.

Scanning electron microscopy was conducted in the Electron Microscope Unit at the University of Sydney and this service is greatly appreciated.

Finally, I wish to thank my wife Lily, and daughter Sylvia for their encouragement, patience and support throughout the course of the work.

CONTENTS

Chapter 1

INTRODUCTION

TEMPCORE is a relatively new type of high strength reinforcing bar with excellent ductility and weldability. The name is a Trademark registered in Australia and is made up from the two major events taking place during the production technology. The process involves a quenching immediately after the bar emerges from the last hot rolling strand and a self-tempering, by the retained heat from the core, hence the core tempered martensitic product, that is: TEMPCORE. The bar in the finished state is made up by tempered martensitic hardened layer and ferrite-pearlite core with an intermediate hardened layer of a mixture of bainite and ferrite in between. Such a composite steel structure offers many advantages over the other types of reinforcing steels, in strength, in ductility, weldability and production cost and therefore, since this technology was invented a considerable expansion took place in the use of TEMPCORE reinforcing steel.

The process is a Belgian invention by the Centre de Recherches Metallurgiques (C.R.M) and the first production tonnage date back to 1974. BHP, the Australian steel maker, started producing this type of reinforcing bars in 1983 under licence agreement with the Belgian inventors. Although the production output increased significantly in Australia, and in the world generally, and in spite of the sophisticated metallurgical composition of the steel itself, literature survey shows a lack of published data on this type of steel.

The primary aim of this thesis is to obtain experimental and analytical information about this composite material in order to understand better the displayed mechanical properties. The investigation centre around four major aspects relating to:

i. Metallurgical and residual stress characteristics;
ii. Mechanical properties in static loading and the related strengthening mechanism;
iii. Cyclic loading behaviour; and
iv. Fatigue properties.

The thesis content may be also divided into four parts: in Chapter 2, 3, 4, and 5 the high strength reinforcing steels, the TEMPCORE technique, mechanical properties of steels potentially used for reinforcing bars and the fatigue properties of deformed reinforcing bars are reviewed from literature. In the second part, Chapter 6 describes the experimental and analytical methods and details. The third part, Chapter 7 presents results and finally in Chapter 8 discussion follows and a model is proposed which appears to be compatible with the results.

In the conclusion section, presented in Chapter 9, the major findings are pointed out as follows:

1. Due to the variation of process control two types of microstructures are observed in the core of TEMPCORE reinforcing bars, i.e., fine ferrite-pearlite, and coarse Widmanstätten ferrite-pseudo-eutectoid.
2. Compressive residual stresses were measured in the hardened layer of the bars.
3. TEMPCORE reinforcing steels exhibit preyield microstrain before the attainment of macro-scale yielding, the magnitude of which depends on the type of microstructure in the core of bars.
4. The preyield microplasticity is attributed to the yield of the soft core and a model is developed which can predict the magnitude of preyield strain.
5. The bars cyclically harden in zero to tension and zero to compression cyclic loading but soften in fully reversed loading below the yield strength.
6. Measurement and calculations show that the surface patterns provided by the deformations produce stress concentration factors with magnitudes reaching 2.5.

7. The fatigue properties of TEMPCORE reinforcing steels are found superior to that of conventional reinforcing bars and these are attributed to the peculiar metallurgical microstructure and residual stresses produced by the process.

Chapter 2

HIGH STRENGTH REINFORCING STEELS

2.1. INTRODUCTION

A brief review is presented on the essential features of reinforced concrete with the basic requirements of reinforcing steels and on some of the problems encountered with conventional types of reinforcing steels.

2.2. REINFORCED CONCRETE

Use of concrete and its cementatious (volcanic) constituents dates back to the days of Greeks, and Romans, and possibly earlier ancient civilisation (Nawy 1985; Hornbostel 1991; Warner et al. 1982). However, intensive use of this material in engineering structures was only made possible when flat bars and wire ropes were used in concrete for reinforcement as documented in 1854 by the Wilkinson patent in England (Warner et al. 1982; Marsh 1909).

Concrete is strong in compression but lacks strength in tension. For example a high strength concrete with 137.9 MPa compression strength has only 12.41 MPa strength in tension (Nawy 1985). Steels are strong in both tension and compression, but much more expensive than concrete. The principles of reinforced concrete is that steel and concrete is arranged in such a way that the cheaper concrete is placed in a compressive region to resist the crushing force, while the steel is put in a tensile region to resist stretching. Take a concrete beam for example (Figure 2-1), when a beam subjected to **P** load, tensile and compression stresses are generated in the bottom and the top respectively. Reinforcing steel bars are then placed at the bottom

of the beam and thus larger **P** can be supported. A composite action is derived from the steel with high tensile strength and high elastic modulus when it is placed in the right position and it bounds with the surrounding concrete.

Steel has an essentially constant elastic modulus of the order of 200 X 10^3 MPa. But the elastic modulus of a concrete varies with the quality of the aggregates used, the consistency, the age and even the applied stress. Nevertheless, the ratio of the modulus of steel to that of concrete is in a range from 10 to 15 (Taylor et al. 1925). This means that in the case of a reinforced concrete member the steel picks up a stress 10 to 15 times higher than the surrounding concrete does and thus the load capacity of a concrete member is significantly increased.

Steel and concrete can develop a good bonding as concrete shrinks slightly on setting, thereby gripping the reinforcing bars firmly. Also, when subjected to changes of temperature, concrete and steel expand or contract almost at the same rate and therefore the two materials do not separate. Additionally, deformed bars, bars with surface ribs of various forms, help to maximise the possible bond.

On the other hand, concrete has a high fire resistance and thus protects the reinforcing bars at high temperatures, and a good quality concrete with sufficient cover would protect the steel from corrosion.

2.3. PROPERTY REQUIREMENTS FOR REINFORCING STEELS

The strength together with ductility, weldability and formability are the most essential quality requirements of reinforcing steel bars. Thus yield strength, together with tensile strength, is the first requirement for reinforcing steel in every national standard and the grade of steel is classified according to the specified minimum yield strength.

Using higher grade steel leads to a great economy as less steel is required for the same loading condition, and the total cost is reduced. This reduction in quantity also reduces the cost in transporting, handling and fixing of the bars during construction.

Additionally, the use of high yield strength steel bars may also permit a reduction in the width of major girders or the size of columns in high-rise buildings, thus it may reduce the cost of concrete and handling.

Currently, Grade 300 (300 MPa minimum yield strength) and Grade 400 are the most commonly used grades but Grade 500 and even higher grade steels are also used in some countries. In contrast, Grade 250 is hardly used anymore for main reinforcement.

Sufficient ductility is required for safety and fabrication considerations. This is particularly important for structures where the possibility of earthquakes is part of the design consideration. From the fabrication point of view, where bending and rebending of reinforcing steel bars are taking place good ductility is very important. The concern regarding ductility is reflected in all current national standards, i.e., the minimum diameter of the pin for 180° bend and the total elongation are generally specified.

As considerable amount of field welding is taking place, the weldability is also a major concern. Several types of welding methods may be used such as manual metal arc welding (MMAW), gas metal arc welding (GMAW), flash welding (FW) and resistance welding (RW). Amongst the several welding techniques, lap and cross welding are the most sensitive to heat affected zone cracking due to the low heat input and the fast heat dissipation.

Other requirements include fatigue resistance, high and low temperature properties, impact properties, corrosion resistance, but these are generally not specified by various national standards although the concern is increasing (Hognestad 1967; ACI Committee 439 1989, 1973).

2.4. TYPES OF REINFORCING STEELS

Several types of reinforcing steels are used with the largest quantities coming from plain round hot-rolled mild-steel bars, deformed hot-rolled steel bars, deformed hot-

rolled high-yield carbon steel bars, deformed hot-rolled high-yield alloying steel bars, cold-worked bars and high-yield TEMPCORE reinforcing steel bars. Other types, namely in-line heat treated bars are also used in some countries.

Plain round hot-rolled mild-steel bars

Ordinary plain round bars are produced from mild-steel by hot-rolling. This type of bars have a yield strength of 250 MPa and tensile strength no less than 1.1 times the yield strength. Grade 250R is produced in accordance with AS 1302-1991 in Australia. This type of bars are mainly used in stirrups (BHP 1993).

Deformed hot-rolled steel bars

This type of bars are basically the same as the plain round hot-rolled mild-steel bars except that on the last mill deformation patterns are rolled on to the surface for better bounding purpose. Due to their low yield strength, this type of bars are not wildly used (Disney and Reynolds 1973). Australia is currently producing such grade steel (AS 1302-250S) only for 12 mm diameter bars (BHP 1993).

Deformed hot-rolled high-yield carbon steel bars

This type of bars were developed in Sweden during World War II (Hognestad 1967) and used world-wide in the 1960s. The bars have a yield strength above 400 MPa. This property is obtained by enrichment in chemistry and high carbon content. In ASTM A615M-84a, ASTM A616-84 and ASTM A617-84 for carbon steel bars there is no chemical composition specified for Grade 60 (415 MPa) bars, but from the work by Helgason et al. (1976) and Mac Gregor et al. (1971) it is known that the carbon content may be as high as 0.41% to 0.52%. Other specifications for this type of bars are listed in Table 2-1.

Deformed hot-rolled high-yield alloying steel bars

High yield strength is achieved in these bars by alloying elements such as manganese and other microalloying elements but the carbon content is restricted to below 0.3% for Grade 60 (ASTM A706-84), and below 0.22% for AS 1203-400Y steels (AS 1302-1991). Other specifications are listed in Table 2-1.

Cold-worked bars

Cold-worked bars are usually mild-steel bars, the yield strength of which is increased by cold-working, generally by twisting or stretching or by the contribution of these two, under controlled conditions. The most common form of cold-worked bars is the twisted square or chamfered-square bars. Although the yield strength may be as high as 460 MPa, the cold working reduces ductility. In AS 1302-1991, cold-worked bars of Grade 410 are no longer included.

In-line heat treated reinforcing steel bars

The rolled bars are strengthened by heat treatment arising from the rolling heat and subsequent controlled cooling and tempering process and thus a yield strength as high as 1,000 MPa can be obtained. According to Chernenko et al. (1987) such reinforcing steel bars were produced in the former USSR since 1967. This technique was intensively studied in the 1970s and 80s (Satskii et al. 1977; Uzlov et al. 1987; Dolzhenkov et al. 1987; Kondratenko et al. 1989; Ivashchenko et al. 1988; Ivashchenko et al. 1976; Shulaev et al. 1986; Babich et al. 1987; Kalmykov 1987, 1989) in the USSR the only country where it was used. Carbon content varied between 0.17% and 0.35 % with alloying elements such as manganese and silicon added to increase hardenability. Weldability of this type of bars would depend on their chemical compositions.

TEMPRIMAR reinforcing steel is also one of the in-line heat treated reinforcing steel bars which technique was developed in the former Federal Republic of Germany (Vlad 1985; Klaus and Vlad 1985). TEMPRIMAR process consists of a series of multiple quench and temper cycles as the bar leaves the finishing strand of the hot rolling mill. Grade 500 weldable reinforcing bars with good ductility can be produced.

High-yield TEMPCORE reinforcing steel bars

This type of bars are strengthened by a specially controlled heat treatment and have many advantages over the other type of bars mentioned above. The details of this type of bars which is the subject of this thesis will be reviewed in Chapter 3.

2.5. DEFORMED REINFORCING STEEL BARS AND DEFORMATIONS

2.5.1. Deformed reinforcing steel

A deformed reinforcing steel bar, as it is defined in AS 1302-1991, is a steel bar which has a rolled raised pattern occurring on the surface at regular intervals. The raised pattern or protrusions are longitudinal ribs and transverse lugs, and these are termed as deformations by most national standard specifications. Figure 2-2 shows a few typical deformed reinforcing steel bars. The use of deformations is intended to inhibit longitudinal movement of the bar relative to the concrete by facilitating bond. Measurable economy may result from the use of such deformations and the increasing working bond stress leads to the use of higher grade bars. Additional hooks and bends at the ends of the bar are generally unnecessary. Total cost reduction is reached by reducing the cost of the steel, transporting, handling, bending and fixing.

2.5.2. Deformations

Longitudinal ribs are usually continuous deformations of uniform height parallel to the longitudinal axis of the bar, while transverse deformations are raised lugs on the surface of the bar at an angle to the longitudinal axis of the bar. Studies have shown that bond strength between the bars and the surrounding concrete strongly depends on the geometry of the deformations (Carirns and Abdullah 1995; Darwin and Zavaregh 1996; Hamad 1995 a & b). Maximum bonding is achieved by large lug height with a flank angle of 60 degree (Hamad 1995 a & b). Requirements for deformations include spacing of transverse deformations, transverse deformation angles, gap between rows of transverse deformations, angle of deformation flanks, height of transverse deformations and height of longitudinal ribs.

Spacing of transverse deformations is measured as the average distance between the corresponding points of transverse deformations, parallel to the axis of the bar. The average spacing, required by AS 1302-1991, should not be less than $0.5d_b$ and no greater than $0.7d_b$, where d_b is the diameter of the bar.

Transverse deformation angle is the acute angle between the transverse deformations and the longitudinal axis of the bar. This angle should be at least 45°.

Gap between rows of transverse deformations is the overall length between the two ends of the deformations on opposite sides of the bar. This should not be greater than 12.5% of the nominal perimeter of the bar.

Height of transverse deformations is measured in two different ways. Average height is the average of measurements taken from the midpoint and two quarter points of a transverse lug. This should be no less than 5% of the nominal diameter of the bar. Peak height is measured from the maximum height. This should not be less than 6.5% of its nominal diameter.

Height of longitudinal rib is required to be no less than 5% of the nominal diameter of the bar and is measured from the midway between two consecutive transverse deformations which terminate on the same side of the longitudinal rib.

Angle of deformation flanks is the included angle at which the sides of the transverse deformations rise from the core of the bar. This is required to be no less than 45°.

The above requirements are taken from AS 1302-1991. Specifications ASTM A 615, A 616, A 617 and A 706 have similar requirements except that the angle of deformation flanks is not included.

Other geometry parameters are defined by several researchers when fatigue properties of the reinforcing steel bars are concerned. These are the lug root radii and lug width. They are expressed by the ratio of lug root radius to lug height (r/h) and the ratio of half lug width to lug height (w/h), respectively. These however are not specified in standards.

2.5.3. Rolling mill identification markings

Identification marks, are special pattern marks indented by rolling on the bar surface for the purpose of identification of the manufacturer. Since these are also protrusions causing stress concentrations when fatigue properties are questioned the effect of identification marks must be also considered.

2.5.4. Measurement of deformation geometry

As deformation details will influence the stress concentrations and thus the fatigue performance, the assessment of these details is very important. Average spacing of transverse deformations, the height of transverse deformations, height of longitudinal rib and angle of deformation flanks are described in AS 1302-1991. In studying the fatigue properties of deformed reinforcing steel bars a detail measurement of the deformation geometry has been developed. Concentrating on the parameters depicting in Figure 2-3 where

r/h: is the ratio of lug root radius to lug height;
w/h: is the ratio of half lug width to lug height;
α: is the flank angle of the lug;
D/h: is the ratio of bar diameter to lug height;

To determine the geometry of deformed reinforcing steel bars, several methods have been used previously. Cutting the bars right through the centre of the bar from the middle of the lugs along longitudinal axes, Grönqvist (1971) measured the geometry of the deformation on enlarged photographs. Since the samples were cut by saw, plastic deformation was introduced. Thus from the photographs the peripheries of the lugs cannot be seen clearly, thereby the accuracy of the measurement may be impaired. In addition, the measurement was only carried out at the middle section of the lugs and it is unclear if that location is the most relevant as it did not coincide with fatigue development.

Methods including direct measurement under stereomicroscope on the sectioned sample and photographing of sectioned plaster casts of the bar samples were attempted by Helgason et al. (1968). These were not so successful due to poor

contrast or by losing periphery details. Later, Helgason et al. conducted a more complicated and systematic study on geometry measurement by finding the most fatigue-prone location on the periphery of the bar. The cleaned samples after rust and mill scale removed were milled to a radial plane containing the critical fatigue location and the milled surface were lapped to smooth finish while the burrs at the edges of the sectioned surface were removed. Finally the machined surface was polished using a 600-grit silicone carbide paper and the measurement of the geometry took place on an enlarged photograph.

2.6. PROBLEMS WITH CONVENTIONAL HIGH YIELD REINFORCING STEELS

Conventional reinforcing high yield steels refer to all deformed high-yield steel bars produced by hot-rolling and cold-working as mentioned before. These steels because of chemistry or cold-working generally show poor ductility and weldability. Due to the poor ductility (Table 2-1), these bars should not be bent to a small radius and cases of failure have been reported when hooks were formed around a pin of two times the nominal bar diameter (Disney et al. 1973). Welding of such bars involves preheating in order to avoid crack.

Although hot rolled microalloyed steels improved ductility and weldability, it led to cost increase. As reviewed by Hognestad (1967) Swedish weldable 57,000-psi (393 MPa) grade steel (0.28%C, 0.6%Si, and 1.6%Mn) was sold at an extra cost of $16/ton in 1967. Additionally, the ductility of this type of steel is still not as good as that of mild steel.

Cold-worked bars do not have the desired ductility and therefore problems arise in fabrication and in safety considerations.

As there is a demand for higher grade steel, such as Grade 500 and Grade 600, the conventional methods reached limitation because production costs.

2.7. SUMMARY

For concrete reinforcement higher grade bars with good ductility and weldability are required. Other properties, such as fatigue resistance, strength loss at elevated temperature, low temperature properties, impact properties, corrosion resistance are generally not required by standards, but there is increasing concern relating to these properties. None of the conventional reinforcing steels can simultaneously and fully meet the requirements of high yield strength, good ductility, weldability and low cost.

Table 2-1. Specification for different types of bars

Bar Type	Grade	$\sigma_{y,\,min}$ MPa	$\sigma_{uts,\,min}$ MPa	Elongation δ_{min} % for bar diameters in mm	Pin diameter for 180° Bend Tests. Diameter in mm	Specification
A	250S & 250R	250	1.10YS	22*	$2d_b$ 12, 16 $4d_b$ 20 and above	AS 1203-91
B	Grade 60	400	600	$9^{\#}$ 11.3 - 19.5 $8^{\#}$ 25.2 $7^{\#}$ 29.9 - 56.4	$4d_b$ 11.3,16.0 $5d_b$ 19.5 $6d_b$ 25.2 $8d_b$ 29.5, 35.7	ASTM Billet 615M-84
B	Grade 50	345	550	$6^{\#}$ 9.52 $7^{\#}$ 12.7 - 19.05 $6^{\#}$ 22.22 $5^{\#}$ 25.4 -35.81	$6d_b$ 9.5-25 $8d_b$ 28-32 for both Grade 50 and 60	ASTM Rail 616-84
	Grade 60	415	620	$6^{\#}$ 9.52 - 19.05 $4.5^{\#}$ 22.22 -35.81		
B	Grade 60	415	620	$8^{\#}$ 9.52 - 22.22 $7^{\#}$ 25.4 - 35.81	$3.5d_b$ 9.5-15.88 $5d_b$ 19.05-25.40 $7d_b$ 28.65 - 35.81	ASTM Axle 617-84
B	Grade 60	415	550	$14^{\#}$ 9.52 - 19.05 $12^{\#}$ 22.22 - 35.81 $10^{\#}$ 43 - 57.33	$3d_b$ 9.52 - 15.88 $4d_b$ 19.05 - 25.40 $6d_b$ 28.56 - 35.81 $8d_b$ 43.00, 57.33	ASTM Low alloy 706-84
B	400Y	400	1.10YS	16*	$3d_b$ 12,16 $4d_b$ 20 and above	AS 1203-91

A: deformed hot-rolled milled-steel bars; B: deformed hot-rolled high-yield bars;

: elongation for 200 mm gage length; * : elongation for 5*d* gage length.

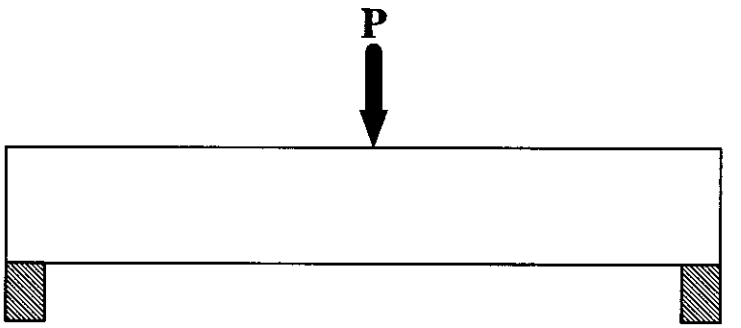

a. Loaded beam configuration

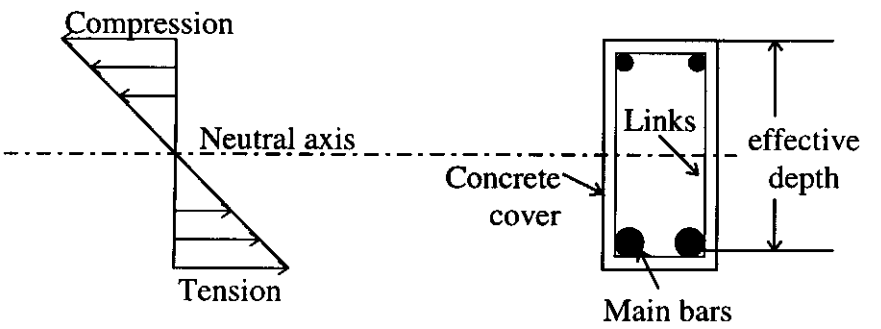

b. Cross sectional stress profile

c. Reinforcing

Figure 2-1. Typical reinforcing application

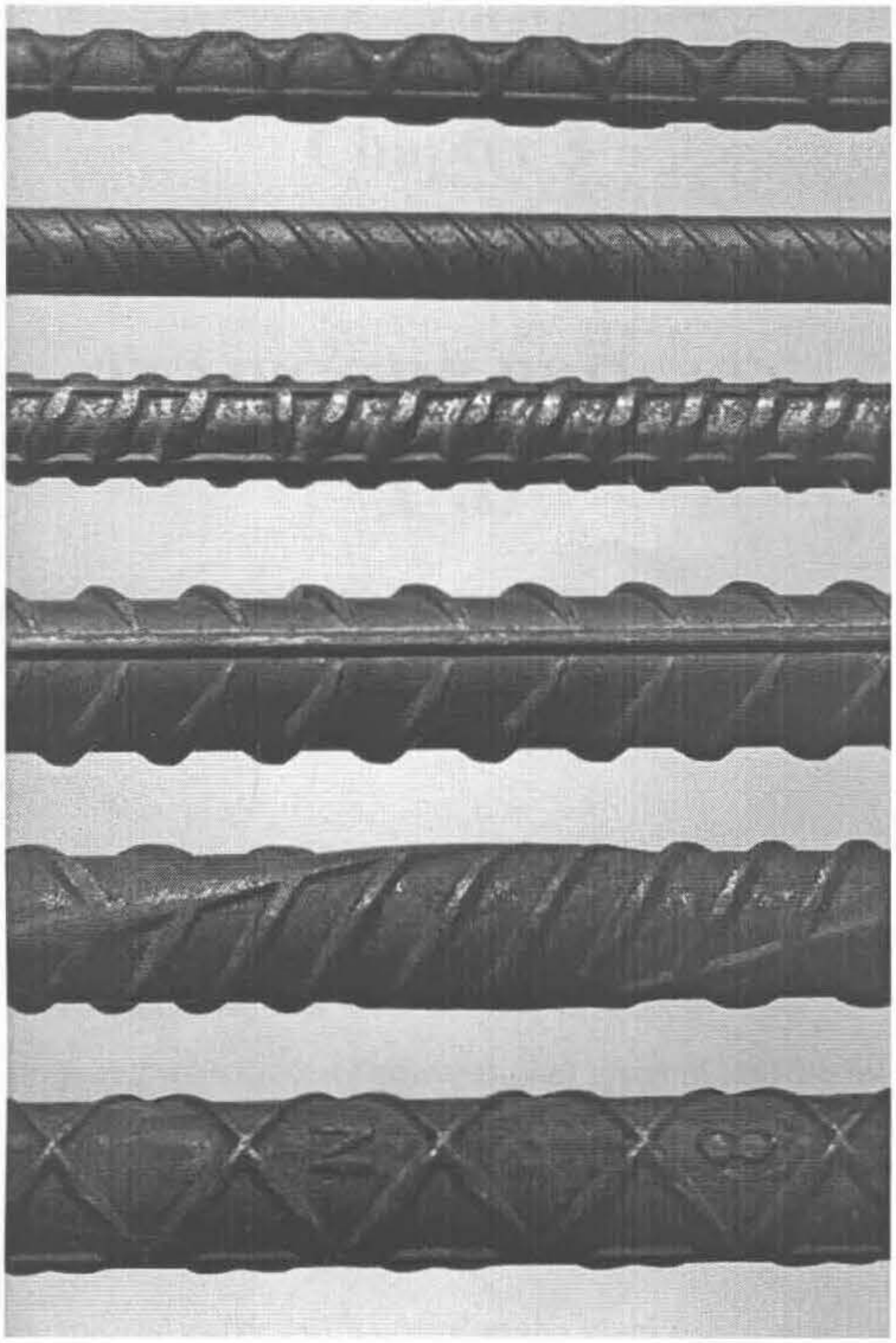

Figure 2-2. Typical deformation patterns of reinforcing steels

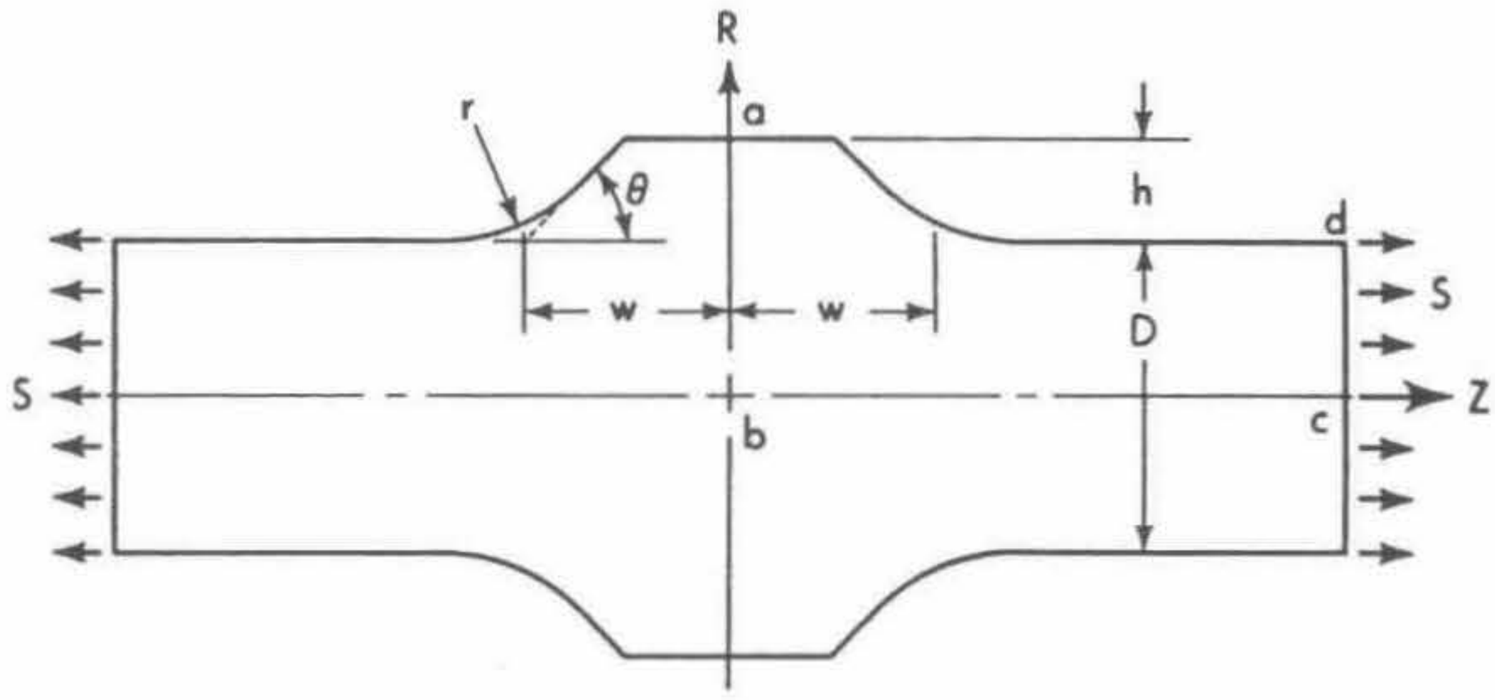

Figure 2-3. Transverse lug geometry

Chapter 3

TEMPCORE PROCESS AND TEMPCORE REINFORCING STEEL

In this chapter the process technique and the general characteristics of TEMPCORE reinforcing steel are reviewed. The superior properties in strength, ductility, formability and weldability of this steel as well as the economic advantages of this technique are compared with those of conventional types of reinforcing steels.

3.1 A BRIEF HISTORICAL BACKGRAOUND

In the late 1960s and the early 1970s, reinforcing steel users were oriented towards high strength reinforcing steels with adequate ductility, good weldability, and thus manufacturers were to develop methods leading to superior bars with relatively low production cost. Conventional methods by hot rolling and cold-working of carbon steels were out of consideration because of the resulting properties, while microalloying methods promised a certain degree of improvement at an extra cost. Heat treatment has come to the foreground and in-line heat treatment, by taking advantage of the rolling heat, appeared to be the economical avenue towards the new product.

As early as 1967 in the former USSR an attempt was made to produce high strength reinforcing steel bars by this method (Chernenko et al. 1987). Another in-line heat treatment technique, named TEMPRIMAR, was developed in the former Federal

Republic of Germany (Vlad 1985; Klaus and Vlad 1985). But amongst the in-line heat treatment methods, the TEMPCORE process became the most successful and the most popular.

This latter method originates from the laboratories of Centre de Recherches Metallurgiques (C.R.M), and in 1972, TEMPCORE process was patented in Belgium (Belgian Patent 790.867 of 31-10-1972). In 1974 the first industrial-scale trials were carried out in Esch-Schifflange Division of S. A. ARBED and this was the beginning of industrial scale manufacturing of TEMPCORE reinforcing steel.

In 1975, Economopoulos et al. (1975) published a paper entitled "Application of the TEMPCORE process to the fabrication of high yield strength concrete-reinforcing bars" in Metallurgical Reports C. R. M., in which the principles of the TEMPCORE process is described together with the laboratory and industrial trial results. In the same periodical, Defourny and Bragard (1977), reported details on the weldability of the steel bars produced by TEMPCORE process. Rehm and Russwurm (1977) systematically assessed the mechanical properties of this type of reinforcing steel. It was demonstrated that the process is capable to produce 500 to 600 MPa grade deformed reinforcing bars with superductility and excellent weldability. These steels full-filled the requirements presented in DIN 4099 and DIN 488. It was also proved that the process itself is quite stable. An analysis on the process was published by Simon et al. (1984b), indicating the economic advantages offered, and Killmore and Warrett (1984) reported that a further improvement can be achieved by microalloying.

Recently the TEMPCORE process is used in European countries, USA and Australia, with annual production of 5 million tones.

3.2 THE TEMPCORE PROCESS

TEMPCORE process, which produces high strength reinforcing bars from plain low carbon steel, is basically an in-line heat treatment process. It consists of quenching and self-tempering from which the name is derived, i.e., a quenched surface layer is TEMPered by the heat dissipating from the CORE.

As it is illustrated in Figure 3-1, steel billets are heated to approximately 1150°C in reheat furnaces and rolled through a sequence of rolling strands which progressively reduce the billets to the final size and shape of reinforcing bars. On leaving the last strand, a controlled cooling is applied in such a way that the bar undergoes three stage metallurgical transformations as it is illustrated by a typical CCT diagram in Figure 3-2.

On leaving the last rolling strand, the bar passes through a water quenching chamber, an intensive cooling forces the temperature within a certain depth from the surface of the bar down to below the martensite transformation starting point (Ms). Martensitic structure is formed within this quenched layer while the core remains austenite and a large temperature gradient is established in the cross-section of the bar.

During the second stage, when the bar leaves the quenching chamber and is exposed to air cooling, the heat retained in the core dissipates through the hardened layer re-heating the quenched martensite, a self-tempering is experienced. Tempered martensite is the result from a "tempering temperature". At the same time, the layer adjacent to the hardened layer starts to transform to bainite and an intermediate and intermediately hardened layer is formed. The core still remains austenite.

During the third stage, the remaining austenite in the core undergoes an essential quasi-isothermal transformation forming ferrite-pearlite structure. Consequently, a TEMPCORE reinforcing steel bar is essentially a composite material consisting of concentrically disposed hard outer layer and soft core with an intermediate and intermediately hardened layer. With relatively low carbon content, TEMPCORE reinforcing steel provides high strength, super-ductility and excellent weldability amongst other advantages.

3.3 CHARACTERISTICS OF TEMPCORE REINFORCING STEELS

3.3.1 Type of steel

TEMPCORE reinforcing steels are basically plain low carbon steels specified for yield strength, ductility, carbon or carbon equivalent and yield to tensile ratio. The maximum and minimum specified carbon content intends to ensure weldability and hardenability. With too low carbon content hardenability of the steel will not be sufficient and thus more sever quenching is required affecting rolling mill design, e.g., speed of rolling mill, length and efficiency of cooling chamber. Semi-killed carbon steel with 0.13% - 0.24% carbon content and the carbon equivalent (CE) < 0.48% has been proved to be the best balance to satisfy the above considerations.

The chemical composition of the steels is shown in Table 3-1 indicating clearly that TEMPCORE reinforcing steel has the leanest chemistry.

3.3.2 Metallurgical phases and microstructures

Typical etched cross section showing the three metallurgical regions and typical microstructures are illustrated in Figure 7-2. Tempered martensite in the form of packets of thin plates with martensitic morphology characterizes the hardened layer; a mixture of bainite and polygonal ferrite is in the intermediate hardened layer; and polygonal ferrite and pearlite develops in the core.

The microstructure is usually fine due to a relative fast cooling in the core and to the thermo-mechanical treatment involved in TEMPCORE process, e.g., polygonal ferrite grains in the core region can be as small as 8 μm diameter and even 3 μm diameter when lower tempering temperature is applied (Killmore and Barrett 1984; Killmore et al. 1985). However, coarse conglomerate of pseudo-eutectoid and Widmanstätten ferrite in the core are also possible outcome of the process. Although this type of microstructure has been only reported in some laboratory work (Economopoulos et al. 1975), it has been observed in the 32 mm and 36 mm diameter bars used in the present case, Figure 7-3.

Vlad (1985) in his article on "A comparison between the TEMPRIMAR and TEMPCORE processes for production of high strength rebars" described that TEMPCORE process has a tendency to form Widmanstätten ferrite due to the "inherent higher equalization temperatures". It is possible that high finishing temperature, and perhaps also insufficient rolling deformation are the major reasons for forming this type of microstructure. High finishing temperature and insufficient rolling deformation results in large austenitic grains at the end of rolling, and thus coarse martensite and bainite develops in the hardened layer and in the intermediate hardened layer during the subsequent quenching. Large austenite grain size in the core prevents the impingement of grain boundary ferrite, thus allowing Widmanstätten ferrite to grow (Honeycombe and Hancook 1981).

3.3.3 Effects of process parameters and steel composition

Naturally if the martensite layer is thicker the retained heat is less and thus the tempering is more modest so that the bar will exhibit higher yield strength and lower elongation. The process parameters and steel compositions play part in the final properties. Longer quenching time, lower finishing temperature and higher intensity of quenching result in thicker martensitic layer and lower tempering temperature. Higher carbon and manganese content increases the hardenability of the steel, and therefore more martensite is formed. Additionally, the strength of tempered martensite increases as the carbon content increases.

Simon (1990), based on the experiences accumulated during the commissioning of more than 25 TEMPCORE installations, developed a model which describes the relationship between yield strength and all influencing parameters. The model was originally used for the design of installations, and it is rewritten as:

$$YS^c = \frac{\tau \cdot q^d \cdot F^e}{K_1 \cdot \phi^a \cdot T_0^b} \qquad \text{and} \qquad TS = K_2 \cdot C^\alpha \cdot Mn^\beta \cdot TY^\gamma \cdot \phi^\delta$$

where

YS = yield strength, MPa;

τ = quenching time, second;

q = linear water flow rate, mm^3/h per meter of line;

F = filling coefficient, i.e., ϕ^2/ID^2 where ID = internal diameter of cooling nozzle;

ϕ = bar diameter, mm;

T_0 = entry temperature of the bar, °C;

C = carbon content of the steel, %;

Mn = manganese content of the steel, %;

TS = tensile strength, MPa;

K_1, K_2, a, b, c, d, e, a, b, g and d are constants.

Although tempering temperature does not appear in this model directly, the finishing temperature, quenching time, bar diameter and water flow rate relate to it quite strongly.

Elongation of TEMPCORE reinforcing steel has a virtually linear correspondence with the yield strength. From the work of Economopoulos et al. (1975) it is seen that for a 0.248%C, 1.12%Mn steel, 30% elongation corresponds to yield strength about 420 MPa, and only 17% elongation is obtained when the process is changed to give 680 MPa yield strength.

3.3.4 Tensile properties

The TEMPCORE process can increase the yield stress by 150 to 200 MPa for a given composition (Economopoulos 1981; Killmore and Barrett 1984) without losing much elongation. The tensile properties of the bars depend on the process parameters and steel composition.

The range of typical yield strength of TEMPCORE reinforcing steel is between 410 to 550 MPa and elongation on a 5d gage length is 30% down to 25% in the same order. Typical stress strain curves from Rehm and Russwurm (1977) and Defourny and Bragard (1977) is show in Figure 3-3. The features are summarized bellow:

- elastic modulus is 200,000 MPa;
- the bar has marked yield point and a Lüders type of yield and therefore the 0.01% proof stress ($\sigma_{0.01}$) coincides with 0.2% proof stress ($\sigma_{0.2}$);

- the ratio of yield stress to tensile strength is approximately 0.85;
- the bar has large elongation (25% to 30%), large Lüders strain and large uniform strain.

TEMPCORE reinforcing steels have two major features when the tensile properties are compared with those of conventional bars:

- higher ratio of yield strength to tensile strength, 0.85 versus 0.65;
- larger elongation, 25% versus 4.5 - 22%.

3.3.5 Formability

Another remarkable properties of TEMPCORE reinforcing steel is that it has excellent bending and rebending properties. Despite the hardened outside layer, minimum bend diameter for a 180° single bend is specified as 1*d* for 12 mm to 28 mm diameter bars and 2*d* for 32 mm and 36 mm diameter bars (BHP 1991). According to BHP (1982 a & b) and Economopulos et al. (1975), the 20 and 28 mm diameter bars can even be bent without mandrel, Figure 3-4. This is far smaller, that is better, than any specification requirement. The bars can also withstand all the bending and rebending tests after aging, satisfying the standard requirements (Economopulos et al. 1975) .

Bending operation requires less energy when compared with other types of bars due to the low tensile strength to yield strength ratio, 1.18 (1/0.85) versus 1.5 (1/0.65) for hot rolled bars. It is estimated that 10% to 20 % energy is saved in bending TEMPCORE reinforcing steel (BHP 1982a).

3.3.6 Weldability

Weldability of a steel is very sensitive to the chemical composition, especially to carbon content and carbon equivalent (CE). Two popular expressions are used, one due to the International Institute for Welding (IIW) and the other due to Ito and Besseyo, covering the high and low ranges of carbon respectively (Honeycombe and Bhadeshia 1995):

$CE = C + (Mn + Si)/6 + (Cr + Mo + V)/5 + (Cu + Ni)/15$

for $C > 0.18\%$, IIW;

$CE = C + Si/30 + (Mn + Cu + Cr)/20 + Ni/60 + Mo/15 + V/10 + 5B$

for $C < 0.18\%$, Ito-Besseyo

The IIW carbon equivalent formula shows less tolerance to substitutional alloying elements than the Ito-Besseyo equation. For the weldability of reinforcing steels, most specifications use the IIW or simplified IIW approach because of the carbon content (Table 3-1).

With the IIW equation, when CE is less than 0.45% the steel is considered weldable with modern techniques (Honeycombe and Hancook 1981). The CE of TEMPCORE reinforcing steel is well below the critical value of 0.45% (Table 3-1) and thus again is superior to other types of reinforcing steels.

The excellent weldability of TEMPCORE reinforcing steel is well demonstrated by the bend test on a cross weld, Figure 3-5 (Defourny and Bragard 1977). There is no sign of HAZ cracking in the weld of a 20 mm diameter bar when it is bent at an angle of 180° on a 3*d* mandrel. The TEMPCORE reinforcing steel in low temperature and or in wet state show remarkable weldability. No preheat and no post heat is necessary according to Defourny and Bragard (1977).

The excellent weldability is also demonstrated by the tensile properties obtained after welding. In flush butt weld no decrease in yield strength was noticed with the fracture located outside the weld (Defourny and Bragard 1977). In a BHP technical publication (1982c), it was shown that under different weld and welding processes no cracks occur in the weld.

3.3.7 Other properties

In addition to high tensile strength, excellent ductility and remarkable weldability, TEMPCORE reinforcing steels exhibit good low temperature toughness, less

sensitivity to surface damage, and the fatigue resistance and sensitivity to heat are also very competitive.

Defourny and Bragard (1977) demonstrated that at -60° C a 20 mm diameter bar with a 1 mm deep cut absorbed 795 Joules in drop weight test without breaking and superior low temperature toughness is reported in BHP technical notes (Table 3-2). Drop weight tests on arc strike damaged 12 mm, 16 mm and 20 mm diameter TEMPCORE reinforcing steel bars show that there is no fracture at -75°C (BHP 1991). Similarly, notch damaged and strain aged bars survive in drop weight test at -60°C.

A limited number of fatigue tests have been conducted on European made TEMPCORE reinforcing steels (Economopoulos et al. 1975; Rehm and Russwurm 1977) indicating that the fatigue properties of TEMPCORE reinforcing steels meet the requirements of German Standard DIN 448. In Australia, Behan and Warner (1984) conducted fatigue tests on a 12 mm diameter TEMPCORE reinforcing bar and reported that it has superior fatigue properties over cold worked bars. Spancer (1985) and Abel et al. (1986) carried out investigations on fatigue properties of TEMPCORE reinforcing steel with interest in the effects of galvanizing. All test results suggested that the fatigue strength of TEMPCORE is as good as those of other types of reinforcing steels with equivalent yield strength.

Properties of heat resistance of TEMPCORE reinforcing steel is of importance because of the possibility of fire damage. This resistance has been evaluated by two ways: tensile strength loss at room temperature after previous heat application and tensile strength loss at elevated temperature. Rehm and Russwurm (1977) showed that after heating in laboratory conditions at temperatures between 250°C and 900°C for half an hour, the room temperature tensile strength increases slightly with preheating up to 500°C and significant drop occurs above that temperature. This property is as good as cold twisted bars and better than those shown by some hot rolled bars. Cold -worked bars start to loss strength at 300°C to 400°C (Neves et al. 1996). Hot rolled British III U steel loss considerable strength from 350°C onwards

(Rehm and Russwurm 1977). Hot-rolled low carbon microalloyed 400 bar starts to show loss in strength from 600°C.

Tensile strength of TEMPCORE reinforcing steels at elevated temperature is similar to cold worked and microalloyed bars with a 20% and 40% reduction in yield strength at 300°C and 500°C respectively (BHP 1982c).

3.3.8 Economic aspects

The TEMPCORE process is an economical method in producing high strength reinforcing bars. Comparing to twisted bars, TEMPCORE process has obvious advantages in saving the cost of the mechanical twisting treatment which is expensive especially for small diameter bars. A further advantage comes from reduced alloying element requirements, off-grade heat, off-grade products, stock piling expenses and some other minor steel making factors. The only factor which increases cost is the rolling operation related to quenching installation and operation. The savings related to the TEMPCORE process is given in Table 3-3 at current prices, Simon et al. (1984b).

Savings on alloying elements compare to non-weldable reinforcing steels (ASTM615-60) amount to approximately 8.5 DM/t, but for weldable bars (KS 60 S) savings can be as high as 50 DM/t.

When the actual composition of the steel is considered unsuitable for its initially planned destination, it is regarded as off-grade heat and saving in off-grade heat is around 1.0 to 13.0 DM/t. With microalloyed steel, off-grade heat has to be diverted to another diameter within the same grade or another grade. Down grade can be very costly. With TEMPCORE process, however, most of these off-grade heats can be salvaged for the initial planned grade by adjusting the cooling power of the quenching installation. According to Simon et al. (1984b) TEMPCORE process has brought a reduction in the percentage of the off-grade heats by a factor of 2 to 5.

TEMPCORE process provides a good quality control: with a deviation of 13.7 MPa, 12.9 MPa and 1.82% in yield strength, tensile strength and elongation, respectively

(Rehm and Russwurm 1977). Saving in terms of reducing off-grade products is up to 0.7 DM/t.

TEMPCORE process has the flexibility to produce different diameter bars and even different grades from the same steel chemistry simply by acting on the cooling power of the quenching installation (Simon et al. 1984a). Thus manufacturers can avoid an expensive stock piling, with a further saving of 0.4 DM/t to 10.7 DM/t.

TEMPCORE process could accept scrap of poorer quality and since the chemical composition has great flexibility, the tap-to-tap time can be reduced. It is believed that the process is on the whole more economical than any other reinforcing bar production method.

3.4 SUMMARY

TEMPCORE process is an in-line heat treatment process which involves quenching and self-tempering. Plain low carbon steel is used in the process leading to advantages offered by the hardened and tempered martensitic outside layer, soft ferrite-pearlite core and the simple chemistry. TEMPCORE reinforcing steels are characterized by high yield strength, super-ductility, remarkable formability, excellent weldability and significant economic benefit. The following chart is a summary indicating the major steps in the process together with some of the property details.

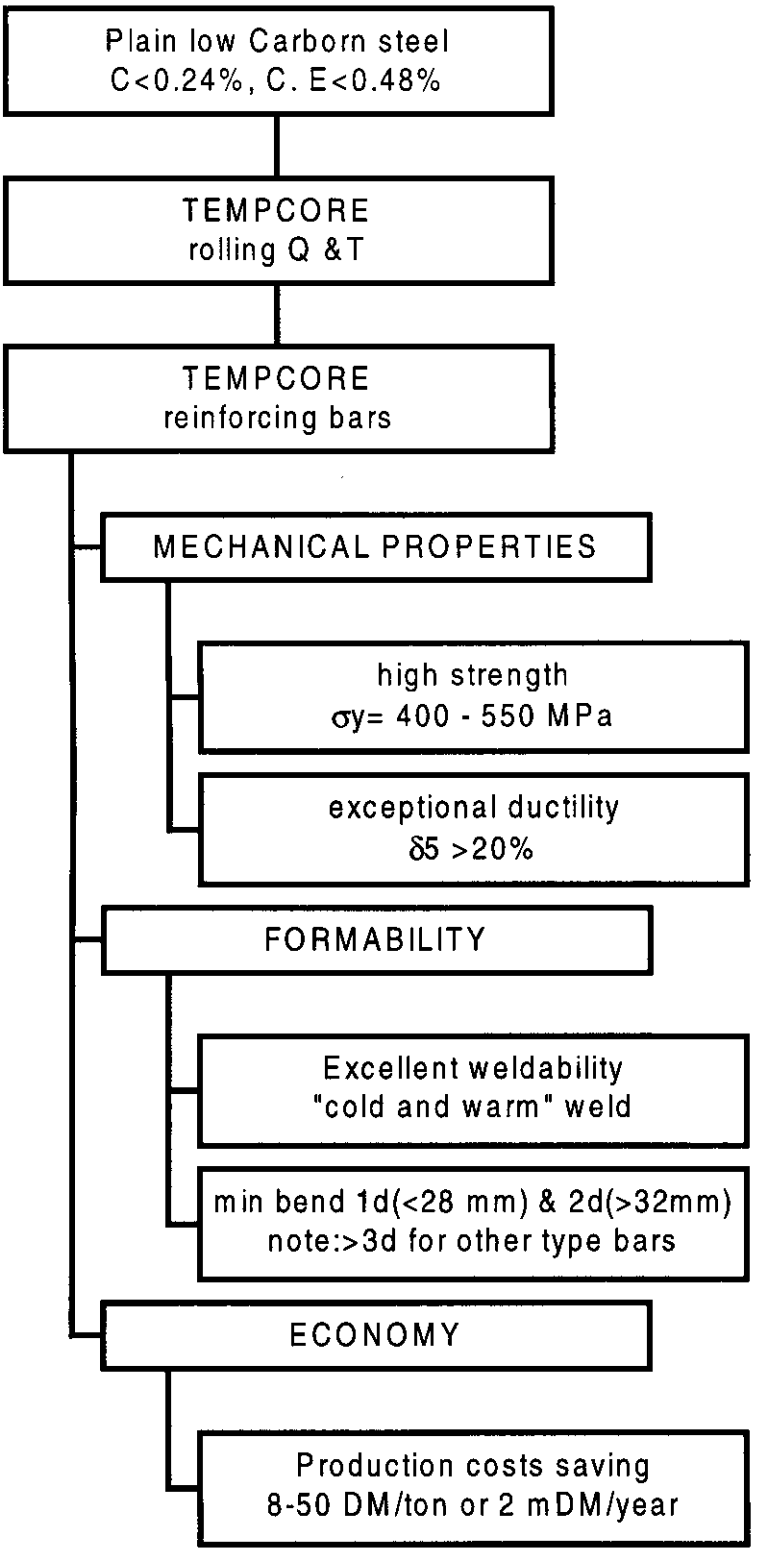
Plain low Carborn steel
C<0.24%, C. E<0.48%
TEMPCORE
rolling Q &T
TEMPCORE
reinforcing bars
MECHANICAL PROPERTIES
high strength
σy= 400 - 550 MPa
exceptional ductility
δ5 >20%
FORMABILITY
Excellent weldability
"cold and warm" weld
min bend 1d(<28 mm) & 2d(>32mm)
note:>3d for other type bars
ECONOMY
Production costs saving
8-50 DM/ton or 2 mDM/year

Table 3-1. Specified chemical composition for 400 MPa reinforcing bars (after BHP 1982c)

	Country	Standard & Grade	Chemical Composition C%	CE %
Hot Rolled	Germany	DIN 488	-	-
		BSt 42/50 Ru	-	-
	USA	ASTM		
		A615/616/617	0.30	0.55 [2]
		ASM A706	-	-
	Britain	BS 4449	0.40	0.51 [1]
	Australia	AS 1302 410Y	0.35	0.60 [3]
	Japan	SD 40	0.29	0.55 [3]
	Holland	Fe B400	0.27	-
	EEC	Fe B400	0.21	-
	France	Fe E400	0.22	0.45 [3]
	Belgium	Be 400S	0.21	0.45 [3]
Cold Twisted	Australia	AS 1302 410C	0.30	0.45 [3]
	Britain	BS 4461	0.25	0.42 [1]
	EEC	Fe B400	0.22	-
	Germany	DIN 488, BSt 42/50/RK	0.20	-
TEMPCORE	Australia	AS 1302 400Y	0.22	0.39 [1]

Note: Chemical compositions listed are ladle percent maximum.

CE: Carbon equivalent.

1. $CE = C + Mn/6 + (Cr + Mo + V)/5 + (Cu + Ni)/15$
2. $CE = C + Mn/6 + Cu/40 + Ni/20 + Cr/10 - Mo/50 - V/10$
3. $CE = C + Mn/6$

Table 3-2. Drop weight test results on notched bars (after BHP 1982c)

Steel type	Diam. mm	Temp. °C	Impact energy J	Fracture	Bend angle
TEMPCORE	20	-60°	1300	No fracture	43°
400 MPa	20	-60°	1300	No fracture	44°
Cold twisted	20	-60°	1300	Brittle fracture	0°
400 MPa	20	-60°	1300	Brittle fracture	0°
	20	+20°	1300	No fracture	43°
Hot rolled	16	-60°	800	Fracture	45°
Micro-alloyed	16	-60°	800	No fracture	45°
400 MPa					

Table 3-3. Production savings when compared with microalloyed steel (after Simon et al. 1984b)

Cost factor	TEMPCORE - Saving	
	DM/t	US$/t
Alloying element	8.0 to 54.0	3.0 to 20.0
Off-grade heats	1.0 to 13.0	0.4 to 4.8
Off-grade products	0 to 0.7	0 to 0.3
Scrap quality	*	*
Tap-to-tap duration	*	*
Level of billets stocking	0.4 to 10.7	0.15 to 4.0
Rolling cost	-0.5 to -1.5	-0.2 to -0.6

Note: 1 US$ = 2.7 DM at the time;

* In favor of TEMPCORE but not quantified.

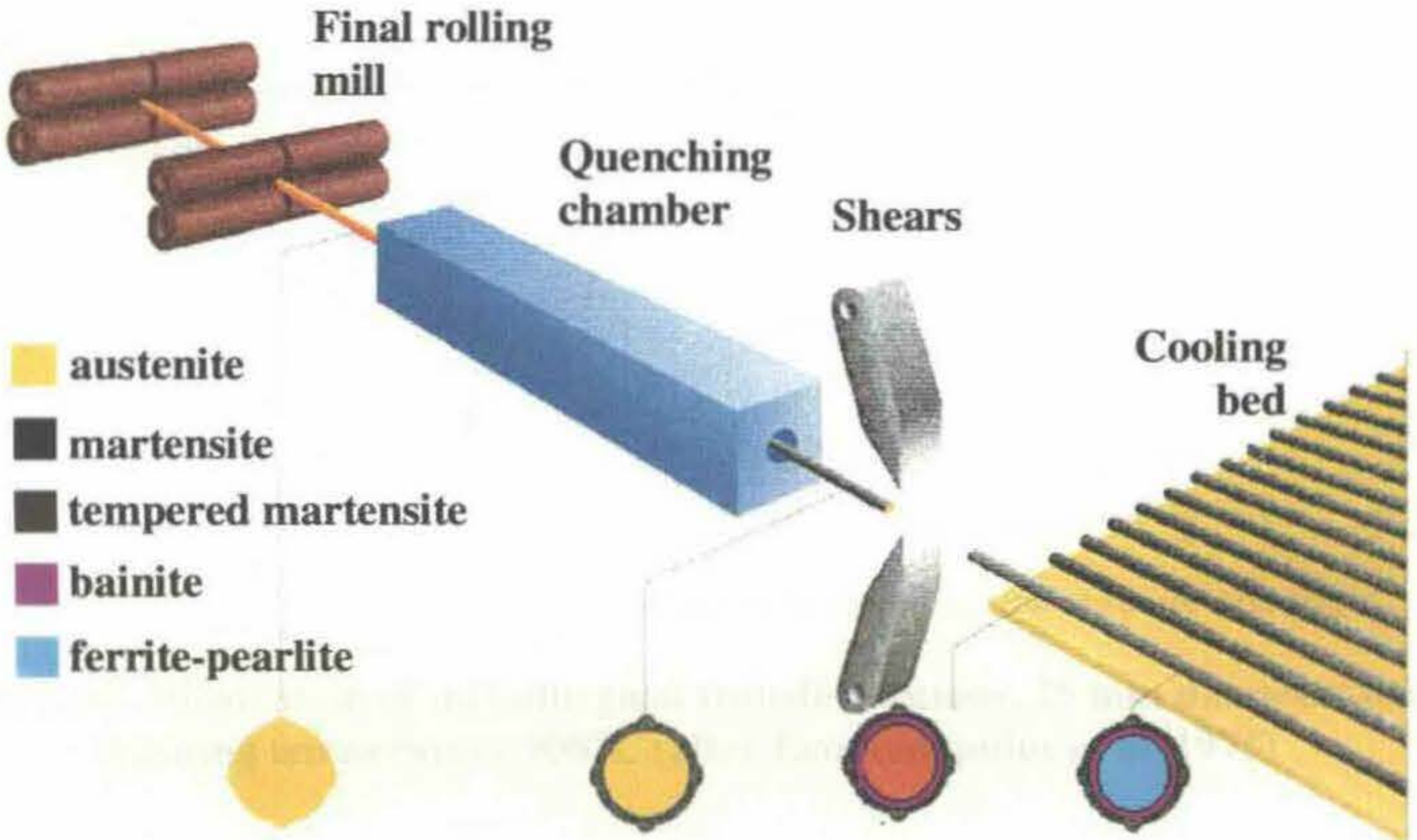

Figure 3-1. Illustration of TEMPCORE process

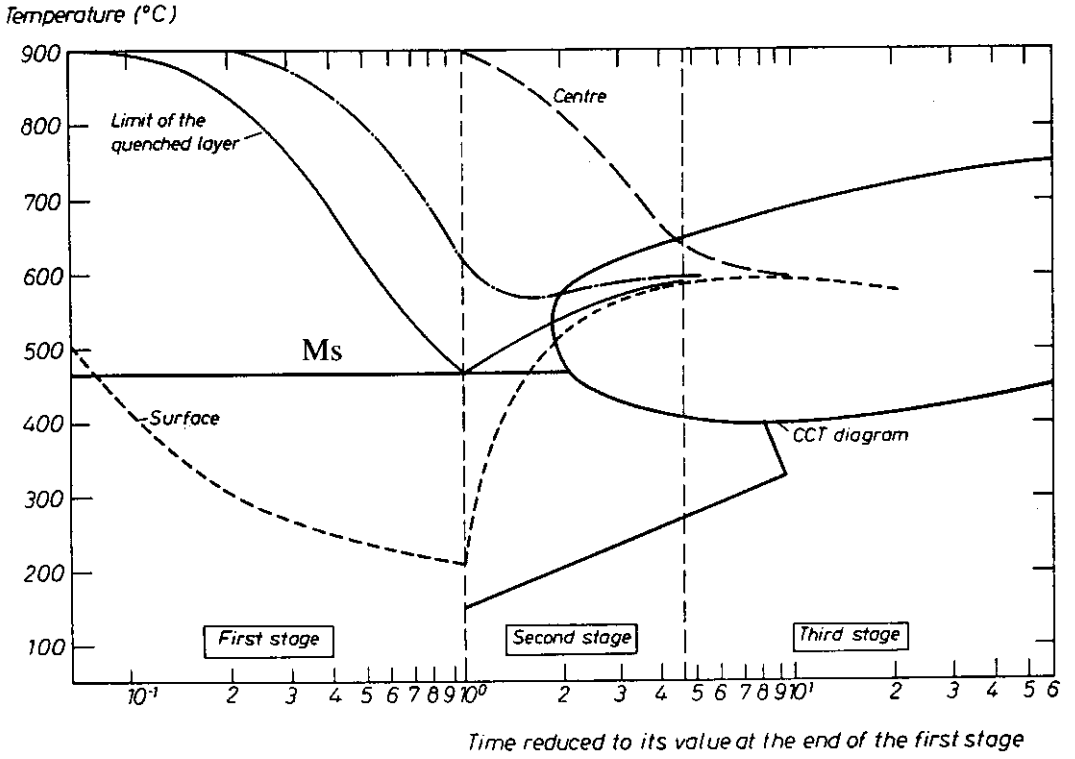

Figure 3-2. Illustration of metallurgical transformations, 25 mm diameter bar, finishing temperature 900°C (after Economopulos et al. 1975)

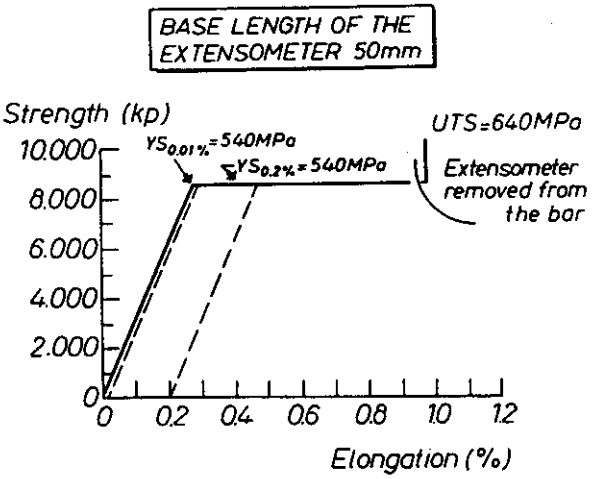

Figure 3-3. Stress strain curve of TEMPCORE reinforcing steel (after Rehm and Russwurm 1977)

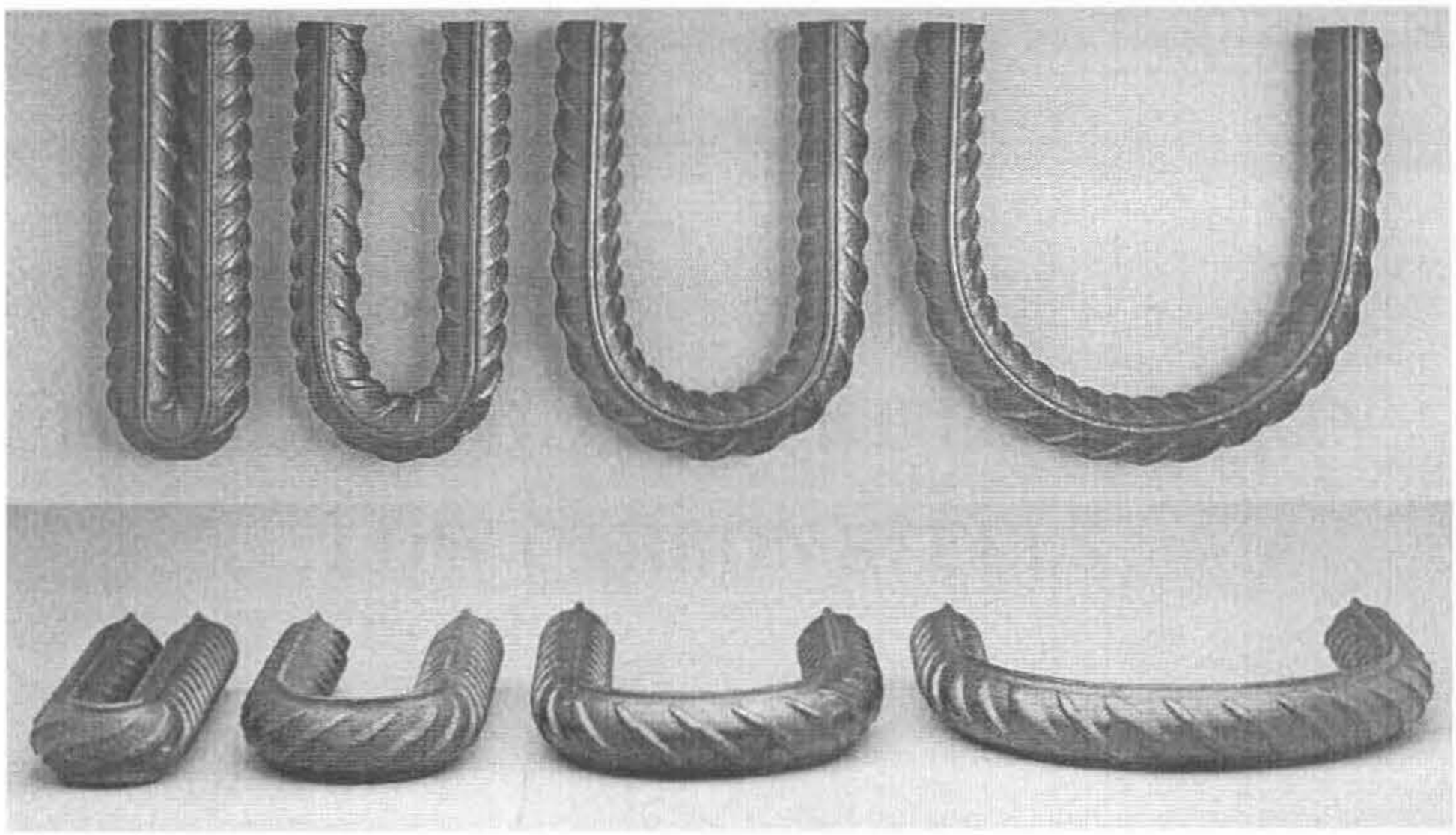

Figure 3-4. Bending of 20 mm TEMPCORE reinforcing steel (after BHP 1982c)

Figure 3-5. Bend test on a 28 x 20 resistance cross weld (after Defourny and Bragerd 1977)

Chapter 4

MECHANICAL PROPERTIES OF PLAIN LOW CARBON STEELS

4.1. OVERVIEW

Plain low carbon steels are generally considered to be steels with carbon content below 0.35% and without deliberate addition of other alloying elements. These steels exhibit yield strengths between 200 MPa and 1200 MPa with various fatigue properties depending on the carbon content and microstructure. In this chapter the tensile and fatigue properties are reviewed so as to provide the necessary background information for comparison purposes when the properties of TEMPCORE reinforcing steels are examined.

4.2. THENSILE PROPERTIES

4.2.1. Strengthening mechanisms

In these steels four different methods or the combination of some of those methods are used for strengthening purposes as outlined below.

4.2.1.1.Solid solution strengthening

The interstitial solid solution of carbon atoms in the ferrite crystals contributes significantly to the strength of steels. Carbon dissolves significantly into face-centred cubic (FCC) lattice forming austenite, but on cooling when the equilibrium conditions demands a transformation into body-centred cubic (BCC) lattice some of the carbon remains in interstitial solid solution distorting iron lattice leading to

interactions with dislocations and therefore strengthening. When oversaturated state is achieved by rapid cooling, the BCC structure is distorted by the entrapped carbon and a body-centred tetragonal (BCT) structure, martensite, is resulted. The distortion, or tetragonality, defined by the ratio between lattice spacing of axes, *c/a*, increases as:

$$\frac{c}{a} = 1 + 0.045\%C$$

Chilton and Kelly (1968) found that the yield strength due to the interstitial carbon atoms is proportional to the square root of carbon content as shown in Figure 4-1. According to Honeycombe and Hancook (1981) other authors expressed such relationship as

$$\tau = \tau_0 + \frac{2G\Delta\varepsilon C^{1/2}}{3}$$

where τ is the yield strength, τ_0 is the strength of pure iron, G is the shear modulus and $\Delta\varepsilon$ (≈ 0.38) is the difference between longitudinal and transverse lattice strain.

4.2.1.2.Grain size

The refinement of the grain size of ferrite provides one of the most important strengthening route via heat treatment and controlled rolling. It has been well established that the lower yield stress of mild steels is proportional to the inverse of the square root of the grain size (Figure 4-2, a), and this was expressed as:

$$\sigma_y = \sigma_0 + kd^{-1/2}$$

where σ_0 and k are constant, and d is the average diameter of grains. This relationship was proposed by Hall, Petch and Low according to Honeycomeby and Hancook (1981), and is generally known as the Hall-Petch relationship.

Hall explained this phenomenon by suggesting that all dislocations are pinned until an applied stress reaches the upper yield point at which one dislocation source in a single grain is activated and starts to generate dislocations which stop at the grain boundary. As these piled up dislocations produce a sufficiently high stress concentration in the adjacent grains, Figure 4-2 (b), a dislocation source in a neighbouring grain will become activated and this way yield spreads from grain to grain.

When the applied stress is σ the stress acting at a distance l from the head of a dislocation pile-up, Figure 4-2 (b), can be expressed as $\sigma(d/4l)^{1/2}$ (Cahn and Haasen 1983) when l is smaller than the width of the pile-up of dislocations that is *d/2*. If a frictional force, σ_f, acts on the dislocation lines, this concentrated stress is reduced to $\sigma_f + (\sigma - \sigma_f)(d/4l)^{1/2}$, and when this stress equals the stress needed to unlock a pinned source, σ', yield starts to spread, i.e.,

$$\sigma' = \sigma_f + (\sigma - \sigma_f)(d/4l)^{1/2} \qquad \text{or} \qquad \sigma = \sigma_f + (\sigma' - \sigma_f)(4l/d)^{1/2}$$

The strengthening arising from grain size is clearly indicated, and furthermore grain size refinement is the only strengthening method which improve the ductility of the steel at the same time.

4.2.1.3.Dispersion strengthening

In low carbon steel particles such as Fe_3C carbide may exist as a second phase in the forms of lamella or randomly dispersed particles. The matrix ferrite, which is strengthened by grain refinement and by solid solution, is further strengthened by dispersion of this second phase. The general trend arising from this type of strengthening is that the yield strength increases as the spacing of the second phase particles or lamellas decreases. Relatively fast cooling a pearlite carbon steel during normalising produces pearlite with finer lamellas thus results in higher yield stress. The relationship of the yield stress to the mean uninterrupted free ferrite path in pearlitic ferrite is described similarly to the Hall-Petch type equation by Takahashi and Nagumo (1970).

In steels with ideally small spheres randomly dispersed in a ferrite matrix, there are well-defined relationships between the yield stress, τ_0 and the mean particle distance, l. Particles could be by-passed at a stress

$$\tau_0 = \tau_s + \frac{2T}{bl}$$

where τ_s is the yield stress of the matrix, T is the line tension of dislocation, and b is the Burgers vector. This equation shows that the yield stress varies inversely as the spacing between the particles.

A more precise form of the above equation takes into account the radius r of the particles:

$$\tau_0 = \tau_s + \frac{Gb}{4r}\phi \ln(\frac{l-2r}{2b})(\frac{2}{(l-2r)})$$

where ϕ is a constant and G is the shear modulus (Honecombe and Bhadeshia 1995).

4.2.1.4.Dislocation strengthening.

Large number of dislocations can be generated by the reaction during the martensite formation and also by plastic deformation, and as the total dislocation density increases the mobile dislocation density decreases and thus the strength of the steel increases.

Considering a steel with a dislocation density of ρ, the mean spacing between dislocations will be $r = 1/\sqrt{\rho}$. If the dislocation distribution is random, with respect to both position and sign, the internal stress due to the dislocations can be written as $\mu b(\rho)^{1/2} / 2\pi$ (Cahn and Haasen 1983) where μ and b are the shear modulus and Burgers vector, respectively. In order to move the dislocation over appreciable distance through the high density dislocations, an external tress of approximately the same amount is required, thus the yield stress is proportional to the square root of dislocation density, or

$$\sigma_y = \mu b(\rho)^{1/2} / 2\pi$$

4.2.2. Tensile properties of ferrite-pearlite steels

4.2.2.1.Tensile strength

Hot rolled and annealed low carbon steels made up from ferrite-pearlite are generally weak. The strength of this type of steels can be increased by refinement of grain size, increasing the proportion of pearlite or work-hardening.

Refinement of grain size may be achieved by normalising, controlled rolling and adding carbide forming alloying elements. Take a 0.16C% steel for example, a ferrite grain size of 20 μm is obtained by conventional hot rolling, while by fast cooling

after hot rolling, the grain size can be lowered to 10 μm or even less. This may lead to a 120 MPa increase in yield strength.

Increasing the proportion of pearlite, by increasing carbon content, does not remarkably affect the yield strength but substantially increases the tensile strength, provided other factors, such as ferrite grain size, are kept constant. This is explained by the low pearlite content in low carbon steels which occupies a small volume in the microstructure, and thus the yield stress is essentially determined by the ferrite matrix. However, the work hardening rate is in a linear relationship with pearlite content hence increases the tensile strength.

Work hardening, by cold rolling, stretching or twisting, significantly strengthens this type of steels as this leads to a significant increase in dislocation density. For example, the tensile strength of a 0.05%C steel subjected to 95% reduction in area by wire drawing is raised by no less than 550 MPa (Honeycombe and Hancook 1981).

4.2.2.2.Lüders yield

A yield drop followed by a flat yield plateau is observed in this type of steels with the characteristic upper yield point and the propagation of a type of plastic wave called Lüders band or Lüders strain at the lower yield stress level. This type of yield is well known as Lüders yield which was first explained by Cottrell (1953) who proposed a dislocation locking and unlocking mechanism. He showed that impurity atoms, such as carbon and nitrogen, tend to be attracted to dislocation lines and thus the dislocation is locked or pinned. As a result, higher stress is required to move this locked dislocation. Once the locked dislocation is "unlocked" by the upper yield stress, the dislocations will be moved by a lower stress.

Another explanation for the Lüders yield was started by Johnston and Gilman (1959) by noting that on yielding a lithium fluoride the pre-existing dislocations never moved during the upper and lower yield, and it was the newly created dislocations which produced the subsequent plastic deformation. Hahn (1962) suggested that there are three main factors leading to discontinuous yielding: a small initial mobile dislocation density, rapid dislocation multiplication and a highly stress-dependent

multiplication mechanism. He argued that the strain consists an elastic and a plastic component and these strain rates equal to $d\varepsilon_e / dt = \frac{1}{\mu}\frac{d\sigma}{dt}$ and $d\varepsilon_p / dt = 0.5bLv$, respectively, where μ is the elastic modulus, b is Burgers vector, L is the length of dislocation line in motion per unit volume, and v is the average velocity of the dislocations.

Here L is assumed to be a fixed fraction f of the dislocation density, and the density is a function of plastic deformation: $\rho = \rho_0 + C\varepsilon_p^a$, where ρ is the dislocation density and ρ_0 represents the growth-in dislocation density, normally 10^6 - 10^8/cm^3. Thus

$$L = f(\rho_0 + C\varepsilon_p^a) \qquad \textbf{(4-1)}$$

It was found that the velocity of dislocation depended on stress (Stein and Low 1960) and with the consideration of strain hardening effect, it is expressed as:

$$v = (\frac{\sigma - q\varepsilon_p}{2\tau_0})^n$$

where τ_0 is the resolved shear stress corresponding to unit velocity, n is a constant (around 35), q is the macroscopic work-hardening coefficient. The strain rate thus can be written as:

$$d\varepsilon / dt = \frac{1}{\mu}\frac{d\sigma}{dt} + 0.5bf(\rho_0 + C\varepsilon_p^a)(\frac{\sigma - q\varepsilon_p}{2\tau_0})^n$$

Without the contribution of elastic strain, the above equation is re-written with respect of stress strain relationship as:

$$\sigma = q\varepsilon_p + 2\tau_0\{\frac{d\varepsilon / dt}{0.5bf(\rho_0 + C\varepsilon_p^a)}\}^{1/n} \qquad \textbf{(4-2)}$$

In real materials local variations of ρ_0 and σ are both likely, the yield starts from where ρ_0 and σ exceed the average. The dislocation density then increases in the yield region by dislocation multiplication (Equation 4-1), thus plastic deformation proceeds at lower stress (Equation 4-2). From Equation 4-2, it is seen that the smaller is the initial dislocation density, the larger is the yield drop. Dislocations generated within the yield band then activates the yield of the neighbouring grains, and the yield band spreads in the specimen.

4.2.2.3.Microplasticity

Preyield microstrain has been observed in low carbon steel (Vreeland et al. 1953) and some iron based alloys and received intensive study (Brown and Lukens 1961; Suits and Chalmers 1961; Worthington and Smith 1964; Brown and Ekvall 1962; Brentnall and Rostoker 1965; Kossowsky and Brown 1966; Abel and Muir 1973 a & b). This preyield microstrain, or microplasticity, refers to the plastic strain up to a few hundreds micro strains (a micro strain is 10^{-6}) before the attendance of macroscopic yield. This microplasticity is attributed to the mobile dislocations with limited potential to move and as the applied stress increases a pile up occurs. Thus the preyield differs from macroscopic yield as no dislocation multiplication takes place.

Brown and Lukens (1961) quantitatively analysed the preyield phenomenon and pointed out that the amount of microplasticity is proportional to the cube of grain size in the following manner.

Suppose the number of dislocation sources per unit volume is uniform throughout the specimen, the strain per *ith* grain will be

$$\gamma_i = n_i D^2 b \rho D^3 / Al \qquad \textbf{(4-3)}$$

where n_i is the number of dislocations emitted by the source in the *ith* grain, D is grain diameter and thus D^2 is the cross-section area of the grain, b is the Burgers vector, A is the cross-section area of the specimen and l is the gage length. The number of piled-up dislocations per source is linear to the back stress, i,e.,

$$n_i = (\sigma - \sigma_0^i) KD / Gb \qquad \textbf{(4-4)}$$

where σ_0^i is the stress to activate a source in the *ith* grain, K is a constant, about 2. The total strain, γ, in the specimen summed over the total number of contributing grains

$$\gamma = \sum \gamma_i f_i Al / D^3 \Delta\sigma_0^i \qquad \textbf{(4-5)}$$

f_i is the fraction of the grains with activated sources by a stress between σ_0^i and $\sigma_0^i + \Delta\sigma_0^i$. With the assumption that the orientation of grains is random, and the ratio of the stress to activate a source in the most favourably oriented grain to that of the least

favourably oriented grain, σ_0^0/σ_0^M, is about 1/2, from equations 4-3, 4-4 and 4-5 the following equation can be deduced:

$$\gamma = C\rho D^3(\sigma - \sigma_0^0)^2 / G\sigma_0^0 \qquad \textbf{(4-6)}$$

indicating that the amount of microplasticity is grain size dependent.

4.2.3. Tensile properties of martensitic steels

Low carbon martensitic steel consist of lath- or plate-like oversaturated ferrite, in respect to carbon, permeated with large dislocation density in the order of 10^{11} - 10^{12} cm^{-2} which is similar to those of very heavily cold-worked steel. The laths are long and about 0.5μ wide and are grouped together in packets with low angle boundaries between them. Thus martensite is strengthened by all the strengthening mechanisms mentioned above, and as the grain size is extremely fine, and auto-tempering and retained austenite are always involved, low carbon martensitic steels are also rather tough.

On tempering martensite the strength is reduced due to the reduction in solid solution and dislocation density, but highly dispersed carbide precipitation takes place and thus the dispersion strengthening increases. The general trend is that strength decreases and ductility increases as the tempering temperature increases. Steels with tempered martensite structure exhibit continuous yielding.

4.3. CYCLIC PROPERTIES

Low carbon steels may exhibit cyclic hardening, or softening, or softening followed by hardening depending on the microstructure and cyclic stress or strain ranges. Klesnil and Lukas (1967) have shown that annealed steels (ferrite-pearlite) cyclically soften and then harden when cycled below their yield points. Three phases can be identified during the course. The initial softening was attributed to the generation of mobile dislocations within discrete plastically deformed zones, and the plasticity is in the microscopic range. The generation of mobile dislocations by cycling may eliminate the upper yield point in a subsequent static tension test (Abel 1973 a & b). Further softening was attributed to the spread of these plastically deformed zones in a

way similar to Lüders yield and the subsequent hardening is attributed to the typical work-hardening mechanism. Cycling at a stress range beyond the yield stress cyclic hardening takes place.

As-quenched martensite steels exhibit cyclic hardening followed by a small and gradual softening (Wilson and Mints 1972; Thielen and Fine 1976). According to Wilson and Mints, the to-and-fro dislocation motion may assist a certain segregation to dislocations and may even lead to a precipitation of ε carbides resulting in cyclic hardening. The minor softening is explained as being due to irreversible damage occurring either at the intersection of the slip band with the surface or at dislocation pile ups.

Tempered martensite steels generally cyclically soften due to: (1) the removal of the dislocation pinning or mechanical generation of unpinned dislocations, which is similar to the softening in ferrite-pearlite steels; and (2) the creation of a fatigue substructure - the uniformly distributed dislocations are rearranged to a highly inhomogeneous bundles of dislocations separated by dislocation free regions - leading to a reduction in the internal stress state.

4.4. FATIGUE PROPERTIES

Steels with martensite and tempered martensite have better fatigue resistance than ferrite-pearlite steels (Forrest 1962; Landgraf 1978; Breen and Wene 1978; Yu et al. 1988). Goto (1991) in a rotating bending fatigue test showed that the fatigue limit of a tempered martensite steel was about twice as high as that of a ferrite-pearlite steel. The microstructure of steels, the constituents, morphology, as well as grain size, affect fatigue properties mainly relating to crack initiation and small crack propagation. Since crack initiation and small crack propagation consumes the majority of the fatigue life (Kerlins 1987; Goto 1991; Shibata et al. 1996; Retchie 1986; Taylor 1989) as shown in Figure 4-3, the following sections will highlight the problem.

4.4.1. Effects of microstructure on fatigue properties

Fatigue crack initiation in many cases has been observed at inclusions, second phase-matrix interfaces, intense slip bands, grain boundaries and grain boundary triple junctions which provide some form of strain localisation. As crack initiation needs heterogeneous deformation, microstructures that distribute the plastic strain homogeneously delaying the fatigue crack initiation. Thus by lowering impurity levels, increasing the fomability of the inclusions or reducing their size, refinement of grain size, and making a microstructure suitable for randomly distributed dislocation network can improve crack initiation resistance.

Crack growth follows different laws according to their size which is classified as (1) microstructural short crack (MSC) length of which having the same order of magnitude as the metallurgical features, (2) physically small crack (PSC) with length in the 50 to 500 μm range, and (3) large cracks beyond 500 μm. Large crack growth can be described by linear-elastic fracture mechanics (LEFM) - the well known Paris law - at low stress level and by elastic-plastic fracture mechanics (EPFM) at higher stress level and it is not sensitive to microstructure. But small fatigue crack growth rate is faster than that predicted by Paris law and thus it is considered "anomalous".

The failure of using Paris law in predicting small crack growth is because the plastic zone at the crack tip is not compatible with the assumptions used in the theory of LEFM. Miller (1987 a & b, 1991) summarised laws governing crack propagation and explained these in the three graphs shown in Figure 4-4. Cracks which initiate above the fatigue limit ($\Delta\sigma_1$ and $\Delta\sigma_2$) continuously grow until failure, while those initiated below fatigue limit ($\Delta\sigma_3$, $\Delta\sigma_4$ and $\Delta\sigma_5$) stop propagating at a certain crack length, b_3, b_4, *and* b_5, as shown in Figure 4-4 (a). Thus fatigue limit can be defined as the maximum stress at which a crack does not grow.

Figure 4-4 (b), known as the Kitagawa diagram (Kitagawa and Takashashi 1976), illustrates the dependency of fatigue limit on crack length. Large cracks, described by LEFM, do not propagate when the applied stress intensity factor range ΔK is below the threshold Δk_{th}. Small crack growth takes place with a decreased rate (Figure 4-4 a

& c) and, under fatigue limit, eventually the cracks stops. The characteristic dimension, $b = b_3$ *or* b_4 *or* b_5, were found to be associated with microstructural barriers. Thus the area enclosed by the contour line in Figure 4-4 (b) represents non-propagation crack. The reduction of propagation rate is related to the cyclic hardening and the rate is expressed as

$$\frac{da}{dN} = A\Delta\gamma_p^{\alpha}(d-a)$$

where A and α are material constants, $\Delta\gamma_p$ is the plastic shear strain range, d is the distance of the strongest barrier and a is the crack length. Grain boundary provides an efficient barrier to crack advancing and thus reducing the grain size of a metal increases the plain specimen fatigue limit. The $\Delta\gamma_p$ term is proportional to $1/\sigma_y$ where σ_y is the yield strength, thus stronger material possess better resistance to MSC growth.

For the physically small crack the growth rate is

$$\frac{da}{dN} = B\Delta\gamma_p^{\beta}a - C$$

where B and β are material constants and C is the longer crack threshold condition. This equation shows that the stronger material possess better resistance to small crack growth.

Figure 4-4 (c) shows that the arrested crack could continue to grow at the same stress range, but only if it could be extended to a length of the fatigue limit threshold condition for a physically small crack, a_3, a_5 for stress ranges of $\Delta\sigma_3$ and $\Delta\sigma_5$, respectively. While cycled at $\Delta\sigma_2$, crack propagation rate slows down before it reaches a certain barrier length and after which the growth rate increases since the barrier length is beyond the fatigue limit threshold condition.

The growth of a large fatigue crack is not sensitive to the microstructure generally (Retchie 1986). The propagation is due to the alternating slip process at the crack tip on two slip systems at roughly 45° to the crack plane, during which the sliding-off is irreversible thus new crack surface is created. The plastic zone at the tip of a large crack is sufficiently large compared with microstructural dimensions, thus the growth

rate is not controlled by the microstructure but instead by the effective stress intensity factor range, ΔK_{eff} in which case the shielding effect of crack closure has been taken away from the applied stress intensity factor range. This is expressed by the Paris law as:

$$da / dN = C(\Delta K_{eff})^n$$

Although large crack growth rate is not affected by microstructures, increasing grain size can increase the LEFM threshold value, thereby increasing the fatigue limit for structures containing large cracks. Thus it has been suggested that a combination of smaller grains on the surface and larger grains in the interior yields better fatigue resistance (Miller 1991).

4.4.2. Crack initiation and crack propagation

A number of papers reported that tempered martensite has a very good resistance to crack initiation, (Stamm et al. 1996; Turnbull and Rios 1995; Rios et al. 1984; Taylor and Knott 1981; Brown and Hicks 1983; Brown et al. 1984; Akinawa et al. 1988; Lankford 1982; Breen and Wene 1978). This is explained by the combined effect of the fine boundaries and high dislocation density found in these metallurgical structures. In a mixed microstructure of ferrite and tempered martensite fatigue cracks initiate only from the soft ferrite (Kunio et al. 1969; Yu et al. 1988; Rios et al. 1992; Solberg 1988). In case-hardened situation fatigue crack origins are shifted from the specimen surface to the sub-surface region (Landgraf and Richman 1975; Starker et al. 1979; Magnusson and Johannesson 1977; Cowing 1986; Qian and Fatemi 1995).

The small crack propagation rate is reduced in tempered martensite because a large number of microstructural barriers have to be overcome by the advancing small crack, such as boundaries of laths, lath packets and former austenite boundaries. In addition to high yield strength, materials with tempered martensite provide good response to fatigue.

The fatigue limits of ferrite-pearlite steels do not increase with tensile strength when strengthened by increasing pearlite proportion as crack initiation always takes place

in ferrite grains (Kurita et al. 1996, 1997). However, by increasing the strength of the ferrite component by adding various alloying elements the fatigue strength of such dual phase steel can be significantly increased (Kurita et al. 1997, 1996; Yanada et al. 1968).

Tests on ferrite-pearlite steels showed that the pearlite bands play an effective role in hindering small crack growth (Rios et al. 1992). In a dual phase steel where ferrite grain is surrounded by a continuous martensite net, it is the martensite which provides an effective barrier to the coalescence of the cracks in the ferrite grains (Nakajima et al. 1997).

4.5. SUMMARY

Plain low carbon steels are generally strengthened by solid solution strengthening, refinement of grain size, dispersion of carbides and dislocations. Ferrite-pearlite steels can be strengthened by refinement of grain size and work-hardening, the first of which improves ductility, but work-hardening impairs ductility. This type of steels yield in Lüders style and this is related to the lack of mobile dislocations. The limited number of mobile dislocations is responsible for the preyield microstrain.

Low carbon martensite or steels with tempered martensite are strengthened by all the possible strengthening mechanisms and thus possess higher strength. Since this type of steels possess fine grain structure and tempering releases some of the internal stresses, these steels are not only strong but also tough.

Generally steels with tempered martensite have better fatigue properties than ferrite-pearlite steels.

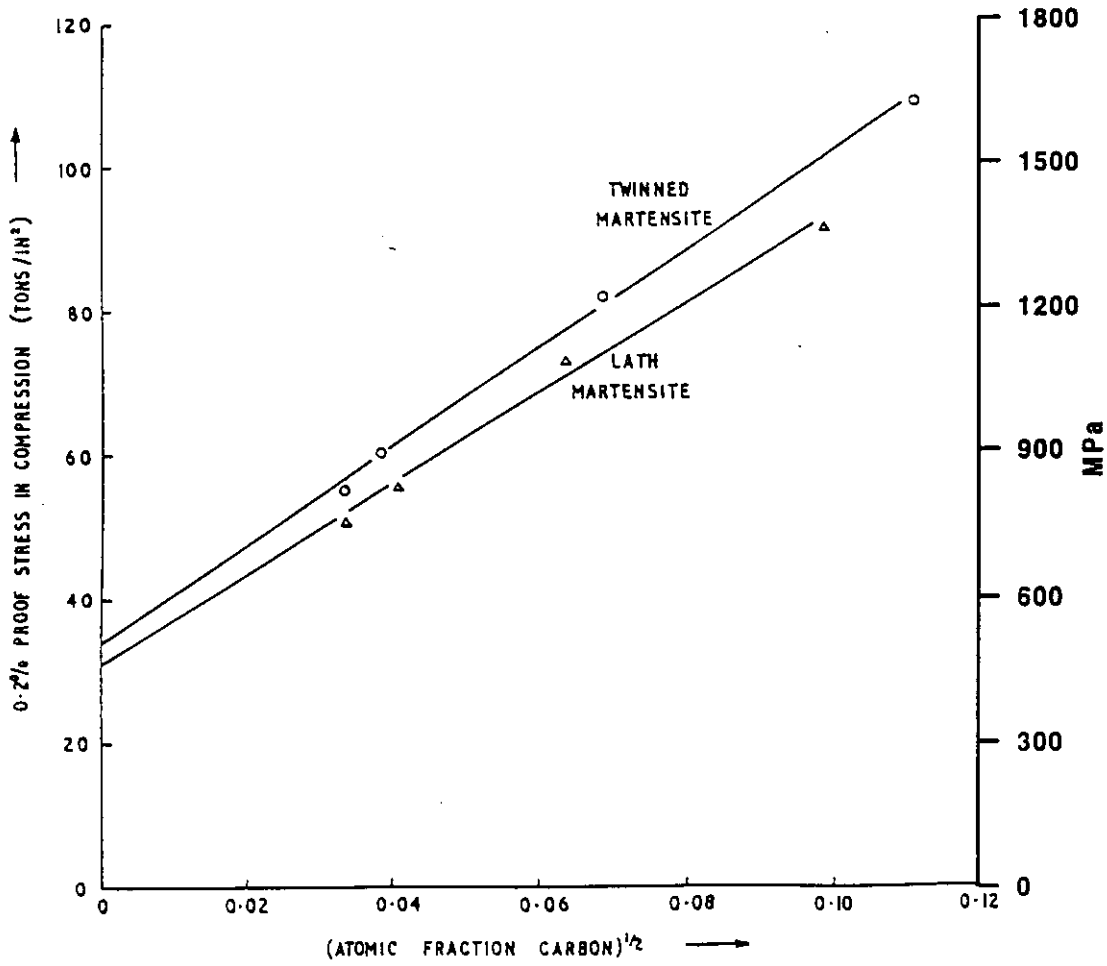

Figure 4-1. The effect of carbon on the yield stress of martensite (after Chilton & Kelly 1968)

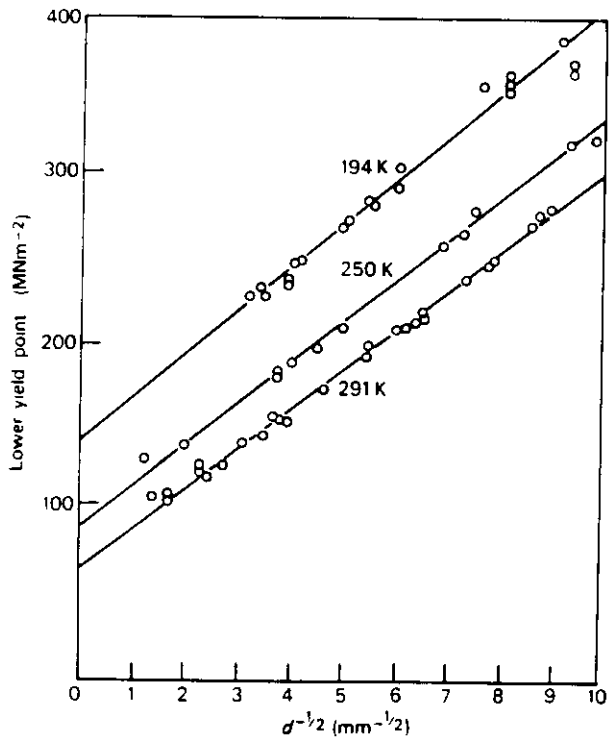

(a) Grain size dependence of the lower yield stress of mild steel (after Honeycombe & Hancook 1981)

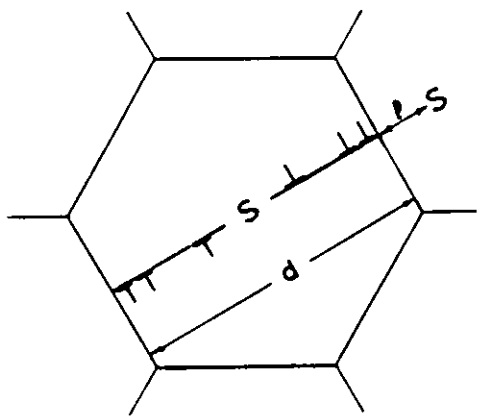

(b) Dislocation pile-up in a grain of diameter *d*

Figure 4-2. Grain size effects on yield strength

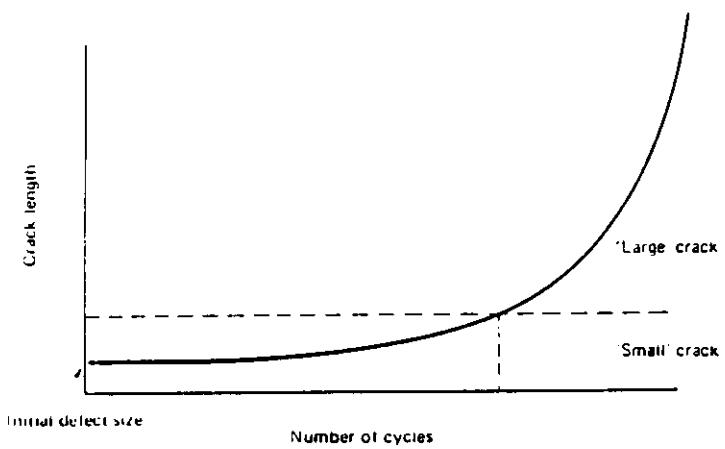

Figure 4-3. Schematic variation of crack length with number of cycles for a crack growing under constant applied stress amplitude (after Taylor 1989)

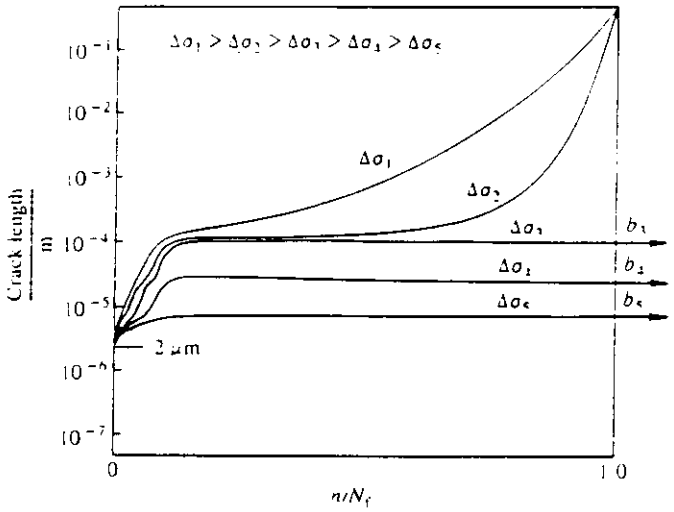

(a) Crack growth behaviour as a linear function of the applied number of cycles

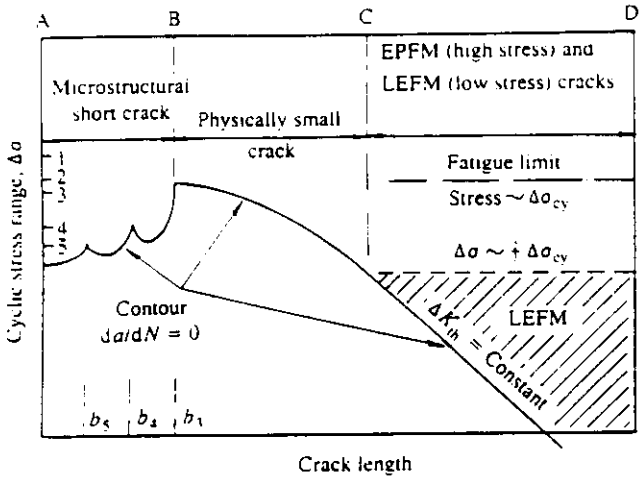

(b) Fatigue limit dependency on crack length

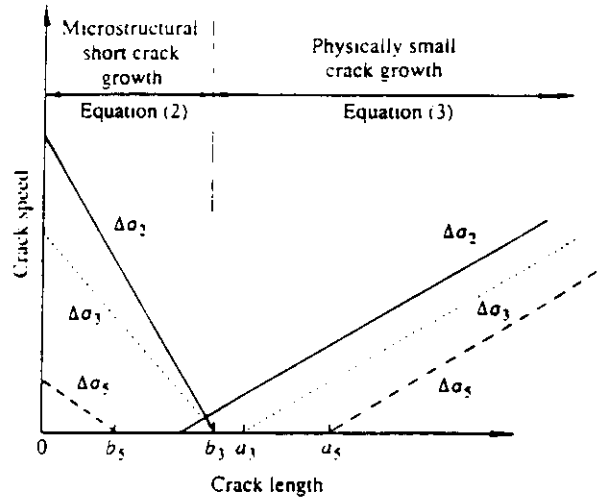

(c) Effects of cyclic stress level and the barrier strength on the propagation of fatigue crack

Figure 4-4. Schematic description of crack propagation (after Miller 1991)

Chapter 5

FATIGUE OF REINFORCING STEELS

5.1 OVERVIEW

Fatigue problems may arise with the use of reinforcing steels in bridges, offshore installations and other structures. A highway bridge may endure 700 million cycles of traffic induced stress states during its 120 years service life and an offshore structure may experience 100 million stress cycles by the action of waves during its 30 years service life. Tests have shown that fatigue limits of high yield deformed reinforcing steel bars are in the range of 150 MPa to 250 MPa. Measured stress by using strain gage method on reinforcing bars of a bridge in Hill County, Texas was 19,810 psi (136.6 MPa) under controlled conditions when test trucks passed (Hardeman 1965). Tests on two other bridge decks showed 103 MPa and 144 MPa stresses under truck loadings (Ruhl and Walker 1975). As the use of high yield bars are increasing, the service stress range of the reinforcing bars tend to increase, and thus fatigue becomes more of a concern.

Since fatigue failure of reinforcing steels has been observed in the laboratory test on concrete bridge (AASHO 1962), the study of fatigue characteristics of reinforcing steels has been intensified. Generally, it has been found that the fatigue limit of deformed reinforcing bars is low, about 1/3 to 1/2 of their yield strengths. Deformed reinforcing steels show well defined S-N curves with clear knees with the following influencing factors, which will be reviewed:

- cyclic stress range;
- minimum stress level;

- stress concentrations associated with bar deformations;
- bar diameter;
- grade of steel;
- manufacturing process; and
- residual stresses.

5.2 TEST METHODS AND STANDARDS

Two major types of tests have been employed to determine the fatigue properties of reinforcing steels, i.e., bending a concrete beam with tested bars embedded and axial tension on bare bars in air. Both have advantages as well as disadvantages, and therefore some standard test procedures have been recommended as shown below.

5.2.1 Bending test on reinforced beam

In this type of test, the tested beams are usually reinforced by either a single reinforcing bar (Pfister and Hognestad 1964; Nakayama 1965; Burton 1965; Mac Gregor et al. 1971; Soretz 1974; Helgason et al. 1976; Roper and Hetherington 1980) or more reinforcing bars in the tensile area (Kokubo et al. 1965, 1968; Kaar and Hognestad 1965). Loading is completed by hydraulic jacks with a sinusoidal constant load amplitude in a way of three-point bending or four-point bending.

The apparent advantage of the beam bending test is that it closely simulates the service conditions such as the interaction between the bar and surrounding concrete, and the existing stress gradient in the bar. However, many disadvantages exit. First of all, test frequency is generally limited within 3 Hz to 8 Hz, and some large scale test can only be run at 0.1 Hz (Centre for Advanced Structure Engineering 1996). For this reason, in many cases, fatigue limit had to be determined at a low cyclic number, e.g., 2 million cycles (Kokubu and Okamura 1968). To facilitate the test method and guarantee fatigue fracture a crack initiator - a plate inserted into the beam - is often used (Burton 1967; Mac Gregor et al. 1971; Soretz 1974). This, however, diverted the test conditions from the actual service conditions. The second disadvantage relates to the cost in preparing the specimens and running the tests which includes material, machine time, space and labour. Finally, it is hard to decide the applied

load, and some assumptions have to be made in calculating the bar stresses. The stresses measured on the reinforcing bars in a concrete bridge using strain gage method has shown such stress differences (Hardeman 1965).

Standards DIN 488 describes the procedure for beam bending tests with strict method relating to concrete embedment of the bars.

5.2.2 Axial test

Axial test involves the loading of the bare reinforcing bars in a conventional fatigue test machine. This is the most convenient method to determine the fatigue properties of reinforcing bars. Although this method is far from the actual service conditions in which the bars are used, it is cheaper in terms of sample preparation and running cost, and the stress calculation is accurate. Since this method gives slightly conservative results compared with beam bending (Tilly 1979; Jhamb and Mac Gregor 1973), the obtained data leads to safer designs and for comparative purposes the results are valid.

The gripping of these bars is, however, a problem. Directly gripped bars will introduce high local stresses resulting fractures at the gripped ends. It is also difficult to avoid bending stresses due to the alignment of the test pieces.

A variety of gripping methods have been developed. In Grönqvist's test (1971) the gripped ends are coated with epoxy in such a way that two layers of 0.7 mm steel-wire is embedded in the epoxy. Gripping is effected through the coated epoxy. Yanopoulos and Edwards (1976) employed leather strips between the grips and the bars. Behan and Warner (1984) used a special bandage consisting of fiberglass wound alternatively with a layer of Araldite coating around the gripped ends of the bar. The banded ends were covered by soft aluminum tubes with 1.6 mm wall thickness. RILEM - FIP - CEB (1973) suggested special grips of collets with the same profile as the tested bar, or of a block of concrete, wood or steel tubes filled with resin. These methods although helped in the gripping problem to a certain degree, are not suitable for higher cyclic loading and for hydraulic grips due to the

lower efficiency in load transfer and to the insufficient strength of the packing or filling materials.

Jhamb and Mac Gregor (1974a), used a rather special gripping method in which the tested bar was embedded into a cylindrical block of high strength steel having a conical hole on one end using epoxy for fill. Thomas and Pasko (1973) developed a technique in which the ends of the specimen were cast in a pair of tapered sleeves using Babbit alloy, so that the cone shaped babbit metal can hold the bar and transforms load through deformations to the bar when jaws grip on the sleeves. This method can be used in hydraulic grips but has difficulty at high applied load.

Spencer (1985) and Abel et al. (1986) improved the above method by welding a washer at each end of the test bar. These washers then act as "plungers" which force the casting into compression between the bar and tapered sleeves producing wedging effect when load is applied axially. This improvement allows a great increase in the testing loads. A further advantage of this method is that it gives good protection for the bar from the squashing by the hydraulic grips, good alignment can be achieved and it is relatively cheap.

The gage length of the test bar is also questionable as sizes from 100 mm to 700 mm, have been used by different authors. Thomas and Pasko (1973) used only 100 mm free length for a 19.5 mm bar testing. Abel et al. (1986) used a gage length of about 240 mm for 12 mm, 20 mm and 28 mm diameter bars, while Behan and Warner (1984) used an effective length of 700 mm for 12 mm diameter bars. It is argued that shorter gauge length can increase experimental scatter and therefore it has been recommended by RILEM - FIP - CEB standard (1973) that the free length should be longer than 30 times the diameter or at least to cover 8 helical ribs (transverse lugs) and in no case should it be less than 500 mm. According to this standard, fatigue limit can be determined at 2 million cycles.

One further advantage of axial testing is that higher frequencies can be used, and although 150 HZ frequency was suggested by Tilly (1979), most testing machines can manage only up to 10 Hz for long specimens.

5.2.3 Test results

It has been shown (Tilly 1979; Jhamb and Mac Gregor 1974a) that axial test yields a slightly conservative result when compared with that of beam bending test results. This maybe explained by the test situation: the potential crack initiator does not necessarily coincide with the largest stress area, while in axial testing, all the defects are subjected to the same cyclic stresses.

Results are generally expressed through the so called S-N curves and typical north American results are shown in Figure 5-1. The fatigue limit and the slope of the curves may vary according to the authors as differences exist in the deformation patterns of the bars and other test conditions.

5.3 EFFECT OF DEFORMATION GEOMETRY

Deformations, as described in Chapter 2, are designed for optimum bond characteristics and not for fatigue considerations. However the deformation geometry influences the fatigue performances, through stress concentrations arising from the root radius, width and flank angles of the deformations. It is shown that these factors have a significant effect on the fatigue behaviour of reinforcing steel bars.

Fatigue tests show that rupture occurs without exception at the bases of lugs or the conjunction of transverse lugs, or longitudinal ribs, or the identification marks of the manufacturer. According to Kokubu and Okamura (1968), the poor fatigue resistance of deformed bars was attributed to the non-uniformity of bar cross-section but later on, it was clarified by many authors that it is the stress concentration associated with deformations that is responsible for the poor fatigue performances.

Mac Gregor et al. (1971) and Helgason et al. (1976) demonstrated that the fatigue strengths of deformed reinforcing steels are much lower than those of smooth bars

machined from the same steels. Bars with different types of deformations (Hanson et al. 1968) and bars produced from rolls which suffered different wearing conditions (Grönqvist 1971) have shown that the radii at the bases of transverse lugs have a major influence on fatigue strength. It was also suggested that the influence of lug geometry may even offset the effect related to the grade of steels (Mac Gregor et al. 1971; Jhamb and Mac Gregor 1974a). The ratio of lug radius to lug height was found to be the prime factor affecting fatigue properties. The smaller is the ratio, the poorer is the fatigue performance. However, the effect of deformation geometry was only assessed qualitatively as the stress concentration factor (SCF) at lug root was unknown. Many other variables, e.g., chemical compositions and microstructures of the steels, may be also involved in this problem.

Jhamb and Mac Gregor (1974b) conducted the first quantitative evaluation of the stress concentrations at the vicinity of the deformations. In that approach the lug was described as an axis - symmetrical projecting lug and defined by the ratios of lug radius to lug height, half width of lug and flank angle. Using finite element method, the authors calculated the stress distribution near the base of a lug and concluded that the SCF decreases with the ratio of base radius to lug height, but increases with the ratio of the half lug width to height. They also concluded that larger flank angles cause higher stress concentrations, but this is not as significant as the other two factors above. Results obtained from their calculation show that a SCF of 2.5 may arise for a sharp and wide deformation (r/h = 0.1, w/h = 2); but SCF decreases to a value of 1.6 and remains essentially unchanged when r/h is larger than 1.25.

To evaluate the effect of SCFs the geometry of the deformation must be determined first and methods used by other authors have been reviewed in Chapter 2.

5.4 EFFECT OF MINIMUM STRESS LEVEL

Some investigators claimed that minimum stress level has no effect on fatigue properties of deformed reinforcing steels (Pfister and Hognestad 1964), but later Helgason et al. (1976) showed that fatigue strength decreases as the minimum stress increases. This finding also applies for cases when the minimum stress level is

negative. The trend is illustrated with the following example: an increase of 21 MPa in minimum stress is equivalent to 6.895 MPa increase in the stress range. According to Mac Gregor et al. (1971) the fatigue strength of high strength hot-rolled bars may be described by a modified Goodman diagram, and Tilly (1979) also showed some similar effects relating to the minimum stress level.

Minimum stress may affect fatigue properties through crack closure and this may be more significant when residual stresses are present.

5.5 EFFECT OF GRADE OF STEELS

There is contradiction in the literature as whether the grade of steels has an effect on the fatigue properties of reinforcing steels. Little effect is reported on the fatigue limit by Pfister and Hognestad (1964), Kokubu and Okamura (1968), Mac Gregor et al. (1971) and Jhamb and Mac Gregor (1974 a & b), while Grönqvist (1971) found that the steel quality may be important. Summarising the published data, ACI Committee 439 (1973) reported that the fatigue strength does not increase much when the yield strength of the bars exceed 420 MPa. Thus it was asserted that this will limit the use of higher grade reinforcing steels. As an explanation of this behaviour Mac Gregor et al. (1971) suggested that decarburisation at the outer surface may be responsible. Jhamb and Mac Gregor (1974a) has also indicated that the strength of surface layer may be important.

However, Kokubu and Okamura (1965) and Helgason et al. (1974, 1976) have shown that the fatigue limit and fatigue life are slightly improved as the strength of the steels increases.

5.6 EFFECT OF BAR DIAMETER

Fatigue strength generally decreases as the bar diameter increases. Helgason et al. (1976) tested bars with five different diameters and concluded that the bar diameter influences the finite-life but the effect is not as significant as stress range and

deformation geometry. ACI Committee 215 (1987) reported similar results when comparing data from three sources.

The bar size effects are generally explained by the idea that larger surfaces have a higher probability of critical surface defects content. In addition, stress gradient in the cross section of the bars may be involved when the beam is subjected to bending.

Jhamb and Mac Gregor (1974b) in his theoretical work did not find bar size effect on stress concentrations associated with the deformation patterns.

5.7 OTHER EFFECTS

Bars produced by the two conventional manufacturing methods - hot-worked and cold-worked - showed no differences in the fatigue properties (Tilly 1979). The TEMPCORE process has not been evaluated, as yet, in this respect.

Mill scale and rust were found essentially no influence on fatigue properties by Jhamb and Mac Gregor (1974a).

The effect of residual stresses were not investigated although it has been mentioned by Helgason et al. (1976) that an association may be present.

5.8 FRACTURE MECHANISM AND FRACTOGRAPHY

Very little has been reported on the fracture mechanism and fractography as related to the fatigue of reinforcing steels. Fatigue crack growth study by Helgason et al. (1976) concluded that the major part of the fatigue crack growth took place during the final 40% of the fatigue life.

Published fractography indicates that fatigue cracks always initiate at the bases of lugs or the conjunction of the transverse lugs, or longitudinal ribs, or the identification marks of the manufacturer where large stress concentrations are present. It appears that the fracture surfaces depend on the deformation patterns and

the ductility of the steels. For American made Grade 60 bars with crossed inclined transverse lugs crack starts from the junction of the crossed lugs. Fatigue fracture is normal to the bar axis and the final fracture is brittle with its surface also normal to the bar axis, Figure 5-2. For hot-rolled bars with inclined transverse lugs crack starts from the lug root and propagate normal to the bar axis. The final fracture is rather ductile, Figure 5-3. Cold-worked bars show similar fractures to hot-rolled bars but fatigue fracture develops along the helical rib, Figure 5-4. In the work of Kokubu and Okamura (1965), one sees fracture surfaces on bamboo shaped bars run along the lug root normal to the bar axis. Fatigue initiation has been observed at one point (Helgason et al. 1976) or more points (Jhamb and Mac Gregor 1974a).

5.9 FATIGUE OF TEMPCORE REINFORCING STEEL

As reviewed in Chapter 3 only limited number of fatigue tests have been conducted on TEMPCORE reinforcing steel.

According to Economopoulos et al. (1975), fatigue tests on TEMPCORE reinforcing steel at Centre de Recherches Metallurgiques (C.R.M) show that the fatigue strength of TEMPCORE reinforcing steels is at least as good as the other type reinforcing bars with equivalent yield strength. This result has been confirmed by tests on girders carried out at the University of Liege. Rehm and Russwurm (1977) experimentally proved that TEMPCORE reinforcing steel meets the German Standard DIN 448. Behan and Warner (1984) showed superior fatigue properties of TEMPCORE reinforcing steel over cold worked bars. From the works of Spancer (1985) and Abel et al. (1986), although concentrating on the effects of galvanising, it can be concluded that fatigue limits of TEMPCORE reinforcing bars are above 200 MPa.

5.10 SUMMARY

There is no international standard procedure for fatigue test on reinforcing steels and only tentative recommendations may be consulted.

Two major methods are used for fatigue testing of reinforcing steel bars. Beam bending test simulates the service conditions but it is a slow process and it is also an expensive method. Axial tests at relatively higher frequency and at a lower cost yield relatively conservative results but not at service conditions.

The two main factors affecting the fatigue properties are cyclic stress range and the deformation pattern on the bar surface. Sharper deformation geometry results in lower fatigue limit, and higher cyclic stress range results in shorter fatigue life in the finite-life region. Other factors, such as the grade of steel, bar diameter and minimum stress level may also influence the fatigue properties but some contradictory conclusions have been reported on the effects of these minor factors.

Generally, fatigue properties of deformed reinforcing steels are in the form of S-N curves. For numerical evaluation the equations of Helgason et al. (1976) indicate the significance of the various factors.

For fatigue limit presented in SI units:

$$\sigma_r = 143.416 - 0.339\sigma_{\min} + 54.7463(r/h) \qquad \textbf{(5-1)}$$

For fatigue life above fatigue limit:

$$LogN = 6.1044 - 0.0059\sigma_r - 0.0026\sigma_{\min} + 0.00103\sigma_u - 0.0000877A + 0.0127d \times r/h \qquad \textbf{(5-2)}$$

where for both equations (5-1) and (5-2):

σ_r = stress range, in MPa;

σ_{min} = minimum stress, in MPa;

σ_u = tensile strength, in MPa;

A = bar area in mm^2;

d = bar diameter, in mm;

r/h = ratio of base radius to height of deformation.

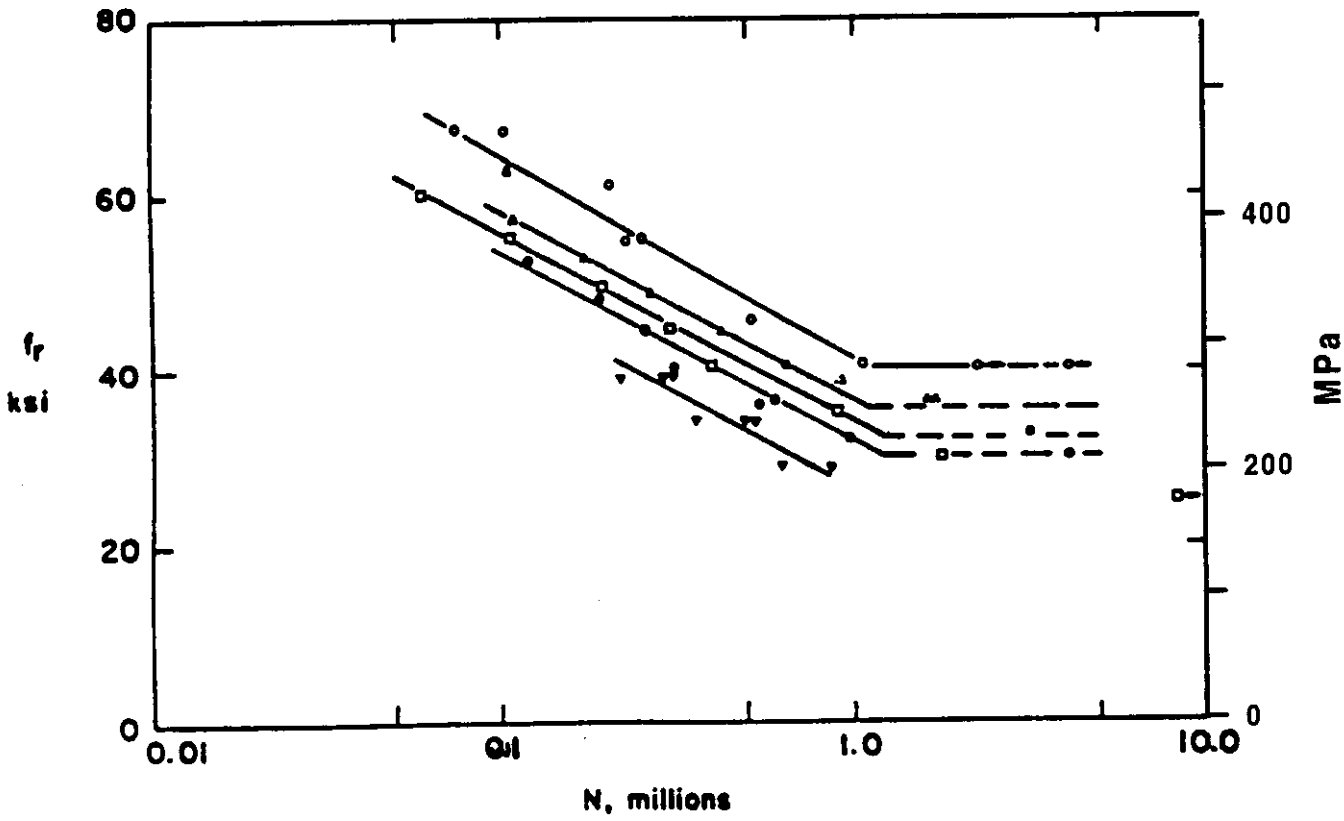

Figure 5-1. Typical S-N curve of deformed reinforcing steel (after Helgason et al. 1976)

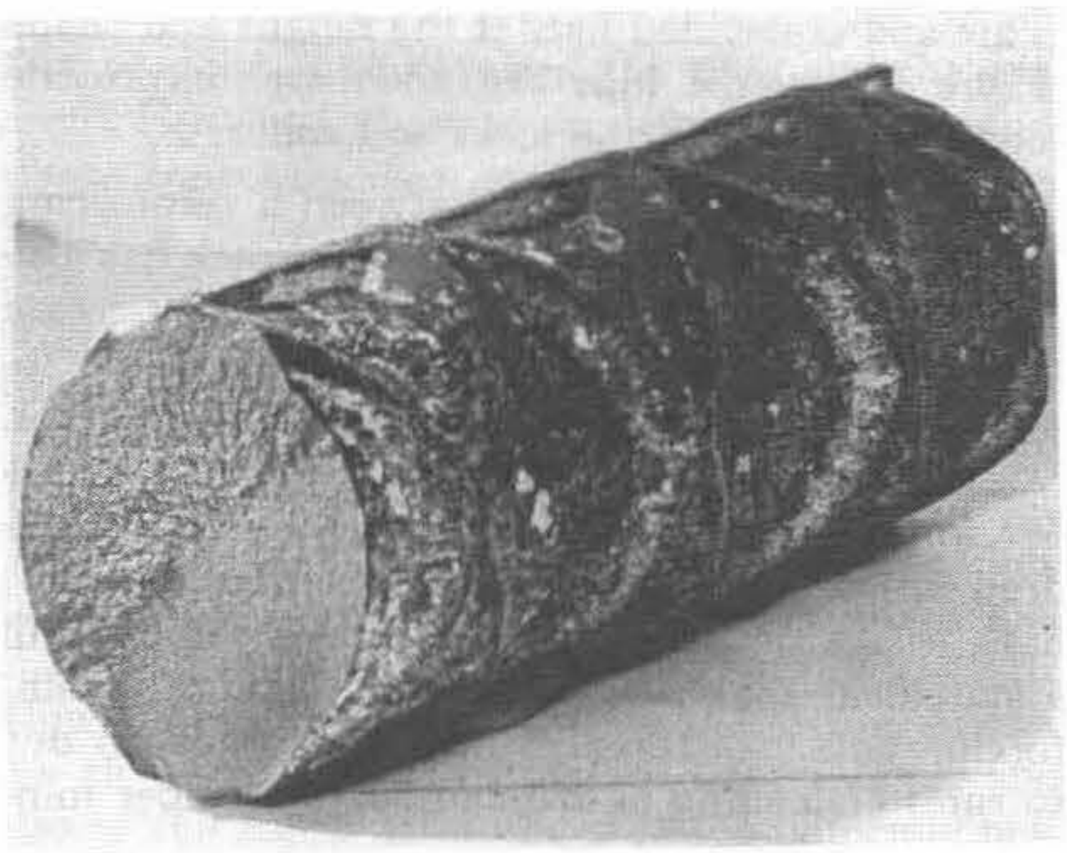

Figure 5-2. Typical fatigue fracture of American Grade 60 bar (after Helgason et al. 1976)

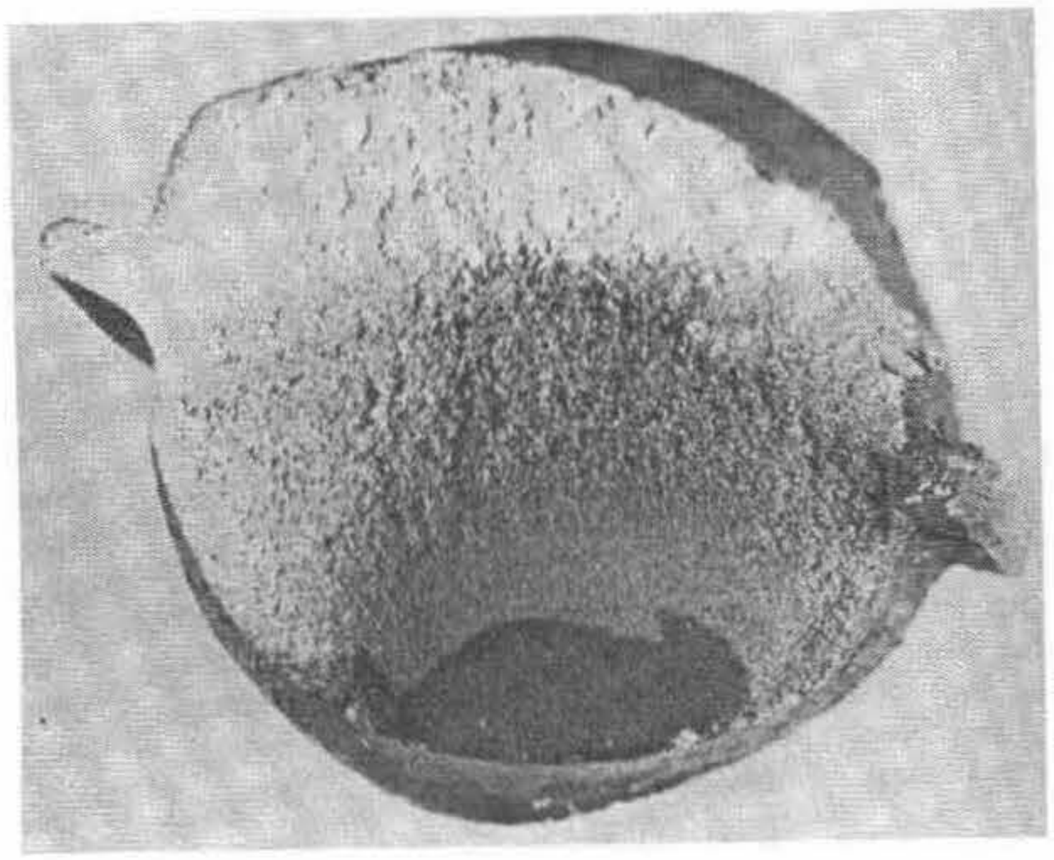

Figure 5-3 Fracture of hot-rolled bar (after Tilly 1979)

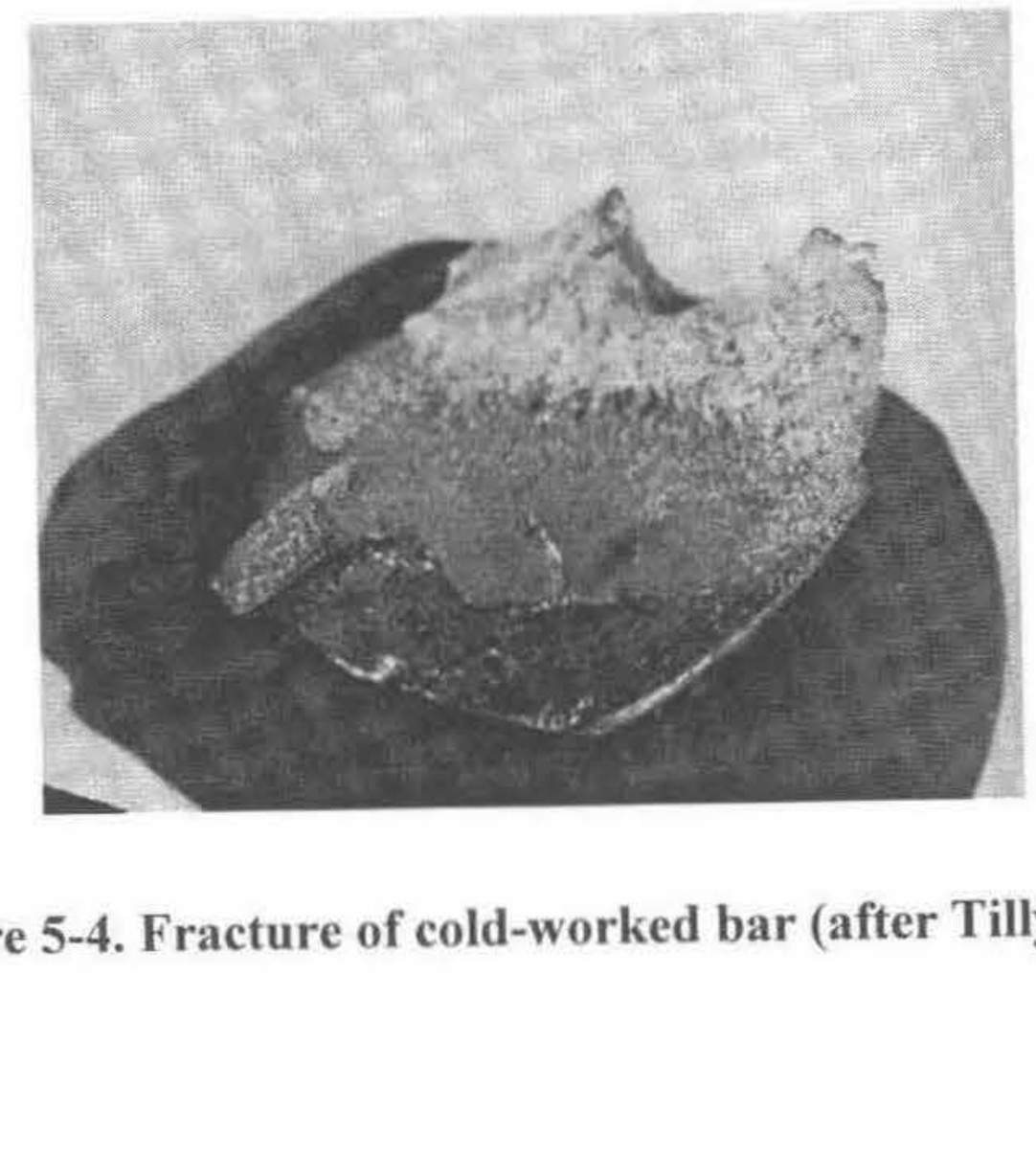

Figure 5-4. Fracture of cold-worked bar (after Tilly 1979)

Chapter 6

EXPERIMENTAL APPARATUS AND PROCEDURES

6.1. EXPERIMENTAL APPARATUS

The used apparatuses are listed below.

1. Leitz MM-6 optical microscope;
2. Wild Heerbragg Stereomicroscope and Zeiss Stereomicroscope;
3. Leitz Wetzlar Miniload-2 micro hardness tester;
4. Philips 505 scanning electron microscope;
5. 11 kW resistance heat treatment furnace;
6. 250 kN Instron testing machine;
7. 300 kN Sentech 65/G MTS testing machine;
8. Instron, model 8500, hydraulic dynamic testing system;
9. 2000 kN Dartec servo-hydraulic testing machine with MTS Teststar control system;
10. Instron 260-603 dynamic extensometer;
11. Model LC-2320 laser displacement meter;
12. "Spectran" computer data log system.

6.2. TEST MATERIAL

Seven size Australian made TEMPCORE reinforcing steel bars (TEMPCORE 400-Y) supplied by Sydney mill and New Castle mill, were studied (Figure 6-1). Their

dimensions, mass and mechanical properties comply to Australian Standard AS 1302 - 1991, and the chemical composition of the steels is given in Table 6-1. These steels can be considered as plain carbon steels, with carbon content in the 0.13% to 0.20% range with carbon equivalent (CE) values in the 0.284% to 0.331% range.

6.3. EXPERIMENTAL PROCEDURES

6.3.1. Metallographic techniques

Cross sectional and longitudinal sections were cut to suitable size and were grounded and polished following a standard procedure described in Metals Handbook (ASTM. 1985). For the etching process a 4% Nital solution (4% nitric acid by volume in ethanol) was used.

The etched samples were examined under stereomicroscope, and the depths of hardened and intermediate hardened layers were measured under a magnification of x10. Photographs of cross sections were taken using a conventional camera with macrolens.

Microstructures were examined by Leitz MM-6 microscope. The samples were marked by Vickers hardness indentations along the radii for reference purposes. Ferrite grain size in the core area was determined by comparison and intercept procedures as described in ASTM standard E 112 (ASTM. 1990).

6.3.2. Hardness tests

The cross section of the samples were hardness tested by Leitz Wetzlar Miniload-2 micro hardness tester with a load of 500 grams. The intervals of the measured positions vary from 0.1 mm to 1.5 mm according to the microstructure change along the radius.

6.3.3. Determination of residual stresses

Residual stress determination was carried out by the Sachs boring-out method, as described by Polakowski (1966).

Figure 6-2 shows the specimen and equipment set-up for determination of residual stresses. Four N22-FA-5-120-11 90° rosette strain gages were arranged symmetrically around the bar surface in longitudinal - circumferential directions.

Boring was performed in a mill with a constant feed speed. Drilling started from about 4 mm diameter and was repeated by approximately 10 to 15 times with increasing drill diameter. Residual stresses possibly induced by boring was minimised by using a sharp tool and slow machining speed. Data acquisition was conducted by using "Spectran" computer data log system which provides a fast and reliable measurement. Reading of the stress release by each boring sequence was taken every 20 minutes until the readings did not change within an hour.

In the calculation of the residual stresses, the elastic modulus and Possion's ratio were assumed to be 2.06 X 10^5 MPa and 0.3, respectively.

6.3.4. Measurement of deformation geometries

Before measurements of deformation geometries on the surface of the bars, the mill scale and rust was removed in an acid bath (as detailed in Appendix 6-1). The cleaned bars are greyish in colour. This surface reflects enough light, so that a laser displacement meter can be used. The preparation does not change the geometry. Profiles of critical longitudinal sections were traced using a laser displacement meter directly on the bar surface and the obtained data was processed by the "Grapher" (1992) software.

Set-up for profile tracing is shown in Figure 6-3 (a) and (b). A laser displacement meter scanning the bar surface measured the changing distance from the bar surface to the meter. Longitudinal displacement of the "scanner" was measured by LVDT transducer. A typical lug profile, as a result of this technique, is shown in Figure 6-3 (c).

6.3.5. Stress relieving

Some specimens were stress relieved in order to asses the effect on mechanical properties without residual stresses. Specimens were heated to 550°C and held for 6 hours followed by furnace cooling. These details were chosen with reference to Howard (1984) and BHP (1993) assuming no microstructural or mechanical property changes.

6.3.6. Tensile testing and tensile cycling

Tensile tests on the as received bars were conducted in the 250 kN Instron, the 300 kN Sintech, and the 2000 kN Dartec machines corresponding to different bar diameters. For the measurement of strain a 50 mm gauge length extensometer and electrical strain gages were used. These tests were conducted according to Australian Standard AS 1391-1991 using a series strain rates, between 10^{-6} / S and 10^{-4} / S.

The core and the case materials, after appropriate machining, were tested on a short specimen, i.e., $L_0 = 5.65\sqrt{S_0}$ or $L_0 = 5d$ with an initial strain rate of 10^{-5}/Sec.

In addition, side-cut and centre-through-cut specimens were used in order to free the core from the restraint of the hardened case, as shown in Figure 6-4 and Figure 6-5. These tests were designed for the study of the interaction between the core and case materials during loading.

There were some tensile cycling tests by loading from zero to a certain level below yield stress before final tension with a strain rate of 10^{-6} / S in order to study the microplasticity effect. For similar purposes compression cycling was also carried out on 40 mm length bar when two electrical strain gages were attached to the bar surfaces.

6.3.7. Reverse cyclic loading

Fully reversed tension-compression cyclic loading tests were carried out for all the seven size bars at a constant stress amplitude of about 80% of their yield stress with a

frequency of 0.01 Hz. This low frequency was intended to avoid intensive heat generation resulted from the possibility of large plastic deformation. Two strain gages on the opposite sides of a specimen were used for strain measurement.

Tests of this type were more intensely used on 16 mm diameter bars with a constant stress amplitude of 300 MPa (70% of yield stress) and 370 MPa (86% of yield stress) at a frequency of 0.01 Hz. Five strain gages were put on different sections along the bar axis to measure strain responses on the specially gripped bars, Figure 6-6.

Babitt alloy (melting point is 272°C) was used to anchor the bars in a pair of steel sleeves. Casting temperature was carefully controlled at 280°C so as to avoid a possible effect on the properties of the bars. Washers were welded at the ends of the specimen and threaded plugs were fastened against the welded ends to assist the anchoring of the specimen.

Testing commenced only after preloading the test specimens to check possible slippage between the sleeves and the bar. Test conditions were kept to ASTM standard for fatigue test, Designation E 466 - 82 (ASTM. 1993).

6.3.8. Fatigue tests

6.3.8.1.Griping

Similar gripping arrangements were used to those applied in reverse cyclic loading. Grinding and wire-brash polishing were applied on the cast parts immediately next to the gauge length to avoid failure in the sleeves. The detailed procedure for sample preparation is described in Appendix 6-2. Typical specimens and their fatigue failure positions are shown in Figure 6-7. The importance of welded washer is shown in Figure 6-8.

The 260 mm gauge length of the specimen covers 50 and 20 transverse lugs, respectively, for diameters of 12 mm and 36 mm the thinnest and thickest bars tested. This meets the requirement of "8 times of the pitch of helical ribs" in gage length

recommended by RILEM-FIP-CEB (1973). In addition, 70% of the specimens also had identification marks in their gauge length.

6.3.8.2.Test methods

Fatigue testes were conducted in Instron model 8500 machine for 12 mm and 16 mm diameter bars, and in the Dartec machine for the bars with larger diameters. Sinusoidal constant axial stress amplitude with $R = 0$ was applied in laboratory air at room temperature with a frequency of 6 Hz. The tests were allowed to run without interruption through to failure. Whenever a specimen survived 5 million cycles that test was termed as a run out and some of these run out specimens were re-tested under a higher stress range.

Some fatigued specimens were tensioned subsequently to yield in order to reveal any small cracks if they developed during fatigue testing.

Crack front marking technique (so-called beach mark) was applied on 16 mm diameter bar by changing the fatigue stress range and stress ratio. This allows one to assess fatigue initiation and propagation after failure took place. Variable amplitudes of 340 MPa and 150 MPa with constant mean were cycled at 1,000 - 1,000 blocks. Test was conducted in Instron dynamic testing machine.

6.3.9. Microscopy

A low power stereomicroscope and Philips 505 scanning electron microscope (SEM) were used for the examination of fracture surfaces.

6.4. FINITE ELEMENT METHOD

Finite element method was used to study stress concentrations arising from bar deformation patterns. Model I simulates an equally spaced transverse lug pattern where each lug is relatively far away from each other, Figure 6-9 (a). This model corresponds to bars marked **b**, **c**, **d** and **e** in Figure 2-2. Model II simulates unequally spaced lugs distributed in such a way that a lug is closer to its neighbour lug on one side but far

away from the one on the other side, Figure 6-9 (b). This model corresponds to the bars marked **a** and **f** in Figure 2-2. The same models were applied in the analysis of identification marks. In the analysis the material was assumed to be elastic and isotropic and loading was through an uniform axi-symmetrical tensile force. Due to symmetry only a quarter of each geometry was modelled and analysed with boundary conditions in such a way that the displacement of nodes along **ad** in axial direction and those along **dc** in radial direction were set to zero.

The mesh of Model I, consisting of 2150 8-node biquardratic (CPE8) elements, is shown in Figure 6-10 (a). Elements along the circumferential direction of the lug root is fixed to be 10 and thus the smaller is the lug root size the higher is the element density around the corner. Mesh of Model II is basically a copy of Model I, Figure 6-10 (b). The calculation was performed employing the ABAQUS 5.5 - commercial program. The largest principal stresses at the surface and layers below the surface were calculated with a sequence incremental of l_0, l_0, l_0/β, l_0/β, l_0/β^2, l_0/β^2, $\cdots$, where $l_0 = 0.002916h$, $\beta = 0.8$ and 0.7 for $r \leq 0.3h$ and $r \geq 0.4h$, respectively.

Appendix 6-1. Sample preparation for deformation profile measurement

Samples were cut to 150 mm length with an identification mark included and the thin layer of mill scale is removed by:

- dipping in a 35% solution of hydrochloric acid for 20 to 30 minutes;
- putting the sample in a neutraliser solution of 5% calcium hydroxide($CaCO_3$);
- rinse sample in water;
- dry the sample with a piece of cloth and then in a hot air; and
- store in a jar to keep it dry.

The treated bars are greyish colour and the rolling defects are visible but no sign of pitting or change in of the geometry are witnessed.

Appendix 6-2. Preparation of specimens for fatigue tests

- The lugs at the cast end and immediately next to the gage length is partially removed by grinding, and sand blast and polish using steel-wire wheel are applied to this part;
- Set up jig and make alignment;
- Pour the 280-290°C Babbit alloy into the sleeve and full fill the sleeve in three pouring;
- Weld washers on the ends;
- Polish the bar immediately next to the cast alloy.

Table 6-1. Chemical composition of the bars

Bar size (mm)	*12*	*16*	*20*	*24*	*28*	*32*	*36*
Heat No.	708179	707114	707904	706965	703672	26189	36819
C	.1500	.1600	.1700	.2000	.1300	.1800	.1700
P	.0080	.0140	.0110	.0120	.0120	.0130	.0160
Mn	.1750	.5600	.5800	.5900	.5500	.7700	.7600
Si	.0260	.1840	.1600	.1670	.1630	.0040	.0080
S	.0700	.0280	.0240	.0200	.0230	.0110	.0130
Ni	.6000	.1000	.0600	.0600	.0800	.0100	.0200
Cr	.0700	.0700	.0800	.0800	.1000	.0200	.0200
Mo	.0100	.0200	.0200	.0100	.0200	.0100	.0100
Cu	.1800	.2200	.1600	.1500	.2400	.0200	.0200
Al	.0030	.0030	.0030	.0030	.0030	.0070	.0050
N	.0090	.0060	.0080	.0080	.0080	.0020	.0030
Nb	.0010	.0010	.0010	.0010	.0010		
Sn	.0160	.0140	.0100	.0100	.0190		
Ti	.0010	.0010	.0010	.0010	.0010		
V	.0060	.0040	.0060	.0040	.0030		
CE	0.284	0.293	0.303	0.331	0.268	0.316	0.305

Chemical analysis as provided by the manufacturers.

$CE = C + Mn / 6 + (Cr + Mo + V) / 5 + (Ni + Cu) / 15$

Bars with 12 - 24 mm diameter were produced in Sydney, the others in Newcastle.

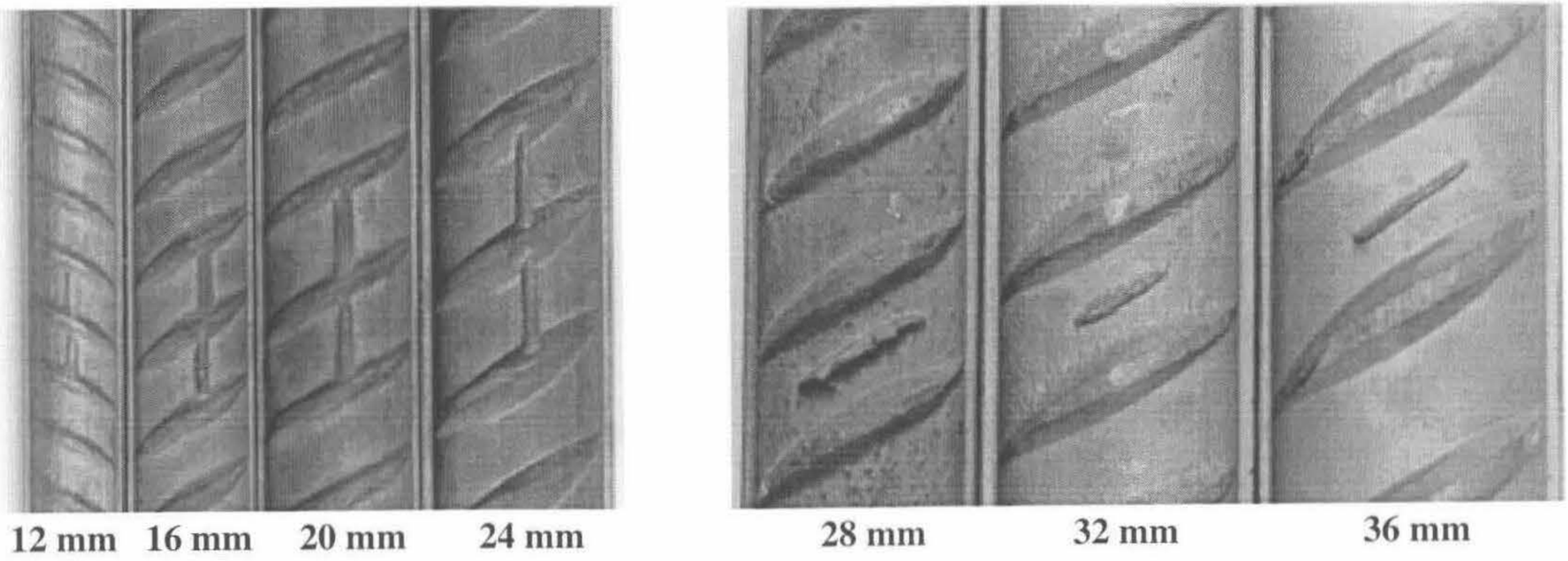

Figure 6-1. Tested TEMPCORE reinforcing steel bar profiles

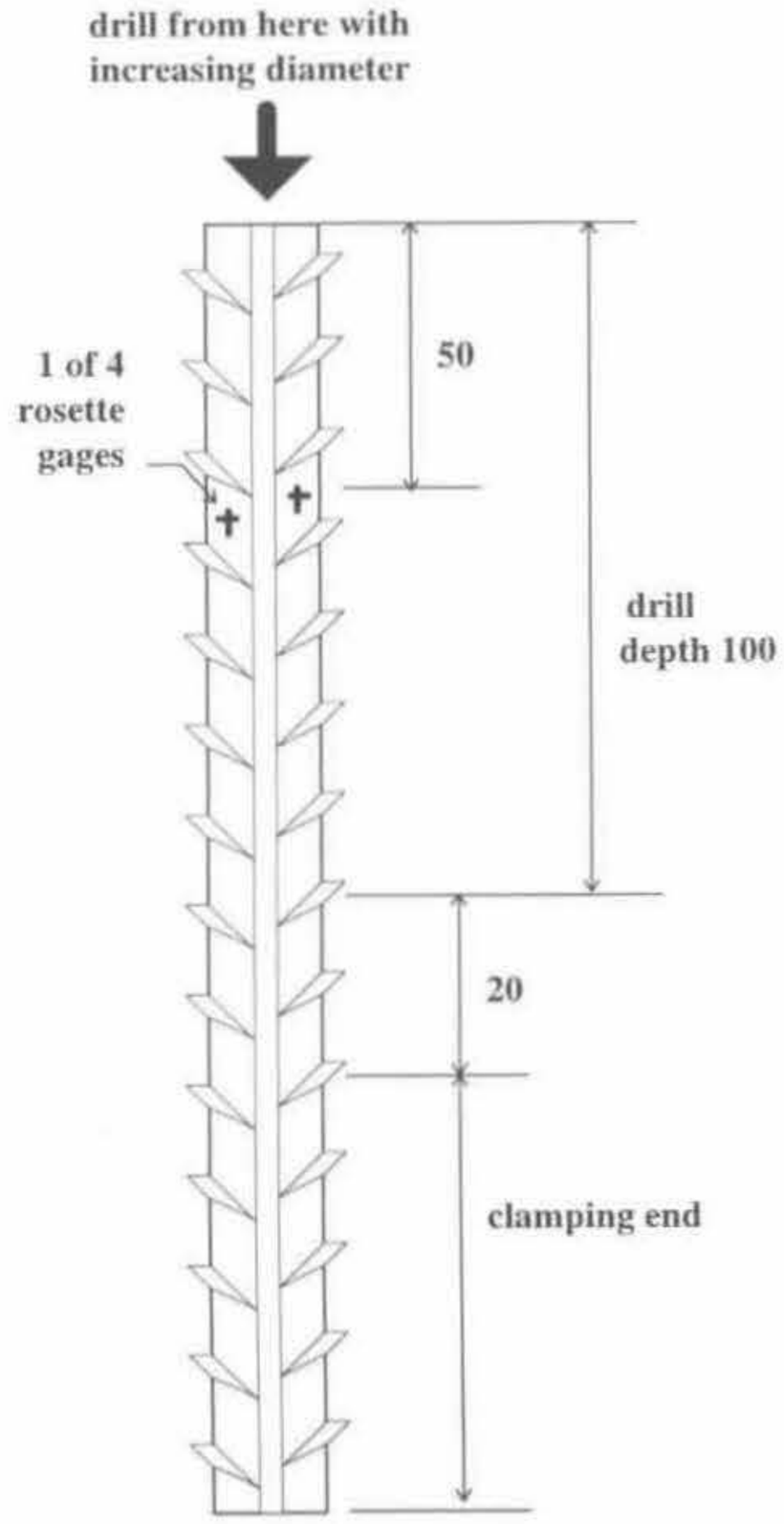

(a) Schematic illustration of the specimen

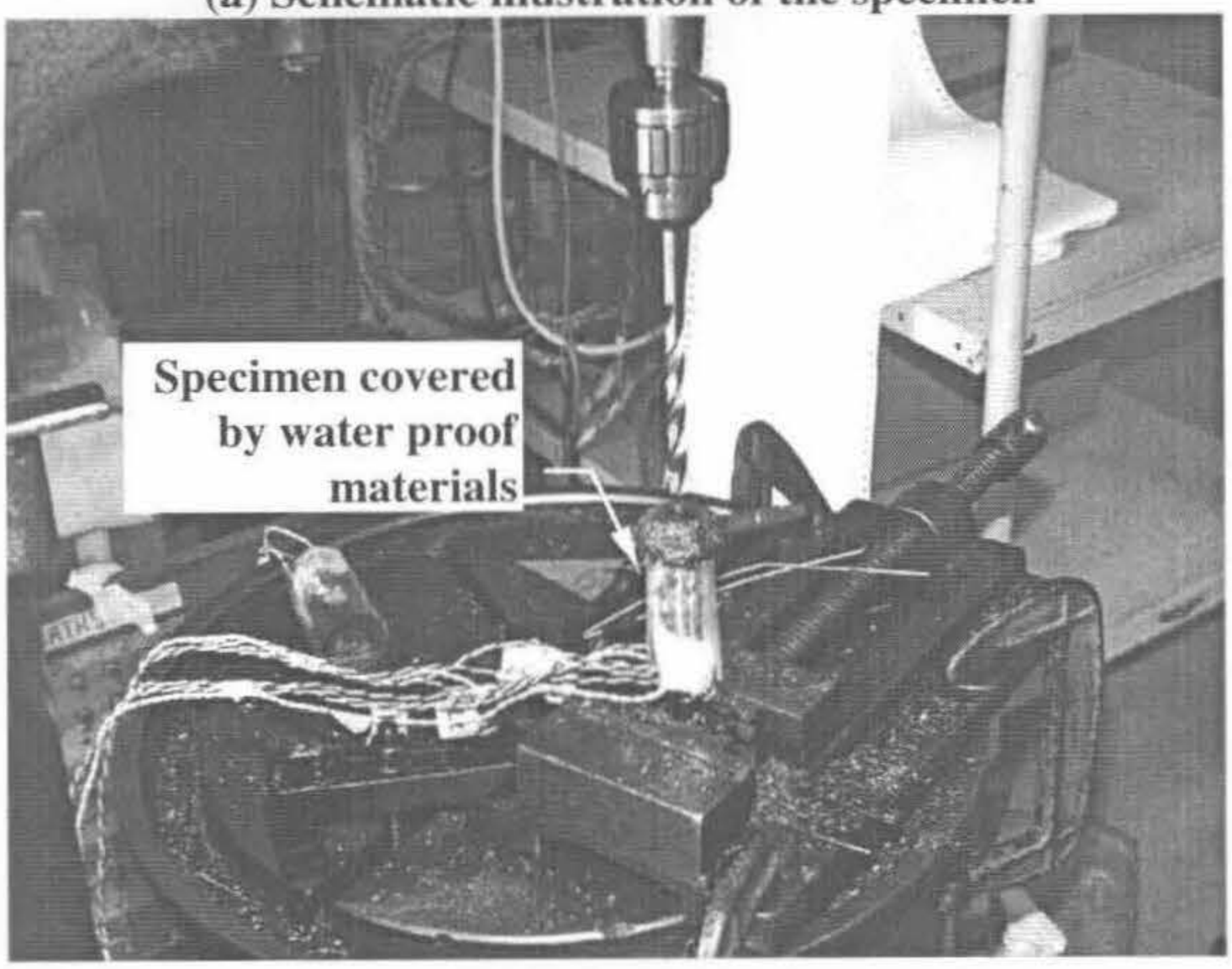

(b) Set-up for residual stresses measurement

Figure 6-2. Residual stress determination

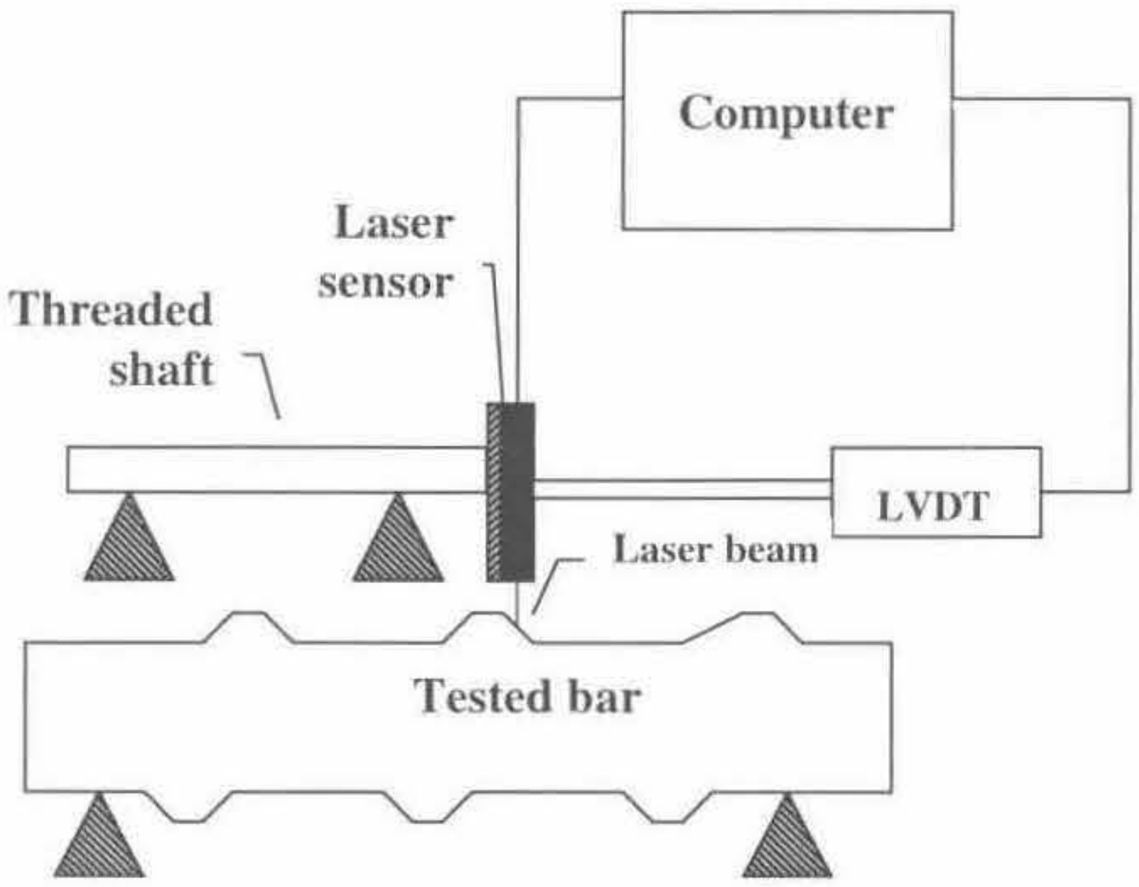

(a) Schematic illustration

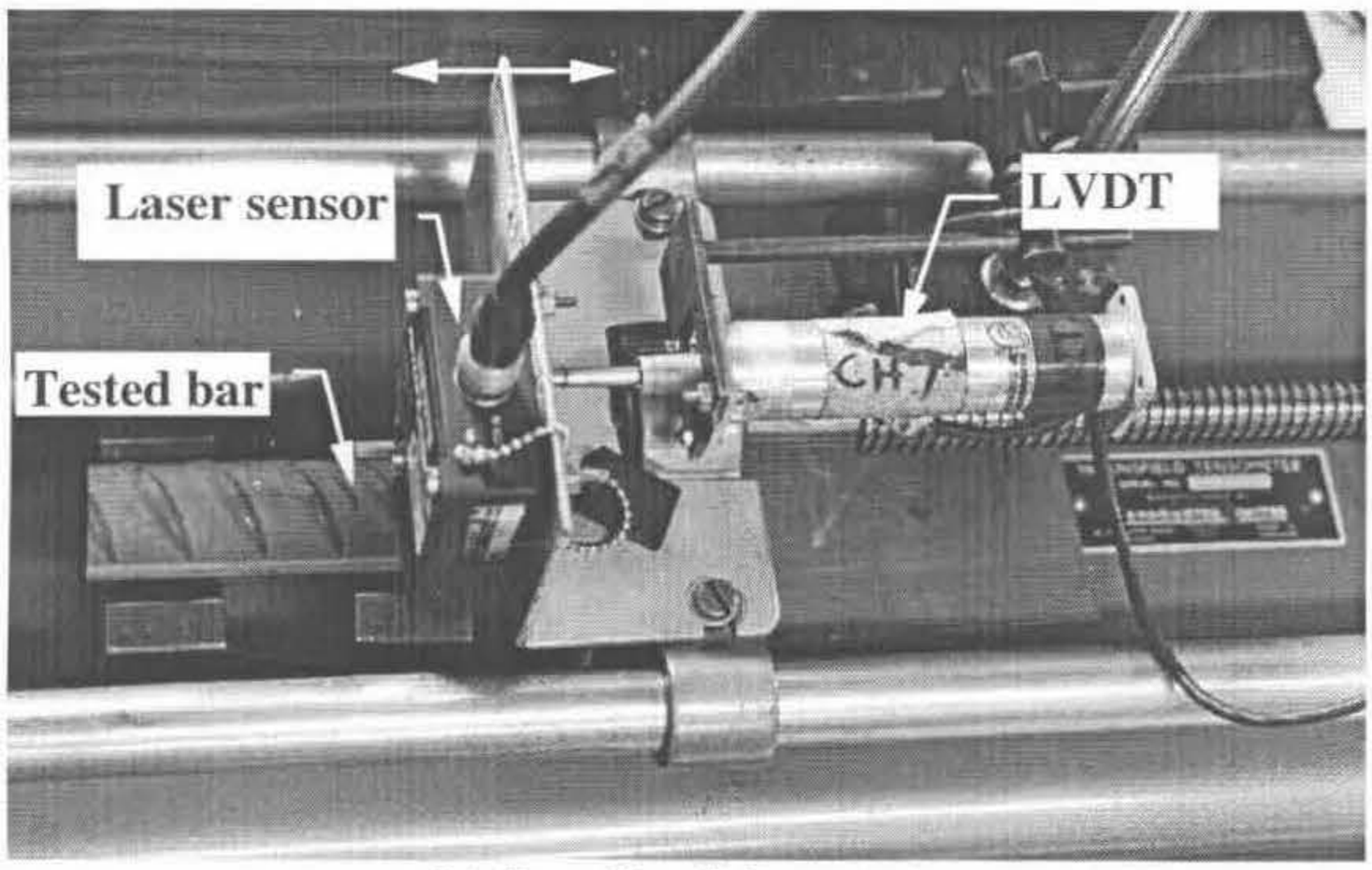

(b) Details of the set-up

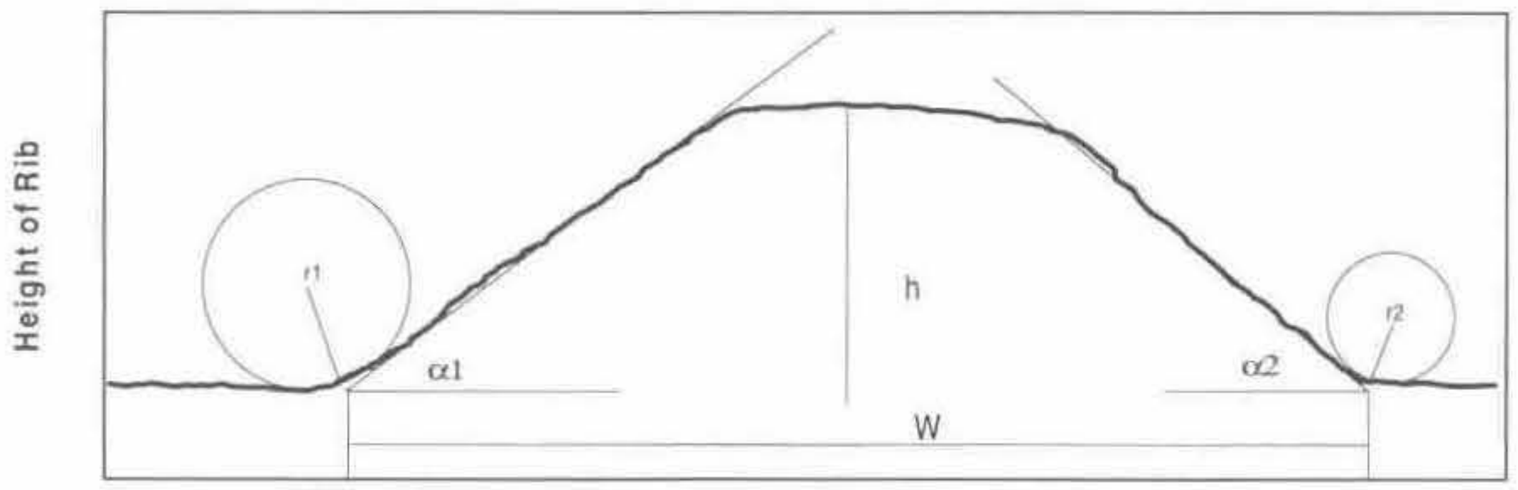

(c) Lug profile measurement

Figure 6-3. Test arrangement for the analysis of deformation profile

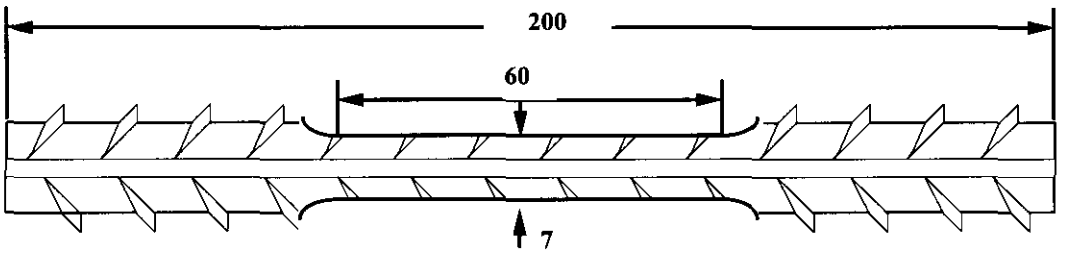

Figure 6-4. Side-cut specimen

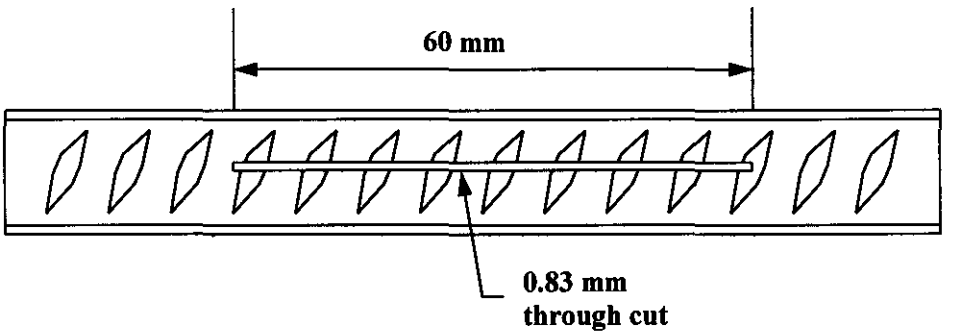

Figure 6-5. Centre-through-cut specimen

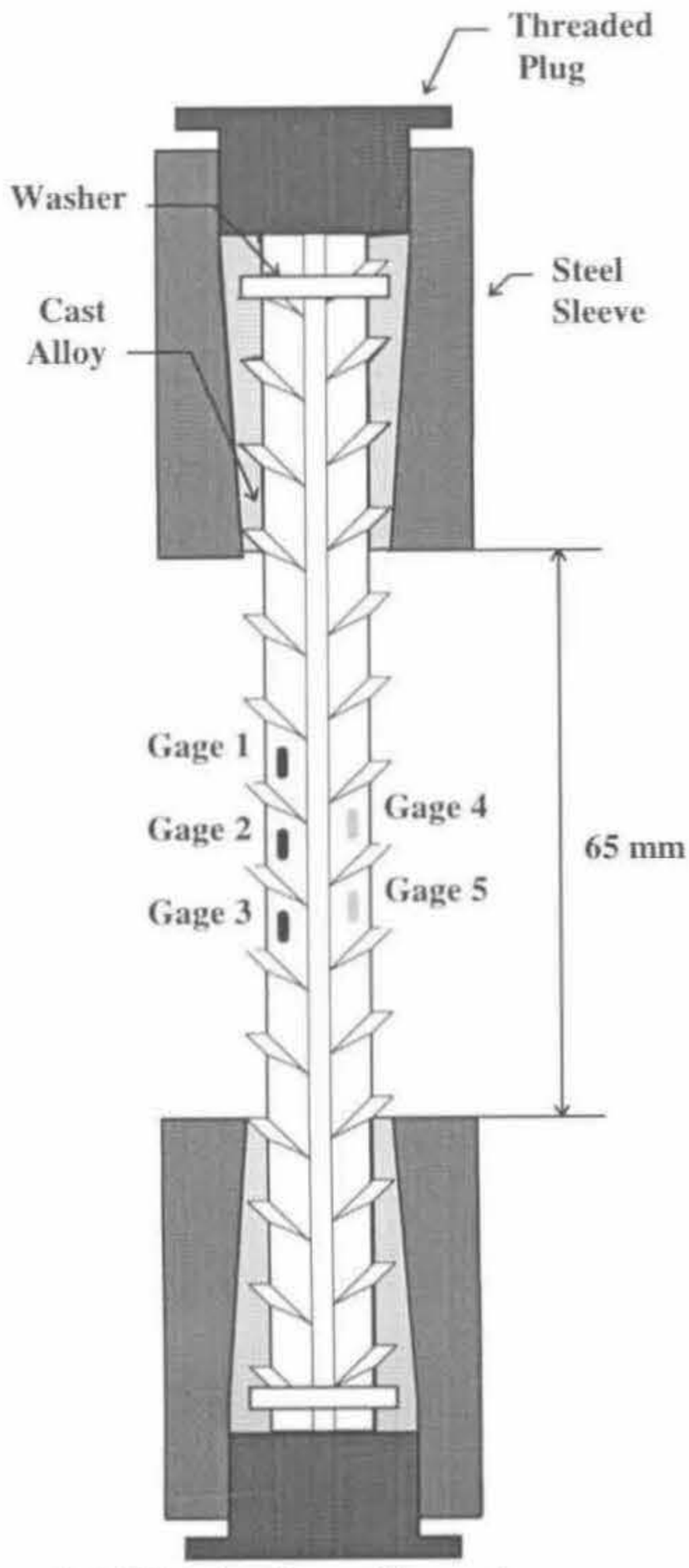

(a) Illustration of specimen

(b) Test machine and set-up

Figure 6-6. Fully reversed cyclic loading in Instron model 8500 hydraulic dynamic testing system

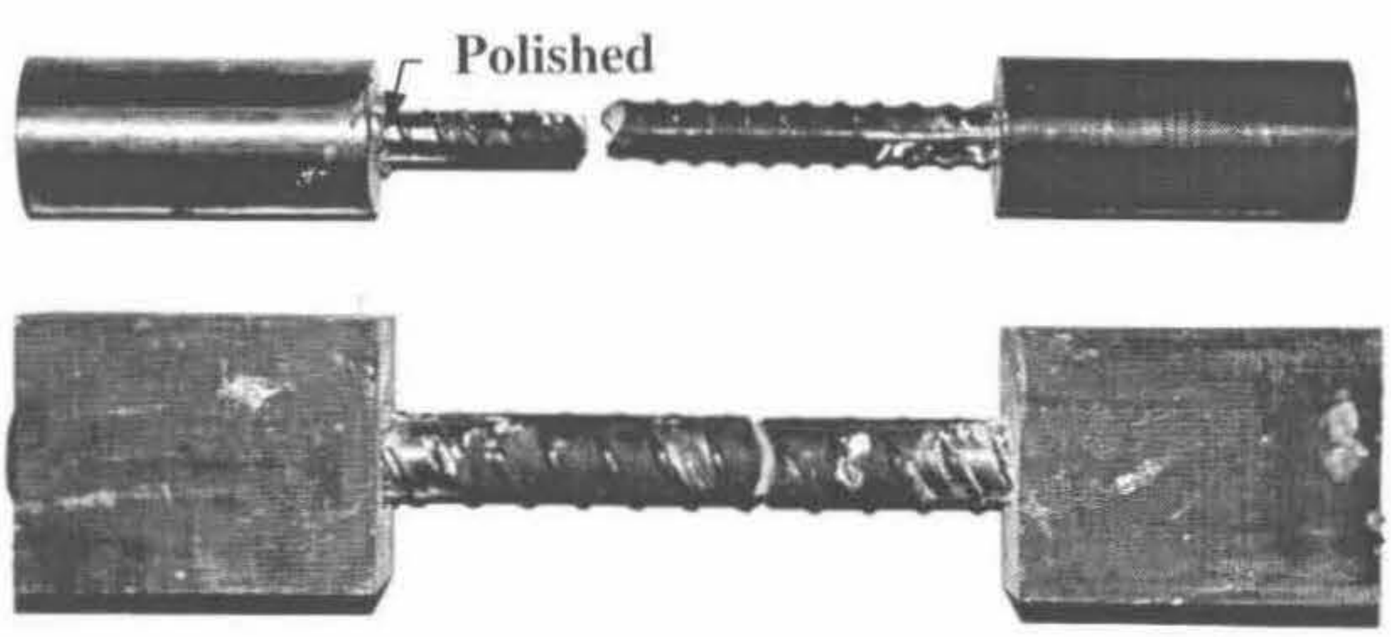

Figure 6-7. Typical fatigue specimens and fracture positions

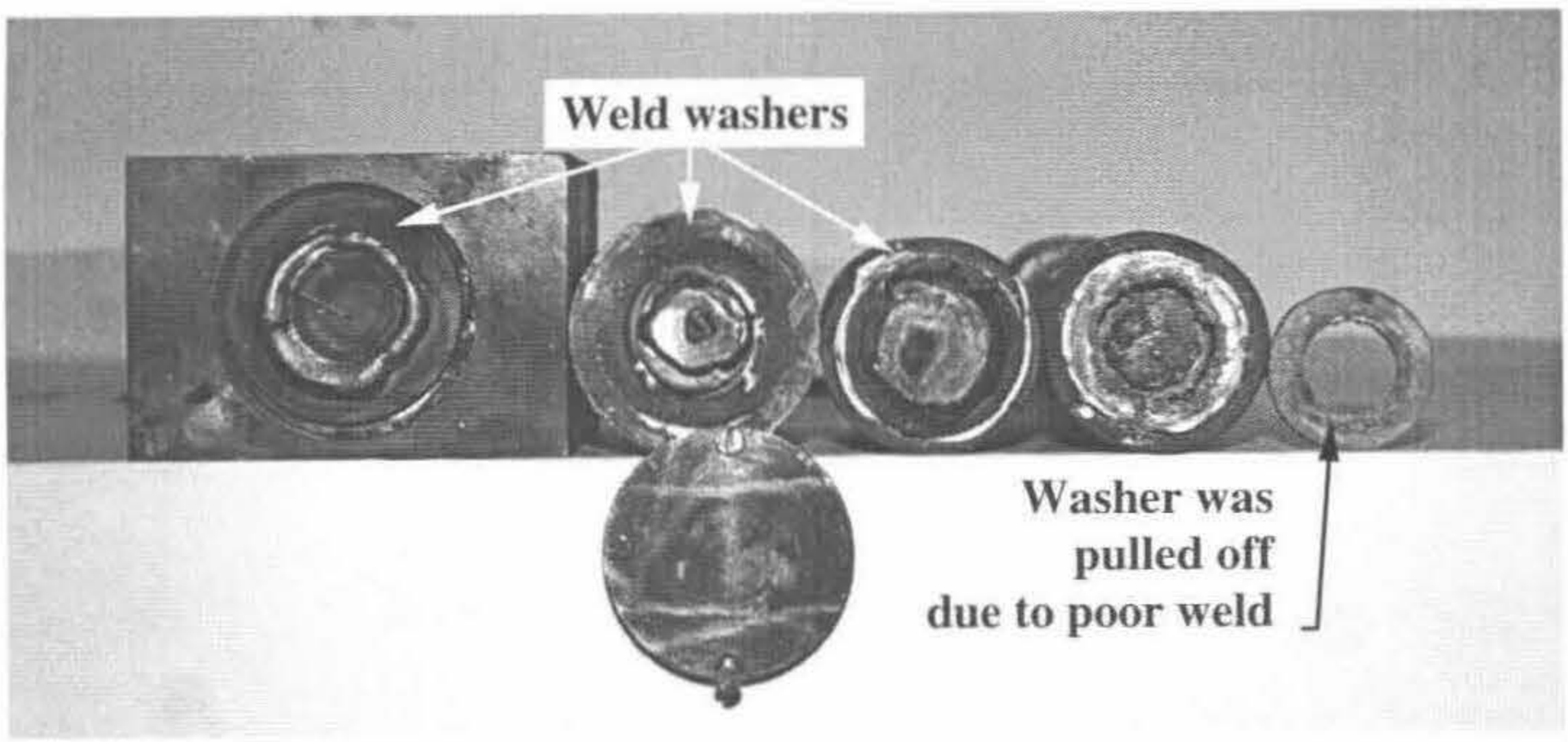

Figure 6-8. Washers used at the cast ends

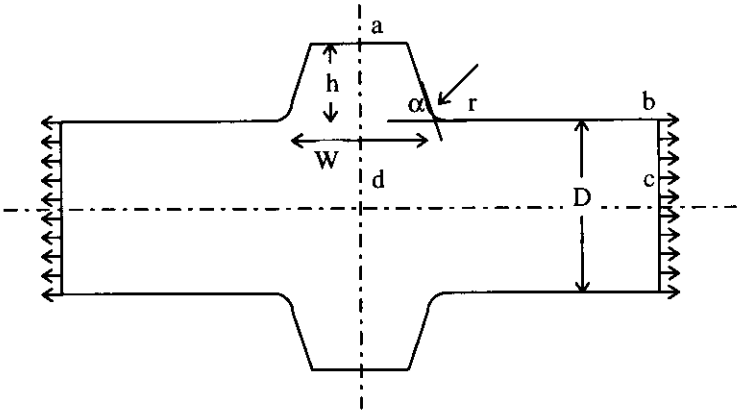

(a) Model I - for long distance spaced transverse lugs

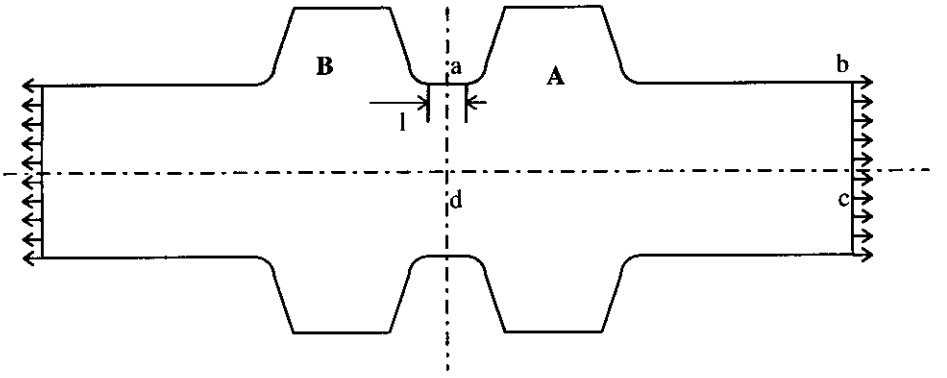

(b) Model II - for unevenly spaced lugs

Figure 6-9. Models used to simulate the geometry of transverse lugs

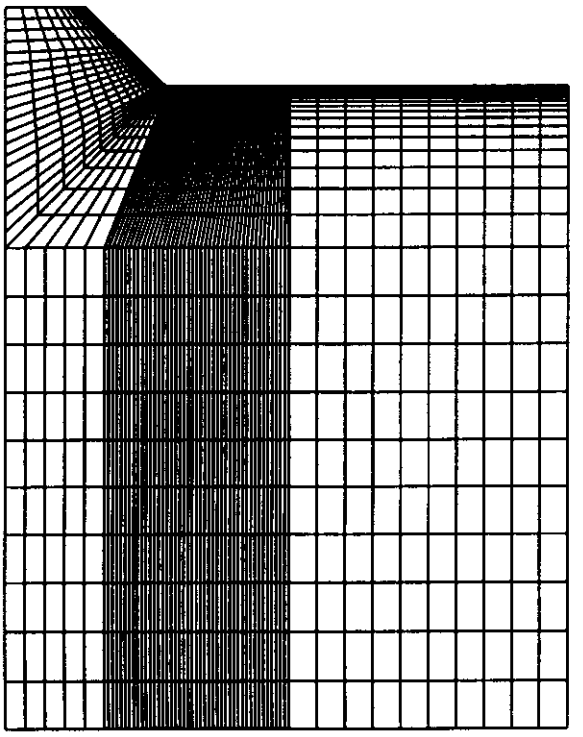

(a) Mesh for Model I

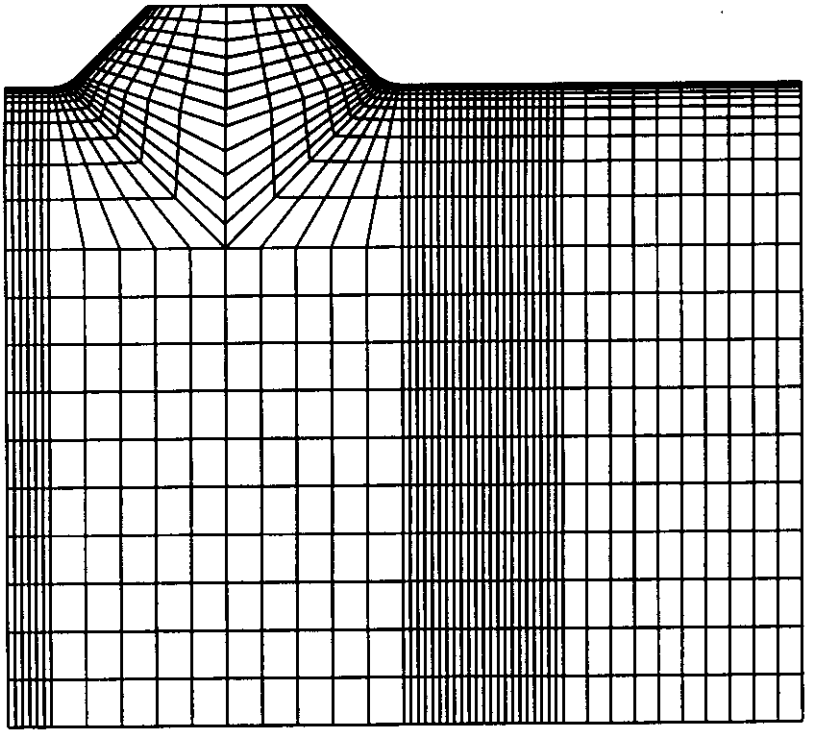

(b) Mesh for Model II

Figure 6-10. Meshes for finite element analysis

Chapter 7

EXPERIMENTAL AND ANALYTICAL RESULTS

7.1. INTRODUCTION

Experimental work was conducted on reinforcing bars with various diameters relating to the metallurgical and physical characteristics, the behaviour in static and cyclic loading, and finally to fatigue properties, while analytical work was carried out on the stress concentrations associated with the surface deformation patterns of the bars.

Investigations on the micro and macro structures, hardness distributions, residual stresses and geometry of deformations were needed to provide basic information for the understanding of mechanical properties of TEMPCORE reinforcing steels.

Further investigations on tensile and cyclic behaviour were designed to provide engineering properties for the TEMPCORE reinforcing steels, as well as to reveal the strengthening mechanism involved in this type of steels. Experimental work was concentrated on the static and fatigue behaviour. It was found that the stress strain response of the bars is very much microstructure dependent, especially the yield behaviour. For this reason the core and case portion of the bars with fine and coarse microstructure were investigated.

Fatigue tests proved that TEMPCORE reinforcing steels have superior fatigue properties when the test data is compared with those of conventional reinforcing bars, and this is due partially to the special microstructures and partially to residual stresses developed in the TEMPCORE process.

Analysis of the stress concentrations arising at surface pattern deformations showed that the stress concentration factor (SCF) strongly depends on the root radius and the spacing of the deformations, and have significant influence on the fatigue performance.

7.2. CHARACTERISTICS OF THE TESTED BARS

7.2.1. Macrostructure

In macro scale the bars exhibit an essentially concentric hardened layer, intermediate hardened layer and unhardened core area as shown in Figure 7-1 and as detailed in Table 7-1.

Although the depth of the hardened layer increases from 0.8 mm to 2.2 mm as the bar size increases from 12 mm to 36 mm this does not change significantly the area percentage, except for the case of 12 mm diameter bar which has the least hardened layer. The depth of intermediate hardened layer, however, increases from 0.3 mm to 4.8 mm, leading to an area percentage change from 19% to 38%. As a consequence the unhardened core area shrinks from 57% to 32% as the diameter increases. Thus immediately at least two conclusions may be drawn: there are difficulties in process control and the correlation between fatigue performance and bar diameter is difficult.

7.2.2. Microstructures

Two distinctive microstructures were identified in terms of ferrite morphology and grain size in the core areas, i.e., fine ferrite and coarse Widmanstätten ferrite, respectively. Bars with 12, 16, 20, 24 and 28 mm diameters belong to the fine ferrite type, while the 32 and 36 mm diameter bars fall into the coarse Widmanstätten

ferrite type. Herein after reference will be simply made to bars with fine microstructure and bars with coarse microstructure.

7.2.2.1. Bars with fine microstructure

Typical fine microstructures are shown in Figure 7-2. In the hardened layer, tempered martensite in the form of packets of thin plates retaining martensitic morphology is observed. The boundaries between tempered martensite packets in different orientations are quite distinct. The hardened layer ends at the point where the last tempered martensite disappears.

In the intermediate hardened layer the microstructure consists a mixture of bainite and polygonal ferrite. The volume of bainite decreases at the expense of ferrite moving towards the centre of the core area. The intermediate hardened layer ends when the first pearlite appears and the bainite vanishes. A further notable feature of the microstructure in the intermediate hardened layer is that the grain size of the polygonal ferrite increases all the way towards the core.

The microstructure in the core area consists of fine polygonal ferrite and pearlite. The ferrite grain size is essentially the same for all the bars of this type with an approximately ASTM micro-grain size number of 10.5 (nominal diameter 9.4 microns). The grain size of pearlite colonies is about one number higher than that of the ferrite grains that is of the order of 6.7 microns.

7.2.2.2. Bars with coarse microstructure

Typical microstructures of this type of bars are shown in Figure 7-3. The microstructure in the hardened layer is basically the same as those in the bars with fine microstructure but the size of the tempered martensite packets is much larger. In addition, some polygonal ferrite is observed at a certain depth of the hardened layer.

The microstructure of the intermediate hardened layer starts with a mixture of large bainite and ferrite grains. As it approaches the core area the microstructure evolves to a mixture of bainite and coarse conglomerate of pseudo-eutectoid and ferrite.

The microstructure in the core area is made up from coarse pseudo-eutectoid colonies surrounded by coarse Widmanstätten ferrite. The size of the Widmanstätten ferrite grain is 45 microns (ASTM micro-grain size number 6.0).

7.2.2.3. Microstructures at the bar surfaces

All the bar surfaces are similar and hardly any unhardened or oxide microstructure is observed as shown by Figure 7-4 representing typical microstructures at the lug roots for both bars with fine and coarse microstructures. Note the microstructures in the middle of the hardened layers: the tempered martensite packets at the surface are finer.

7.2.3. Hardness distributions

Hardness as a function of normalised radius from surface to the centre, i.e., the ratio of distance from the centre to the radius, is plotted in Figure 7-5. A hardness variation, higher on the way from the core to the surface reflects the microstructure variation.

The hardness of the hardened layer of bars with different diameters varies from HV 225 to HV 265 (also see Table 7-1). The thicker bars with fine microstructure exhibit higher surface hardness. The 32 and 36 mm diameter bars with coarse microstructure contain ferrite grains in the hardened layer at a certain depth resulting fall in hardness.

Hardness in the core area between HV 148 to HV 156 does not vary much with bar size. The hardness gradient in the intermediate hardened layer however significantly varies and it is in line with the thickness of the intermediate hardened layer which increases as the bar size increases.

7.2.4. Residual stresses

Residual stress measurement was obtained on the 16, 24, and 32 mm diameter bars. With similar results and typical distributions are presented in Figure 7-6 for the 24 mm diameter bar. The case material is under compressive stresses in both longitudinal and circumferential directions and reach peak values in the order of 90

MPa. Tensile residual stresses with much lower magnitudes, are concentrated in the intermediate hardened layer.

During the residual stress measurement some discrepancies in readings were observed, and this can be associated with the transverse lugs which may have some influence although minor, on the symmetry of the residual stress distributions. The measured axial and circumferential residual stresses generally balance themselves and radial stresses do vanish at the surface.

7.2.5. Geometry of the deformations

The deformation patterns and rolling mill identification marks of the bars, as shown in Figure 6-1, have been analysed and the profiles of the representative lugs and the identification marks are plotted in Figure 7-7 and Figure 7-8. In the figures arrows indicate critical sites for potential fatigue initiation. All the measured geometry parameters are presented in Table 7-2.

The data show clearly that the lug roots of the 24, 32 and 36 mm diameter bars are sharper than those of the rest of the bars. Taking the 24 mm diameter bar for example, the *r/h* ratio is 0.15 and the highest flank angles is 46.7° on the steeper side of the lug. The *r/h* ratio of the 16 mm bar, however, is as large as 1.08 and thus another problem arises besides the metallurgical variations in presenting a single correlation between bar size and fatigue performance.

The identification marks of the bars manufactured by Newcastle mill are parallel to the transverse lugs and merge to the bar base sharply. The size of identification marks of 32 and 36 mm diameter bars are very small compared to their transverse lugs. The size of identification mark of the 28 mm diameter bars is comparable to its transverse lugs, being 88% as high as the lugs. The *r/h* ratio on the deeper side of those high identification marks is nearly zero with a flank angle of 90°. The identification marks on bars manufactured in Sydney are parallel to the bar axis and merge into the transverse lugs. However an incomplete merging of the mark and transverse lug is found on the 16 mm diameter bar, Figure 7-8, which has a gap between mark and lug with a radius comparable to the lug root. The effect of these

identification marks on the fatigue behaviour will be discussed in the relevant section.

7.3. STATIC AND CYCLIC LOADING RESULTS

7.3.1. Tensile results

Stress strain curves of the tested bars in static tension are shown in Figure 7-9 to Figure 7-15 and the mechanical properties are listed in Table 7-3. Generally all the tested bars exhibit high yield strength (> 410 MPa), high ratio of yield to tensile strength (around 0.80), large uniform elongation (15% to 26%), large total elongation (22% to 32%) and generally flat yield plateau.

It was found that the performances of the five smaller size bars are distinctively different in yield behaviour when compared with the two bigger bars. Smaller size bars exhibit marked yield point and Lüders style yielding in a similar way to mild steel but without yield drop, regardless of strain rate. Lüders yield is illustrated in Figure 7-16 for a 16 mm diameter bar and these five bars generally exhibit large Lüders strain, 2.0% to 3.2%, with the value decreasing as the bar size increases.

In contrast, the two larger size bars exhibited a departure from elasticity before macro yielding took place. The amount microyielding was as large as 600 and 1000 microstrain (10^{-6}) for the 32 and 36 mm diameter bars, respectively. This phenomenon is similar to the preyield or microyield observed in other metals as reviewed in Chapter 4. Although preyield was followed by Lüders yield, it is not as distinctive as has been observed on the other smaller bars. Additionally, the Lüders strain is much smaller, Figure 7-17, only 0.4% and 0.32% for 32 and 36 mm diameter bars, respectively.

The different performances in tension however do not relate to the bar size but to the microstructure. This point was proved on a 36 mm diameter bar, 36F, possessing fine microstructure. These results are presented in Figure 7-18 and Table 7-4 indicating

no preyield, large Lüders strain (1.5%) and large elongation (30%) similar to those observed on the other five small size bars with fine microstructure.

The preyield of the 36 mm diameter bar starts from around 310 MPa and as a result, the $\sigma_{0.2}$ proof stress equals $\sigma_{0.1}$ and these are larger than $\sigma_{0.05}$ or $\sigma_{0.01}$. The bar with fine microstructure, 36F, the two values for $\sigma_{0.01}$ and $\sigma_{0.2}$ coincide, Table 7-4.

7.3.2. Zero to tension and zero to compression cycling prior to tensile testing

The nature of microyielding was studied by cycling below the yield strength. In zero to tension cyclic loading, the performances of the bars with fine and coarse microstructure are different. Figure 7-19 and Figure 7-20 show typical stress-strain curves for the 24 and 36 mm diameter bars representing bars with fine and coarse microstructure, respectively. Each loading cycle is illustrated separately and the final tensile response is plotted on the left hand side of the diagrams. Fine microstructure bars showed essentially elastic responded when cycled at stresses below the yield strength value, while bars with coarse microstructure responded with an open mechanical hysteresis.

In the first cycle to 400 MPa, the 36 mm diameter bar preyielded to the value of 400 x 10^{-6} and this microstrain response has reduced to only 33 x 10^{-6} plastic deformation in the second cycle to the same stress level. Increasing the applied stress in the subsequent cycle to 420 MPa plastic strain of 267 x 10^{-6} developed between 400 and 420 MPa. During the subsequent tensile test the bar preyielded to the order of 250 x 10^{-6} before macroyielding. The accumulated preyield strain was about equal to the microplastic response in a simple static tension which is of the value of 1000 x 10^{-6}.

In zero to compression cyclic loading, the performances of bars with fine and coarse microstructure were similar to those observed in the zero to tension cyclic loading tests, Figure 7-21 and Figure 7-22. The 24 mm diameter bar responded elastically, while the 36 mm diameter bar started showing an open mechanical hysteresis at 310 MPa.

7.3.3. Fully reversed cyclic loading

In fully reversed cyclic loading at stress amplitude of 85% to 90% of yield strength, all bars showed gradually expanding hysteresis, i.e., the bars exhibited cyclic softening at the "elastic range". But once again, the bars with fine and coarse microstructure behaved differently. Bars with fine microstructure showed a very slow expansion of plasticity in the first 200 cycles, Figure 7-23, followed by gradual expansion over some hundred cycles and eventually large scale yield took place. In contrast, bars with coarse microstructure showed large plasticity in the very first cycle and the hysteresis expanded much quicker, leading to large scale yielding after tens of cycles, Figure 7-24 and Figure 7-25.

To explore the cyclic response of the bars with fine microstructure, a 16 mm diameter bar with 5 strain gages along the bar axis was tested at $\pm$ 300 MPa (70% of yield strength) up to 1500 cycles followed by $\pm$ 370 MPa (83% of yield strength) cycling up to failure. In the first cycle sequence, no microplastic response was observed, Figure 7-26. However, cycling at $\pm$ 370 MPa, cyclic softening was observed as shown in Figure 7-27. In the first 1000 cycles plastic deformation reached only 500×10^{-6} strain level with an uniform distribution along the bar axis but the strain amplitude increased linearly reaching 1.5×10^{-6} per cycle at the 1000^{th} cycle. During the following 250 cycles, the softening rates in different parts of the bar were no longer uniform, gages 1, 3 and 5 indicating fast softening rates and plastic deformation soon reached macro scale. At gages 2 and 4 macroyield took place 100 cycles later.

7.3.4. Mechanical properties of the case and the core materials

Only the 16 and 36 mm diameter bars were selected for investigation but this way the fine and coarse microstructures were represented.

Test results are listed in Table 7-5, and the stress strain curves of the materials are shown in Figure 7-28. The case materials yield continuously and exhibit higher yield strengths than the corresponding strengths of the core materials. Differences also exist between the 36 and 16 mm diameter bars with yield stresses 607 MPa and 495

MPa, respectively. Although the case material has been hardened it is quite ductile, with elongation being larger than 13%.

The core material of both types of bars yield in Lüders style with yield drop. It is seen that the upper yield strength of the core with fine microstructure is approximately 70 MPa higher than that of the core with coarse microstructure. Lüders strain of the former is about four times as much and additionally, fine microstructure core material exhibits larger yield drop.

7.3.5. Properties of side-cut and centre-through-cut specimens

Tensile test results on the 16 mm diameter bar in the cut state are presented in Figure 7-29. Side-cut specimen yield at 380 MPa in Lüders style, while the centre-through-cut specimen started to depart from elasticity from around 380 MPa and yield in Lüders style at 422 MPa with total preyield of approximately 250 x 10^{-6}.

The centre-through-cut specimen exhibited lower yield strength than the as received bars although it possesses 2% more hardened materials than as received bar. On the other hand side-cut specimen, despite of containing 34% hardened and intermediate hardened material, yielded at the upper yield stress of the core material.

7.3.6. Fractography

All the as received bars exhibited large necking with typical cup-and-cone tensile failure, Figure 7-30. Dimples are observed on the fracture surfaces, Figure 7-31, and no differences were observed relating to bars with coarse and fine microstructures.

The core and case materials, from bars with fine or coarse microstructure, also fractured in a cup-and-cone model and the case material showed extensive amount of dimples, Figure 7-32.

7.4. FATIGUE TESTS

7.4.1. Results in the form of S-N curves

Fatigue results in the form of S-N curves are represented in Figure 7-33 and details of the test results are tabulated in Table 7-6 to Table 7-12. Fatigue limits and ratios of fatigue limit to yield strength ($\sigma f/\sigma_y$) and tensile strength ($\sigma f/\sigma_u$) are given in Table 7-13. Fatigue limits for the 16 and 20 mm bars are as high as 310 MPa which equates approximately 60% and 70% of tensile strengths and yield strengths, respectively. The 24, 32 and 36 mm diameter bars have lower fatigue limits: 240 MPa, and the 28 mm diameter bar has the lowest fatigue limit, 230 MPa. Fatigue limit of the 28 mm diameter bar was determined on identification mark free specimens as bars with identification marks showed even lower fatigue limits. The ratios of $\sigma f/\sigma_u$ and $\sigma f/\sigma_y$ are however well above 0.4 and 0.5, respectively.

In the finite-life region, fatigue life in logarithm scale shows a linear relationship with the cyclic stress range and the lines for different diameters are parallel to each other. The best fatigue life was exhibited by the 20 and 16 mm diameter bars being twice as much as achieved by the 24 mm bar when cycled at the same stress range. The worst fatigue life was given by the 28 mm diameter bar with identification marks.

7.4.2. Fatigue fractures

Typical fracture surface topographies are shown in Figure 7-34. Except those of the 16 and 28 mm bars, cracks initiate from transverse lug roots which provide high stress concentrations (Figure 7-34 a and b). In these bars no cracks started from identification marks despite the fact that 70 % of the specimens had such marks. In contrast, in the case of the 16 mm diameter bar 2 out of 4 specimens containing identification marks failed at the gaps of the mark and lug, while the other 2 at transverse lugs. These failure positions however did not affect the fatigue lives significantly as presented in the S-N curve. In the case of 28 mm bars when identification marks were present the cracks initiated there (Figure 7-34 c) while in the absence of identification marks cracks initiated at the transverse lug roots.

Failure at lug root was observed to be either single initiation (Figure 7-34 a) or multiple initiation at the same flank side of the transverse lugs (Figure 7-34 b) depending on the applied stress level and *r/h* ratio of the lug. Higher stress range and lower *r/h* ratio promote multiple initiation. In the case of the 12 mm bar for example, under 320 MPa applied stress range single initiation took place, beyond that stress level multiple initiation was observed. This stress related fatigue initiation position for the 24 mm diameter bar, with the sharpest geometry, $r/h = 0.15$, is as low as 280 MPa. In some rare cases fatigue fracture starts from opposite transverse lugs (Figure 7-34 d).

In every case of fatigue failure, large amount of plastic deformation was observed on the final rupture surface.

Examination under SEM revealed that all the cracks initiated from surface flaws, usually at tiny peaks of surface roughness, Figure 7-35 and Figure 7-40 (d). The early stage propagation, up to 200 mm, is illustrated in Figure 7-35 (arrows indicate propagation direction). Two major regions may be identified. Small crack region, shorter than 150 mm, is reflected in the featureless character and this is followed by large crack region in which noncystalline striations are clearly shown. Detailed examination revealed irregular striation-like fluctuations in small crack region, Figure 7-36. The fractography is similar to stage I propagation observed in martensitic 300-M steel (Ritchie 1986, Figure 11 a) and a short crack of Titanium alloy (Petit et al. 1992), and the fluctuations may be termed as stage I striations as described by Laird (1967) which is the results of plastic blunting process along slip bands. In large crack region fine striations are observed on the tempered martensite laths, Figure 7-37 (a), indicating stage II propagation with a propagation rate of the order of 0.13 mm/cycle. A perspective of the crack propagation illustrated in Figure 7-37 (b) shows that the crack changes direction at the boundaries between martensite packets and it also diverges within the martensite packets. In the unhardened area the fracture surface becomes rougher with large secondary cracks, Figure 7-38, and the propagation rate becomes faster. Next to the terminal failure region large amount of

dimples are observed together with striations indicating that significant plastic deformation preceded the final failure, Figure 7-39.

7.4.3. Fatigue and tensile tests

Tensile testing parts of the specimens which have failed in fatigue revealed small cracks at every lug root as they are shown in Figure 7-40. Single and multiple initiations are indicated clearly by these tests, Figure 7-40 (a) and (b), and after initiation the cracks propagated away from the transverse lug on the bar surface into the body of the bar normal to the bar axis. This suggests that crack initiation is governed by the maximum stress concentrations but propagation is driven by the maximum axial stresses. The 16 mm diameter bar which failed at the lug root showed fatigue cracks at lug root as well as at the gaps of identification marks and transverse lugs, Figure 7-40 (c). This indicates that the lug root and the gap between identification mark and lug are equally suitable for fatigue crack initiation for this bar size.

It is interesting to note that these cracks are small in depth semi-elliptic in shape normal to the loading axis and none of them reaches the intermediate hardened material layer as shown in Figure 7-40 (d).

Small cracks were also observed on a specimen fatigued to 83% of the fatigue life (specimen 28F360-1), while no cracks appeared on the specimens fatigued only to 69% of fatigue life (24F250-3) or on run out specimens.

Unlike ASTM 615 bars in similar tests (Helgason et al. 1976), fatigue did not affect tensile properties, and tensile failure did not necessary start from those small fatigue cracks. Ductile rupture at the front of a small fatigue crack shown in Figure 7-41 is actually at the hardened layer and this clearly indicates the superior ductility of the case material of TEMPCORE reinforcing steel.

7.4.4. Crack growth

In two tests, 16Fb340-1 and 16Fb340-2, beach marks are visible under optical microscope, Figure 7-42. The general feature of the marks are semi-elliptic in shape

and there is no obvious change in curvature of the crack front when the crack propagated in different hardened layers.

Examinations revealed, for these 16 mm bars, that 458,000 cycles developed a 2.2 mm crack, at that stage of cycling 95.5% of the total fatigue life has been exhausted. These results together with the observations made on fatigued and subsequently tensile tested bars it may be concluded that the fatigue life and fatigue limit of TEMPCORE reinforcing steels are essentially dominated by the characteristics of the outside hardened layer only.

The crack lengths versus cyclic numbers is given in Figure 7-43 (a) showing essentially a similar growth rate at points A, B and C as indicated in the Figure 7-43 (c). The stress intensity factor ranges are calculated according to the model proposed by Astiz (1986) and propagation rates are plotted against this values in Figure 7-43 (b), indicating the propagation may be described by Paris law for cracks longer than 2.2 mm.

Unfortunately, surface marks in the vicinity of crack initiations were not resolved by optical microscope or SEM, thus it was not possible to measure the initial crack propagation rates.

7.4.5. Fatigue of stress relieved bars

Figure 7-44 shows fatigue test results of stress relived bars when the minimum applied stress was zero. Stress relieving caused a fatigue life reduction of 49% and 38% at stress ranges of 280 MPa and 320 MPa, respectively, but it caused only 10 MPa reduction in fatigue limit. Approximately the same results were obtained with the as received bars when cycled at the same stress amplitude but with the minimum applied stress set to +80 MPa.

7.4.6. Comparisons with other high strength reinforcing steels

In Table 7-13 the fatigue strength of the tested bars, together with the ratios of fatigue limit to yield and tensile strengths, are compared with data obtained from

other high strength reinforcing steels and it is clear that the fatigue strength of TEMPCORE reinforcing steel is significantly better.

Another interesting comparison is made in Figure 7-45 in which typical S-N curve of Grade 60 North American high strength reinforcing steel obtained by Helgason et al. (1976) is superimposed onto the present results. Comparisons show that although the slope of the S-N curves are parallel the present results show higher fatigue limits with much higher fatigue lives generally.

Comparing the present test results with the prediction based on the equations proposed by Helgason et al. (1976), as reviewed in Chapter 5, the data in Table 7-13 and Figure 7-46 indicates a significant discrepancy.

7.5. STRESS CONCENTRATION ARISING FROM DEFORMATIONS

7.5.1. **Model I** (evenly spaced transverse lug pattern)

7.5.1.1.Stress distributions

Totally 135 cases with different geometry parameters were studied and the results of maximum stress concentration factors (SCFs) at the surface and at the point *0.013h* below surface are given in Table 7-14 and Table 7-15, respectively. Typical stress concentrations along the bar axis at different depths below the surface are presented in Figure 7-47. It is quite clear that stress concentrations are limited in a very small area and volume in the vicinity of the lug root and the maximum stress is at the lug root junction with the base material. On the surface and along the longitudinal direction the SCF drops to 50% of the peak value at a distance of *0.01h* from the lug root, and it becomes negligible at *0.5h* from the lug root. Beyond a distance of *2.5h* there is essentially no stress concentration. The lug itself does not carry large stress and at the top surface of the lug there is no stress at all.

Along the radial direction the stress concentration gradient is rather large and increases as the *r/h* ratio decreases. It is shown in Figure 7-47 that *0.013h* bellow the surface the SCF drops 6.6% and 24.7% for *r/h* ratios of 0.5 and 0.1, respectively.

7.5.1.2.Effect of bar size

Calculations show that when *D/h* varies in the practical range of 8 to 16 the change of SCF is less than 2%. Thus it can be concluded that the stress concentration is independent from bar size at least within the investigated range. This is in agreement with the result obtained by Jhamb and Mac Gregor (1974b).

7.5.1.3.Effects of lug radius

The great influencing effect of the *r/h* ratio on the magnitude of the SCF, is shown in Figure 7-48. Regression analysis (Appendix 7-1) shows that a polynomial function of an order of 6 is more appropriate to describe such relationship than the logarithmic function presented by Jhamb and Mac Gregor (1974b). Some of the differences between the present results and those reported by Jhamb may be attributed to the analysis of the latter where the average SCF values were taken at *0.026h* below surface. It is believed that the SCF at the surface is more important than the average value at a certain depth in fatigue related problems since cracks develop from the plastic deformation of crystals at the very surface.

7.5.1.4.Effect of lug width and flank angle

Generally, the SCF increases as the lug width and flank angle increase, but these influences are much smaller than that of the *r/h* ratio as shown in Figure 7-49. The data in Table 7-14 indicate that the change in the value of *w/h* by 0.5 leads to no more than 5.3% change in SCF, while the change in flank angle α by 15 degree results in 3.5% change in SCF at the most. In addition, these effects decrease as *r/h* increases and the effects of flank angle become negligible when $r/h > 0.5$.

7.5.2. Model II (unevenly spaced transverse lug pattern)

This analysis shows that as the distance between the two neighbouring lugs diminishes the SCF increases at the inner side of the lugs, Figure 7-50. This increase

in the value of SCF reaches a maximum of 2.65 when the two lugs merge. On the outside of the lug, the maximum increase in the SCF values is only 2%.

7.5.3. Analytical results on the tested bars

The calculated SCFs for the sharpest geometry parameters for seven TEMPCORE reinforcing bars and their measured fatigue limits are listed in Table 7-16, indicating a general trend that the fatigue limit decreases with increasing SCFs.

7.6. SUMARRIES

7.6.1. Features of tested bars

1. TEMPCORE reinforcing steel bars are essentially a concentric composite of a hardened layer, intermediate hardened layer and core material. The percentage of the hardened cross-section varies little, being 30-32% except for the 12 mm bar where this value is only 24%. The intermediate hardened area increases from 19% to 38% as the bar size increases from 12 to 36 mm and thus the percentage of the core area decreases from 57% to 32%.
2. Fine microstructures were detected in the core of the 12-16- 20-24 and 28 mm diameter bars with an average grain size of 9.4 microns and HV 150 hardness. The microstructures in the hardened layer is fine tempered martensite with hardness values of HV225 to HV265.
3. The 32 and 36 mm diameter bars are characterised by coarse microstructure in the core with coarse Widmanstätten ferrite + pearlite with ferrite grain size of 45 microns and HV150 hardness value. The microstructure in the hardened layers is tempered martensite with large packet size. The hardness in these layers is HV232 and HV255 for the two sizes, respectively.
4. There is no unhardened microstructure observed on the bar surfaces.
5. Compressive residual stresses of the order of 90 MPa exist on the surfaces of the tested bars.
6. The geometry of the transverse lugs of 24, 32 and 36 mm diameter bars are sharper than those of the other bars. The identification marks of the 28 mm diameter bar are large and sharply merge into the bar base producing large SCFs.

The identification marks of the 16 mm diameter bar incompletely merge into the transverse lugs producing also high SCFs.

7.6.2. Behaviour under static and cyclic loading

1. In tension tests all the bars exhibit high yield strength (> 410 MPa), high yield to tensile strength ratios (0.80) and large elongation (22% to 32%).
2. The yield behaviour of the bars is significantly influenced by the microstructure. Bars with fine microstructure exhibit marked yield point with large Lüders strain, while bars with coarse microstructure preyield significantly before macroyielding and exhibit much smaller Lüders strains.
3. The Lüders style yielding of TEMPCORE reinforcing steel is not exhibiting sharp yield drop regardless of strain rate.
4. In zero to tension and zero to compression cyclic loading below the yield strength the response is elastic with fine microstructure bars, while bars with coarse microstructure respond with wide open mechanical hysteresis when loaded beyond the preyield stress level and exhibit cyclic hardening in both tension and compression cycling.
5. Fully reversed cyclic loading well below the yield strength but with sufficiently high stresses produces cyclic softening. The softening rate with coarse microstructure is much faster and macroyield is induced within tens of cycles. In contrast, fine microstructure bars soften slowly within the first hundreds of cycles and further cycling is needed to induce macroyielding.
6. Case materials exhibit higher yield strength and yield continuously in ductile manner.
7. The core materials yield in Lüders style and the core with fine microstructures exhibit higher yield strength and larger Lüders strain than core materials with coarse microstructures.
8. Cut out specimens of 16 mm diameter bar show different yield behavior from as-received bars, and this provides information about the interaction between case and core materials during loading.

7.6.3. Analysis of tress concentrations arising from surface pattern deformations

1. The root radius is the prime factor affecting the value of SCF and a polynomial function of an order of 6 is to describe such relationship. Smaller root radius naturally results in a higher stress concentration factor.
2. Stress concentration increases as the deformation width and flank angle increase but these influences are much smaller than those relating to the *r/h* ratio. The effects of deformation width are more significant than those of flank angles.
3. Stress concentration increases as the lug spacing approaches zero.

7.6.4. Fatigue tests

1. TEMPCORE reinforcing steels have superior fatigue properties over the other type of high strength reinforcing steels. The fatigue limits of the tested bars are as high as 40% of the measured tensile strength and in some cases this value reaches 60 to 70%.
2. The fatigue properties of TEMPCORE reinforcing bars are essentially determined by the hardened outside layer.
3. TEMPCORE reinforcing steel is rather tough and considerable plastic deformation takes place before the final stages of failure.
4. Stress relieving significantly reduces fatigue lives but has an insignificant effect on the fatigue limit.
5. The fatigue lives of as received bars when cycled at the same range but at a minimum stress level set to +80 MPa are the same as the fatigue lives of stress-relieved bars cycled from zero minimum stress.
6. The existing model for fatigue life and fatigue limit calculation underestimates the fatigue properties of TEMPCORE reinforcing steel.

Appendix 7-1. Regression results for the relationship between SCF and *r/h*.

w/h = 4.0; $\alpha = 65°$

$$SCF = 5.9972(r/h)^6 - 32.812(r/h)^5 + 71.994(r/h)^4 - 81.191(r/h)^3 + 50.306(r/h)^2 - 17.241(r/h) + 4.6629;$$

w/h = 4.0; $\alpha = 45°$

$$SCF = 5.1408(r/h)^6 - 28.031(r/h)^5 + 61.293(r/h)^4 - 68.951(r/h)^3 + 42.799(r/h)^2 - 14.906(r/h) + 4.3359;$$

w/h = 3.0; $\alpha = 65°$

$$SCF = 5.1524(r/h)^6 - 28.274(r/h)^5 + 62.262(r/h)^4 - 70.497(r/h)^3 + 43.855(r/h)^2 - 15.067(r/h) + 4.1992;$$

w/h = 3.0; $\alpha = 45°$

$$SCF = 4.6015(r/h)^6 - 25.153(r/h)^5 + 55.143(r/h)^4 - 62.191(r/h)^3 + 38.679(r/h)^2 - 13.455(r/h) + 3.9643$$

Table 7-1. Area percentages and hardness of different regions of the tested bars

Bar size	*Hardened layer*	*Intermediate layer*	*Core*	*Hardness*
	Depth /Area	*Depth / Area*	*area*	*HV*
mm	*mm / %*	*mm / %*	*%*	*Surface/Core*
12	0.8 / 24	0.3 / 19	57	225/150
16	1.1 / 32	1.1 / 24	44	231/148
20	1.3 / 33	1.2 / 25	42	240/153
24	1.5 / 33	2.4 / 29	38	256/150
28	1.7 / 32	2.8 / 32	36	265/153
32	2.0 / 32	4.2 / 36	32	232/156
36	2.2 / 30	4.8 / 38	32	255/150

Note: Areas of transverse lugs were excluded in the calculation of the percentages of the areas.

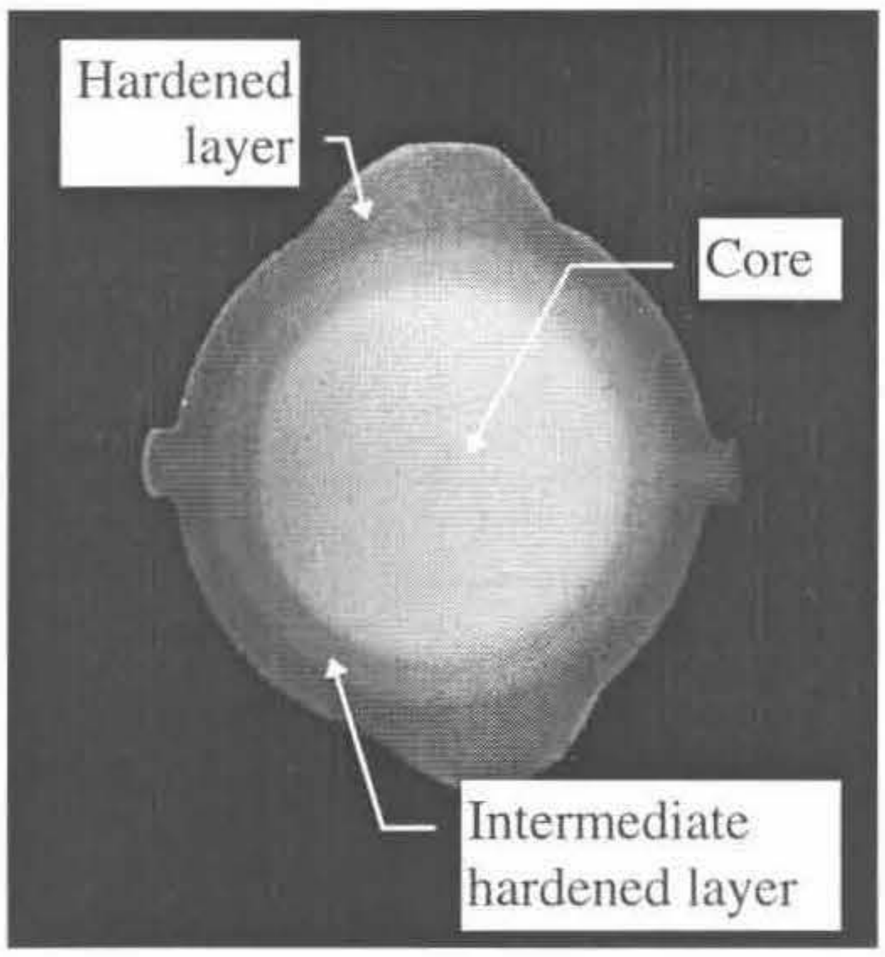

Table 7-2. Geometry parameters related to lugs or identification marks

Bar size (mm)	r_1	r_2	α_1	α_2	*h*	*w*	*L*	*r/h*	*w/h*
Lugs									
12	0.76	1.03	35.6°	36.0°	0.78	3.09	7.77	0.9	4.0
16	1.10	1.87	40.8°	42.0°	1.02	4.28	11.06	1.08	4.20
20	1.48	1.19	38.7°	44.3°	1.23	5.01	13.73	0.96	4.07
24	1.60	0.4	32.6°	46.7°	2.73	7.62	16.36	0.15	2.79
28	1.11	1.14	41.2°	41.7°	2.29	7.81	18.32	0.48	3.4
32	3.09	0.78	32.0°	37.5°	2.52	9.19	20.20	0.31	3.65
36	1.11	0.91	35.2°	39.4°	3.00	11.1	26.1	0.30	3.7
ID marks									
16	1.03*	-	-	-	-	-	-	-	-
28	1.55	-	32.5°	90°	2.01	3.48	-	-	1.73
32	1.82	0.57	39.8°	64°	0.97	3.2	-	0.59	3.3

Note: * radius of the gap valley between mark and lug, as shown in Figure 7-8;
ID marks = identification marks.

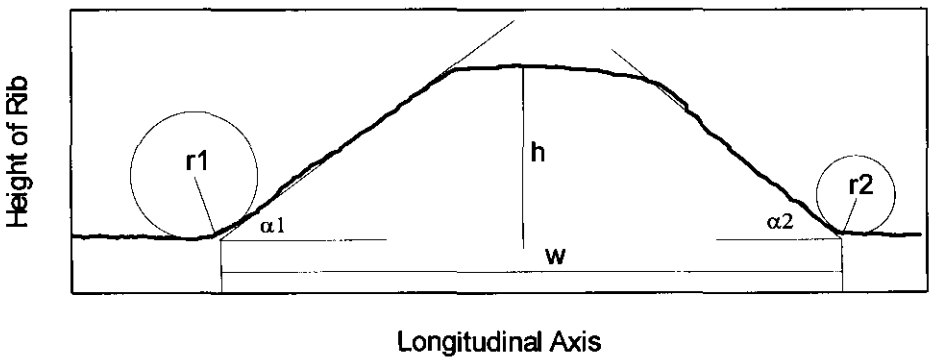

Table 7-3. Mechanical properties of TEMPCORE bars

bar size *mm*	$\sigma_{0.2}$ *MPa*	σ_{uts} *MPa*	σ_y / σ_{uts}	δ_5 *%*	$\delta_{L\ddot{u}ders}$ *%*	δ_{uni} *%*	*preyield strain* 10^{-6}
12	438	521	0.84	32.4	3.2	26.2	undetectable
16	443	537	0.83	32.1	2.7	25.2	undetectable
20	430	527	0.82	30.9	2.6	22.5	undetectable
24	455	557	0.82	25.8	2.2	21.5	undetectable
28	441	541	0.82	25.0	2.0	21.5	undetectable
32	416	538	0.77	22.1	0.4	17.0	600
36	433	556	0.78	22.2	0.32	15.5	1000

Note: Tested under strain rate = 10^{-5}/S.

$\sigma_{0.2}$: 0.2% proof yield strength;

σ_{uts} : Tensile strength;

δ_5: Elongation of 5*d* gage length;

$\delta_{L\ddot{u}ders}$: Lüders strain;

δ_{uni}: Uniform elongation.

Table 7-4. Mechanical properties of 36 mm diameter bars with different microstructures

Test No.	$d\varepsilon/dt$ *1/S*	$\sigma_{0.2}$ *MPa*	$\sigma_{0.1}$ *MPa*	$\sigma_{0.05}$ *MPa*	$\sigma_{0.01}$ *MPa*	σ_{uts} *MPa*	δ_5 *%*	$\varepsilon_{L\ddot{u}ders}$ *%*	*Pre-yield*
36C	10^{-6}	428	428	406	335	548	23.0	0.18	Yes
36C	10^{-5}	433	433	410	348	551	22.5	0.32	Yes
36F	10^{-6}	425	425	425	425	535	30.0	1.5	No

Note: **C** for coarse microstructure and **F** for fine microstructure.

Table 7-5. Mechanical properties of the core and case sections

Material	*Yield Strengths MPa*	*UTS MPa*	*Yield Style*	ψ %	δ_5 %	$\delta_{L\,Lüders}$ %
Case 16	$\sigma_{0.02} = 465$ $\sigma_{0.1} = 486$ $\sigma_{0.2} = 495$	573	Continue	–	15	–
Core 16	$\sigma_u = 380$ $\sigma_l = 354$	481	Lüders	67	31	3.25
Case 36	$\sigma_{0.02} = 540$ $\sigma_{0.1} = 596$ $\sigma_{0.2} = 607$	680	Continue	-	13	-
Core 36	$\sigma_u = 308$ $\sigma_l = 297$	476	Lüders	71	28	0.73

Note: Results of core materials of 16 and 36 mm diameter bars represent bars with fine and coarse microstructure, respectively.

Table 7-6. Fatigue results for the 12 mm diameter bar; zero to tension cycling

σ_{max} MPa	test No.	fatigue life No. of cycles	Failure position	Fracture features	remarks
260 ↓	12F260-1	run out			run out and cycled again at higher stress
340	12F340-1	313,385	at lug root	multiple initiation	tensile loading after fatigue revealed cracks
270 ↓	12F270-1#	run out			run out and cycled again at higher stress
320	12F320-1#	522,824	at lug root	single initiation	
300	12F300-4	645,025	at lug root	single initiation	
280	12F280-1	1,000,921	at lug root	single initiation	
270	12F270-2#	run out			tensile loading after fatigue did not reveal cracks

Note: # Specimen without identification marks;

Table 7-7. Fatigue results for the 16 mm diameter bar; zero to tension cycling

σ_{max} MPa	Test No.	Fatigue life No. of cycles	Failure position	Fracture features	Remarks
310	16F310-2	run out			run out and cycled again at higher stress
380 ↓	16F380-1	287, 513	at lug root	multiple initiation	
300	16F300-1	run out			run out and cycled again at higher stress
360 ↓	16F360-1	339, 853	at ID mark		
310	16F310-1	run out			run out and cycled again at higher stress
340 ↓	16F340-1	484, 983	at lug root	single initiation	tensile loading revealed cracks at lug and IDmark
340	16F340-2#	467, 357	at lug root	single initiation	block loading revealed beach-mark
340	16F340-3#	480, 076	at lug root	single initiation	block loading revealed beach-mark
320	16F320-1	600, 977	at ID mark		

Note: # Specimen without identification marks;

Table 7-8. Fatigue results for the 20 mm diameter bar; zero to tension cycling

σ_{max} MPa	Test No.	Fatigue life No. of cycles	Failure position	Fracture features	Remarks
380	20F380-1	226, 954	at lug root	multiple initiation	
300	20F300-1	run out			run out and cycled again at higher stress
360 ↓	20F360-1	323, 717	at lug root	multiple initiation	
310	20F310-1	run out			run out and cycled again at higher stress
340 ↓	20F340-1	431,797	at lug root	single initiation	
320	20F320-1	708, 831	at lug root	single initiation	

Note: # Specimen without identification marks;

Table 7-9. Fatigue results for the 24 mm diameter bar; zero to tension cycling

σ_{max} MPa	Test No.	Fatigue life No. of cycles	Failure position	Fracture features	Remarks
240 ↓ **360** ↓	24F240-1# 24F360-1#	run out 201, 000	at lug root	multiple initiation	run out and cycled again at higher stress tensile loading after fatigue revealed cracks
240 ↓ **340** ↓	24F240-2 240F340-1	run out 233, 858	at lug root	multiple initiation	run out and cycled again at higher stress
320	20F320-1#	378, 050	at lug root	multiple initiation	
280	24F280-1	740, 130	at lug root	single initiation	
250	24F250-2#	1, 043, 240	at lug root	single initiation	
250	24F250-3	-	-	-	terminated at 741,080 cycles, gripp smashed, subsequent tensile loading did not revealed cracks
250	24F250-4	1, 104, 908	at lug root	single initiation	

Note: # Specimen without identification marks;

Table 7-10. Fatigue results for the 28 mm diameter bar; zero to tension cycling

σ_{max} MPa	Test No.	Fatigue life No. of cycles	Failure position	Fracture features	Remarks
230 ↓	28F230-1#	run out			run out and cycled again at higher stress
360 ↓	28F360-1#	-	-		terminated at 200, 650 cycles, washer pulled out, tensile loading after fatigue revealed cracks
360	280F360-2#	241, 960	at lug root	multiple initiation	
360	28F360-3#	251, 310	at lug root	multiple initiation	tensile loading after fatigue revealed cracks
320	28F320-1#	536, 420	at lug root	multiple initiation	
280	28F280-1#	859, 820	at lug root	single initiation	
260	28F260-1#	1, 363, 520	at lug root	single initiation	
240	28F240-1	1, 347, 460	at ID mark		
240	28F240-2	674, 350	at ID mark		
240	28F240-3#	2, 340, 410	at lug root	single initiation	
240	28F240-4	1, 220, 000	at ID mark		
240	28F240-5#	1, 533, 160	at lug root	single initiation	
240	28F240-6#	2, 300, 082	at lug root	single initiation	
230	28F230-2	1, 480, 000			

Note: # Specimen without identification marks;

Table 7-11. Fatigue results for the 32 mm diameter bar; zero to tension cycling

σ_{max} MPa	Test No.	Fatigue life No. of cycles	Failure position	Fracture features	Remarks
230	32F230-1	run out			run out and cycled again at higher stress
360 ↓	32F360-1	180, 510	at lug root	multiple initiation	
320	32F320-1#	308, 730	at lug root	multiple initiation	
230	32F230-2#	run out			run out and cycled again at higher stress
300 ↓	32F300-1#	414, 570	at lug root	multiple initiation	
240	32F240-2	run out			run out and cycled again at higher stress
300 ↓	32F300-2	467, 500	at lug root	multiple initiation	
280	32F280-1#	775, 980	at lug root	multiple initiation	
260	32F260-1	833, 440	at lug root	single initiation	
240	32F240-3	run out			run out and cycled again at higher stress
250 ↓	32F250-1	949, 770	at lug root	single initiation	

Note: # Specimen without identification marks;

Table 7-12. Fatigue results for the 36 mm diameter bar; zero to tension cycling

σ_{max} MPa	Test No.	Fatigue life No. of cycles	Failure position	Fracture features	Remarks
240	36F240-1	run out			run out and cycled again at higher stress
300 ↓	36F300-1	527, 549	at lug root	multiple initiation	
220	36F220-1	run out			
280	36F280-1	611, 860	at lug root	multiple initiation	run out and cycled again at higher stress
250 ↓	36F250-1	1, 264, 495	at lug root	single initiation	

Table 7-13. Comparisons of mechanical properties.

Steels	σ_f MPa	σ_y MPa	σ_u MPa	σ_y/σ_u	σ_f/σ_y	σ_f/σ_u	Predicted # σ_f MPa	Test Condition	Data Source
TEMPCORE 12 mm	**270**	413	503	0.82	**0.65**	**0.54**	193		
TEMPCORE 16 mm	**310**	430	506	0.85	**0.72**	**0.61**	203		
TEMPCORE 20 mm	**310**	428	521	0.82	**0.72**	**0.60**	196		
TEMPCORE 24 mm	**240**	455	557	0.82	**0.52**	**0.42**	152		
TEMPCORE 28 mm	**230**	440	543	0.81	**0.59**	**0.52**	170		
TEMPCORE 32 mm	**240**	416	538	0.77	**0.58**	**0.45**	160		
TEMPCORE 36 mm	**240**	432	556	0.78	**0.56**	**0.43**	155	axial in air	present tests
A432#5	221	454	753	0.60	0.49	0.29			
A321#5	252	616	842	0.73	0.41	0.30			
A432#8	204	452	752	0.60	0.45	0.27			
A432#8	210	582	851	0.68	0.36	0.25			
A432#10	197	443	762	0.58	0.44	0.26			
A432#10	200	572	755	0.76	0.35	0.26		beam bending	Mac Gregor (1971)
Hot rolled bars	250	420	630	0.62	0.59	0.39			
(2 millions cycles)	250	510	680	0.75	0.49	0.39		beam bending	Kokubu (1968)
Grade 60 (3 millions cycles)	179	423	667	0.63	0.42	0.27		axial test in air	Jhamb (1973)
British high strength	227	-	-	-	-	-		unknown condition	
Unisteel 410	200							axial test in air	
Torbar (16 mm)	220							axial test in air	
Torbar (40 mm)	150							axial test in air	Tilly (1979)
Cold worked 410 bar	185	431	544	0.79	0.43	0.34		beam bending in air	Roper (1980)

Helgason's equation (see Chapter 5).

Table 7-14.Maximum SCFs as calculated by finite element method at the surface of deformation root (Model I)

	w/h = 3.0			*w/h = 3.5*			*w/h = 4.0*		
r/h	**α = 45°**	**α = 55°**	**α = 65°**	**α = 45°**	**α = 55°**	**α = 65°**	**α = 45°**	**α = 55°**	**α = 65°**
0.1	2.953	3.039	3.072	3.093	3.194	3.234	3.215	3.327	3.373
0.2	2.389	2.429	2.449	2.496	2.543	2.565	2.589	2.642	2.665
0.3	2.129	2.154	2.174	2.218	2.246	2.265	2.296	2.328	2.345
0.4	1.972	1.996	2.015	2.053	2.073	2.095	2.123	2.144	2.163
0.5	1.861	1.886	1.902	1.931	1.955	1.973	1.996	2.016	2.035
0.6	1.780	1.804	1.818	1.843	1.868	1.883	1.900	1.924	1.939
0.7	1.717	1.739	1.761	1.778	1.796	1.818	1.829	1.847	1.867
0.8	1.667	1.691	1.711	1.722	1.743	1.764	1.771	1.789	1.810
0.9	1.625	1.650	1.670	1.676	1.699	1.719	1.725	1.743	1.762
1.0	1.592	1.616	1.635	1.639	1.663	1.681	1.685	1.704	1.722
1.1	1.564	1.587	1.605	1.607	1.631	1.649	1.651	1.670	1.688
1.2	1.539	1.561	1.580	1.580	1.603	1.621	1.622	1.641	1.657
1.3	1.517	1.539	1.559	1.557	1.579	1.596	1.595	1.615	1.631
1.4	1.497	1.519	1.541	1.536	1.557	1.575	1.572	1.592	1.607
1.5	1.480	1.501	1.524	1.517	1.538	1.557	1.551	1.571	1.586

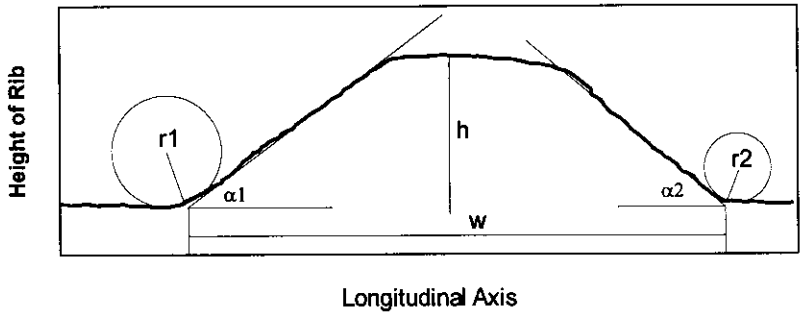

Table 7-15. Maximum SCFs as calculated by finite element method at the point 0.013h below surface (Model I)

	w/h = 3.0			*w/h = 3.5*			*w/h = 4.0*		
r/h	**α = 45°**	**α = 55°**	**α = 65°**	**α = 45°**	**α = 55°**	**α = 65°**	**α = 45°**	**α = 55°**	**α = 65°**
0.1	2.376	2.446	2.472	2.480	2.561	2.595	2.569	2.659	2.699
0.2	2.127	2.159	2.183	2.218	2.257	2.283	2.297	2.341	2.368
0.3	1.964	1.989	2.010	2.045	2.071	2.094	2.116	2.142	2.167
0.4	1.820	1.847	1.865	1.892	1.918	1.937	1.955	1.980	2.000
0.5	1.745	1.771	1.786	1.808	1.836	1.852	1.866	1.893	1.909
0.6	1.689	1.711	1.725	1.747	1.771	1.785	1.799	1.824	1.838
0.7	1.640	1.663	1.684	1.698	1.717	1.738	1.746	1.764	1.785
0.8	1.599	1.625	1.645	1.653	1.675	1.695	1.702	1.720	1.739
0.9	1.568	1.593	1.612	1.615	1.640	1.659	1.664	1.682	1.701
1.0	1.542	1.565	1.584	1.586	1.610	1.628	1.631	1.650	1.668
1.1	1.518	1.541	1.559	1.561	1.584	1.602	1.603	1.622	1.639
1.2	1.498	1.520	1.538	1.538	1.561	1.578	1.578	1.597	1.613
1.3	1.479	1.501	1.518	1.518	1.540	1.557	1.555	1.575	1.590
1.4	1.463	1.584	1.503	1.500	1.522	1.538	1.535	1.555	1.570
1.5	1.448	1.469	1.491	1.484	1.505	1.521	1.516	1.537	1.552

Table 7-16. Calculated SCFs and the obtained fatigue limits

Bar size	α	r/h	w/h	Calculated SCF	Fatigue limit
12 mm	36.0°	0.9	4.0	1.700	270 MPa
16 mm	42.0°	1.08	4.20	1.665	310 MPa
20 mm	44.3°	0.96	4.07	1.704	310 MPa
24 mm	46.7°	0.15	2.79	2.562	240 MPa
28 mm	41.7°	0.48	3.4	1.930	230 MPa*
32 mm	37.5°	0.31	3.65	2.174	240 MPa
36 mm	39.4°	0.30	3.7	2.216	240 MPa

* determined on specimens without identification mark.

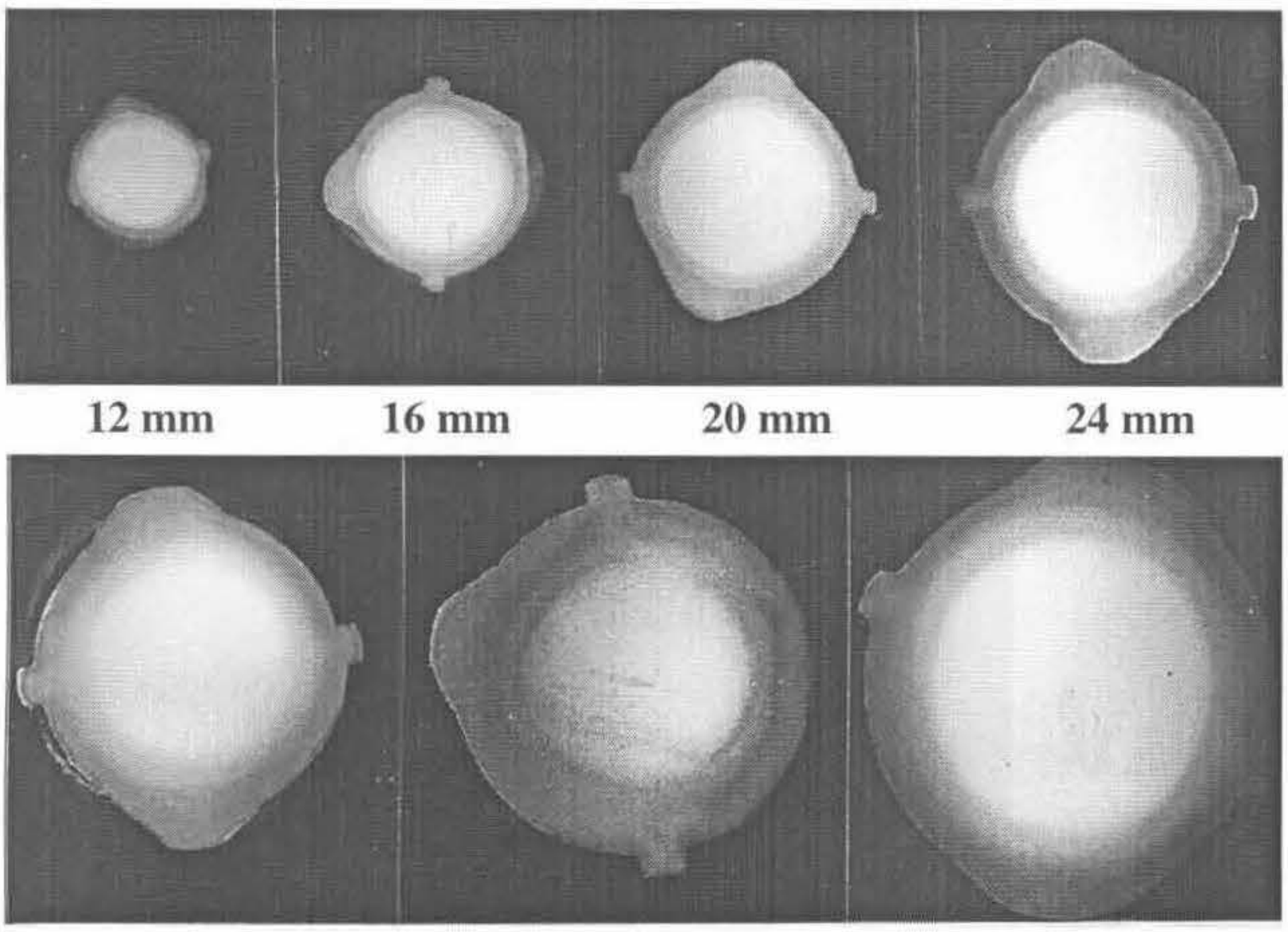

Figure 7-1. Etched cross sections of the tested bars

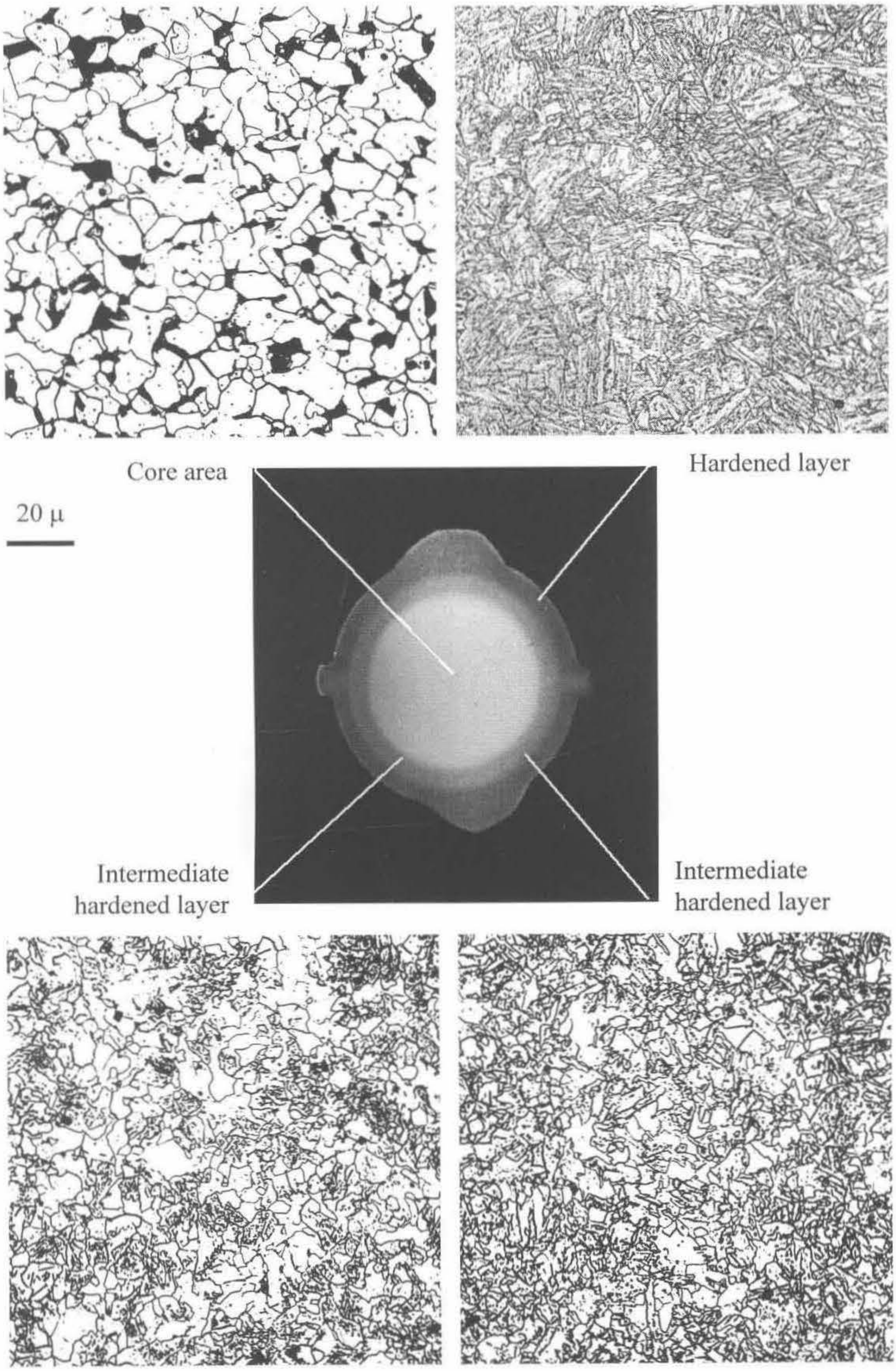

Figure 7-2. Bars with typical fine microstructure

Core area

20 μ

Hardened layer

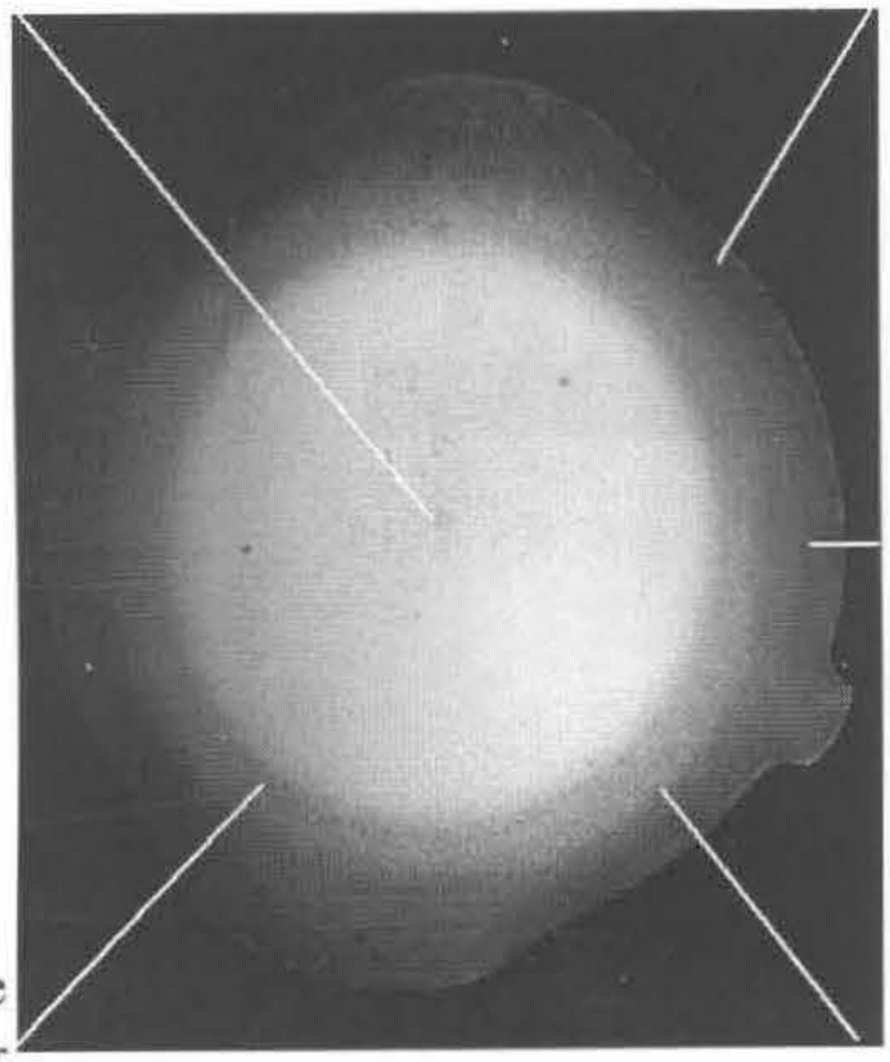

Intermediate
hardened layer

Hardened layer close to
intermediate hardened layer
Intermediate
hardened layer

Figure 7-3. Bars with typical coarse microstructure.

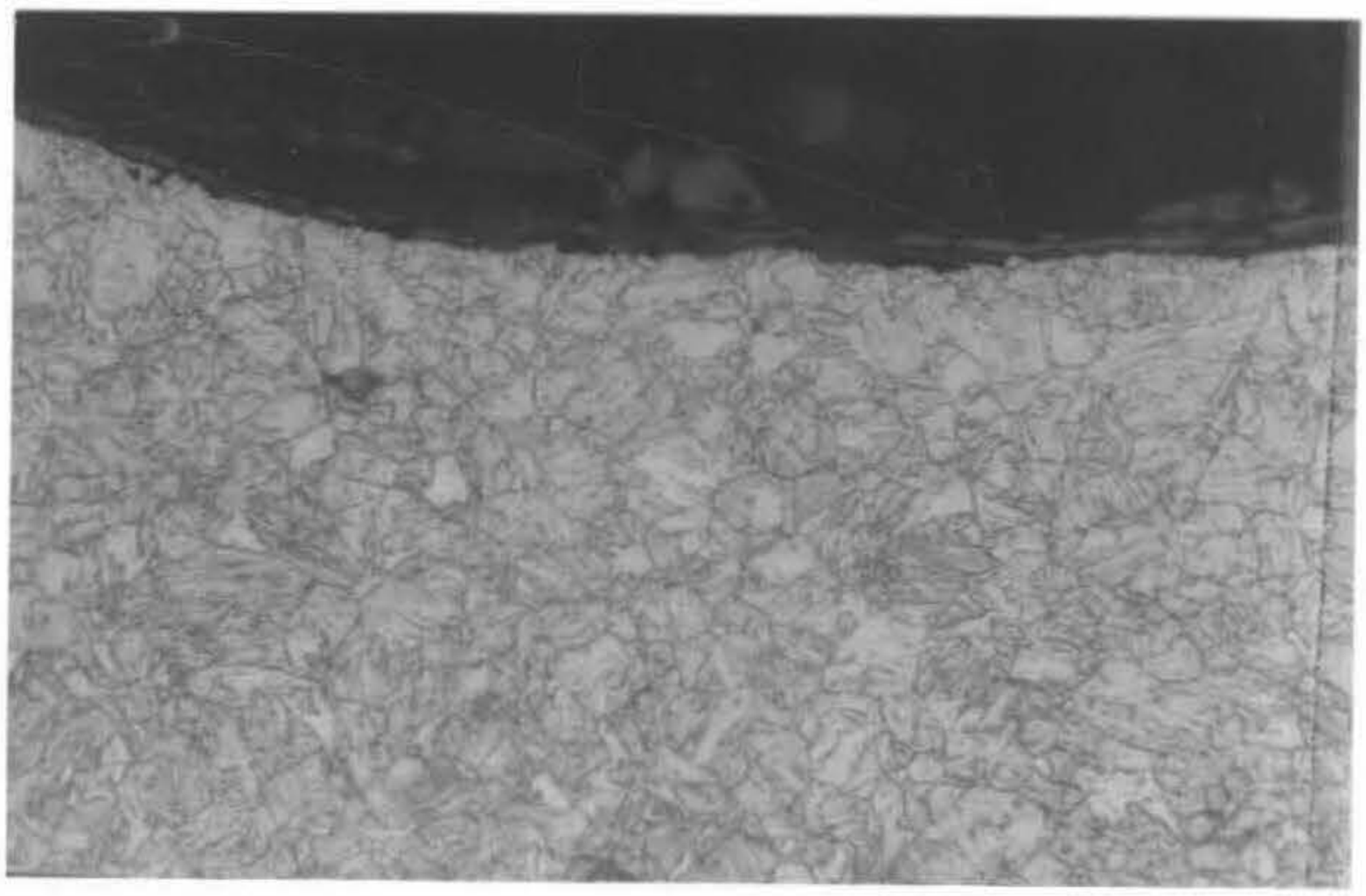

(a) 24 mm bar

(b) 36 mm bar 20 μ

Figure 7-4. Microstructures at the bar surface.

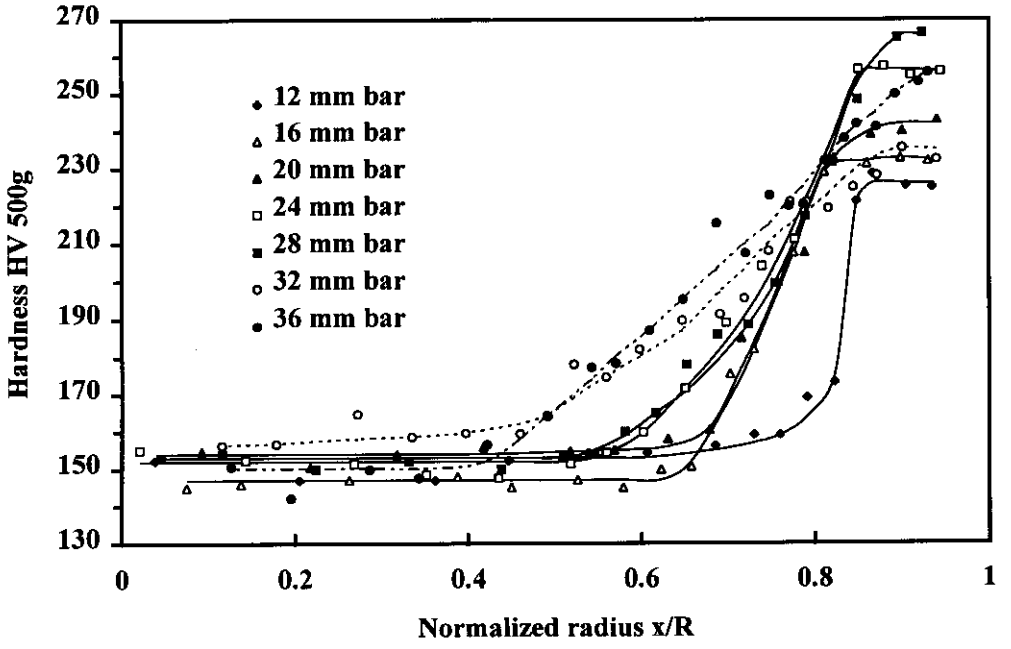

Figure 7-5. Hardness distributions along the radii of the bars

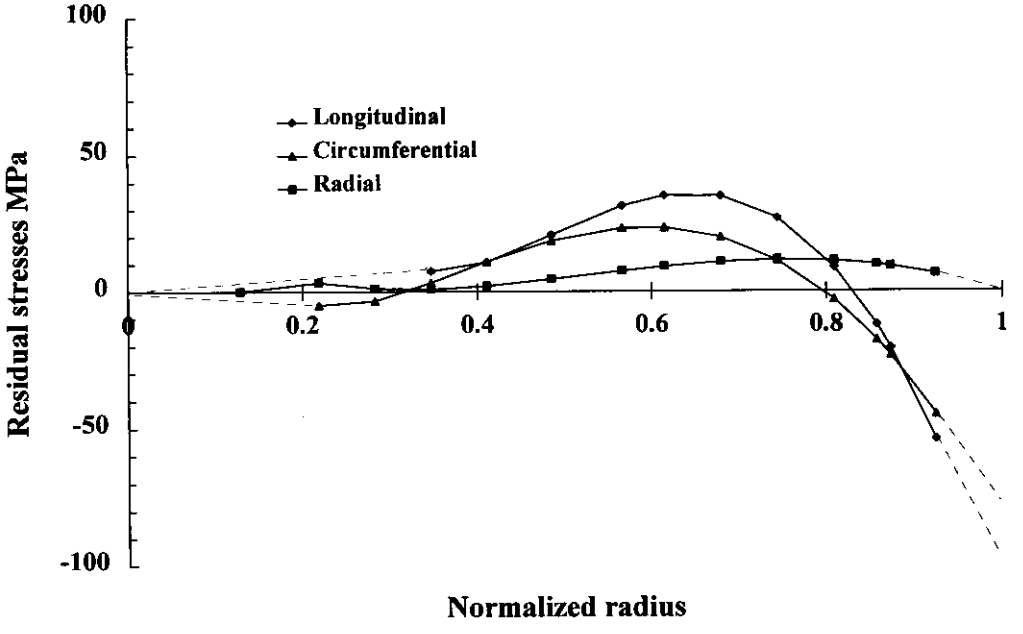

Figure 7-6. Residual stress distribution; bar diameter 24 mm

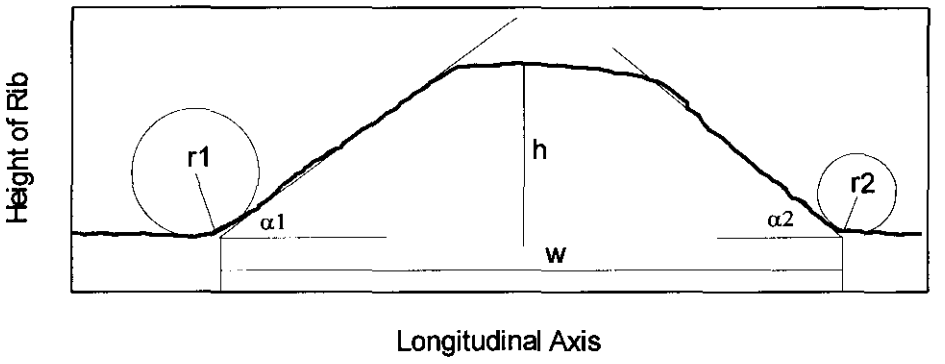

(a) Illustration of typical lug profile measured by laser displacement meter

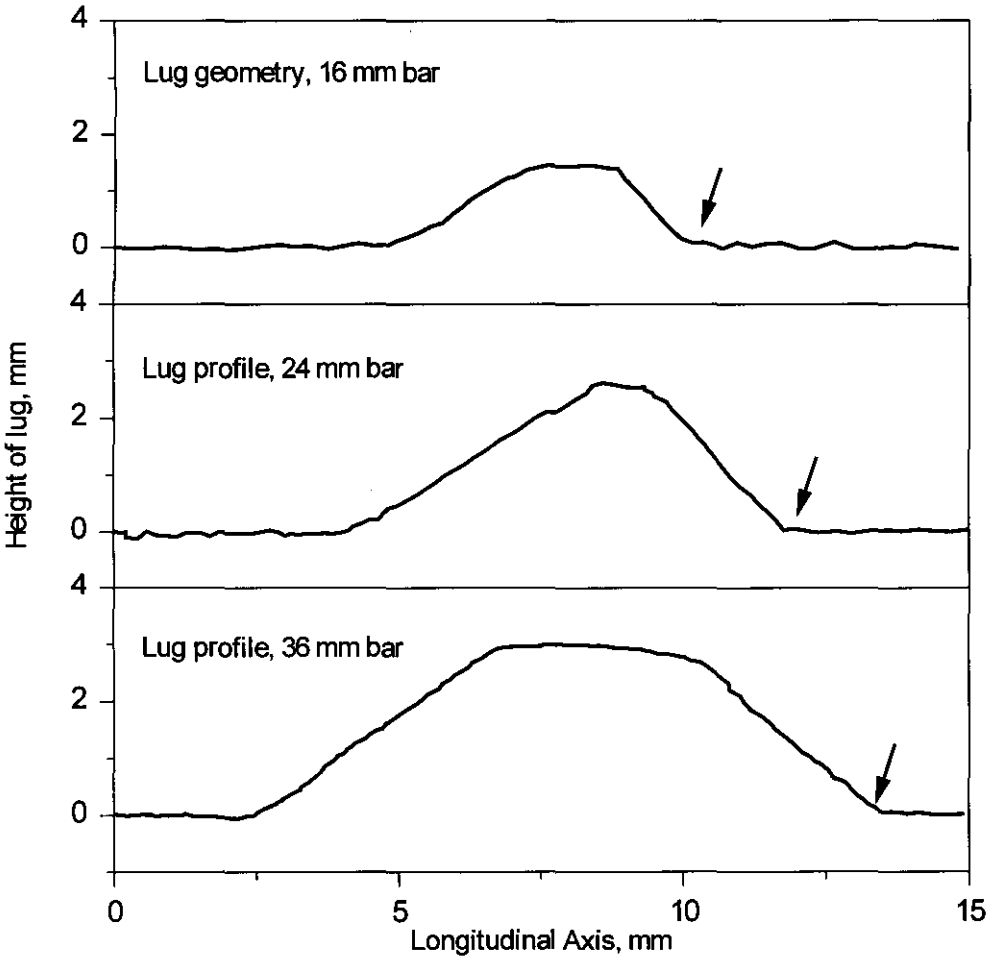

(b) Actual measurements

Figure 7-7. Representative lug profiles (x 7.5)

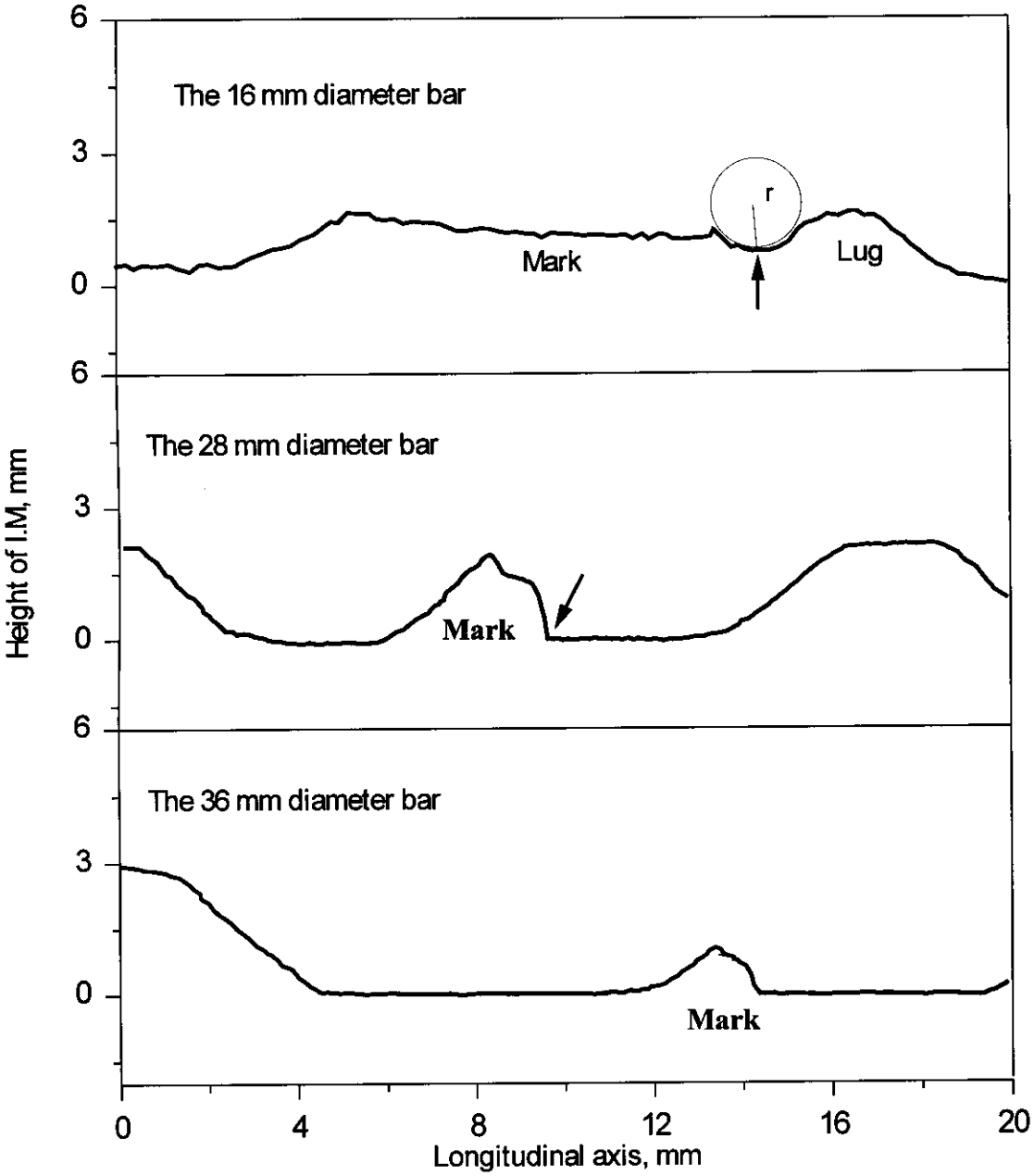

Figure 7-8. Profiles of representative identification marks (x 6)

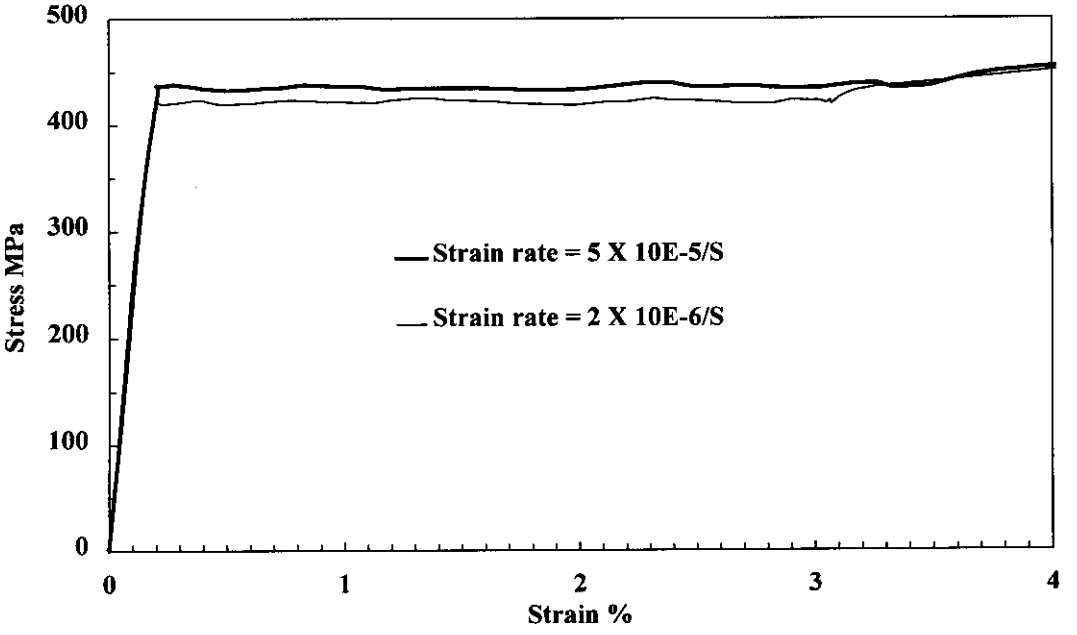

Figure 7-9. Tensile stress-strain curves; 12 mm bar

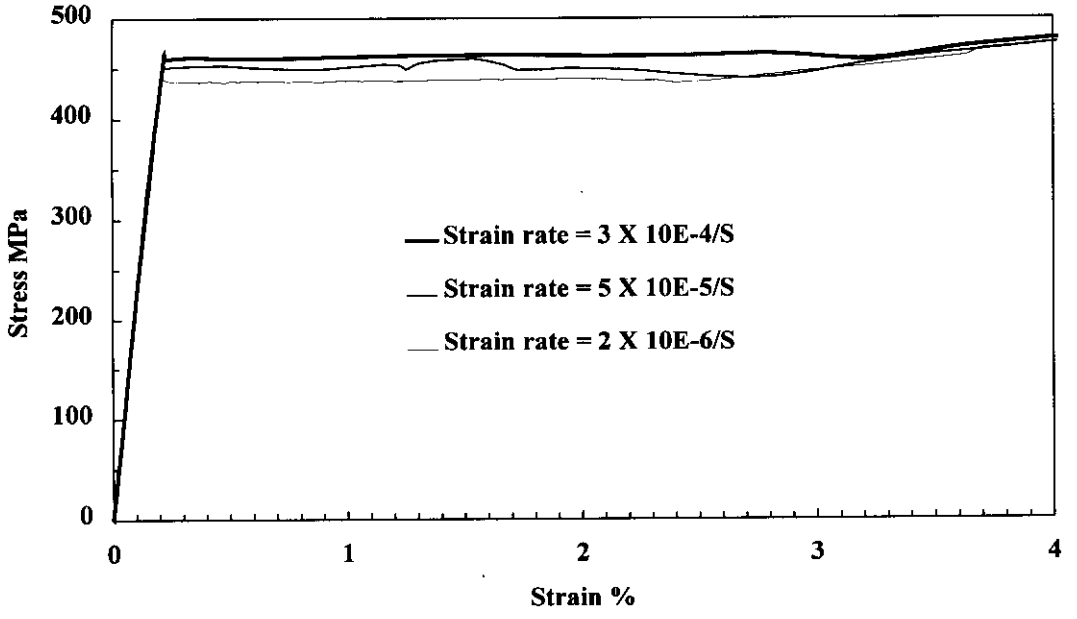

Figure 7-10. Tensile stress-strain curves; 16 mm bar

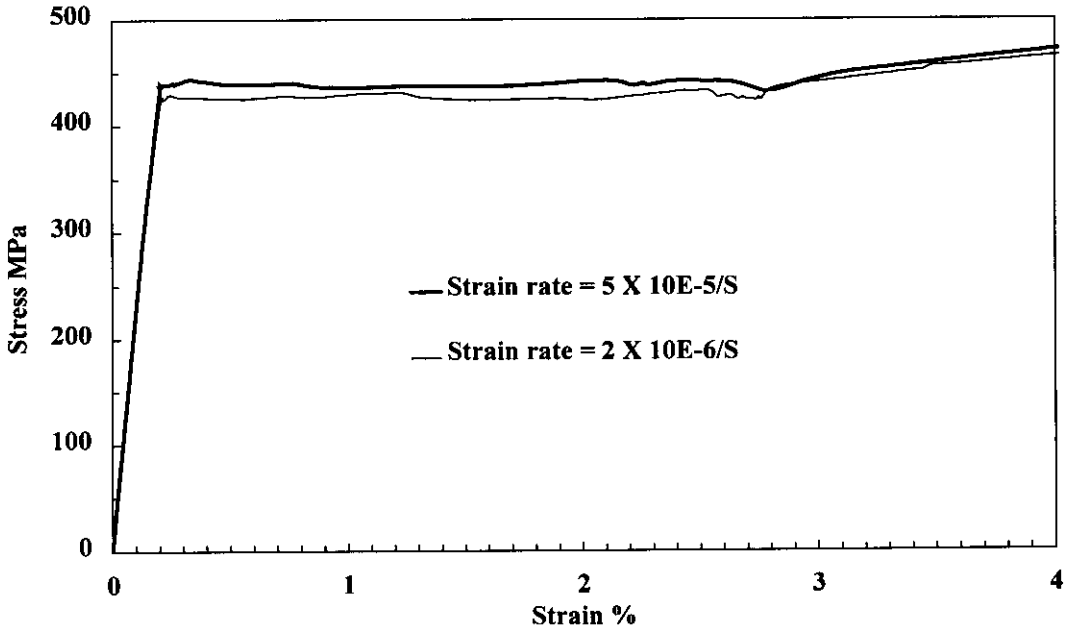

Figure 7-11. Tensile stress-strain curves; 20 mm bar

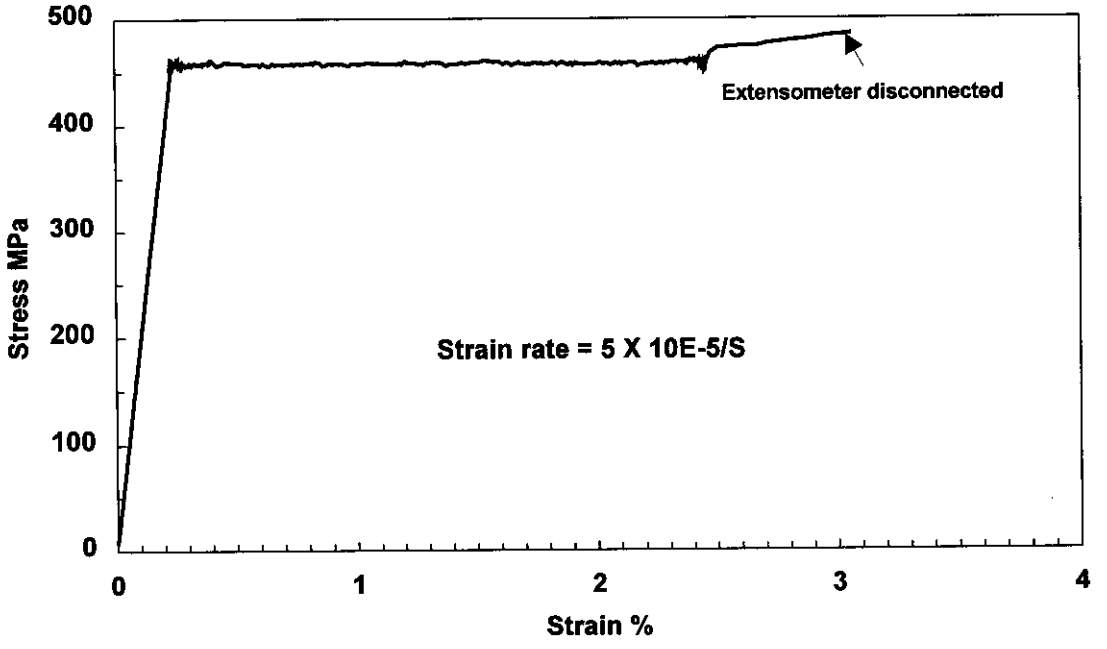

Figure 7-12. Tensile stress-strain curve; 24 mm bar

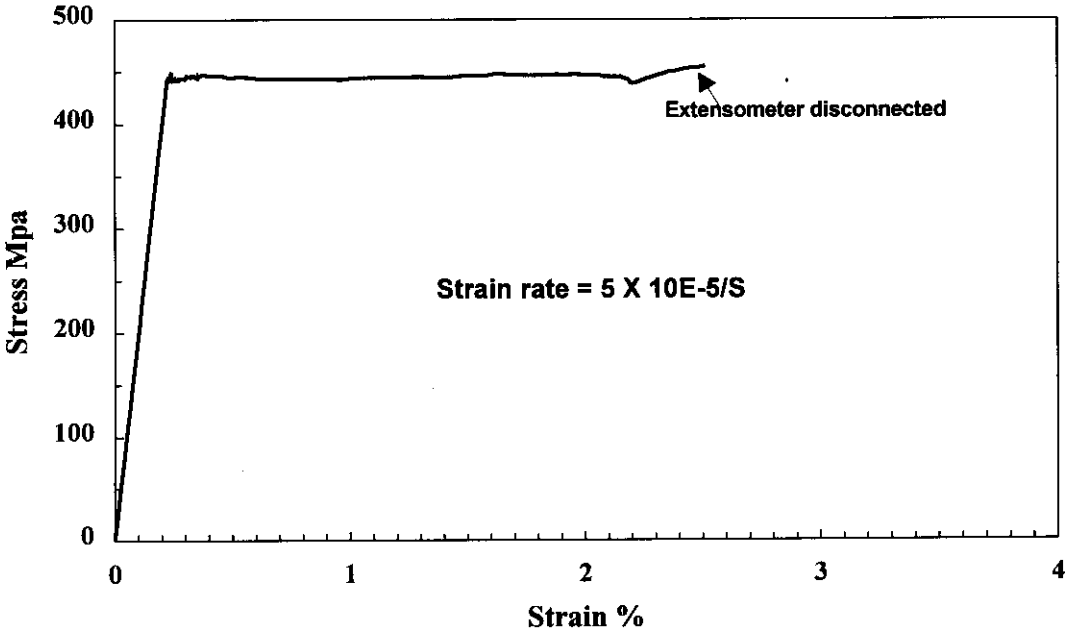

Figure 7-13. Tensile stress-strain curve; 28 mm bar

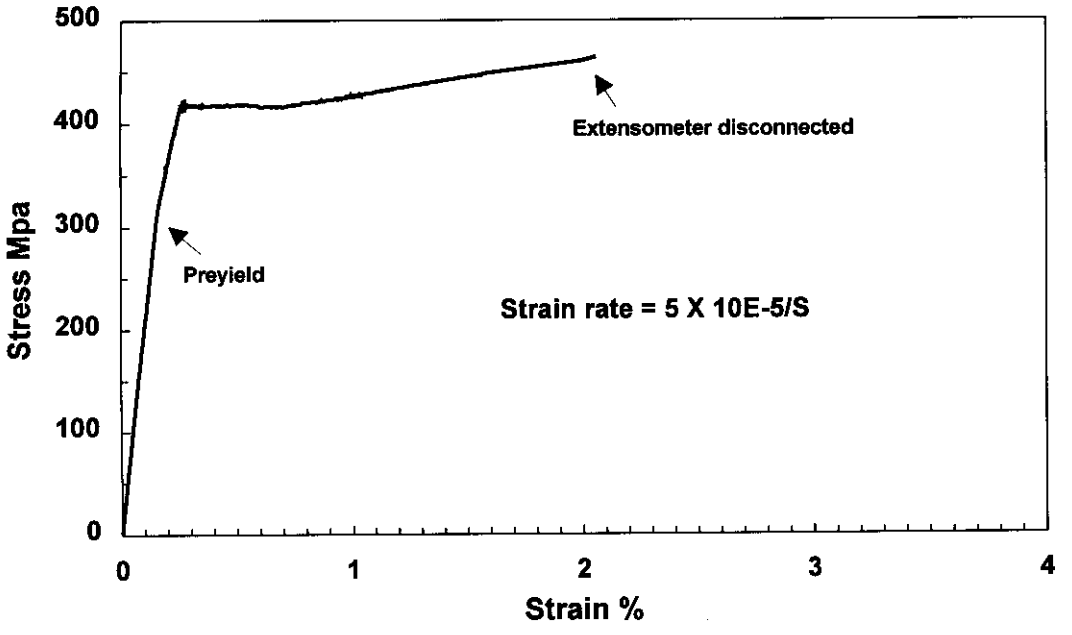

Figure 7-14. Tensile stress-strain curve; 32 mm bar

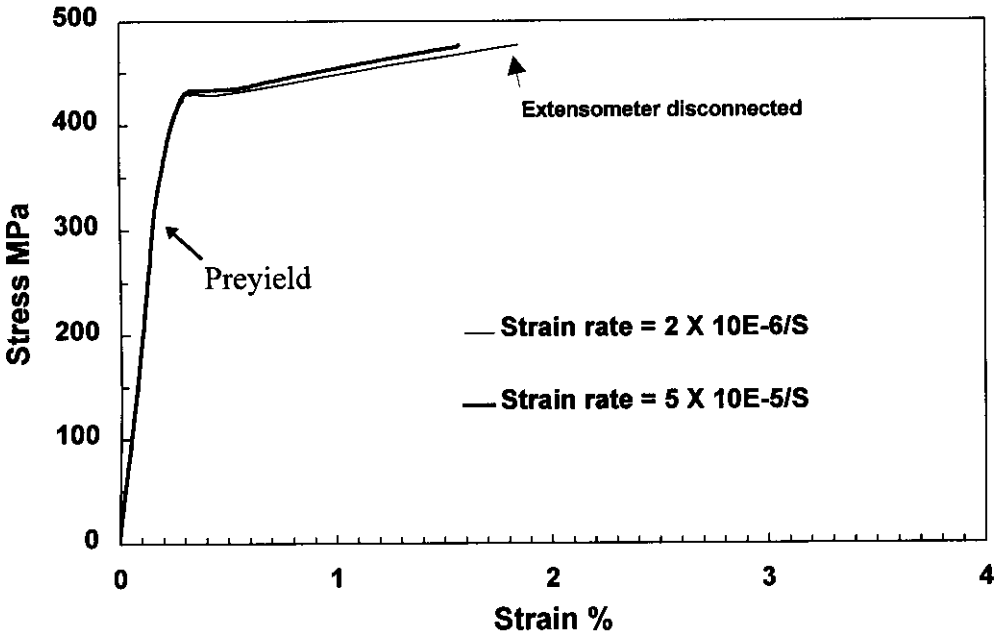

Figure 7-15. Tensile stress-strain curves; 36 mm bar

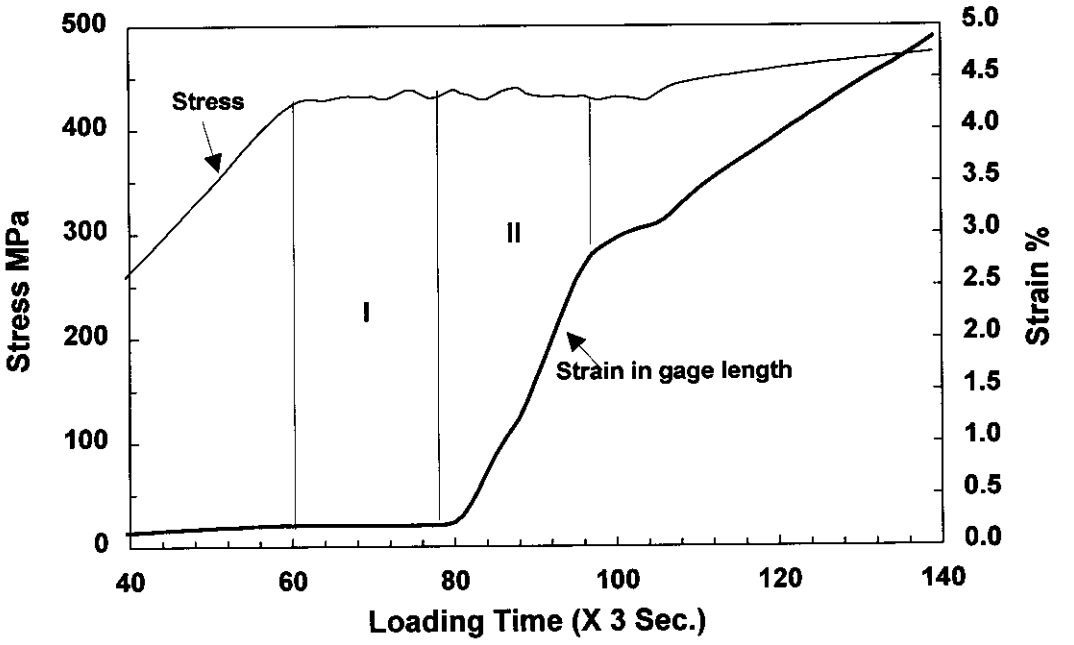

Figure 7-16. Stress-strain response versus loading time; 16 mm bar

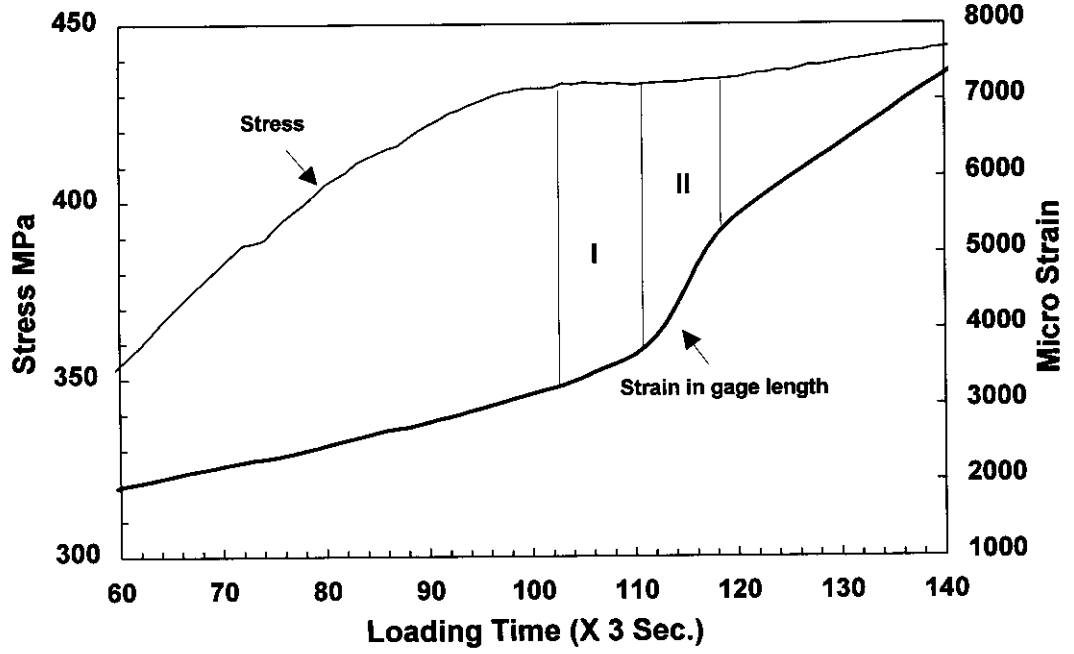

Figure 7-17. Stress-strain response versus loading time; 36 mm bar

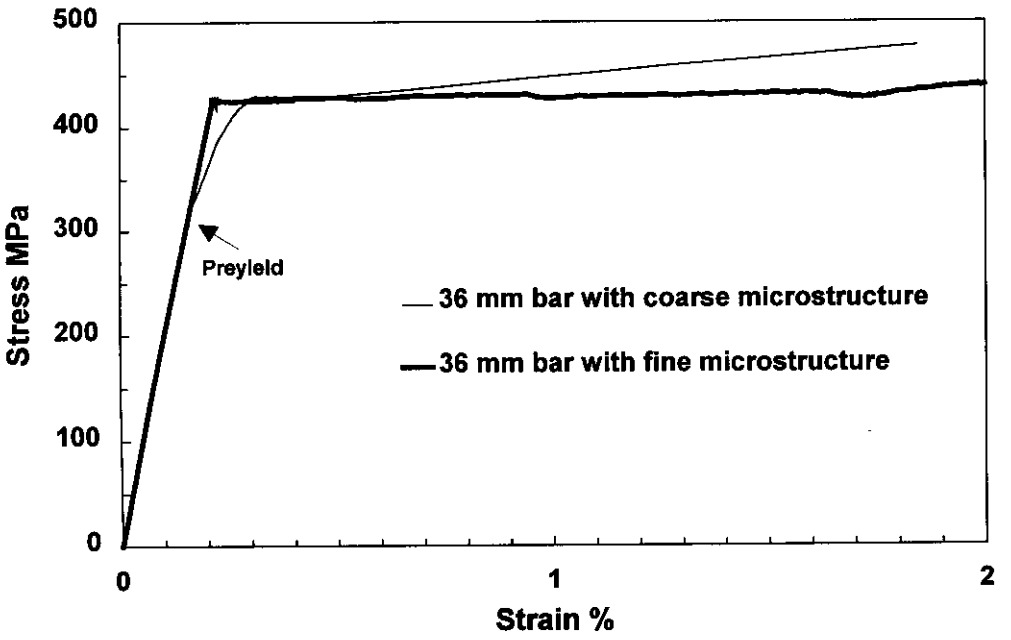

Figure 7-18. Comparison of stress-strain curves of fine and coarse microstructure bars

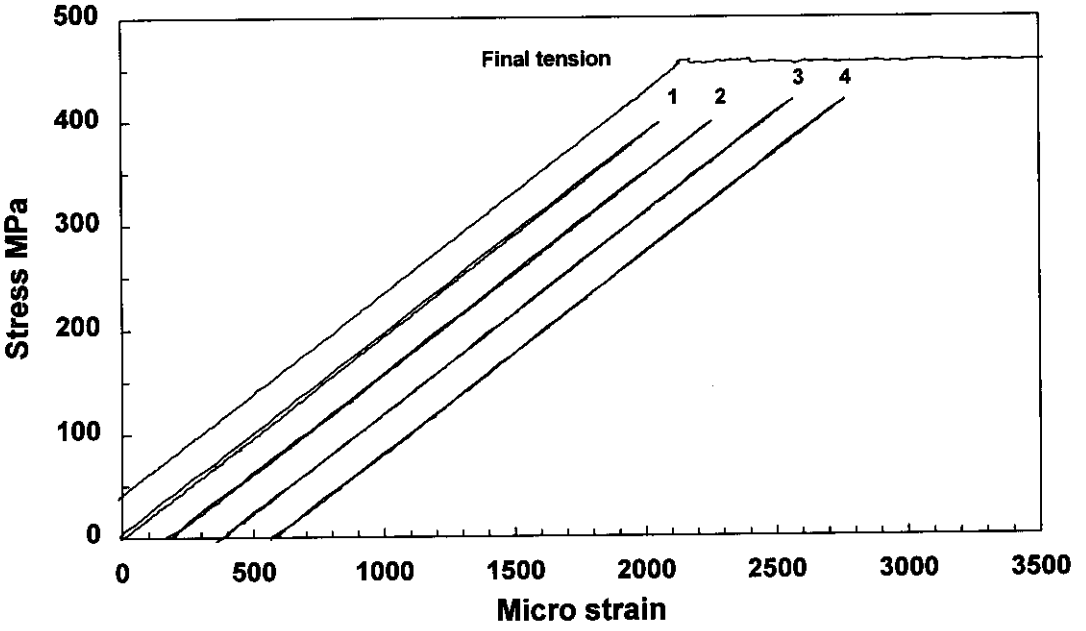

Figure 7-19. Typical stress-strain curves of fine microstructure bar in zero to tension cyclic loading (24 mm diameter bar)

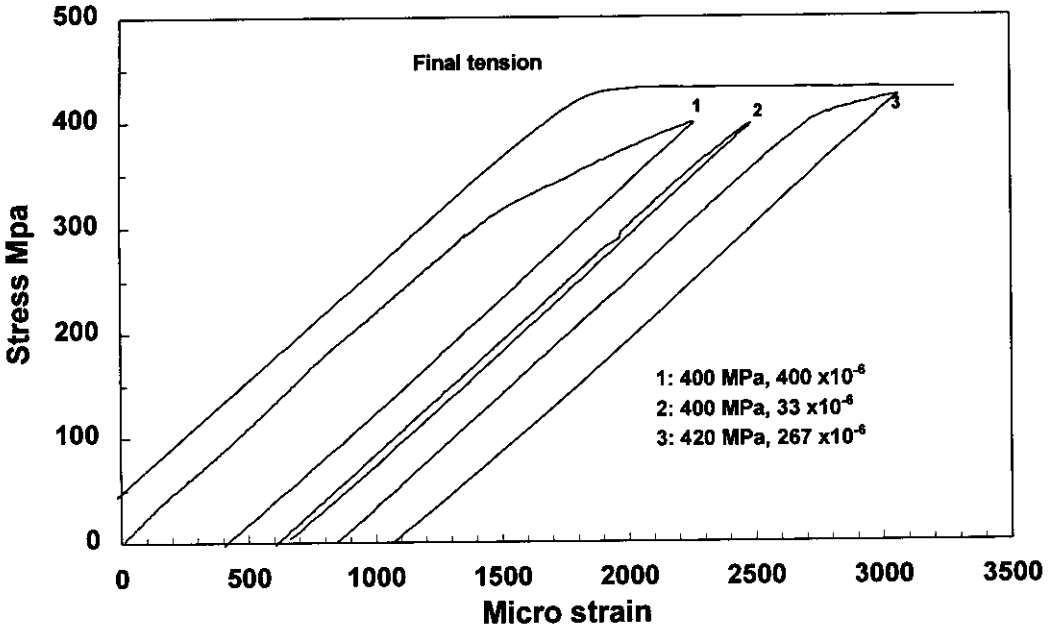

Figure 7-20. Typical stress-strain curves of coarse microstructure bar in zero to tension cyclic loading (36 mm bar)

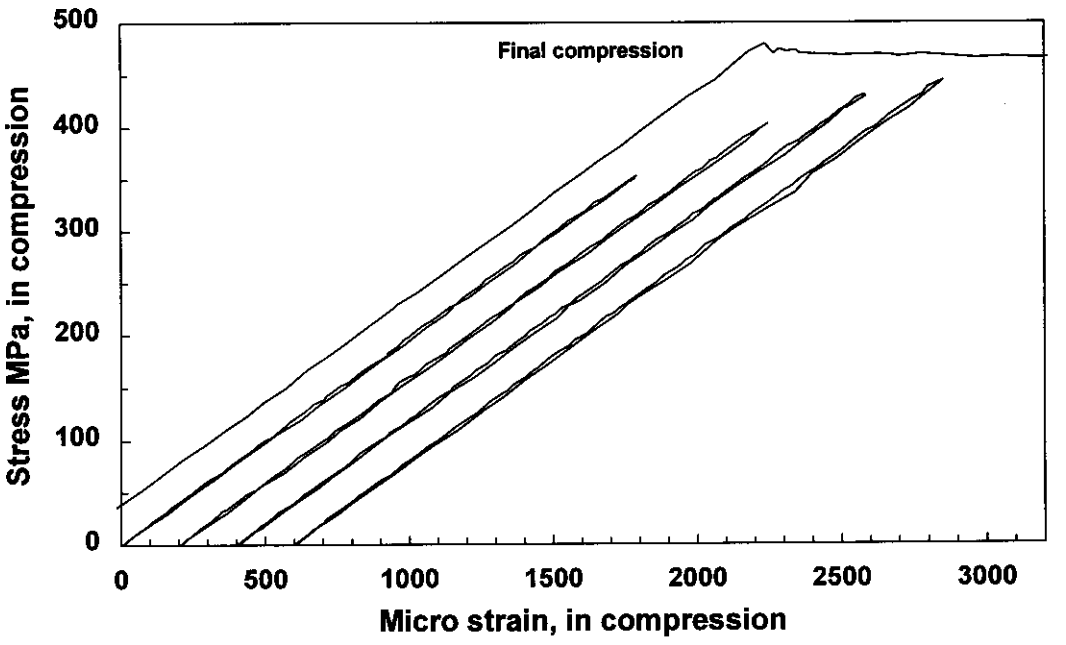

Figure 7-21. Typical stress-strain curves of fine microstructure bar in zero to compression cyclic loading (24 mm diameter bar)

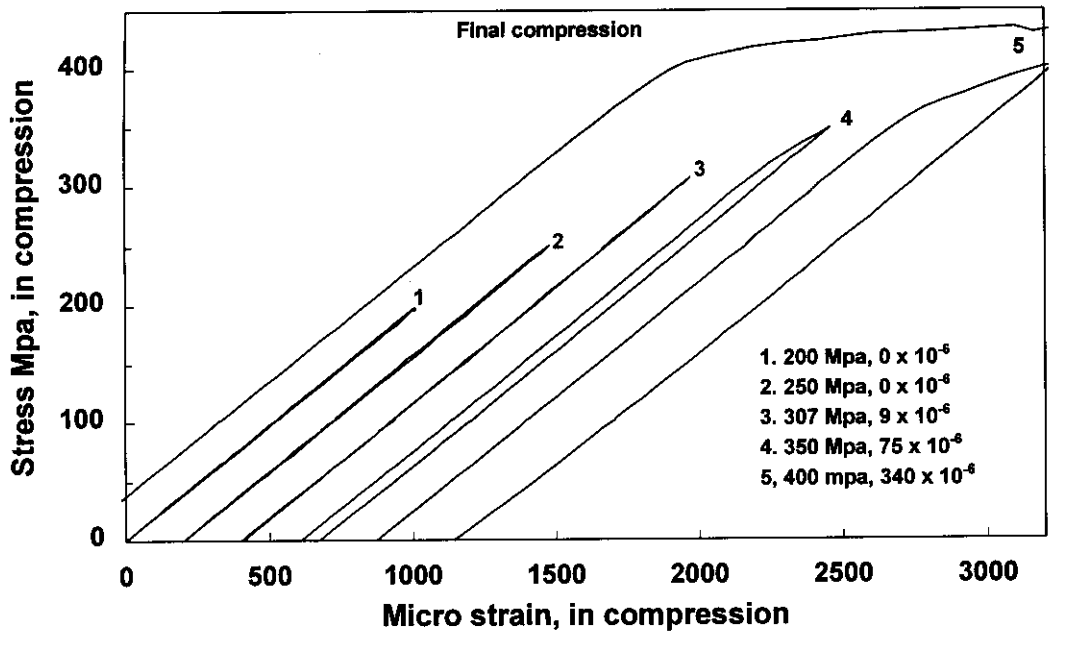

Figure 7-22. Typical stress-strain curves of coarse microstructure bar in zero to compression cyclic loading (36 mm diameter bar)

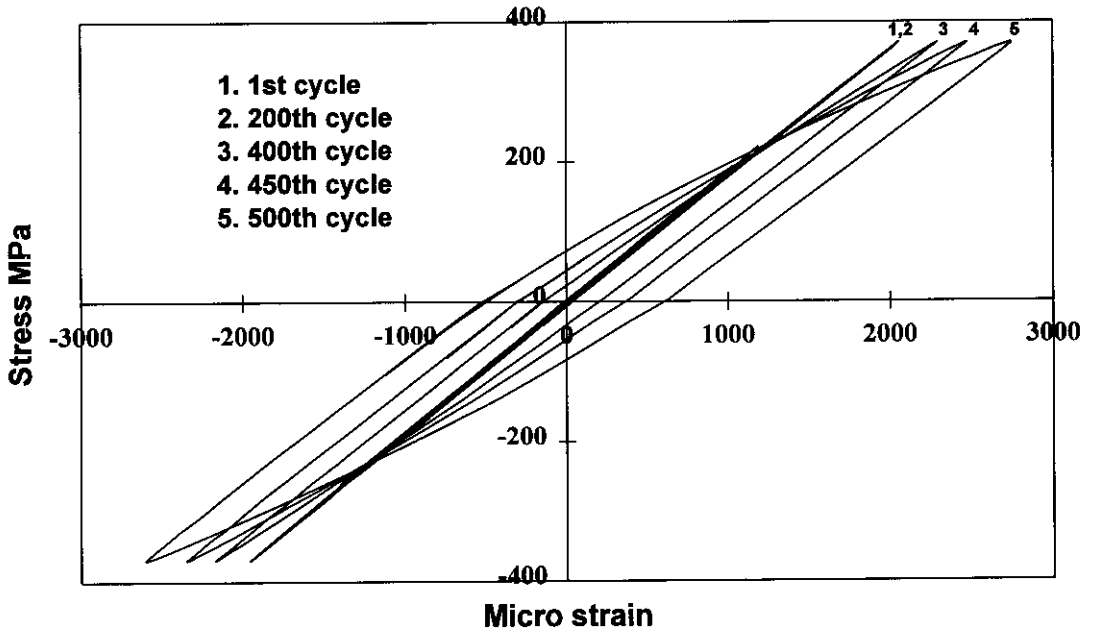

Figure 7-23. Typical hysteresis of fine microstructure bar (12 mm bar cycled at ± 372 MPa)

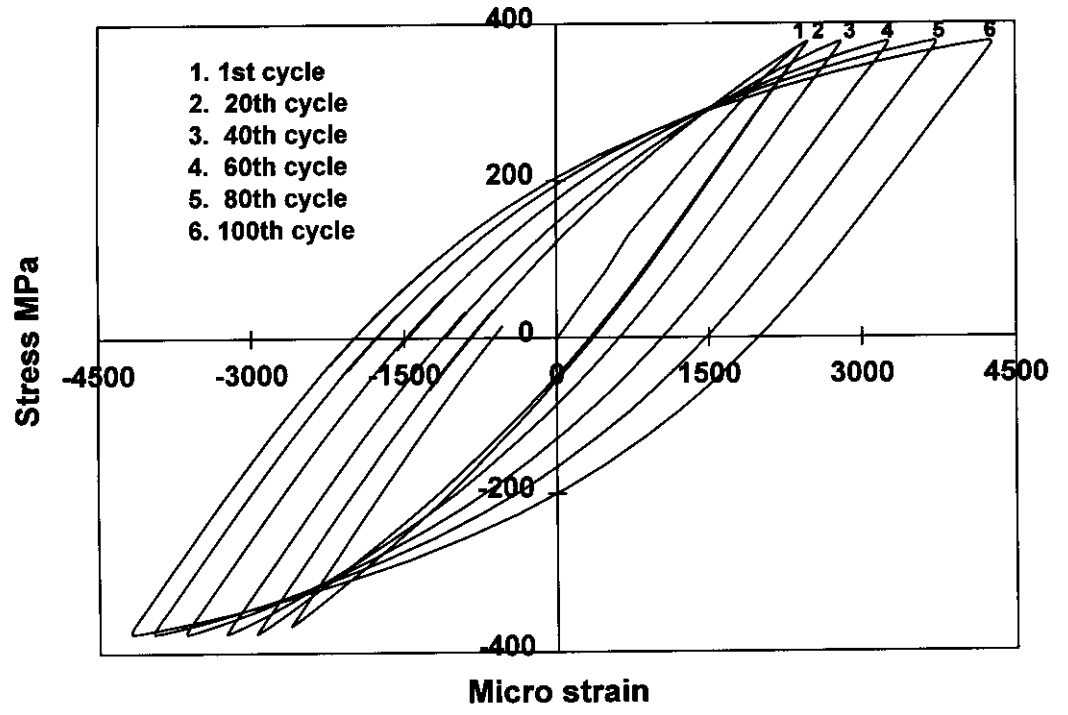

Figure 7-24. Typical hysteresis of coarse microstructure bar (32 mm bar cycled at ± 375 MPa)

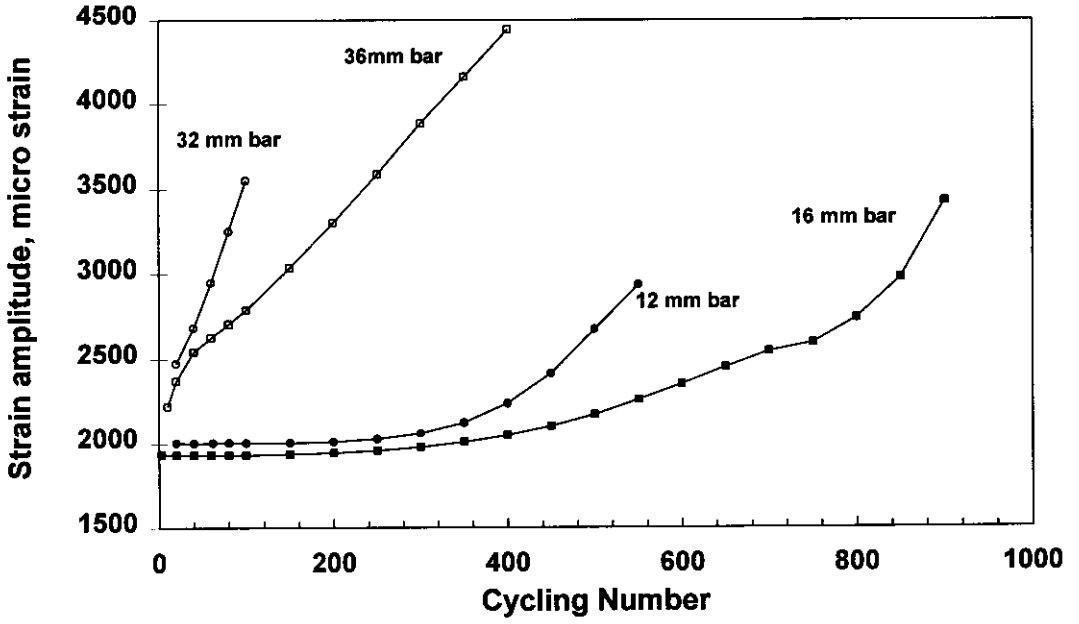

Figure 7-25. Strain softening at fully reversed loading (± 85% yield strength)

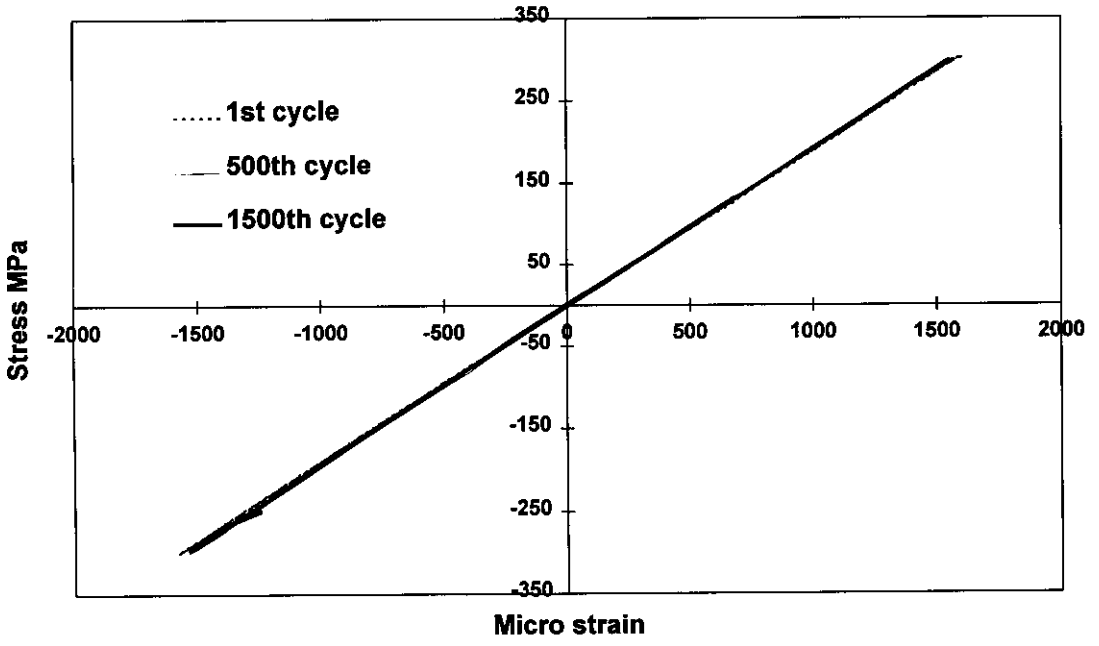

Figure 7-26. Stress-strain relationship of 16 mm bar cycled at ± 300 MPa

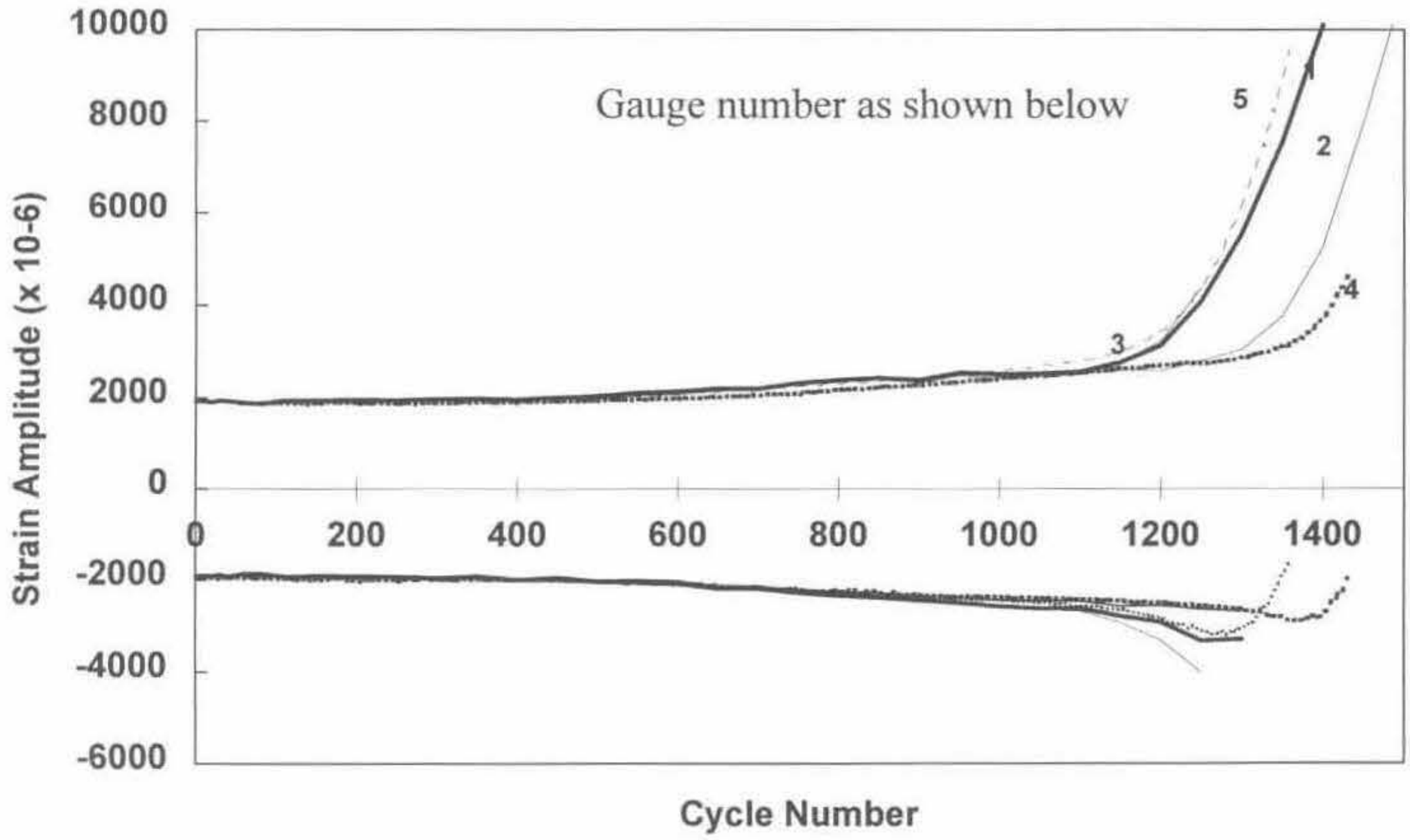

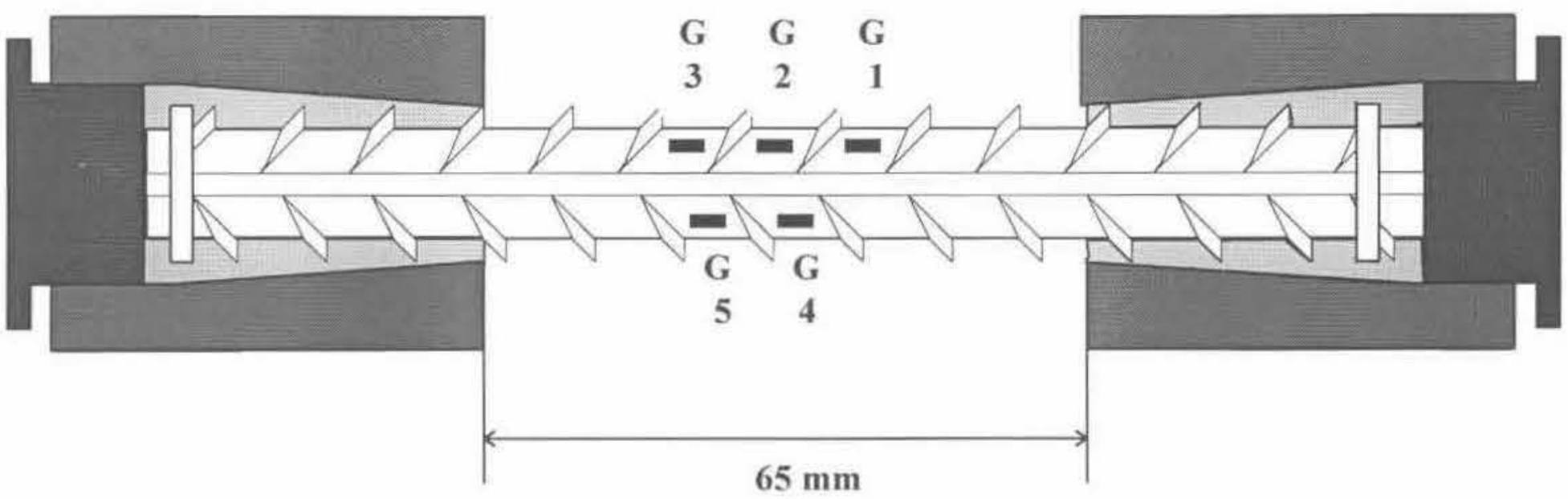

Figure 7-27. Strain response at the five gages; 16 mm bar cycled at ± 375 MPa

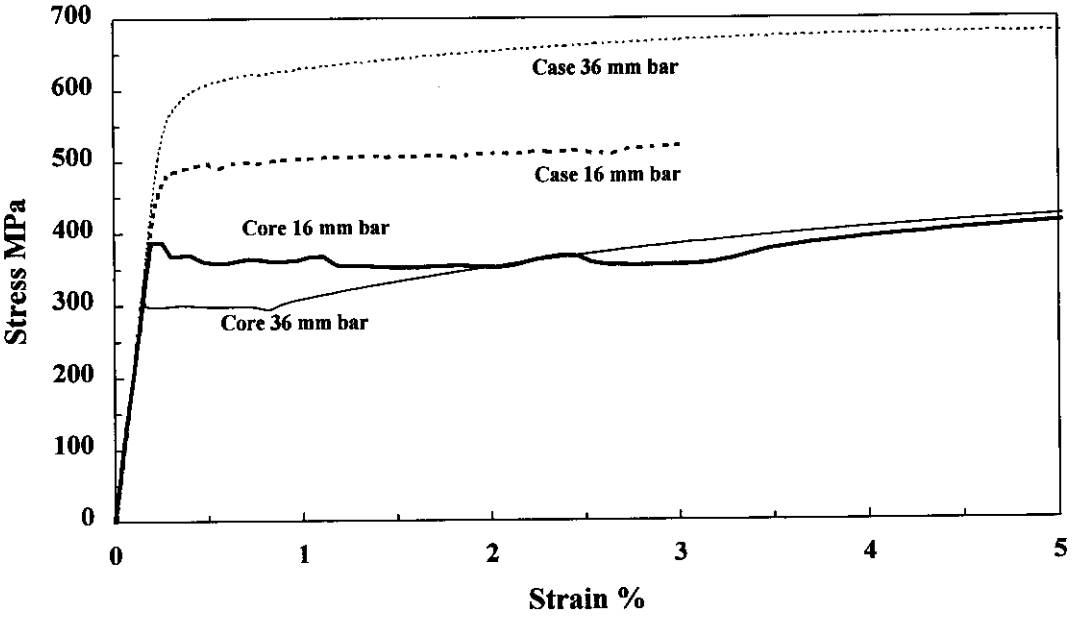

Figure 7-28. Stress strain curves of case and core materials

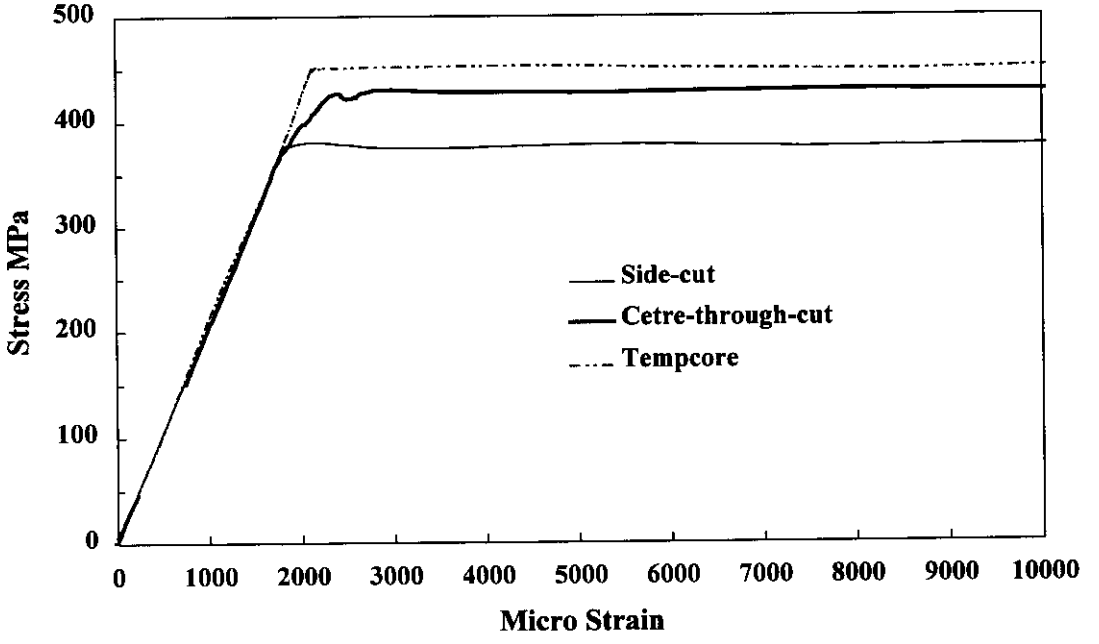

Figure 7-29. Stress-strain curves of cut-specimens and as received bar

(a) 16 mm diameter bar

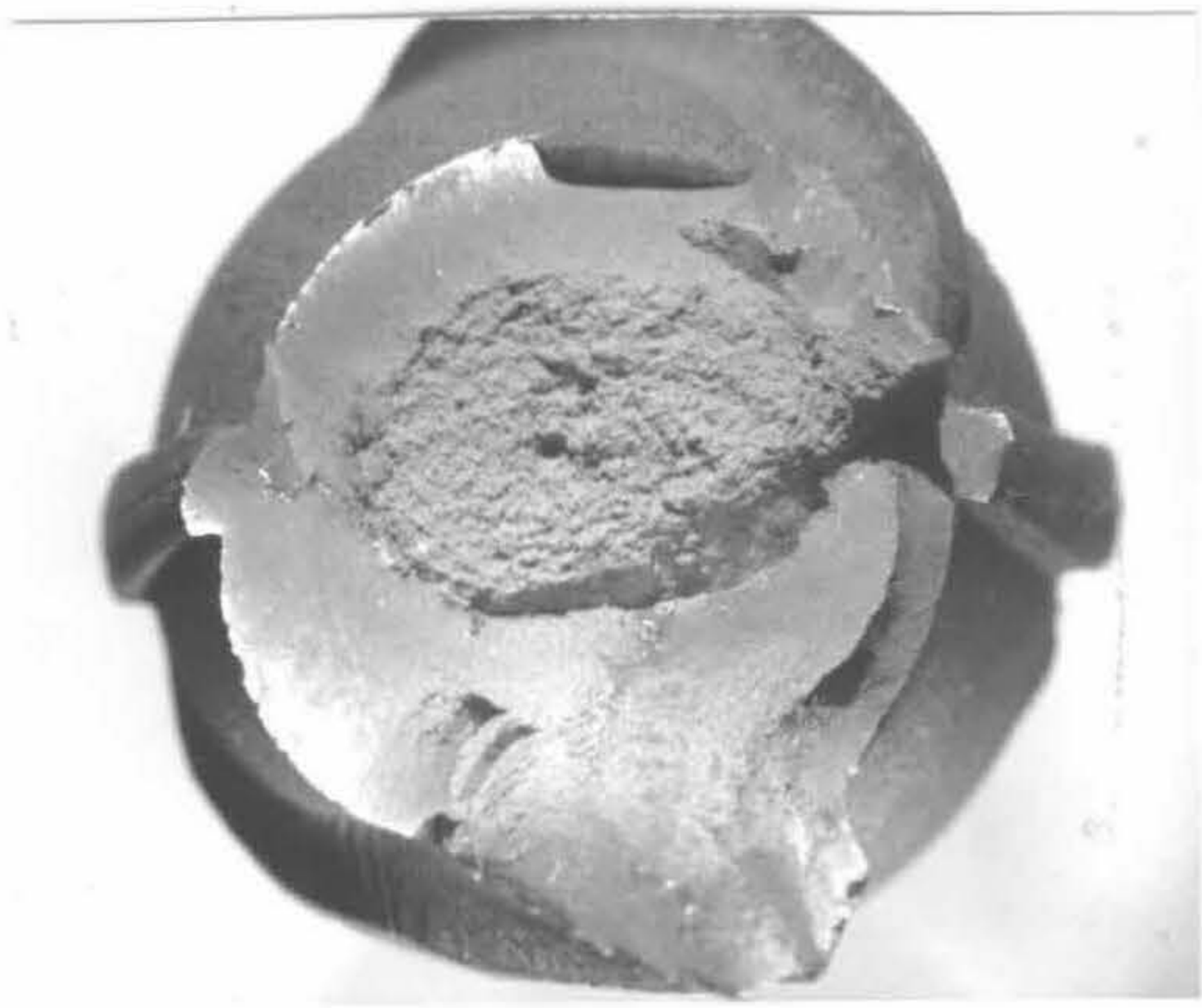

(b) 36 mm diameter bar

Figure 7-30. Typical fractures in tension, TEMPCORE reinforcing steels

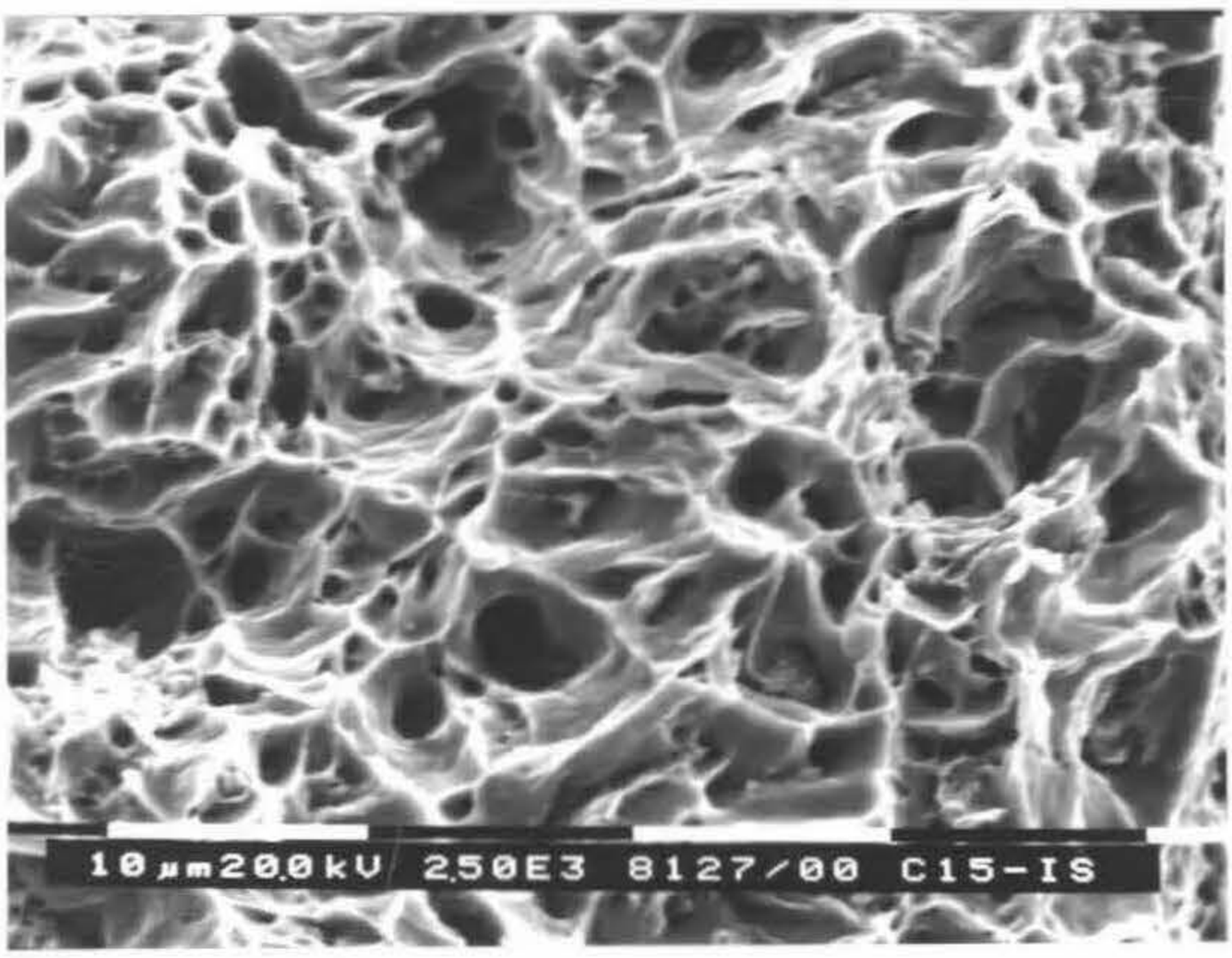

(a) 16 mm diameter bar

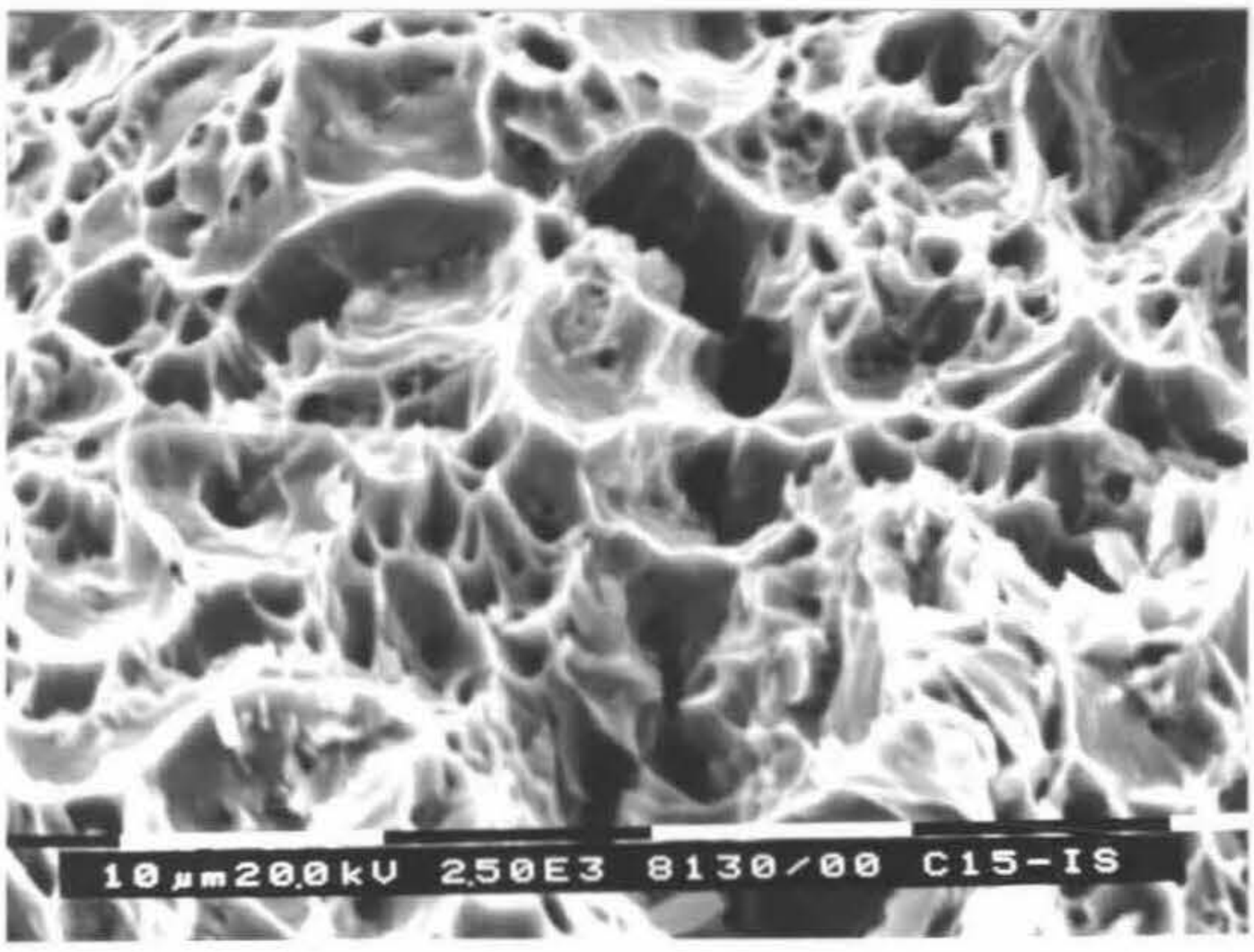

(b) 36 mm diameter bar

Figure 7-31. Dimples at the bottom of the fractured cup-section

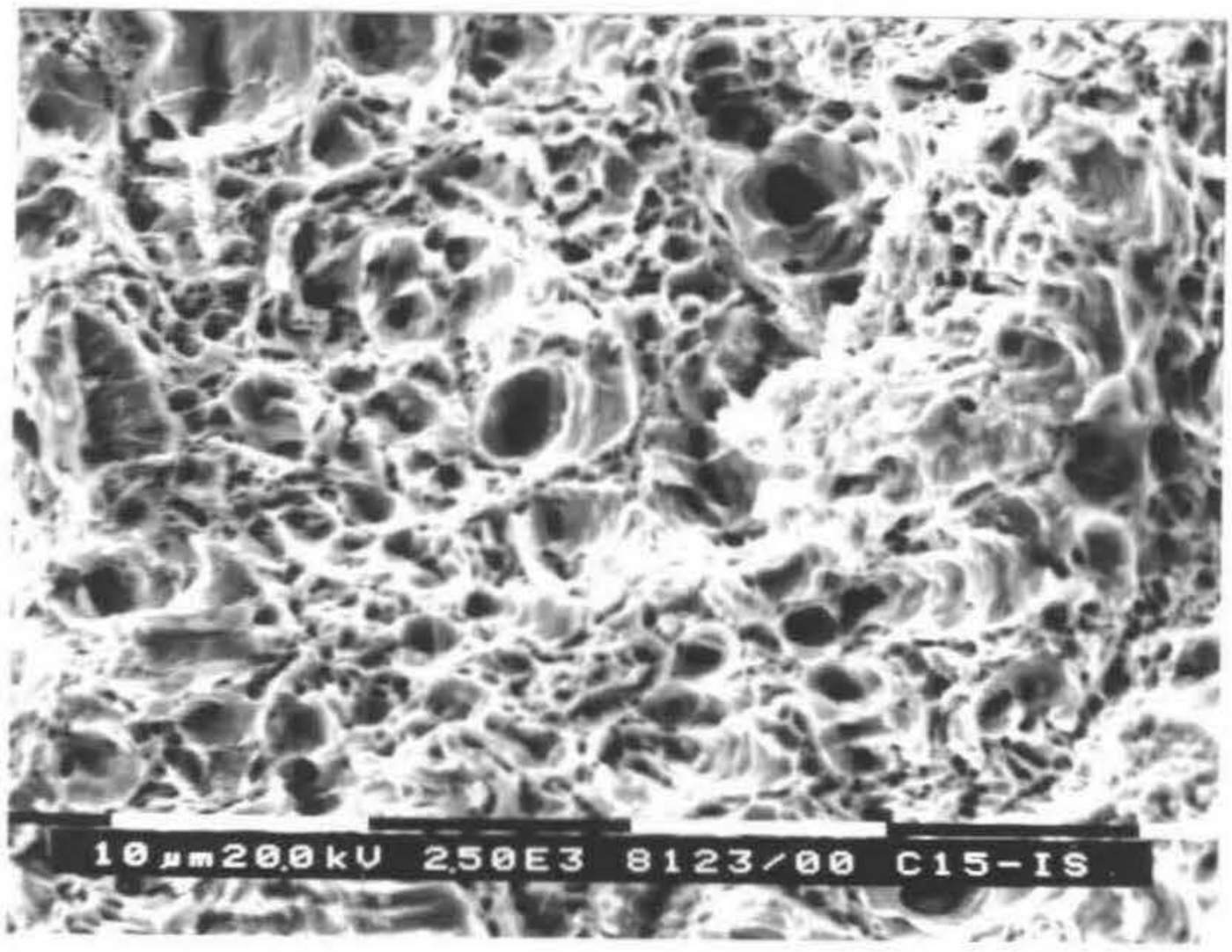

(a) 16 mm diameter bar

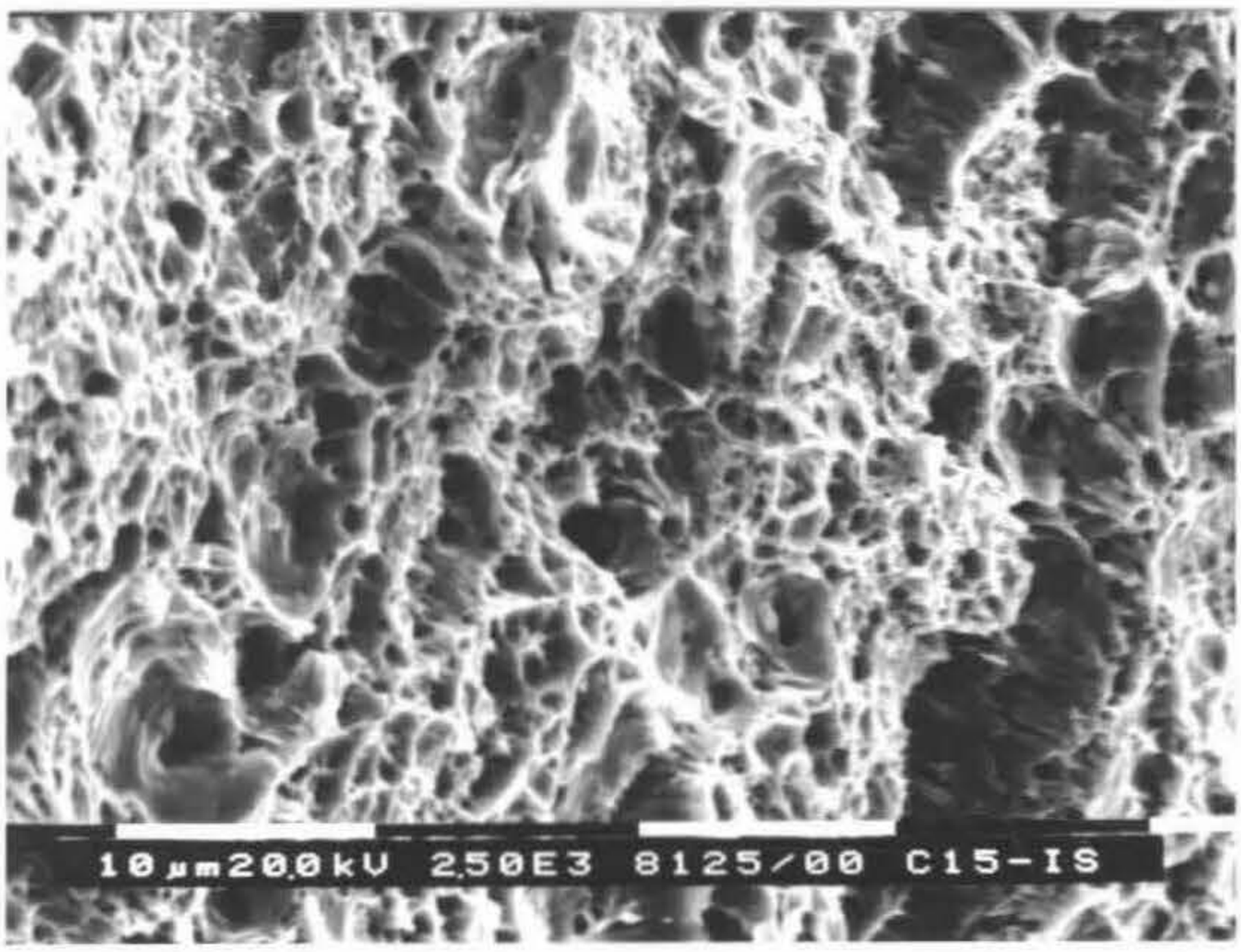

(b) 36 mm diameter bar

Figure 7-32. Case materials in tension tests showing excessive dimples

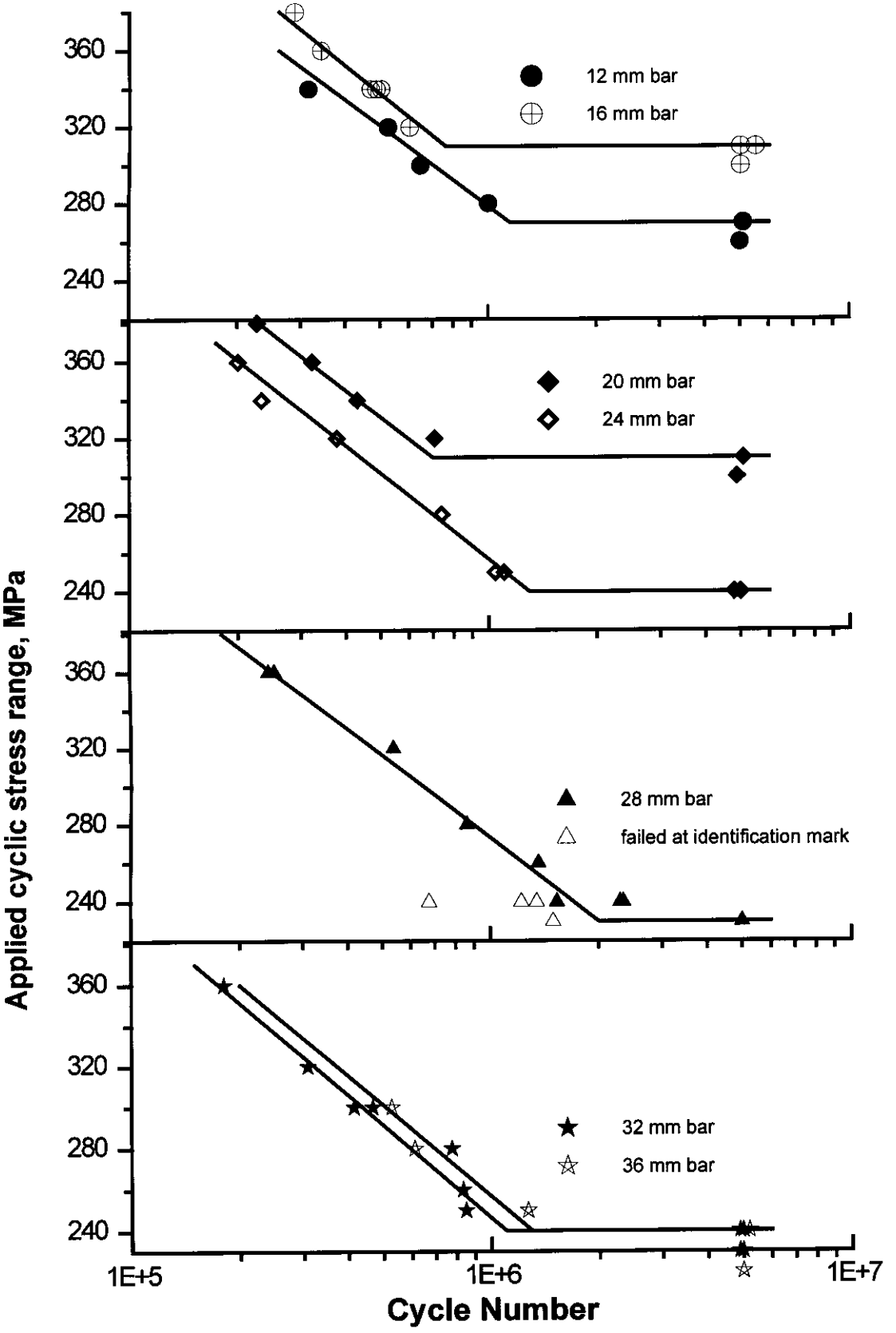

Figure 7-33. S-N curves of TEMPCORE bars

Figure 7-34. Typical fatigue fractures

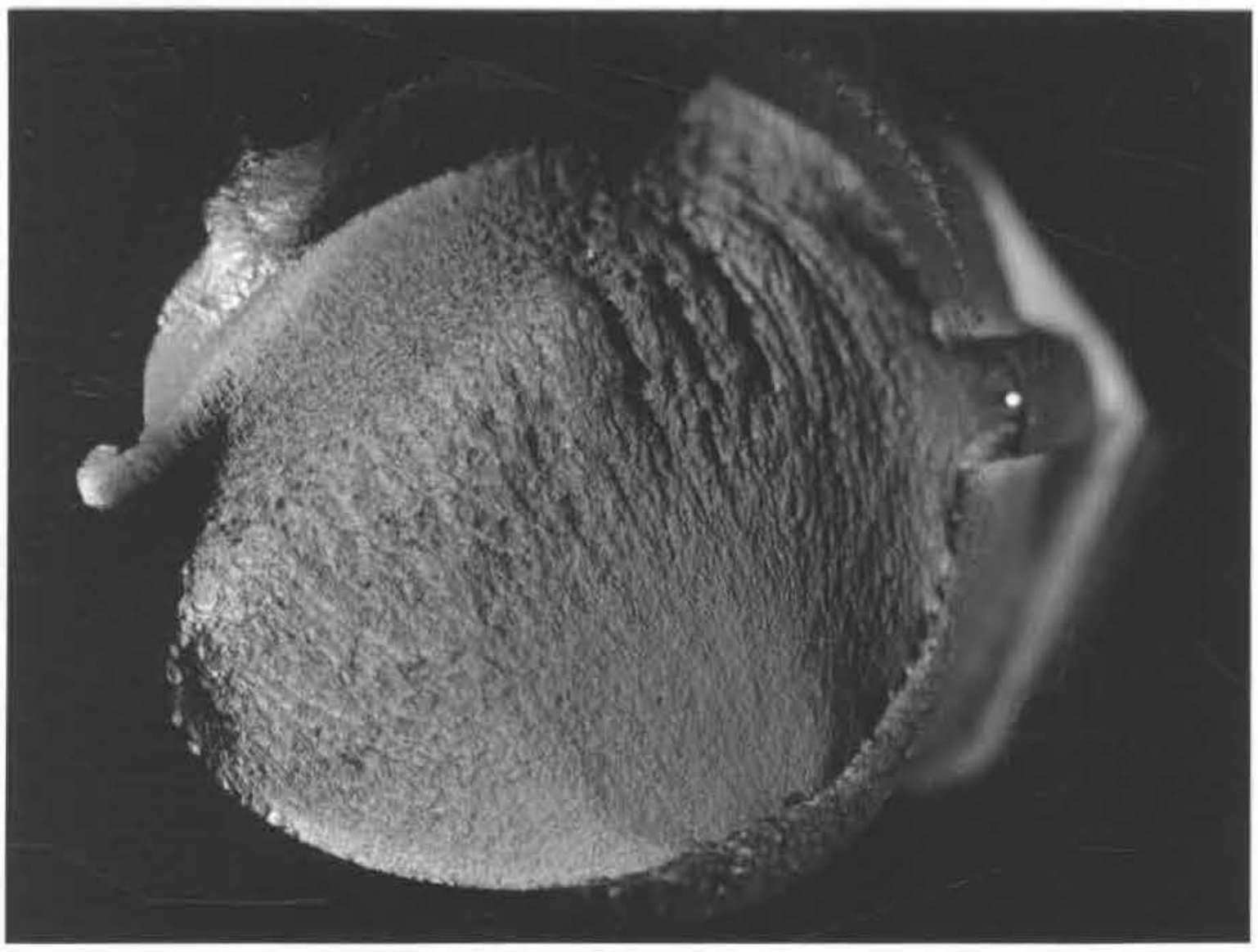

(a) single initiation at lug root (36 mm bar, $\Delta\sigma$ = 250 MPa)

(b) multiple initiation at lug root (32 mm bar, $\Delta\sigma$ = 360 MPa)

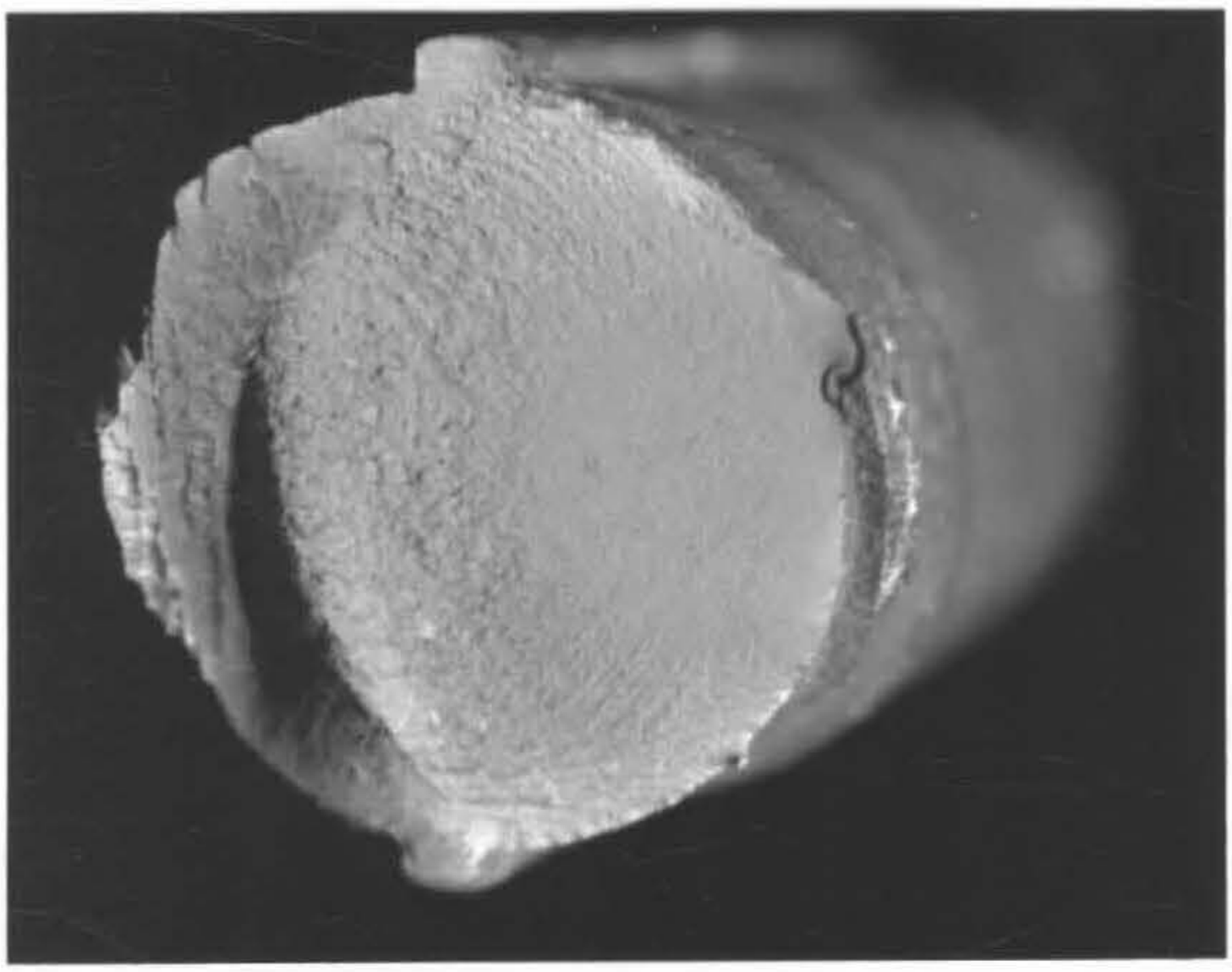

(c) initiation at identification mark (28 mm bar)

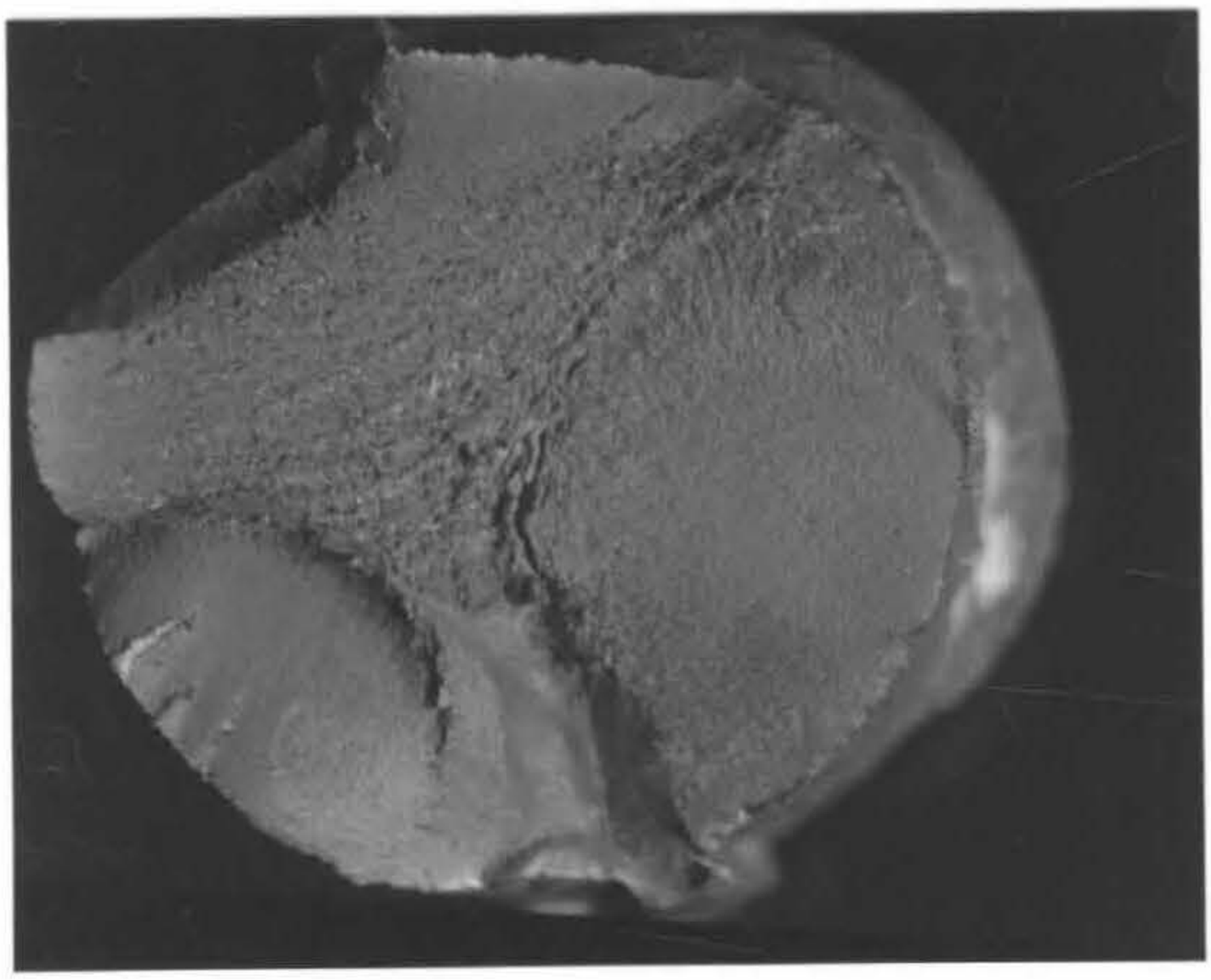

(d) initiation at opposite transverse lugs (28 mm bar, 320 MPa)

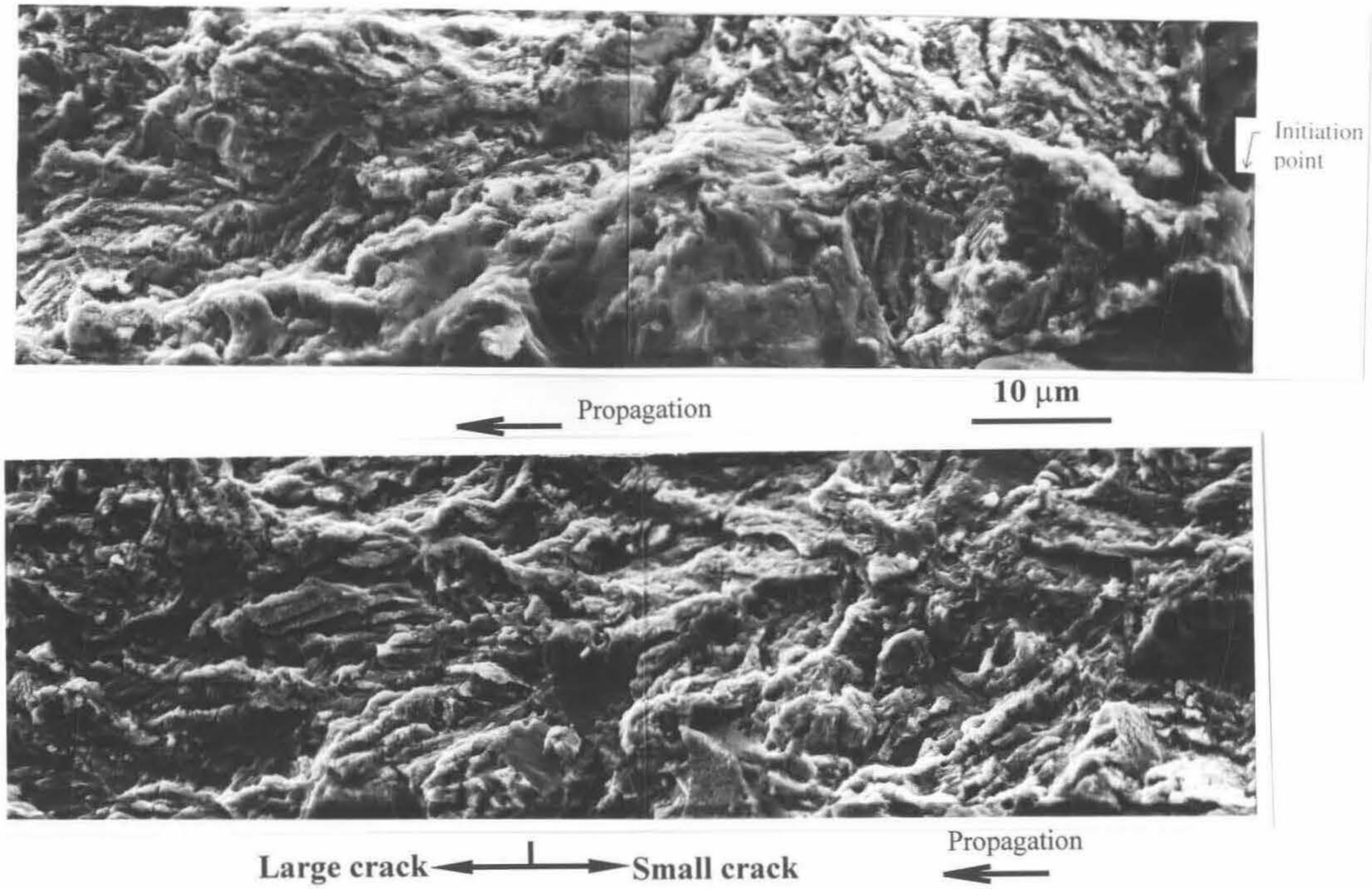

Figure 7-35. Fatigue fracture of early crack (16F340-1)

Figure 7-36. Fracture at 40 µm away from initiation point (16F340-1)

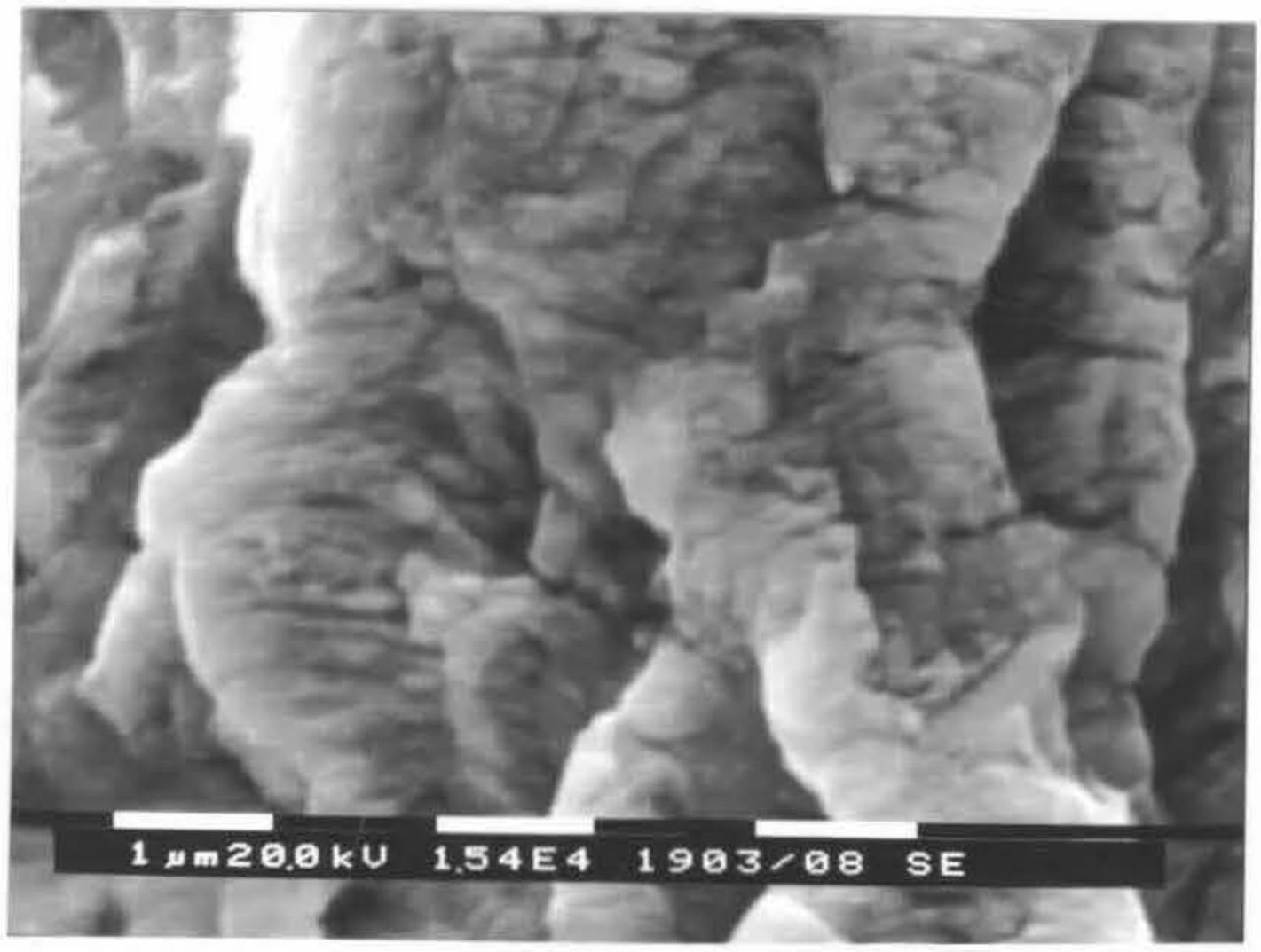

(a) SEM image

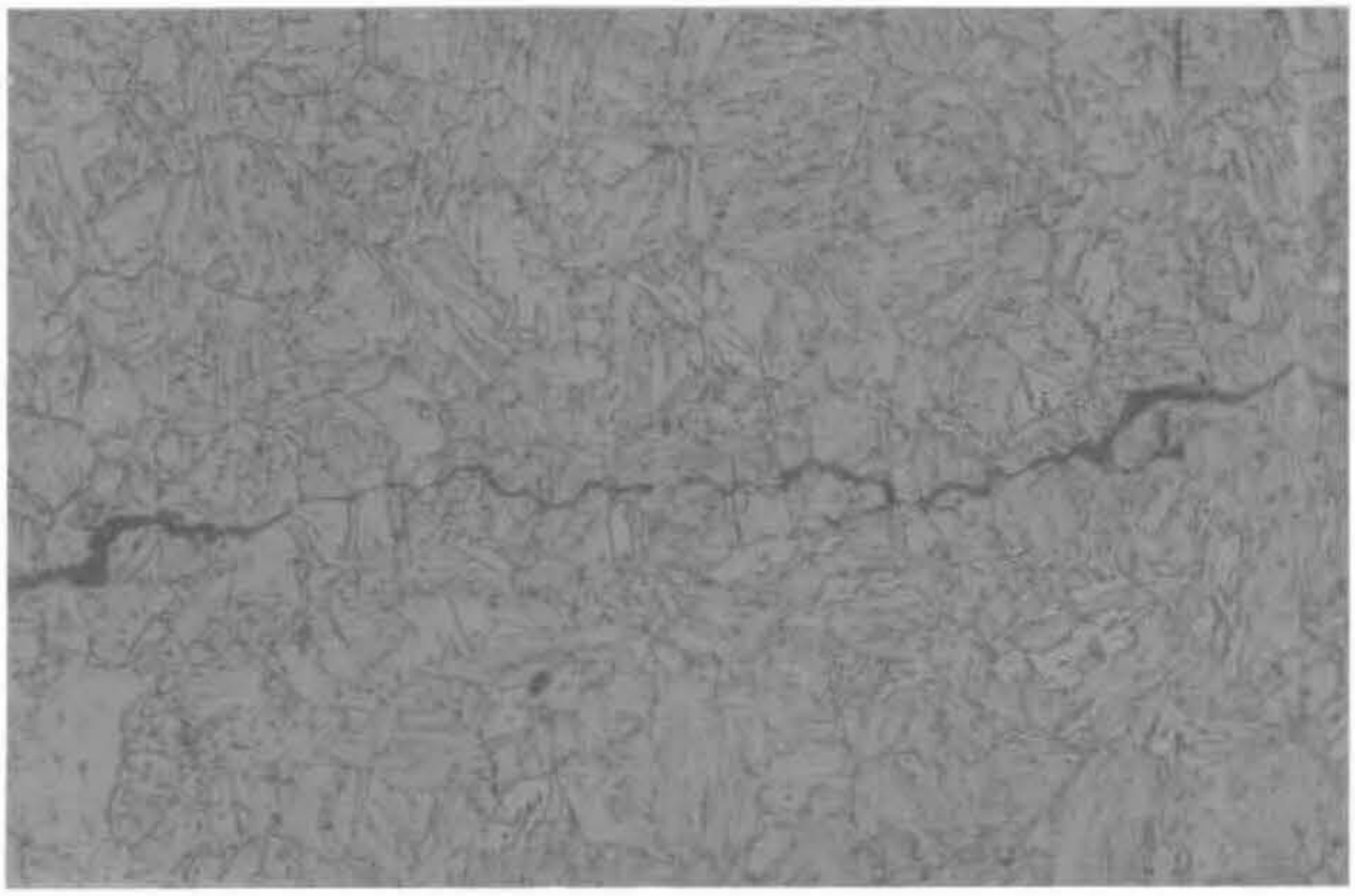

(b) Perspective of propagation in hardened layer (x 800)

Figure 7-37. Fracture at 165 μm away from initiation point (16F340-1)

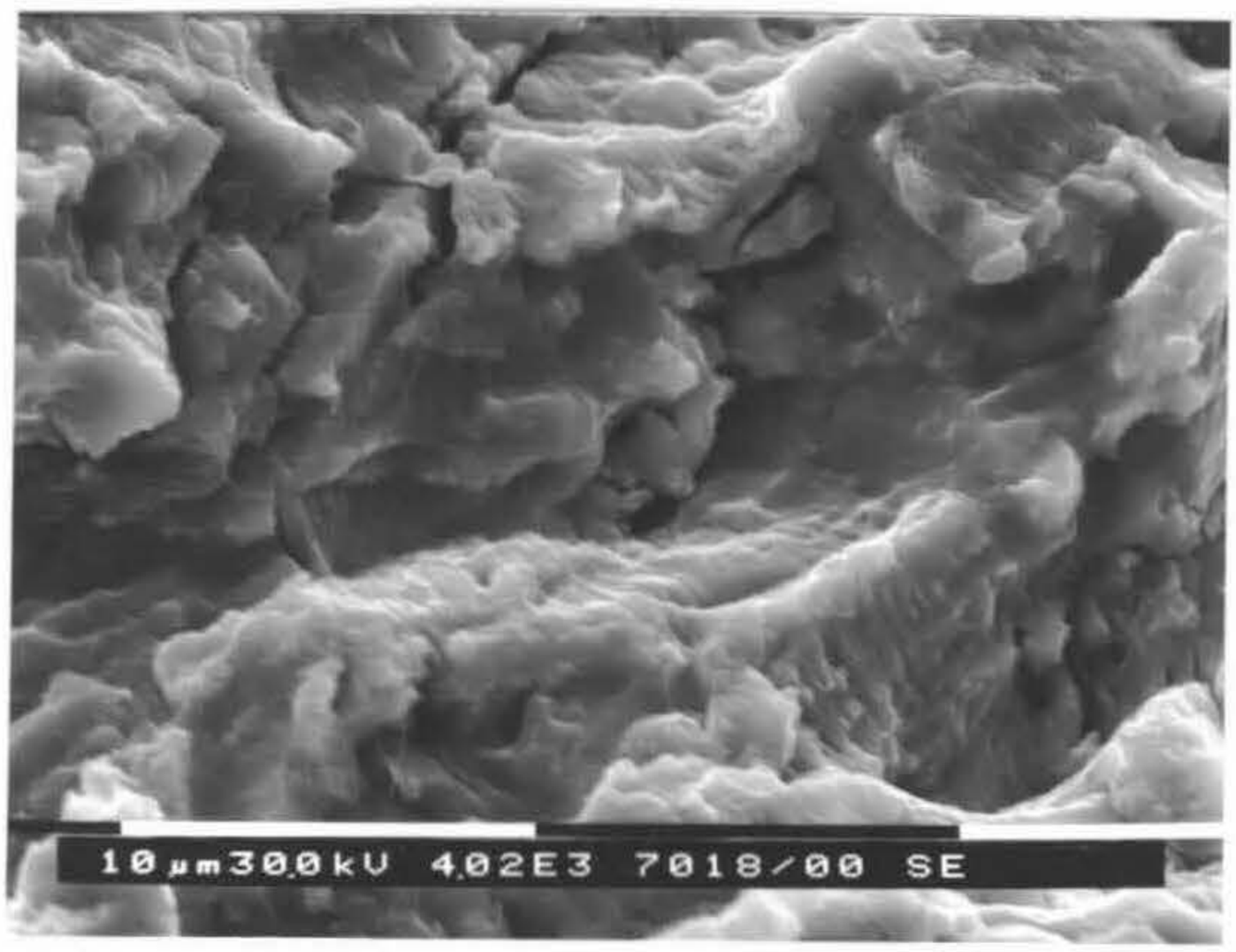

Figure 7-38. SEM image of fatigue fracture in unhardened area (16F340-1)

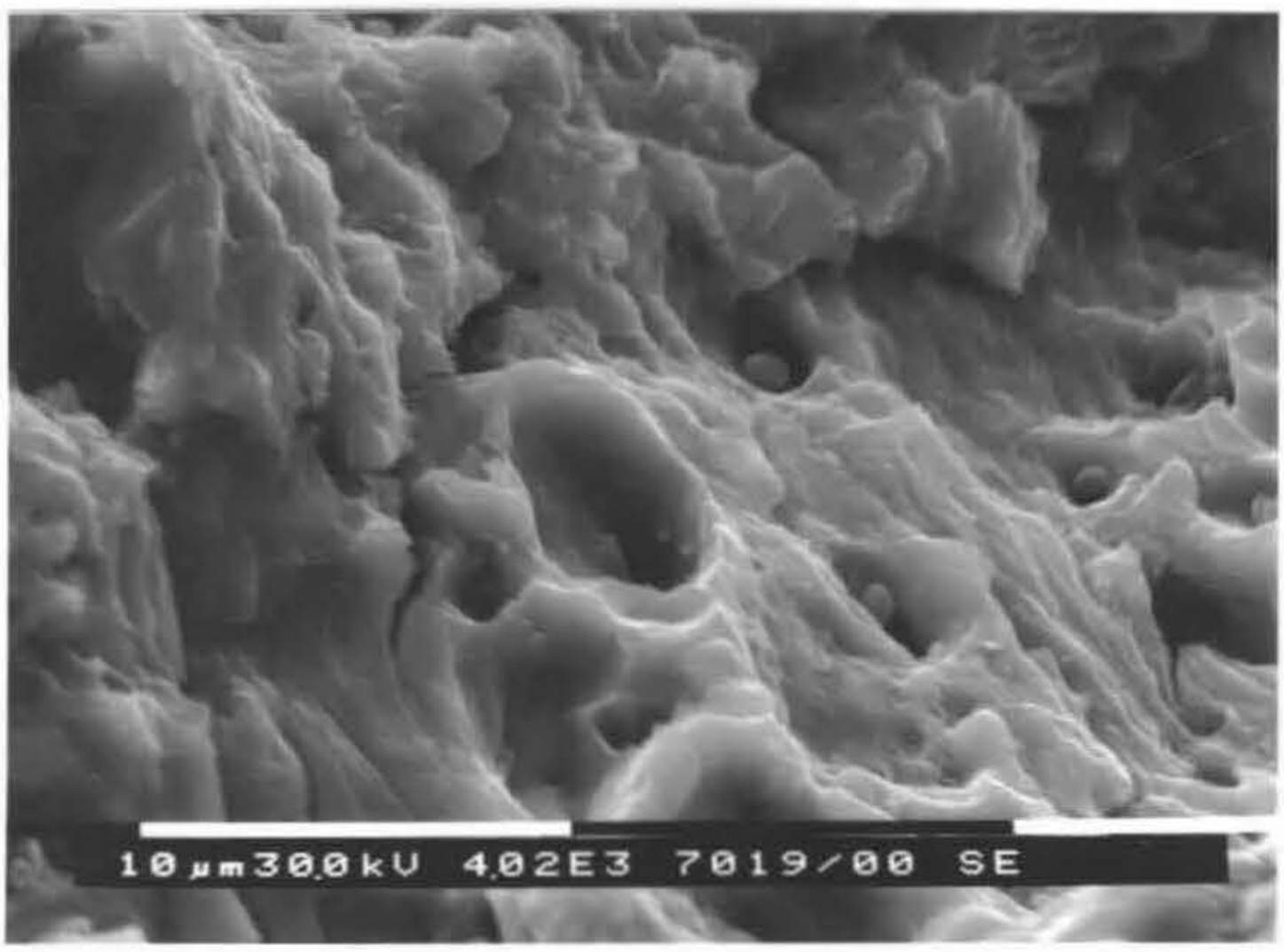

Figure 7-39. SEM image next to final rupture (16F340-1)

Figure 7-40. Small cracks revealed by tensile fatigued specimens

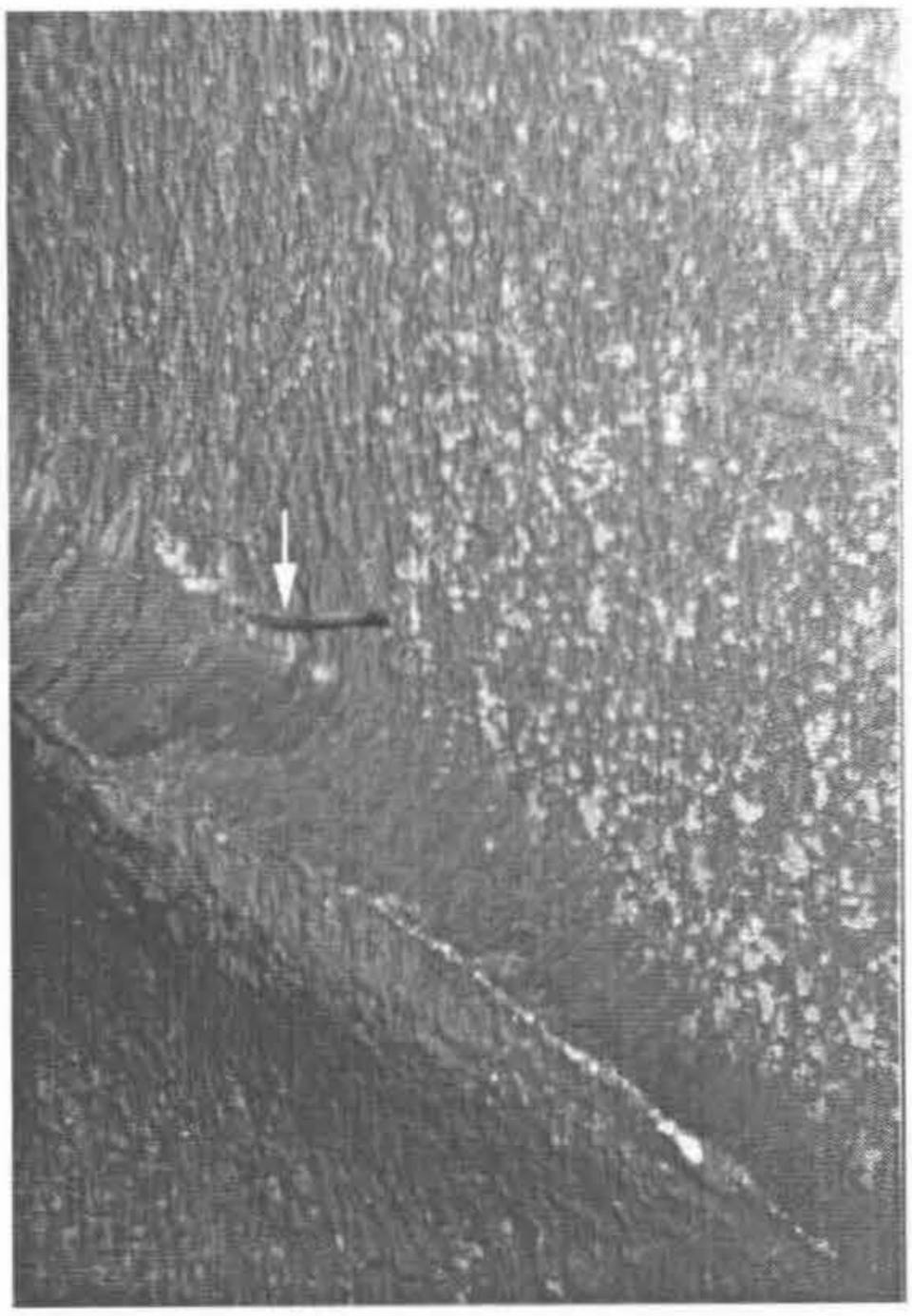

(a) single initiation at the lug root (16 mm bar, 340 MPa)

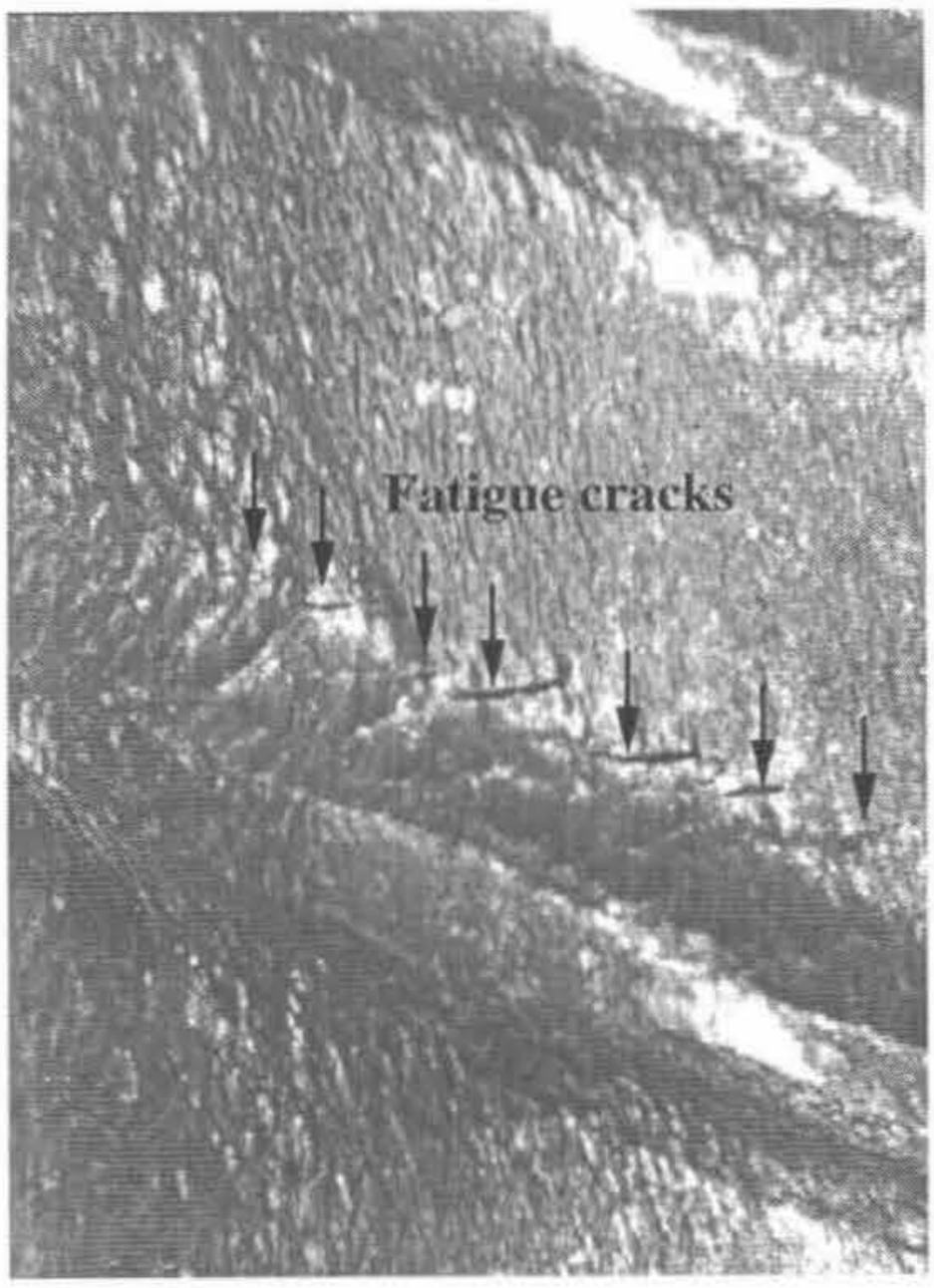

(b) multiple initiation at the lug root (12 mm bar, 340 MPa)

Figure 7-40 continue

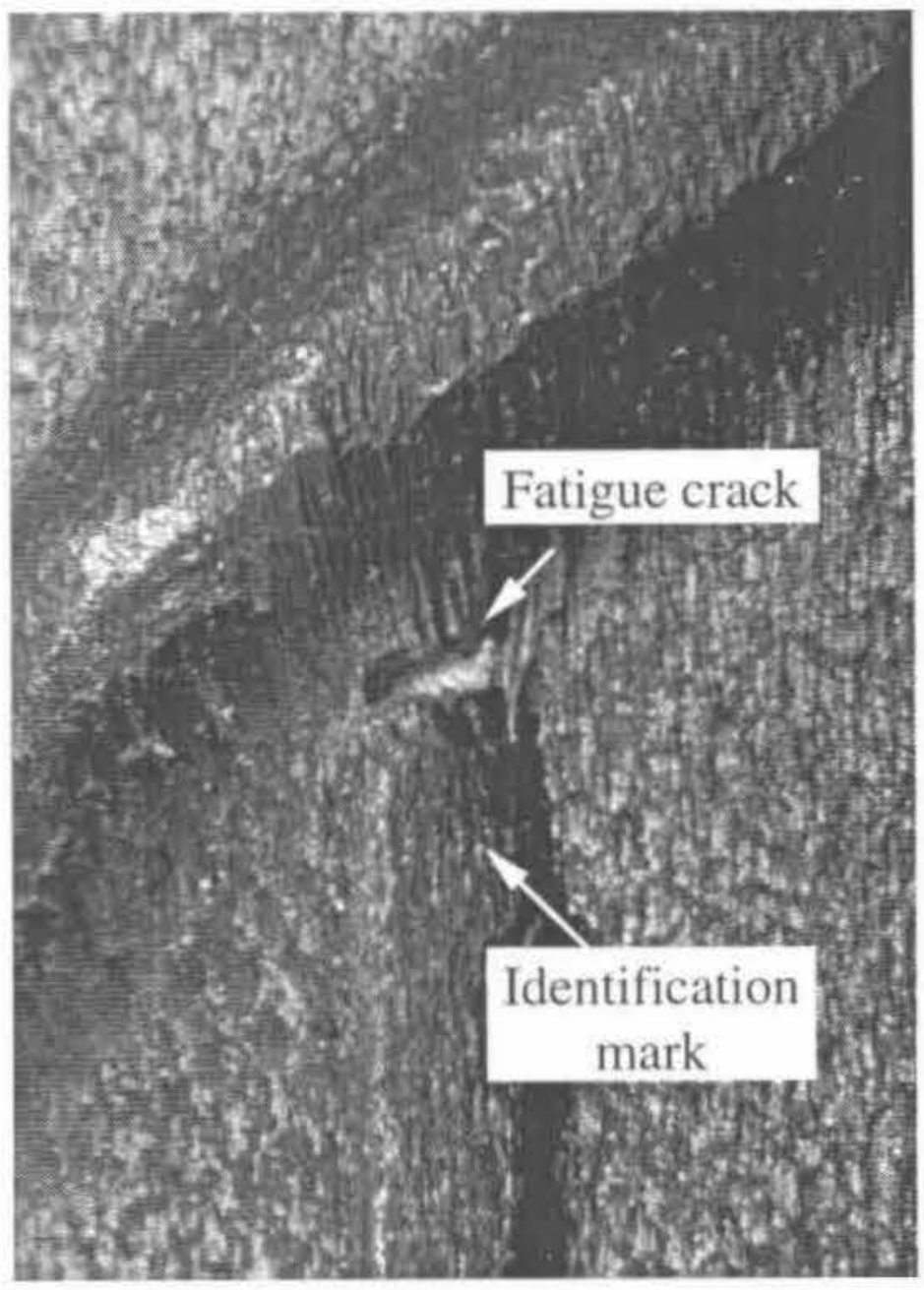

(c) initiate at identification mark (16 mm bar)

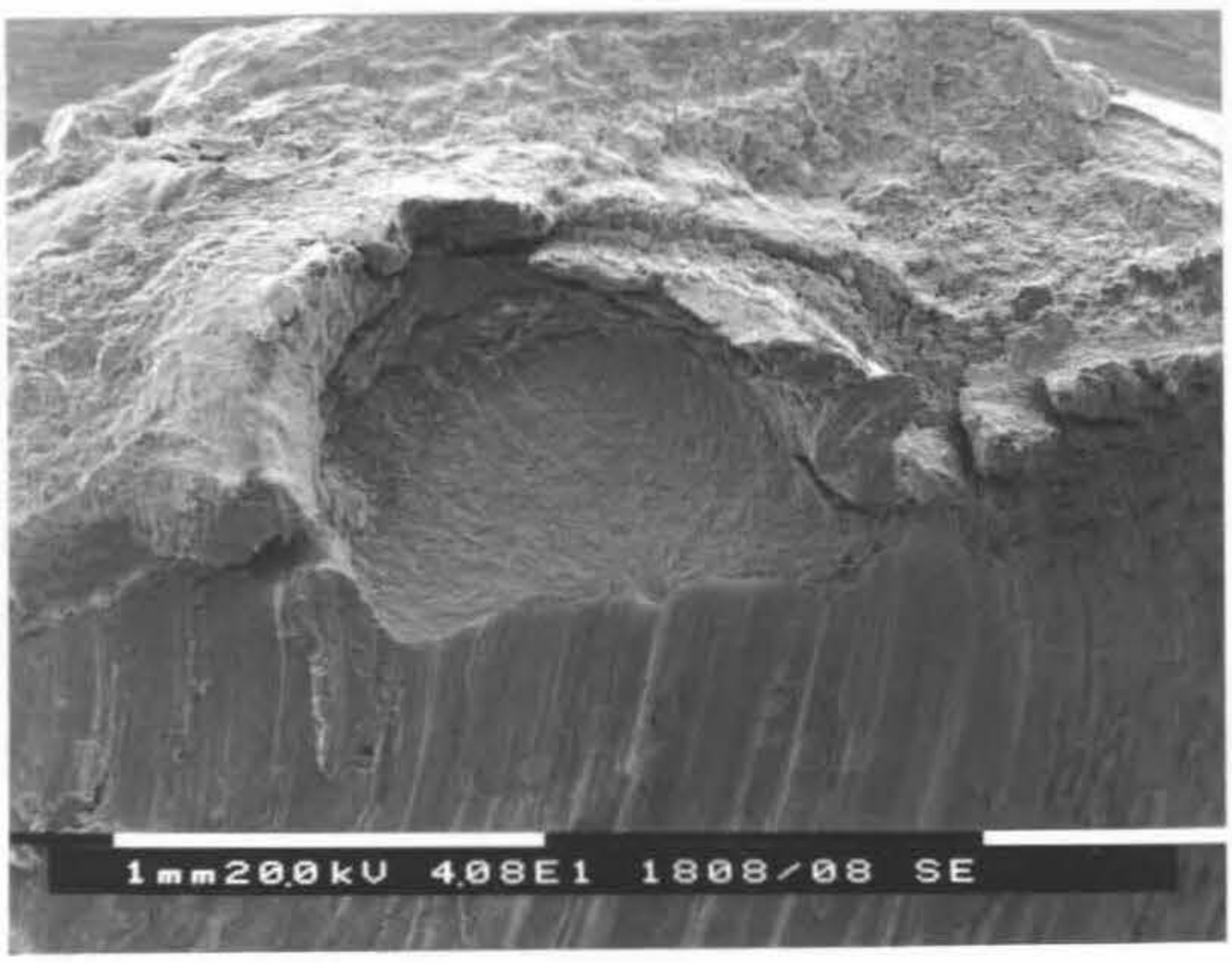

(d) cross sectional view of a small fatigue crack

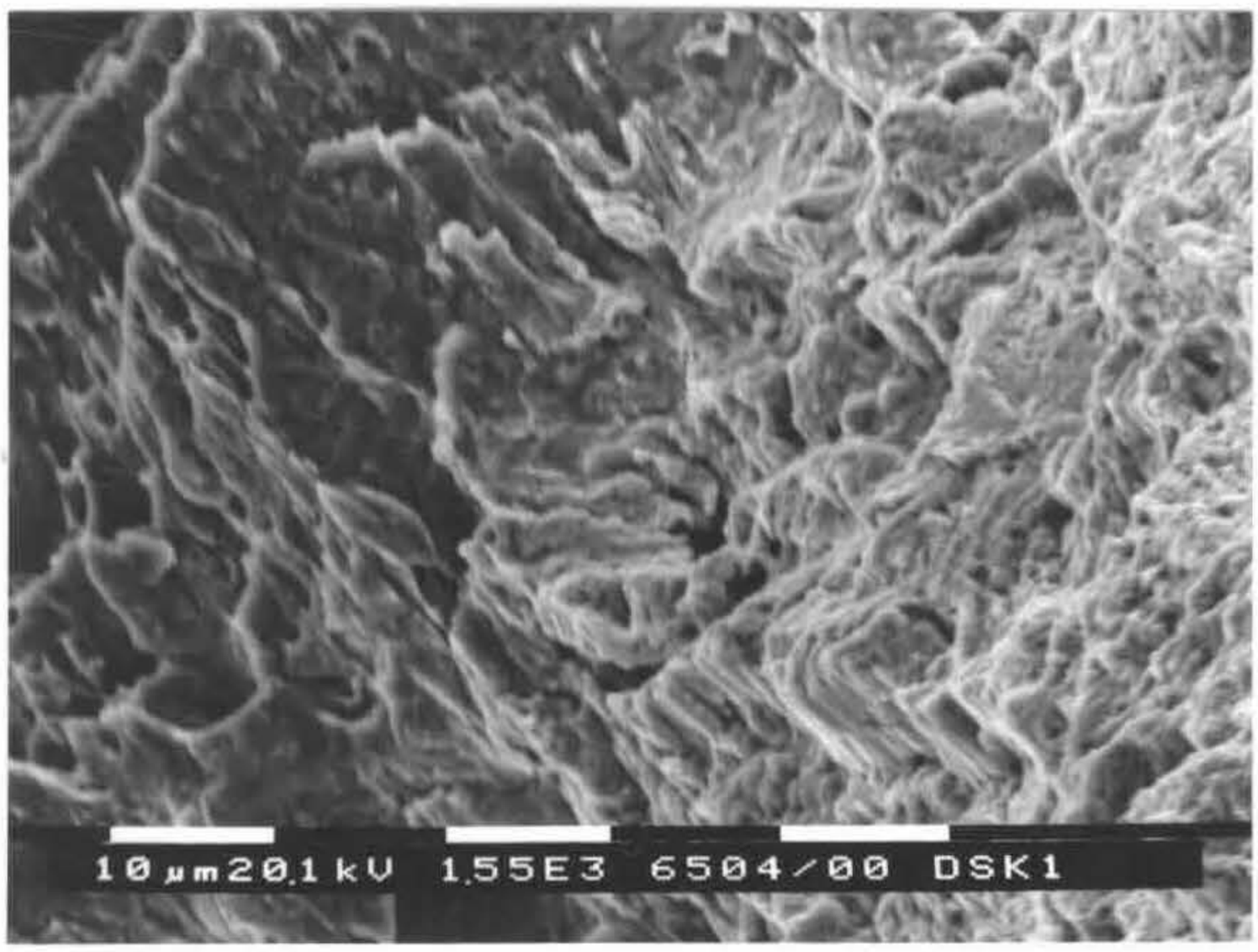

(a) Fracture showing fatigue and ductile rupture in subsequent tensile loading

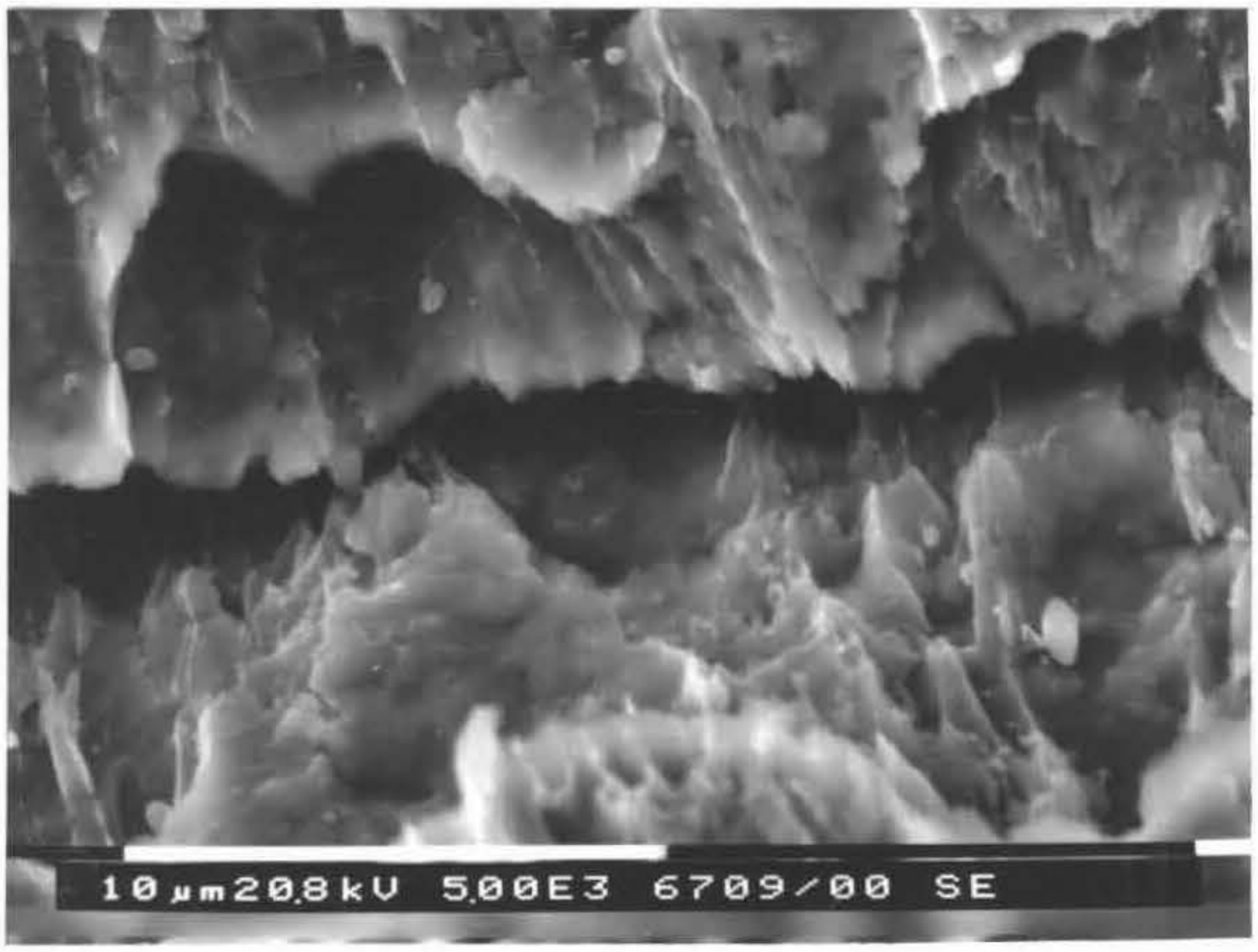

(b) Ductile rupture near crack tip in subsequent tensile loading,

Figure 7-41. Ductile rupture at the crack tip: tensile fracture after fatigue

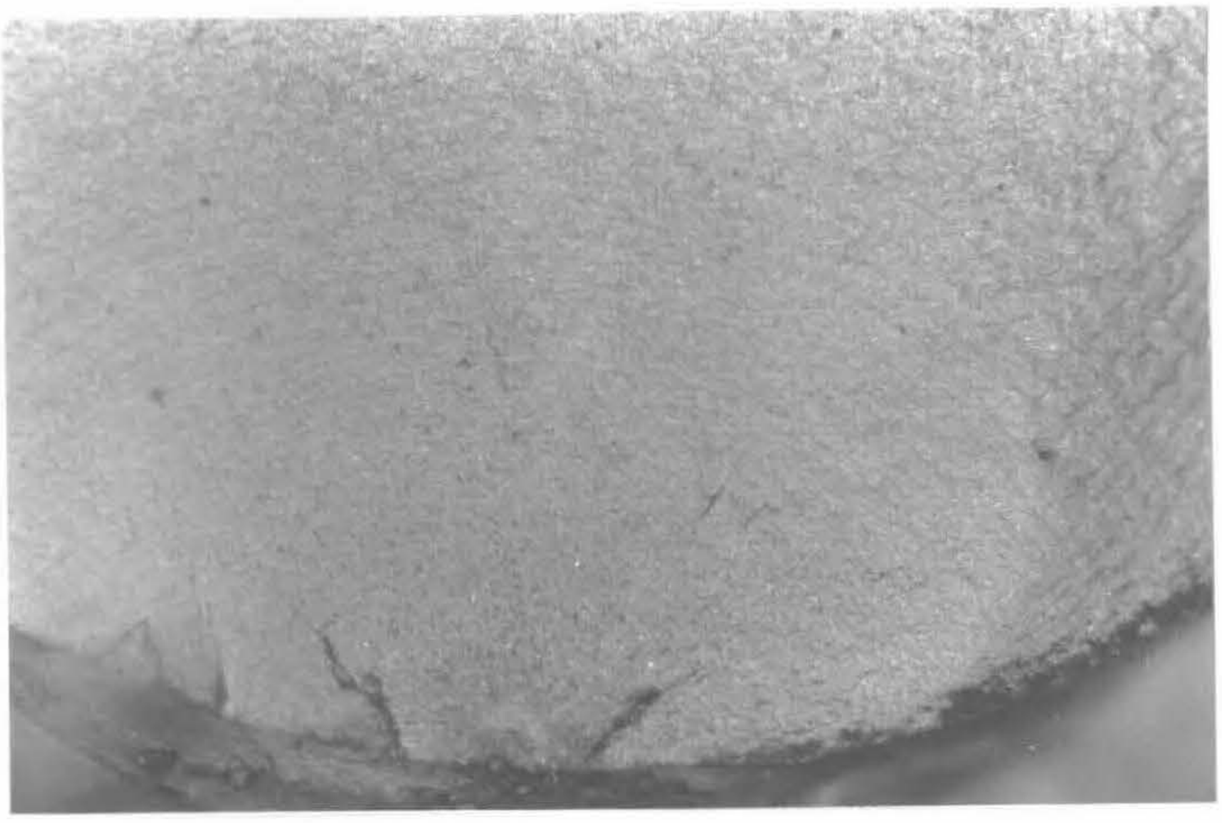

Figure 7-42. Beach marks indicating fatigue propagation

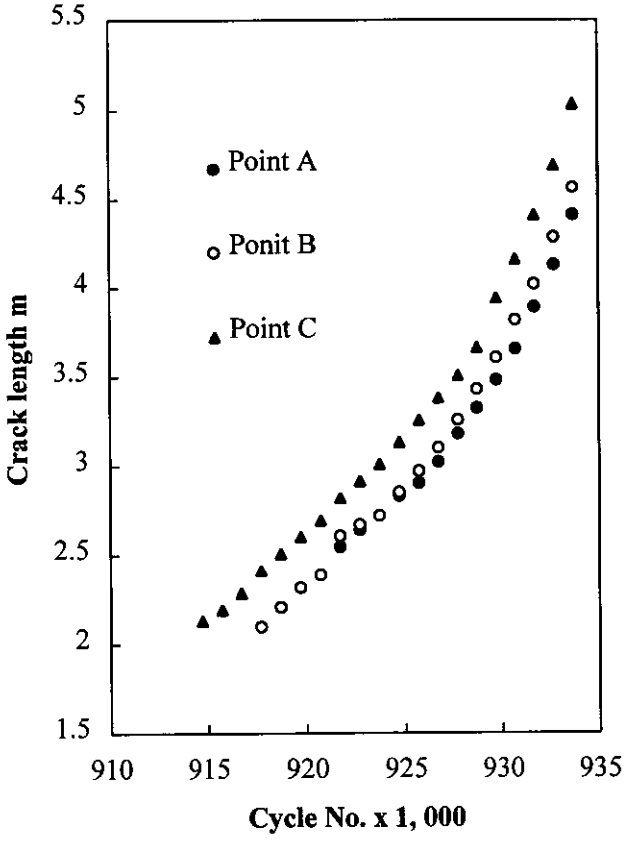

(a) Crack length via cycle number

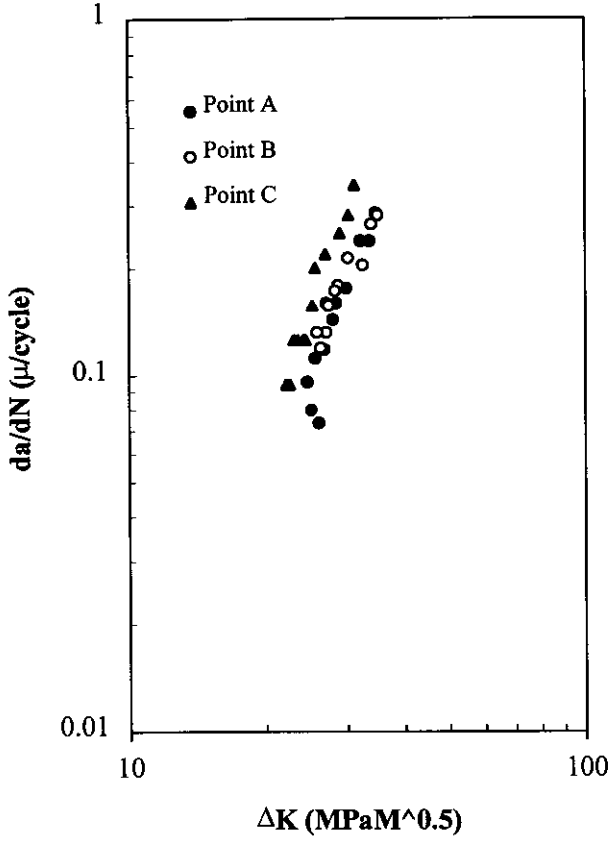

(b) Crack growth rate via ΔK

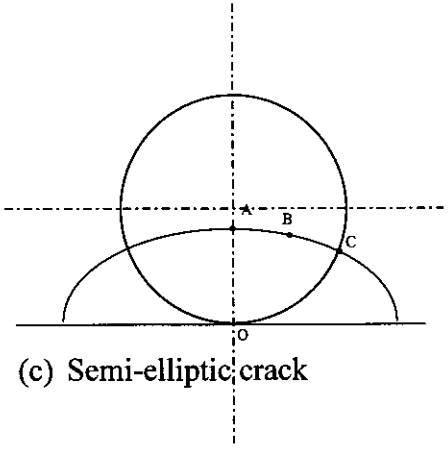

(c) Semi-elliptic crack

Figure 7-43.Crack growth data for 16 mm bar fatigue at $\Delta\sigma$ = 340 MPa

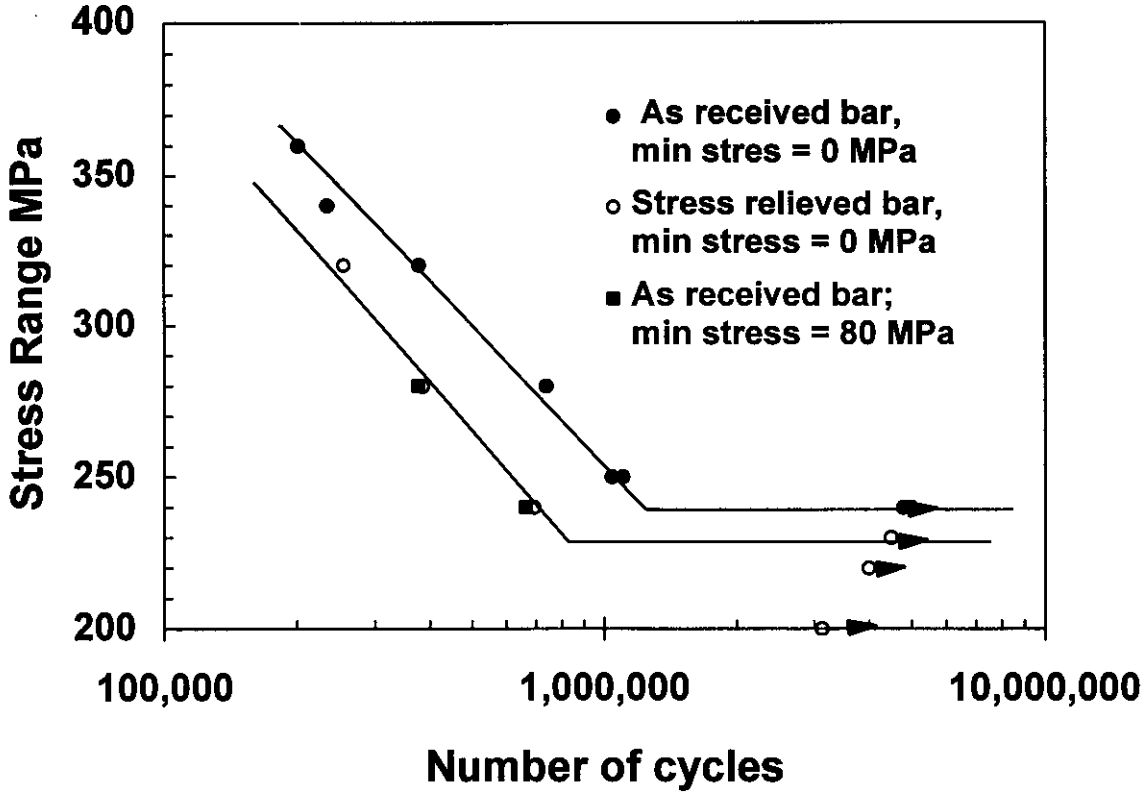

Figure 7-44. The effect of stress relieving and minimum cyclic stress

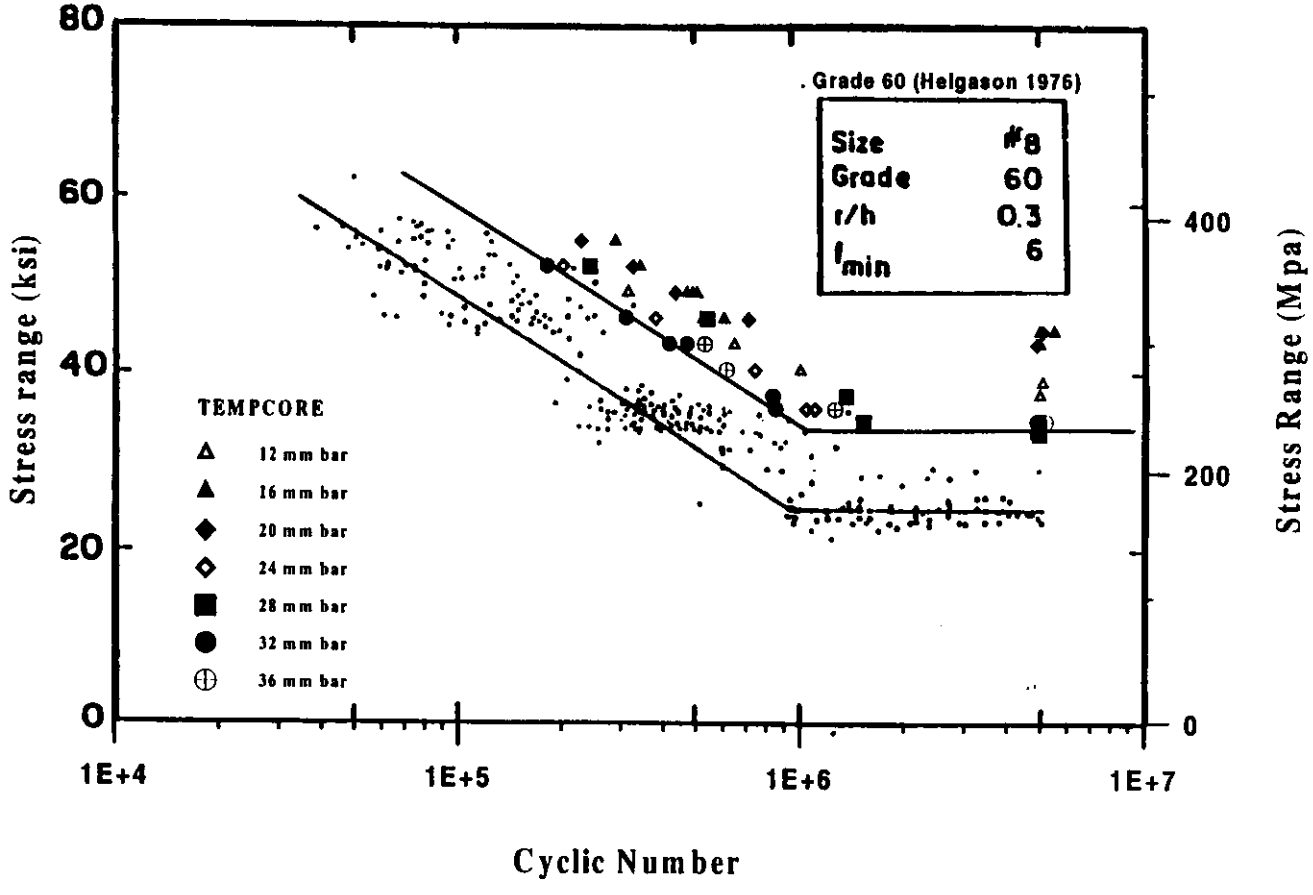

Figure 7-45. Comparison fatigue results with Grade 60 reinforcing steel

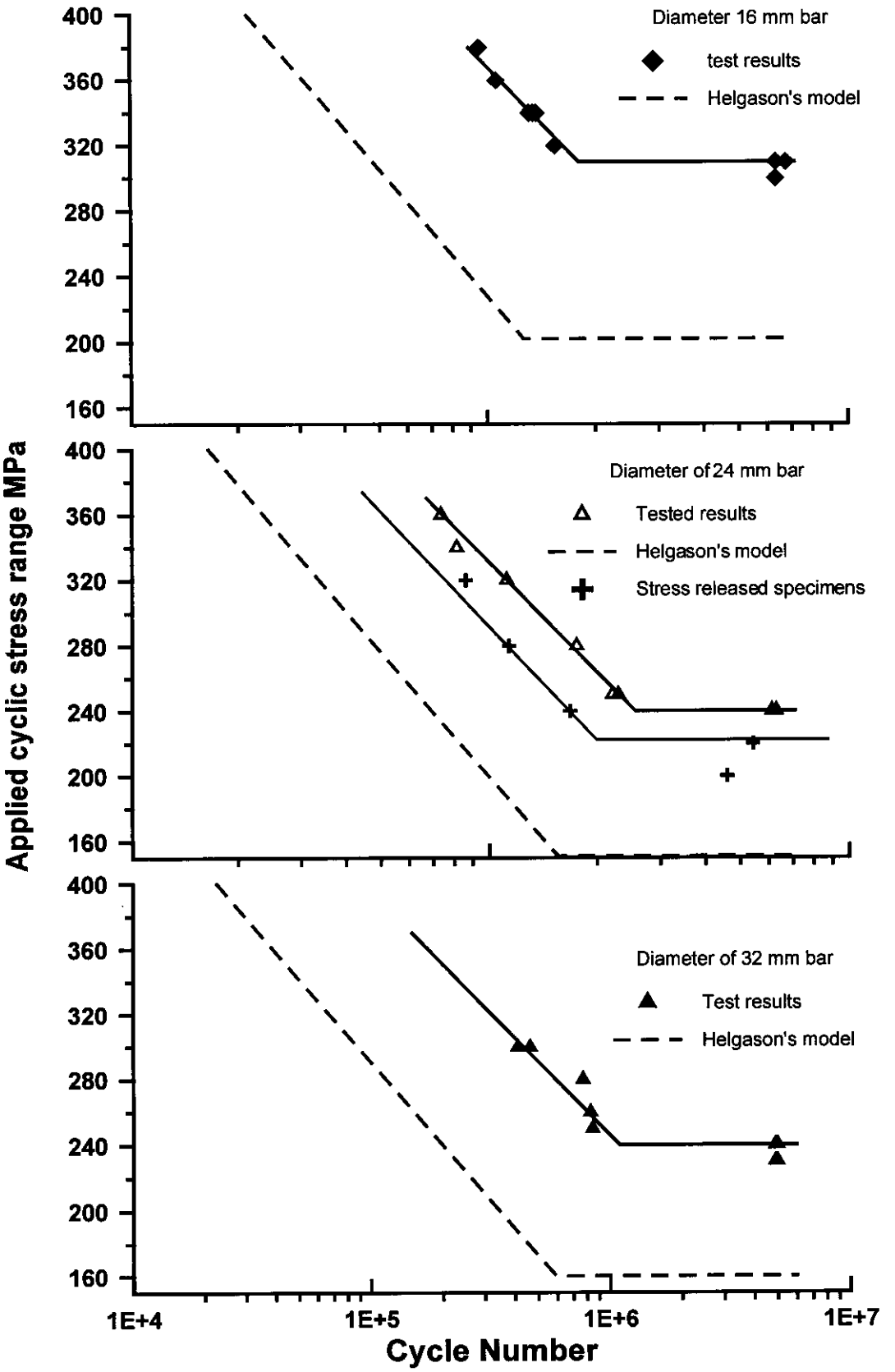

Figure 7-46. Comparison of test results with the predicted results

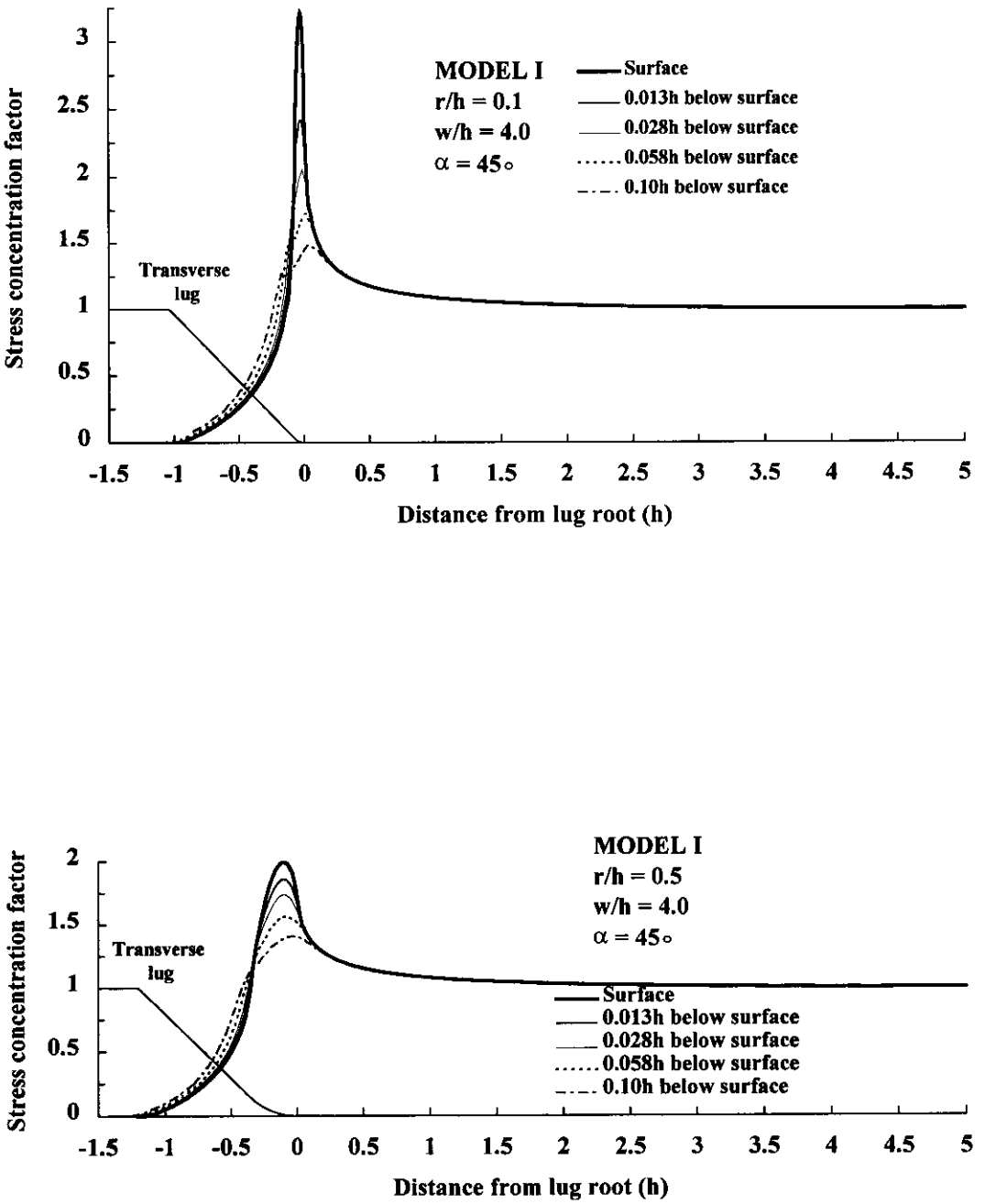

Figure 7-47. Analytical results - stress distributions along longitudinal axis

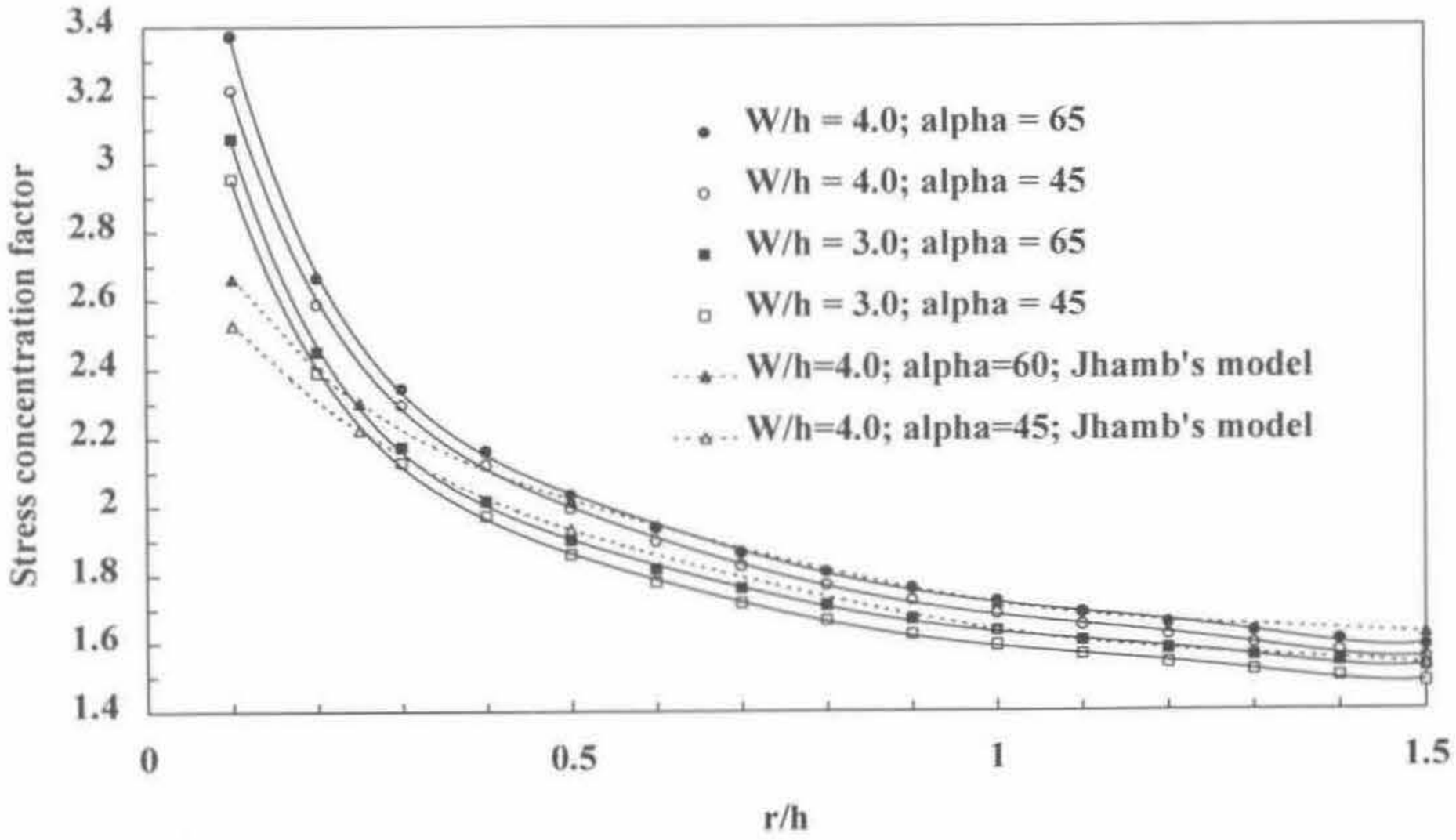

Figure 7-48. Stress concentration factor changes as a function of *r/h*

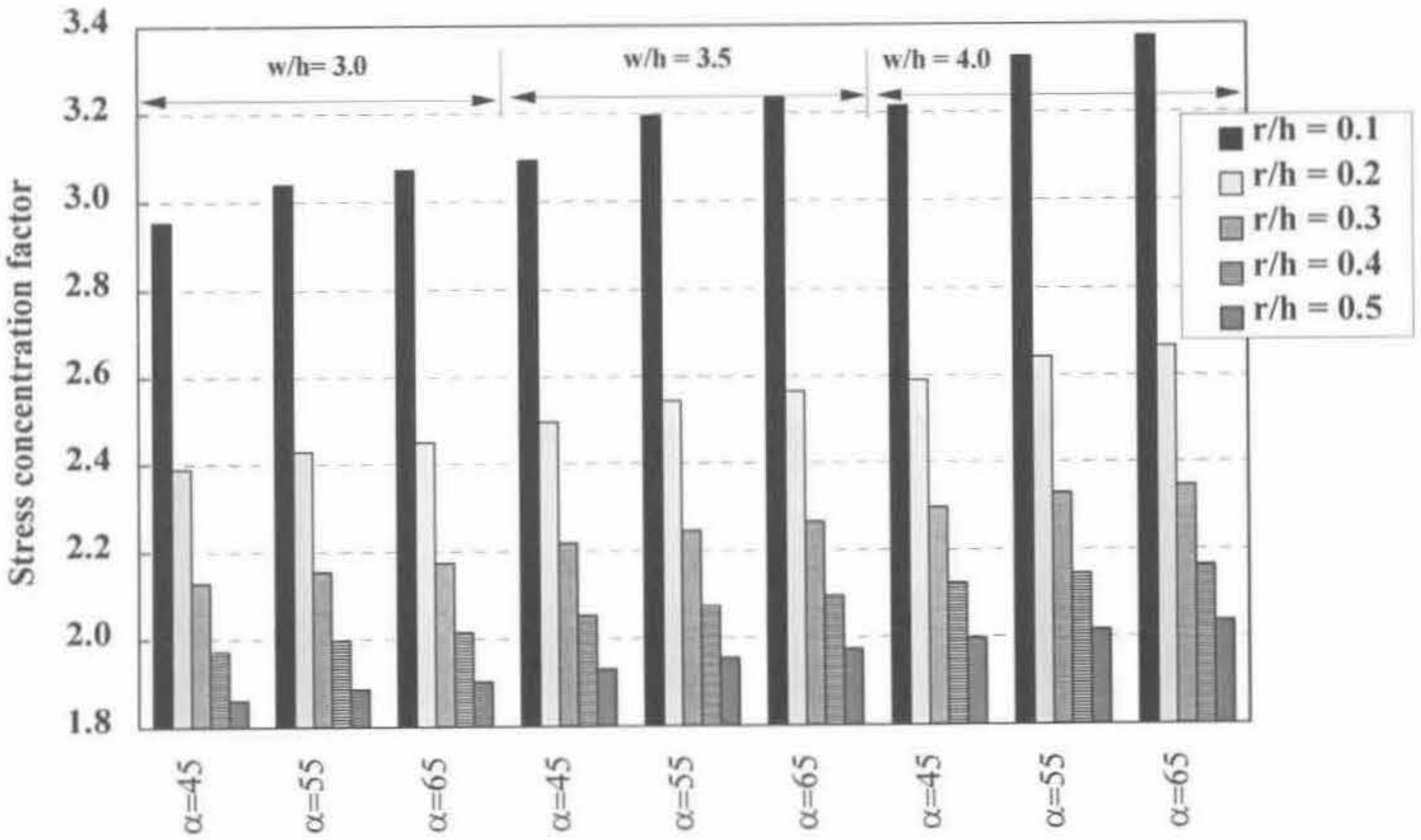

Figure 7-49. Stress concentration variation with lug widths, flank angles and *r/h* ratios

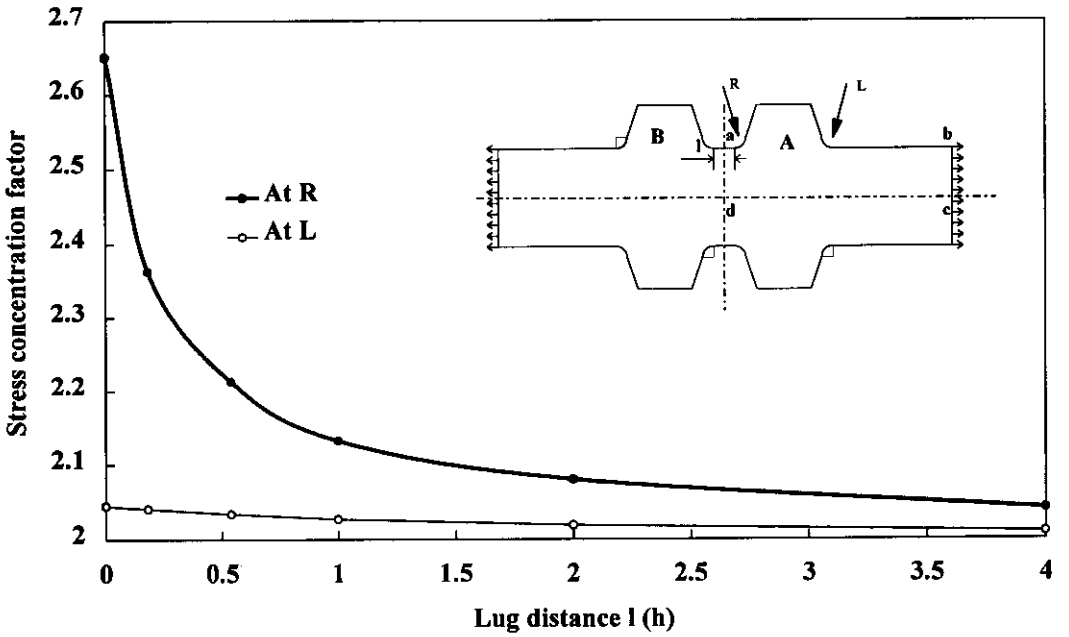

Figure 7-50. Analytical results; Model II

Chapter 8

DISCUSSIONS

Discussion is organised along the main facets of this work relating to microstructures, tensile properties, cyclic behaviour, residual stresses and fatigue performance. All of theses are the direct consequence of the manufacturing process which leads to a product with excellent properties, but which at the same time is too difficult for fine tuning to produce the same end results in bars with different diameters.

8.1. CHARACTERISTICS OF THE TESTED BARS

8.1.1. Microstructure in the core

As reviewed in Chapter 3 typical microstructure of TEMPCORE reinforcing steel has been described as a composite consisting fine ferrite and pearlite core and tempered martensite case. The formation of the fine microstructure is due to the fast cooling rate and the effect of thermomechanical treatment.

However, coarse core microstructure has been observed in laboratory trials (Economopoulos et al. 1975) and in some thermomechanically strengthened reinforcement bars which are similar to TEMPCORE (Ray et al. 1997), and it has been referred to as the preferred product of the TEMPCORE process (Vlad et al. 1983; Vlad 1985). During the present investigation the two larger size bars, 32 and 36 mm diameters, showed coarse microstructures in the core, but it was also found in smaller diameter bar from another trial. On the other hand, fine microstructure was found in a 36 mm diameter bar (see Chapter 7) and therefore the process technology should be questioned. It is believed that coarse microstructure is caused by high

finishing temperature and insufficient rolling deformation, which lead to large austenite grains preventing the impingement of grain boundary ferrite and thus allowing Widmanstätten ferrite to grow. Conclusion is therefore that fine or coarse microstructure can be produced in any bar diameter with the appropriate adjustment of production technology details. Which of these microstructures becomes the preferred one will be examined in the following sections.

8.1.2. Mechanical properties of the case and core sections

All the tested bars possess tempered martensite to various depths from the surface but differences exist in hardness, and thus in strength, indicating a large degree of sensitivity to process details. As thicker bars generally exhibits harder case material one may deduct that the balance between the severity of cooling and the retained heat favoured the former.

The core with fine microstructure, 9.4 μm grain size, exhibits 70 MPa higher yield strength than the core with coarse microstructure. The yield strength of the core with fine microstructure is 130 MPa higher than an ordinary hot rolled steel with similar carbon content but larger grain size (16.2 μm).

A core with coarse microstructure yields at around 310 MPa which is also higher than that of an ordinary hot rolled steel with similar chemical composition and this is due to the larger portion of pearlite resulting from pseudo-eutectoid reaction during the fast cooling. For the same reason, cores with coarse microstructure provide shorter Lüders strains than the cores with fine microstructure. It follows then that the high yield strength of TEMPCORE reinforcing bars is made up from the contributions of both the case and the core sections which is true even when the latter is made up from larger crystals.

8.1.3. Residual stresses

The cooling and the phase transformation sequences involved in TEMPCORE process produce residual stresses in a similar way as in any other surface heat treatments. When the surface of the bar is quenched, the case material contracts first due to cooling and then expands due to the formation of martensitic structure. At this

stage the core strength is low and the ductile austenite core deforms plastically to accommodate the shape change of the case. On further cooling in the air, however, after the core undergoes a transformation to ferrite and pearlite and when it eventually cools to the room temperature, the core shrinks. The rigid case does not follow this shrinkage to the same extent and thus residual stresses are generated.

The magnitude of the measured residual stresses is smaller than in other surface quenching processes, such as induction quenching and carburization. This seems compatible with the fact that during the course of residual stress generation the case is undergoing a 500 to 600°C tempering and thus a certain degree of stress relieving takes place by dislocation annihilation (Plumbridge and Knee 1985) and by the precipitation of carbides.

The remaining compressive residual stresses at the surface, of the order of 90 MPa, however significantly improve the fatigue performance as shown in Figure 7-44.

8.2. BEHAVIOUR IN STATIC LOADING

8.2.1. Preyield microplasticity and strengthening mechanism

Typical stress-strain relationship of TEMPCORE reinforcing steels has been described as having a marked yield point and large Lüders strain in the related literature. This is generally true if the bars possess a fine microstructure in the core. However, large amount of preyield microplasticity has been observed with bars having coarse microstructure. Similar phenomenon was also observed on a quenched and tempered angle section and in some in-line interrupted quenching and self-tempering reinforcing bars (Kugushin et al. 1986) and this preyield was attributed to the variable mechanical properties across the sample including the residual stresses.

The coincidence of the onset of preyield (310 MPa) with the yield strength of the core material of the bars with coarse microstructure no doubt indicates that the preyield behaviour may relate to the yield of the core material. Accordingly, the bars with fine microstructure should also exhibit preyield at around 380 MPa but it is not

the case. Thus the preyield phenomenon requires a plausible explanation and an attempt is made in the following sections to provide one.

8.2.1.1. Mechanical approach - the rule of mixture

In this approach, the bar is simplified as a rotational symmetric composite of a high strength outer layer with yield strength = σ_y^{case}, a low strength elastic-plastic core with yield strength = σ_y^{core} and an intermediate layer with a linear interpolation strength according to the hardness distributions, as shown in Figure 8-1. Materials in the cross-section are assumed to be independent from each other. Loaded under the yield strength of the core section, all sections perform elastically with the same modulus, and a liner stress strain relation is observed, i.e.,

$$\sigma = E.\varepsilon \qquad \textbf{(8-1)}$$

When the average stress, σ, exceeds σ_y^{core}, according to the rule of mixture one has:

$$P = P_1 + P_2 + P_3 = \sigma_y^{core}.\pi.r_1^2 + \int_{r_1}^{r} 2\pi.r.\sigma_r.dr + \pi.(R^2 - r^2)\sigma_c, \text{ and}$$

$$\sigma = \frac{r_1^2}{R^2}.\sigma_y^{core} + \frac{2}{R^2}.\{\frac{1}{3}.k.r^3 + \frac{1}{2}.(\sigma_y^{core} - kr_1).r^2 + \frac{k}{6}.r_1^3 - \frac{\sigma_y^{core}}{2}.r_1^2\} + \frac{R^2 - r^2}{R^2}.\sigma_c$$

where P_1, P_2, P_3 are loads taken by the core, the yield part of intermediate hardened layer (from r_1 to r) and the elastic case (from r to R), respectively, $k = \frac{\sigma_y^{case} - \sigma_y^{core}}{r_2 - r_1}$,

and $\sigma_c = k.(r - r_1) + \sigma_y^{core} = E.\varepsilon$, and therefore

$$\sigma = \frac{R^2 - r^2}{R^2}.E.\varepsilon + \frac{r_1^2}{R^2}.\sigma_y^{core} + \frac{2}{R^2}.\{\frac{1}{3}.k.(\frac{E.\varepsilon - \sigma_y^{core}}{k} + r_1)^3 + \frac{1}{2}.(\sigma_y^{core} - kr_1).(\frac{E.\varepsilon - \sigma_y^{core}}{k} + r_1)^2 + \frac{k}{6}.r_1^3 - \frac{\sigma_y^{core}}{2}.r_1^2\} \qquad \textbf{(8-2)}$$

Comparing Equations (8-1) and (8-2), it is clear that the "effect" of the Elastic modulus of the composite bar becomes smaller as the core and intermediate hardened layer yields. The elastic relation gives in and a different slope in the stress-strain relation develops.

Taking the appropriate parameters, this approach leads to a prediction for the 16 and 36 mm diameter bars, representing fine and coarse microstructures respectively, as shown in Figure 8-2. This method of prediction fails in the case of the 16 mm diameter bar.

8.2.1.2.Elastic-plastic approach

The failure of the rule of mixture in describing the stress-strain relationship of the tested bars may relate to the assumption about the yield and elastic part as being independent. For a composite as shown in Figure 8-3 and based on the work of Ebert et al. (1965, 1968 and 1978) the following consideration is proposed. Below the yield point of the weak core material, the whole cross-section of the bar deforms elastically with a Poisson's ratio of about 0.3. Assuming that the core is Lüders type elastic-plastic material, at yield the core tends to deform with Poisson's ratio of 0.5, while the hardened outer layer remains elastic with Poisson's ratio of 0.3. This means that the core material tends to volumetrically contracting in the ratio of 0.5/0.3 that is 1.67 times as much as the hardened case. This however is restricted by the rigid unyielded case.

Using Hook's law with boundary conditions of

$U_{r=a}^{case} = U_{r=a}^{core}$ at the interface of core and case; and

$\sigma_r = 0$ at $r = b$ (bar surface)

where a is the core and b is the bar radius.

Stresses and strain in longitudinal, circumferential and radial directions at the elastic case can be written as:

$$d\sigma = Ed\varepsilon_z + 2\mu k\Gamma(A + \mu d\varepsilon_z)/(1+\Gamma)$$
$$\sigma_r = k(A + \mu d\varepsilon_z)[\Gamma - (1-2\mu)a^2/r^2](1+\Gamma) \quad \textbf{(8-3)}$$
$$\sigma_t = k(A + \mu d\varepsilon_z)[\Gamma + (1-2\mu)a^2/r^2](1+\Gamma)$$

where

U = radial displacement;

σ = principal stress;

$d\sigma$ = incremental change in stress;

r = subscript denoting radial component or arbitrary specimen radius;

t = subscript denoting tangential, or circumferential component;

z = subscript denoting axial component;

ε = strain;

$d\varepsilon$ = incremental strain;

E = elastic modulus;

μ = Poisson's ratio

k = $E/(1+\mu)(1-2\mu)$, material constant

Γ = $(1-2\mu)(x^2/b^2)$;

A = $[1/(1 + de_z)^{-1/2}] - 1$.

In the core part, both radial and circumferential stresses are generated, and $\sigma_r^{core} = \sigma_{r,r=a}^{case}$. According to Tresca's criterion, the core material is strengthened and the longitudinal stress is written as

$$\sigma_z^{core} = \sigma_y^{core} + \sigma_r^{core} = \sigma_y^{core} + \sigma_t^{core} = \sigma_y^{core} + \sigma_{r,r=a}^{case} \quad \textbf{(8-4)}$$

Where $\sigma_y{}^{core}$ is the yield strength of the core material.

Using Equations (8-3) and (8-4), and applying the rule of mixture, the average longitudinal stresses across the composite bar can be calculated. The prediction of the stress - strain curve for a 16 mm diameter bar, also shown in Figure 8-2, leads to similar results to that of the role of mixture, and thus the method is not successful.

8.2.1.3.Microplasticity approach

The two models above fail in describing the preyield behaviour of the bars with fine microstructure and the most obvious reason seems to be that microstructure parameters, such as grain size, is not taken into account. The fact that the preyield is essentially microplastic with very high hardening rate followed by Lüders yield indicates that the core material cannot be simply assumed to be an elastic-plastic component, when it is restrained by a surrounding hard case. A microplastic

mechanism with limited potential is needed for the explanation and therefore dislocations are brought into the foreground. Assuming some dislocation sources are operating below the macroscopic yield it is most likely that the slip is greatly limited and the created dislocation pile-ups stop the operation of the source. This type of event can be related to the grain size as reviewed in Chapter 4. Increasing stresses activates some other sources leading to the observed microplasticity and at even higher stresses the case yields. When the case yields, and the restraint on the core changes, the composite bar yields in Lüders style. This strengthening mechanism is similar to the surface film effects observed in other metals (Gilman 1955; Brame and Evans 1958) where the coated film inhibits the passage of dislocations out of the surface of the crystal.

Using this approach the stress strain response of the soft core and hard case at an average stress σ^{bar} can be described. As the case performs elastically and the core provides microplasticity a departure from elasticity is achieved by the composite bar as shown in Figure 8-4. Accepting the grain size dependence in this model the theory of Brown (1961, also Chapter 4) may be applied, i.e.,

$$\varepsilon_{pl}^{core} = \rho D^3 (\sigma^{core} - \sigma_0^0)^2 / 2G\sigma_0^0 = C(\sigma^{core} - \sigma_0^0)^2 \qquad \textbf{(8-5)}$$

where ρ is the density of dislocation sources (sources/cm^3), D is the grain diameter, σ^{core} is the applied stress on the core material, σ_0^0 is the stress to activate the first dislocation source in the core and G is the shear modulus. The term $\rho D^3 / 2G\sigma_0^0$ can be expressed as a constant for a given material and it will be simply C.

The stress of the yielded core member (Figure 8-4) can be written as:

$$\sigma^{core} = E(\varepsilon - \varepsilon_{pl}^{core}) \qquad \textbf{(8-6)}$$

where ε is the strain of the bar under an average bar stress, σ^{bar}.

As microyielding commences with the activation of a dislocation source, that is $\sigma_0^0 = \sigma_y^{core}$ with the use of Equations (8-5) and (8-6), the stress acting in the microyielding core can be written as:

$$\sigma^{core} = \sigma^{case} - EC(\sigma^{core} - \sigma_y^{core})^2$$

With the condition that $\sigma^{core} - \sigma_y^{core} > 0$, the solution is:

$$\sigma^{core} = \frac{\sqrt{4EC(\sigma^{case} - \sigma_y^{core}) + 1} - 1}{2EC} + \sigma_y^{core} \qquad \textbf{(8-7)}$$

If the fraction of core and case in the cross section are A and B, respectively, according to the rule of mixture:

$\sigma^{bar} = A\sigma^{core} + B\sigma^{case}$

thus

$$\sigma^{bar} = A\{\frac{\sqrt{4EC(\sigma^{case} - \sigma_y^{core}) + 1} - 1}{2EC} + \sigma_y^{core}\} + B\sigma^{case} \qquad \textbf{(8-8)}$$

When the case is still in the elastic state, that is $\sigma^{case} = E\varepsilon$, from the above equation the stress strain curve of the bar can be calculated.

Equation (8-8) shows that the stress-strain plot of the composite bar is not only core strength dependent but it also depends on parameter C in which the grain size and the density of dislocation sources of the core material are included. Taking the yield strength of the core material as 300 MPa and A = 0.6 for example, the calculated stress-strain curves for various C parameters are different as shown in Figure 8-5. When $C \leq 10^{-8}$ very small preyield takes place, while with $C \geq 10^{-6}$ large preyield occurs. For example if $C = 10^{-8}$ the preyield microstrains are only 1, 20 and 26 x 10^{-6} when the composite bar is loaded to 20, 40 and 50 MPa beyond the yield strength of the core, respectively. In contrast, the corresponding preyield microstrains for $C = 10^{-6}$ are 95, 200 and 270 x 10^{-6}. When $C = 10^{-5}$ the prediction is close to that predicted by the rule of mixture.

As parameter C is directly related to grain size and dislocation source density, the smaller is the grain size in the core for a given dislocation source density, the higher is the hardening rate of the core material and thus the smaller is the preyield microstrain of the bar, Figure 8-6. Finer grain size in the core, say $C = 10^{-8}$, the core takes nearly as much stress as the case does thus the bar is nearly elastic in the

microplastic range. With coarse grains in the core, $C = 10^{-5}$ for example, the core takes a stress only slightly higher than its yield strength thus the composite bar performs as predicted by the rule of mixture.

Assuming one dislocation source in each grain with 9.4 μm grain size (core of the bars with fine microstructure) the dislocation source density will be 0.925 X $10^{15}/m^3$, and thus the C parameter will be of the order of 10^{-8}. If the dislocation source density with the 45 μm grain size (core of the bars with coarse microstructure) is the same to that of fine microstructure, the C parameter will be of the order of 10^{-6}. This approach is compatible with the observed behaviour, and can explain that bars with fine microstructure exhibit undetectable preyield, while the bars with coarse microstructure exhibit large amount of preyield microplasticity before the attainment of macroyield. Since the appropriate values of dislocation sources are as yet not well defined for fine ferrite and coarse Widmanstätten ferrite, the use of the model requires a number of assumptions.

8.2.1.4.Residual stress and preyield

As the bars behaved similarly in both tension and compression tests it may be concluded that residual stresses are not playing part in the preyield phenomenon and this is reasonable conclusion as the magnitude of residual stresses in the soft core part are low.

8.2.1.5.Experimental results on cut-specimen

Test results of specimen with cut out section provide a great support for the validity of the proposed model. The model works only when the core behavior is entirely restricted by the hard case. If the core material is freed from the restraint no dislocation pile-up mechanism will operate but normal dislocation multiplication takes place. In that event specimens should exhibit large preyield which can be predicted by the rule of mixture even when the core is made up from fine small crystals.

The results obtained with the 16 mm diameter bar support the above. The centre-through-cut specimen with the freed core, Figure 6-5, preyielded at 380 MPa and the

microplasticity reached 250 x 10^{-6} before macroyielding at 422 MPa, Figure 7-29. There was no preyield with the intact specimen, and furthermore, the cut out specimen contained larger proportion of hard case section than the intact specimen. This leads to the logical conclusion that the core yields if permitted by the surroundings. This result can be explained by the rule of mixture.

8.2.2. Lüders yield and Lüders strain

The proposed strengthening mechanism due to the restricted dislocation activity ends when the stress in the case reaches its yield strength and at that stage normal dislocation multiplication commences in the core leading to macro yielding in the composite bar. Once this takes place, the core takes less stress than in the preyield stage as the limited strengthening mechanism diminishes, this forces the case to take larger stress and large yield plateau is achieved. The yield style is determined by the characteristics of the core while the magnitude of the Lüders strain is mainly determined by the hardening rate of the case. Thicker bars and bars with coarse microstructure tend to contain larger portion of hardened layer, thus exhibit smaller Lüders strain.

8.3. BEHAVIOUR IN CYCLIC LOADING

Understanding the behaviour in cyclic loading is based on the interaction of the yielding core and elastic case. On forward loading in zero to tension or zero to compression, beyond the yield stress of the core but under the yield strength of the bar, the core yields to a certain degree at the peak load. On unloading to zero load, only the elastic part of the deformation recovers thus an interaction between the core and case is generated, i.e., the case is stretched by the core and the core is compressed by the case and thus further restraint is created. On the subsequent loading to the same peak load the restraint leads to cyclic hardening. More plastic deformation takes place, however, in the same manner as it is loaded beyond the previous peak load. Bars with fine microstructure, since they preyield little, do not exhibit notable open mechanical hysteresis.

On fully reversed cyclic loading, the stresses generated by the interaction between the core and case during the forward loading simply help to lower the yield strength of the core in the reverse loading and thus gradually expansion of mechanical hysteresis is observed, cyclic softening occurs. This cyclic softening mechanism also provides an explanation to the phenomenon reported by Behan and Warner (1984): when a 12 mm diameter TEMPCORE bar was fatigue tested at applied cyclic stress between -10% and 80% of the static tensile strength "marked heat" was generated, since large plastic deformation took place.

8.4. FATIGUE PROPERTIES

It has been shown clearly that the TEMPCORE steel has superior fatigue property over other types of high strength reinforcing steels. The composite metallurgical microstructure and the residual stresses generated during the TEMPCORE process are the contributing factors as it will be discussed below.

8.4.1. The most important negative factor

Test results show that fatigue cracks initiate from either the root of the transverse lugs or from the identification marks both of which provide high stress concentrations. The analysis carried out on the geometrical patterns of the surface deformations of the bars were directed entirely from the fatigue point of view. The discussion that follows therefore ignores the concrete-to-bar bonding efficiency which is after all the main purpose of having surface deformations on the reinforcing bars.

According to the analysis, sharper merging of a deformation geometry into the base of the bar substantially increases the SCF, therefore, initiates fatigue crack at lower stress range and reduces fatigue crack initiation time in the finite-life region. The 28 mm diameter bars contained large and sharp identification marks, and cracks initiated at the marks without exception, Figure 7-34 (c). Thus bars exhibited much lower fatigue limit and fatigue life than the bars free from such marks, Figure 7-33. Calculated SCFs and measured fatigue strengths, Table 7-17, indicates a good correlation: when the r/h increases from 0.3 (32 and 36 mm bars) to 1.0 (16 and 20

mm bars) the SCFs decrease approximately by 23%. This reduction in the value of SCFs increases the fatigue limit by about 30%, and fatigue life in the finite-life region increases by 100%, Figure 7-33. Some scatter exists when the fatigue limit is plotted against the calculated SCFs, Figure 8-7, but this may be attributed to other influencing parameters, e.g., residual stresses, microstructures which do show a variation between the various bar diameters. In addition, the calculated SCFs did not include a surface roughness related factor and this may also contribute to the scatter.

Analytical results also showed that the SCF increases as the gap between deformations decreases. This explains the fact that cracks initiated at the identification mark of the tested 16 mm diameter bar, Figure 7-40 (c), where the mark and the transverse lug can be regarded as two independent deformations close to each other. This effect is also verified by other tests as shown in Figure 8-8 in which fatigue crack initiated at the intersection points of transverse lugs and in Figure 8-9 where identification marks are close to transverse lugs.

8.4.2. Effect of stress range

Stress range is the primary factor influencing fatigue life in the finite-life region, and there is a limiting stress range, the fatigue limit, below which no fracture takes place in this type of material. The stress range versus fatigue life in log scale are parallel to each other (Figure 7-33) and parallel with other types of bars (Figure 7-45) suggesting that the TEMPCORE reinforcing steel does not have an anomalous fatigue characteristic. The fatigue limits were declared after 5, 000,000 cycles when no signs of fatigue initiations were detected by the subsequent tensile test.

Along the root of a lug the SCFs vary according to the local *r/h* ratio, thus at lower cyclic stress range only the sharpest point reaches critical situation and thus single initiation takes place. At higher cyclic stress multiple initiation is promoted by raising the stress threshold well into locations with adequate SCFs for crack initiation. For the same reason, the 24 mm diameter bar with much smaller *r/h* ratios along lug roots developed multiple initiation at relatively low cyclic stress range.

8.4.3. Effect of microstructures

The two factors alone, geometrical and stress range, are not adequate in explaining the fatigue properties of the bars, as these factors would be approximately the same for all the other type of reinforcing bars. Therefore the peculiar microstructure associated with the composite nature of the material must be examined next.

According to the facts observed by Kerlins (1987), Goto (1991) and Shibata et al. (1996) fatigue crack initiation and early stage propagation make up the majority of the fatigue life. This applies to the present case also as the fatigue properties of the TEMPCORE reinforcing steels are essentially determined by the outermost case material which is tempered martensite. In Chapter 4 it has been shown that tempered martensite has much better fatigue properties than structure with ferrite-pearlite composition, and these results on TEMPCORE bars with a the tempered martensitic outer layer are substantiating these expectations.

As the hardened case material is so important, the application of the model developed by Helgason et al. (1976) on the TEMPCORE bars will be reconsidered. When the tensile strength of the case material is used instead of the tensile strength of the composite bar the predictions are better as shown in Figure 8-10 and Figure 8-11. The discrepancies are still significant. As residual stresses are not included in the model the predicted results should be the same as for the stress relieved specimens, but Figure 8-11 indicates that the model of Helgason fails.

The observed higher fatigue limit is related to the metallurgical features of the surface structure. The fine laths, randomly dispersed fine carbide particles, small martensite packets (Figure 7-4), all inhibit heterogeneous plastic deformation under a certain cyclic loading. Thus the higher strength of this microstructure increases fatigue limit. Even when a crack is initiated as a microstructural small crack, or MSC, it may stop at metallurgical barriers in tempered martensite, namely at packet boundaries and at former austenite grain boundaries. It is more difficult to overcome these barriers than it is in ferrite steels, inhibiting the advance of MSC. Martensite packet boundaries are so effective barriers that they even retard the propagation of

large cracks, Figure 7-37 (b). Non-propagation MSC may exist at the surfaces of run out specimens but they were not revealed by tensile tests carried out subsequently as these cracks are too small.

The test results indicate that crack initiation and small crack propagation in the hardened layer occupy at least 90% of the fatigue life leading to featureless fracture surface, extending up to 150 μm, Figure 7-35. Although monitoring the propagation rate of small cracks was not possible, examinations revealed that cracks did not appear up to 69% of the total fatigue life, which is already better than or at least equal to the total fatigue life of conventional bars. With similar fracture characteristic the propagation rate in a titanium alloy is reported to be 3×10^{-11} m/cycle (Petit et al. 1992).

8.4.4. Effect of residual stresses

It is well known that surface compressive residual stresses are beneficial while tensile residual stresses are harmful in terms of fatigue resistance (Parker 1982; Fletcher et al. 1988; Kang et al. 1990; Okamoto and Nakamura 1990). Accordingly some techniques have been developed for improvement of fatigue properties of components. Carburising, induction quenching and shot peening all generate compressive residual stresses at the surface, and stress relieving treatment reduces tensile stresses. Residual stress effect on fatigue properties are generally treated to be equivalent to the effect of a mechanically applied stress that changes the mean (Fletcher et al. 1988; Leis et al. 1997), and this approach is discussed below.

Compressive residual stresses lower the local mean load or local R-ratio as shown in Figure 8-12 (a) and (b), by shifting the applied stress intensity factor down. The effective stress intensity factor range is

$\Delta K_{eff} = (K_{\max} + K_{rsi}) - K_{cl}$

when $K_{\min} + K_{rsi} \le K_{cl}$, $R = 0$ for example, Figure 8-12 (a);

$\Delta K_{eff} = K_{\max} - K_{\min}$

when $K_{\min} + K_{rsi} > K_{cl}$, $R >> 0$ for example, Figure 8-1 (b).

where K_{max} and K_{min} denote the maximum and minimum stress intensity factor due to the applied load, K_{rsi} is the stress intensity factor induced by residual stress field, K_{cl} is crack closure - the stress intensity factor at which crack surface mating occurs behind the crack tip, and $R = \sigma_{min}/\sigma_{max}$. The above equations indicate that under compressive residual stresses and with small R-ratio the crack tip will not experience the full stress intensity factor range imposed by the applied loading. In the case of sufficiently high R-ratio however full applied stress intensity factor range will be experienced.

In case of large crack propagation the weight function method can be used to calculate K_{rsi} (Okamoto and Nakamura 1990; Parker 1982; Kang et al. 1990). For near threshold crack growth cases the residual stress can be simply treated as an additive stress to the applied stress to calculate ΔK, e.g., $K_{\max,eff} = Y(\sigma_{\max} + \sigma_{rsi})\sqrt{\pi a}$, where Y is a parameter relating to specimen geometry. This approach has been successfully used by Fletcher et al. (1988) to explain the crack front shapes. Specimen with compressive residual stresses in the middle part and tension residual stresses at the two quarter sections fatigued at R = 0.2 have curved fronts as shown in Figure 8-13, but straight fronts when fatigued at R = 0.8.

As-received bars used in this project contain 85-90 MPa compressive residual stresses at the surface and the gap between the results of as-received bars and the stress relieved bars is shown in Figure 7-44 and Figure 8-11. When cycling with R = 0 the residual stresses shield part of the stress intensity factor range thus the crack propagation rate is reduced. When the applied stress is increased to the residual stress level in tension (σ_{min} = +80 MPa) the shielding effect vanishes and the full range of ΔK_{app} is acting at the crack tip. In these cases the fatigue life should coincide with that of the residual stress free specimens and this is demonstrated by the results obtained on bars with 24 mm diameter.

The results shown in Figure 8-11 indicate that the residual stresses in the 24 mm diameter bar provide a shift in the S-N curve in the order of 40 MPa, and this

differences directly due to the TEMPCORE process by providing residual stresses to the outside layer.

8.4.5. Effects of bar size

From the obtained results there is no way to asses the bar size effect if any. This is due to other influencing factors which cannot be precisely controlled by the process itself, i.e., deformation pattern, microstructure and residual stresses. Any variation in any of these may mask the size effect. However, the applied analysis leads to reliable SCF values which is perhaps the most important single parameter related to fatigue performance.

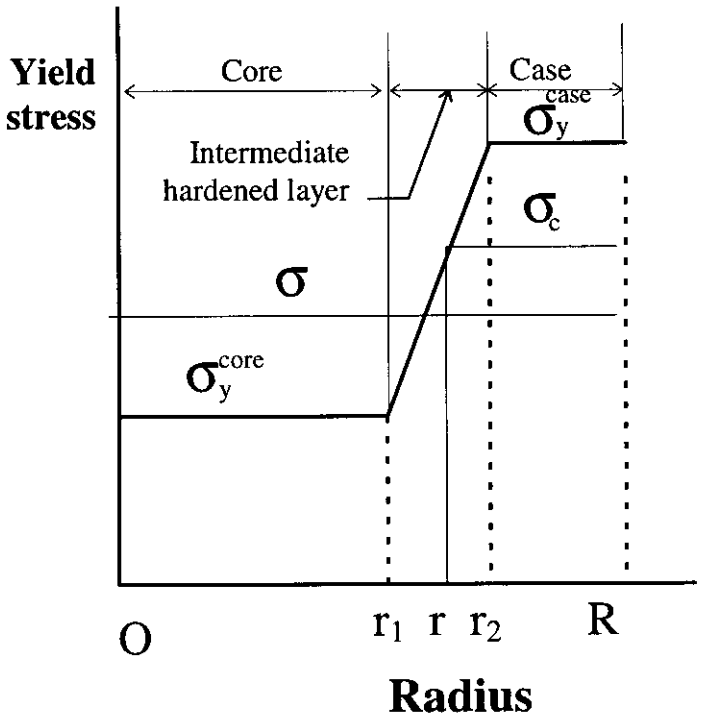

Figure 8-1. Schematic illustration of the variable yield strength along the radius of the bar

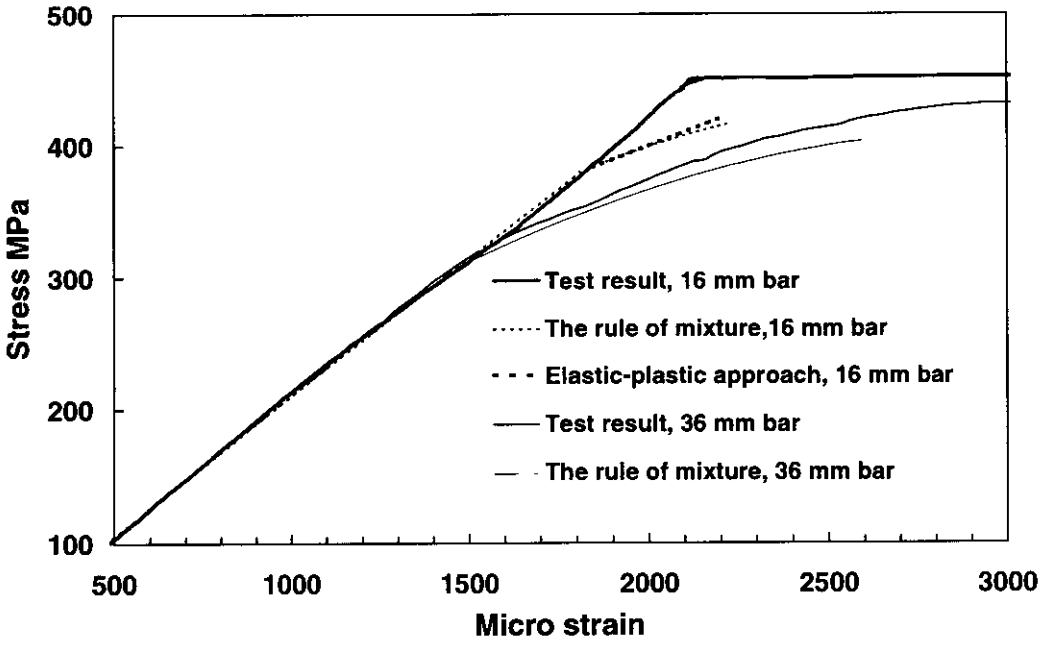

Figure 8-2. Preyield microplasticity

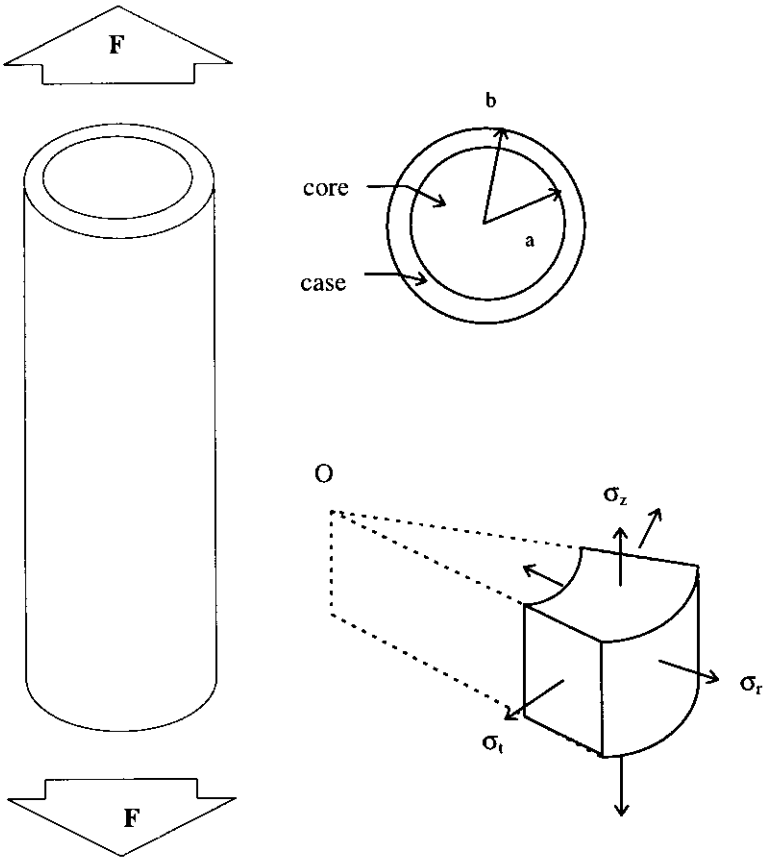

Figure 8-3. Rotationally symmetric composite model and representative volume element

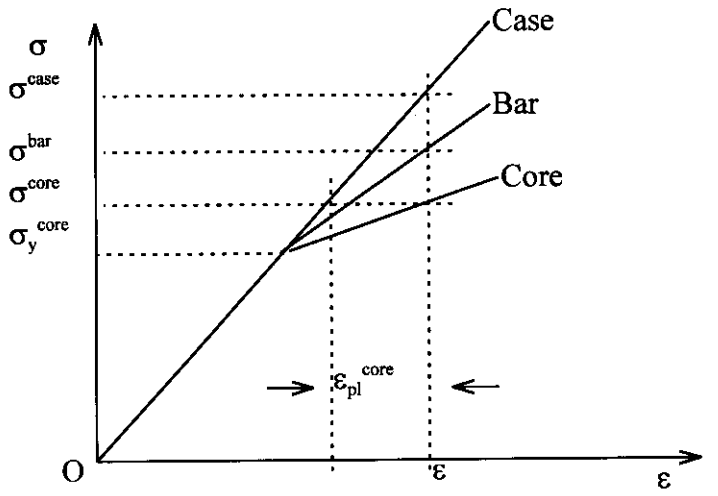

Figure 8-4. Schemic illustration of stress strain relation of bar sections in tension

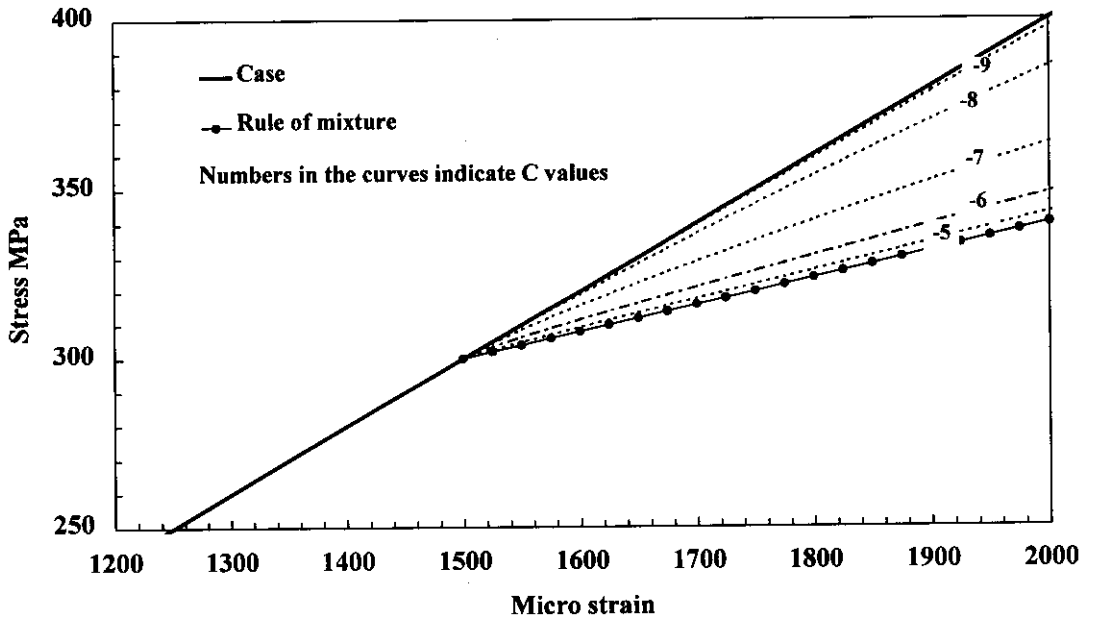

Figure 8-5. Microstrain predictions by the developed model

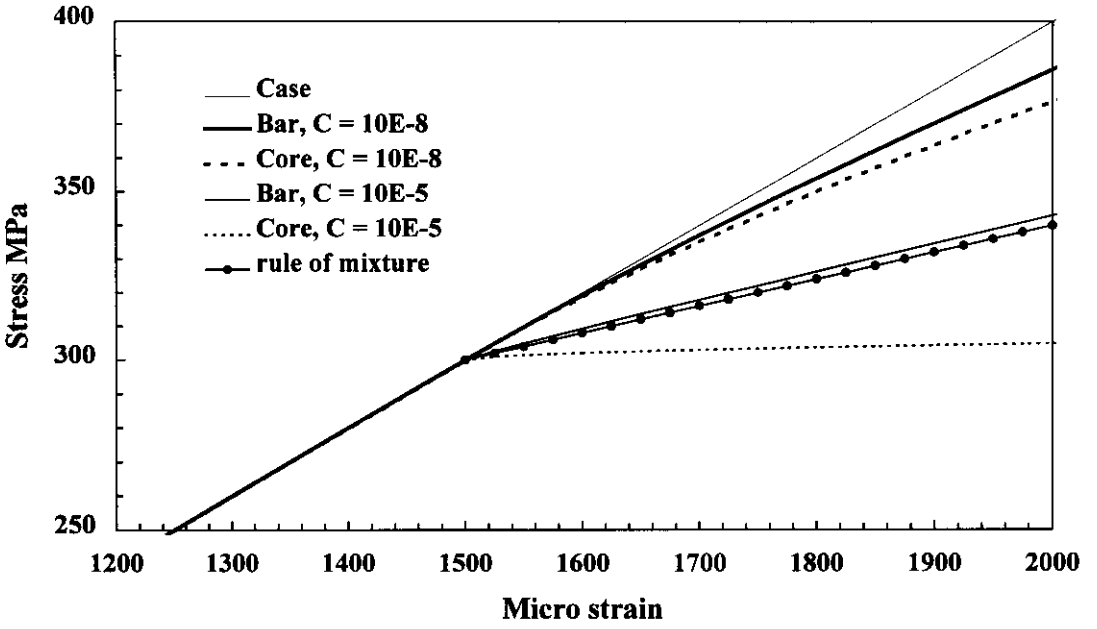

Figure 8-6. Stress-strain predictions by the developed model

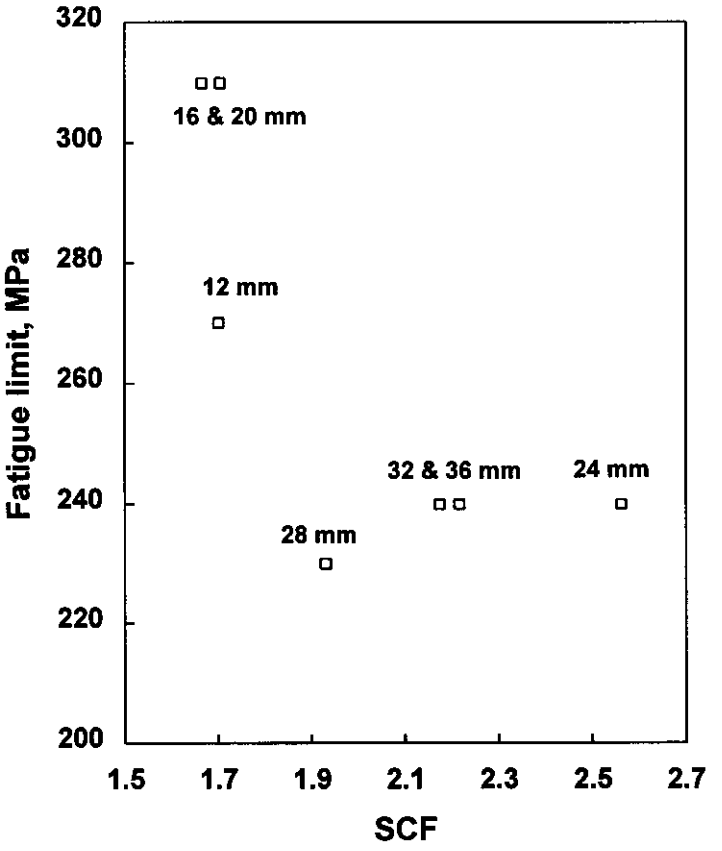

Figure 8-7. Fatigue limit of the tested bars versus the calculated SCFs

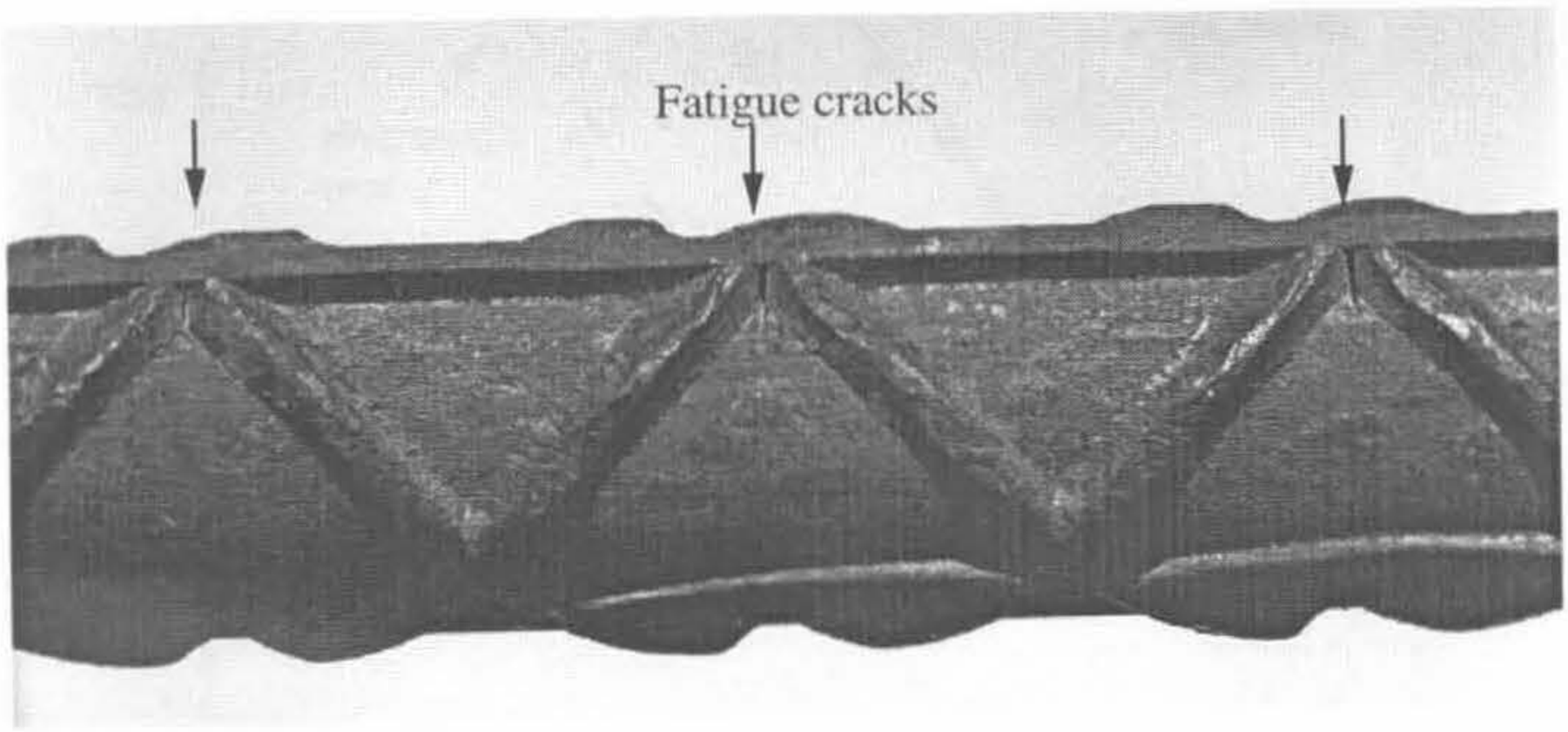

Figure 8-8. Crack initiations at intersection points with maximum SCF values

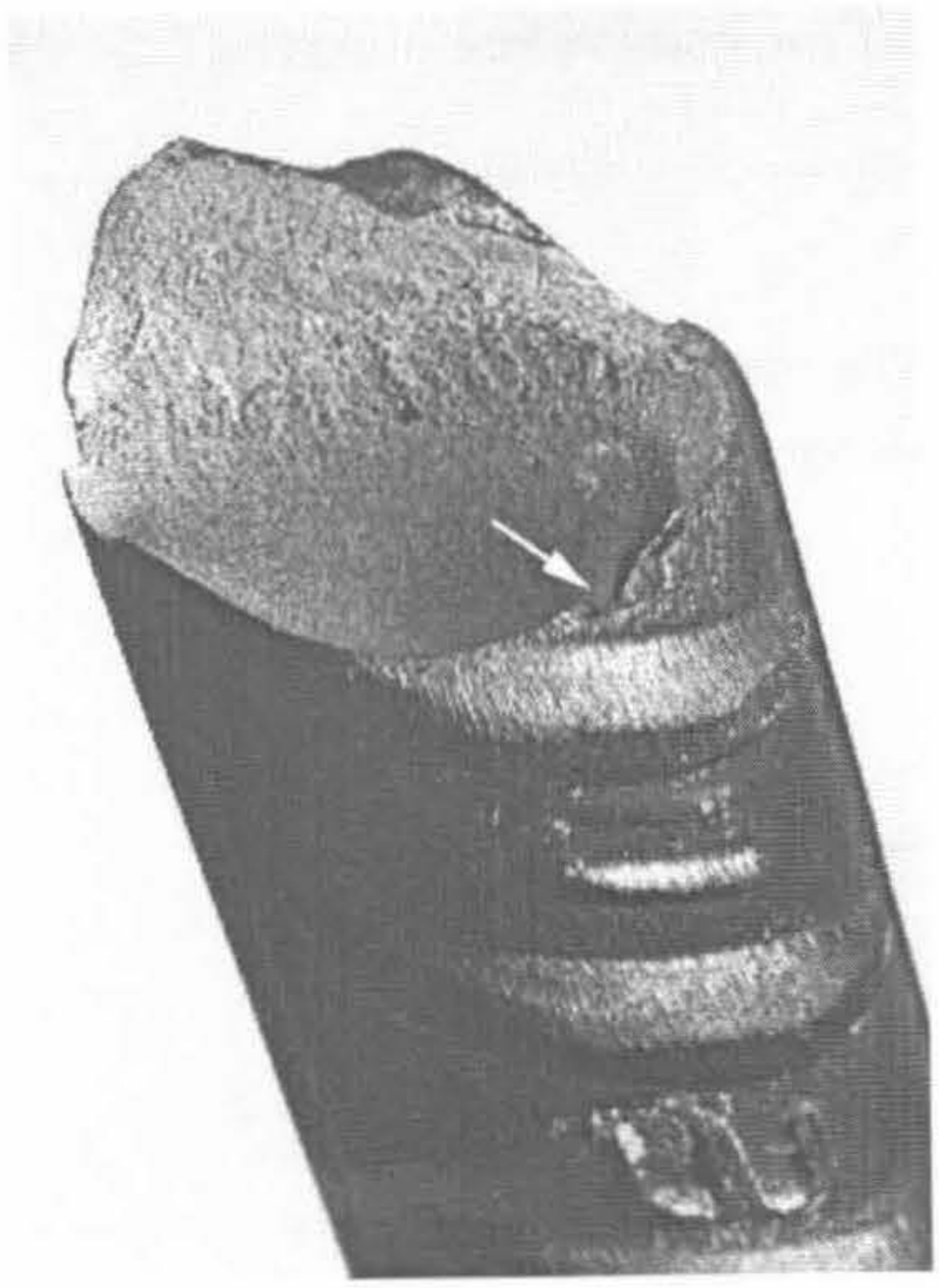

Figure 8-9. Crack initiation from a sharp identification mark close to a transverse lug

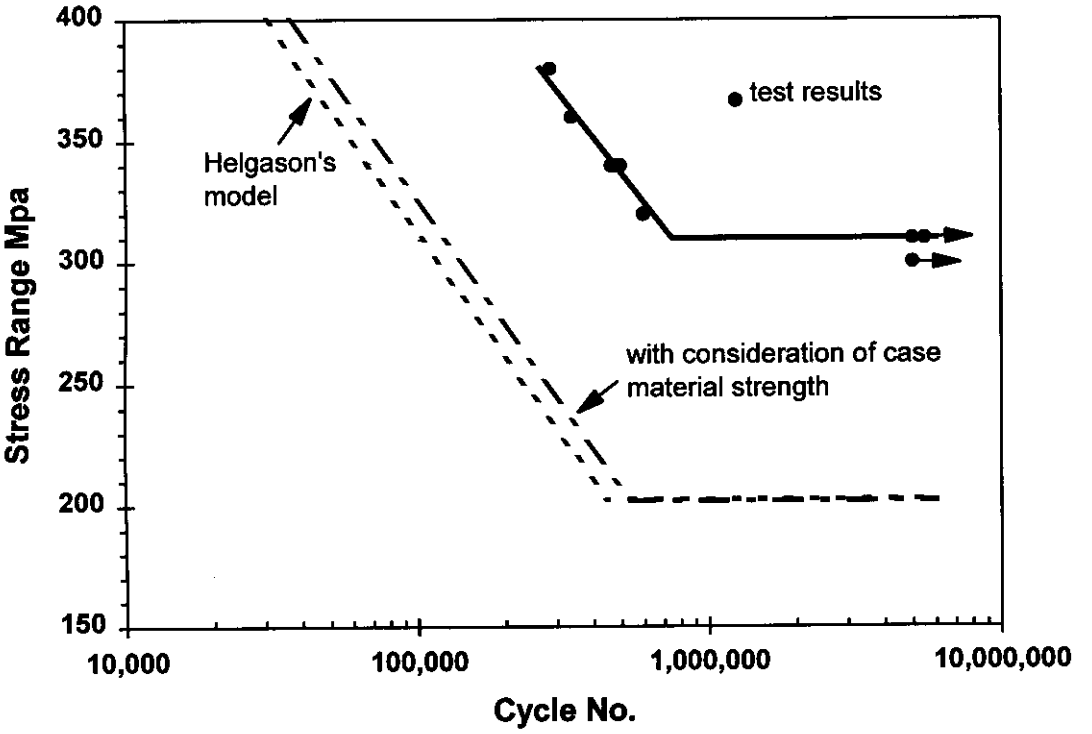

Figure 8-10. Test results and predictions; 16 mm bar

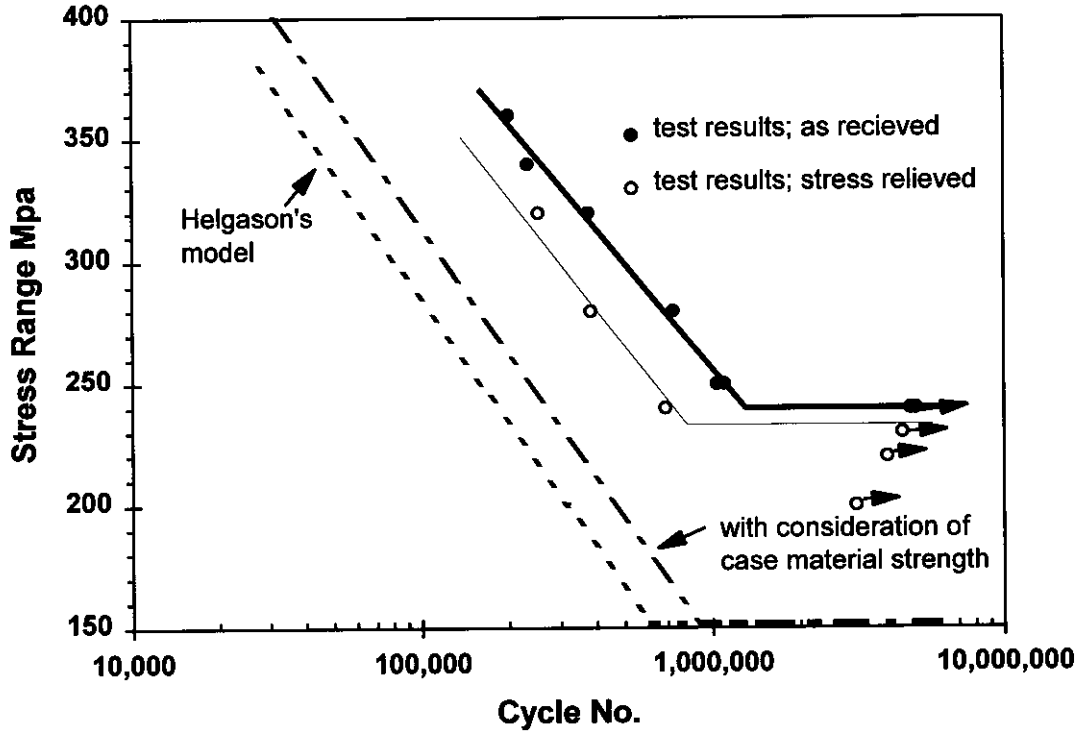

Figure 8-11. Test results and predictions; 24 mm bar

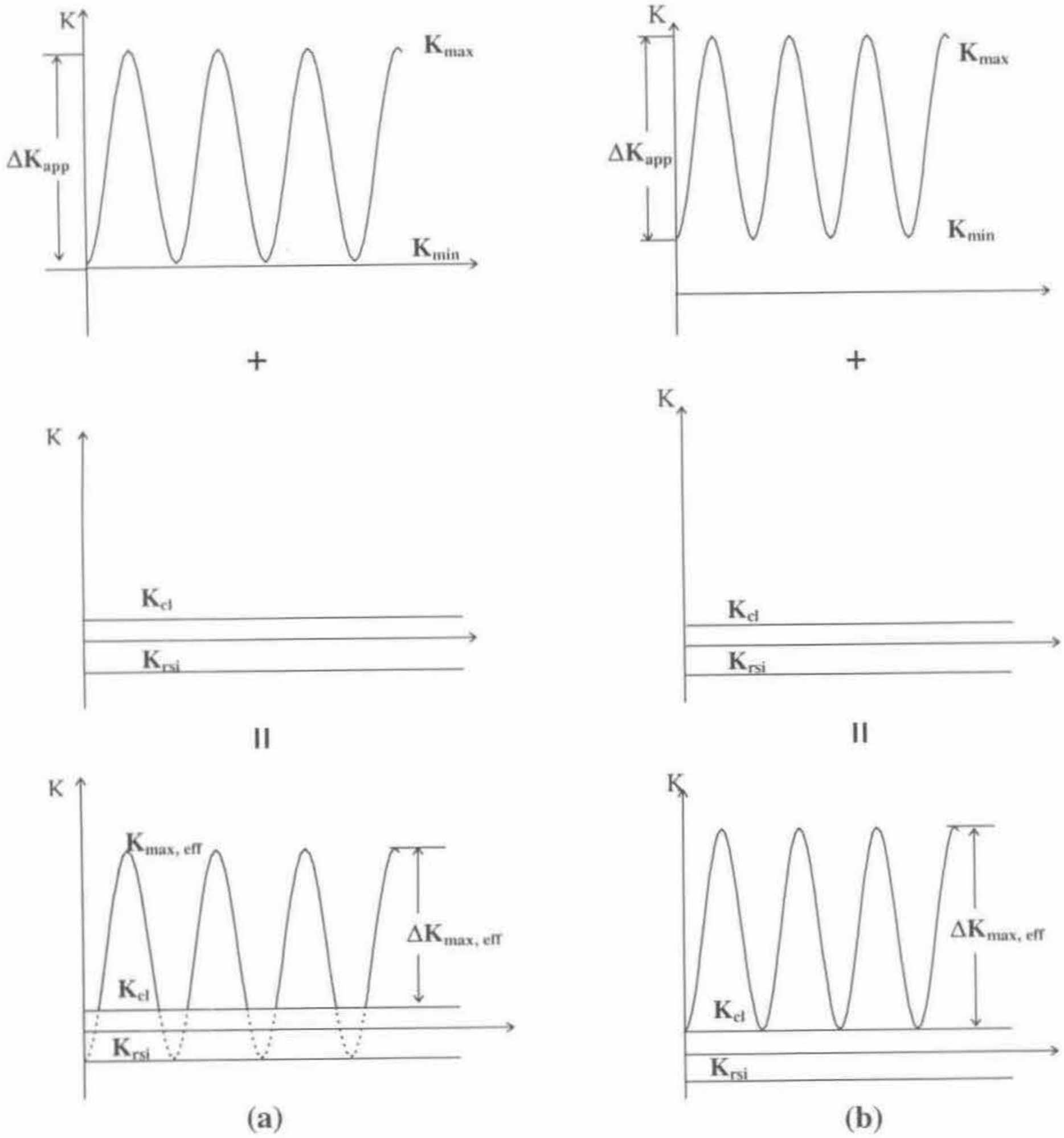

Figure 8-12. Effect of compressive residual stress on stress intensity factor range, (a) R = 0, (b) R>>0

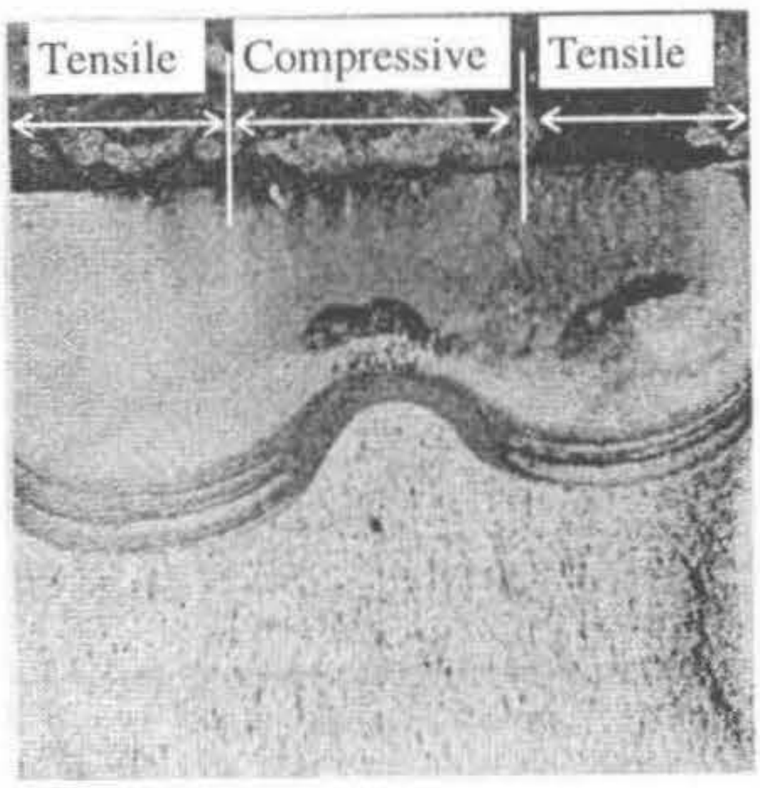

Figure 8-13. Crack front shape (after Fletcher et al. 1988)

Chapter 9

CONCLUSIONS

In general terms the following conclusions are made: the TEMPCORE reinforcing steel bars can be considered as a composite material made up from a hardened surface layer, an intermediate hardened layer and a relatively soft core section. The static and cyclic properties are greatly influenced by the microstructure in the core section, while the fatigue properties are controlled by the case material. Fatigue crack initiations are associated with the deformation patterns on the bar surface which provide high stress concentration factors. The fatigue performance of TEMPCORE reinforcing steel is significantly superior when compared with the other type of reinforcing steels.

In more specific terms the conclusions are detailed below.

A. Metallurgical features

1. Based on metallurgical assessment it can be stated that the TEMPCORE reinforcing steels represent a composite material made up from three very different microstructures. The concentrically arranged sections contain a hard case with a soft core jointed by an intermediately hardened transition zone.
2. The surface of the bar, extending to a certain depth, consists of tempered martensite, constituting the "case" which is strong, nevertheless possessing high toughness.
3. At the surface of the bars, due to the sequence of thermal and metallurgical events during the cooling process, a compressive residual stress state develops with the order of 90 MPa in the longitudinal direction. This compressive residual stress plays a significant role in the fatigue performance of the bars.

4. The intermediate hardened layer consists a mixture of bainite and ferrite with increasing width as the bar size increases.
5. In the core area due to some slight variation in the process technology two types of microstructure are found: fine ferrite-pearlite, coarse Widmanstätten ferrite and conglomerate of pseudo-eutectoid.

B. Static properties

6. The bars generally exhibit high yield strength (> 410 MPa), high yield to tensile strength ratios (0.80) and large elongation (22% to 32%).
7. Bars with fine core microstructure exhibit marked yield point with large Lüders strain, while bars with coarse microstructure in the core section preyield significantly before macroyielding with much smaller Lüders strains.
8. The preyield of the steels is associated with the response of the core, while macroyield commences with the yield of the case.
9. A model has been developed, culminating in a mathematical expression, which explains the preyield dependency on the prevailing core microstructure of the bar.
10. The experimental and analytical results show that larger is the grain size of the core microstructure, larger is the preyield of the bar.
11. The tested bars do not exhibit sharp yield drop regardless of strain rate.
12. The case material exhibits higher yield strength of the order of 495 MPa and 607 MPa for the 16 mm and 36 mm diameter bars respectively, and yield continuously with considerable ductility.
13. The core materials yield in Lüders style and the fine microstructure core exhibits higher yield strength (380 MPa) and larger Lüders strain (>2.5%) than those core materials with coarse microstructure. Both kind of core materials possess a yield strength higher than that of conventional hot rolled bars with similar composition.

C. Cyclic response

14. In zero to tension and zero to compression cyclic loading below the yield strength the response is elastic with fine microstructure bars, but bars with coarse

microstructure develop open mechanical hysteresis loops when loaded beyond the preyield stress level, and exhibit cyclic hardening in both types of loading.

15. Fully reversed cyclic loading with sufficiently high stresses, but well below the yield strength, produces cyclic softening. The softening rate of the bars with coarse microstructure is much faster and macroyield is induced within tens of cycles. In contrast, fine microstructure bars soften slowly within the first hundreds of cycles and further cycling is needed to induce macroyielding.

D. Fatigue performance

16. TEMPCORE reinforcing steels exhibit superior fatigue properties when compared with other type of high strength reinforcing steels.
17. The fatigue properties of the steel are essentially determined by the hardened outside layer which is tempered martensite.
18. Once the crack has propagated through the hardened layer the fatigue life has been expanded to approximately 90%.
19. Compressive residual stresses at the bar surface significantly increase fatigue life but have little effect on the magnitude of the fatigue limit.
20. The fatigue limits of the tested bars are as high as 40% to 60% in relation to tensile strength and in some cases this value reaches 60 %.
21. The deformation patterns on the surface of the bars produce large stress concentration factors which however are very similar when compared with other types of reinforcing steels.
22. The deformation patterns on the surface of the bars were examined only from the point of view of fatigue and the negative aspects may be overruled by the load characteristics.
23. Analytical work shows that the ratio of the root radius to the lug height is the prime factor affecting the value of stress concentration factor and a polynomial function of an order of 6 is proposed to describe such relationship.
24. When the distance between two deformation patterns is short the interaction leads to larger stress concentrations providing areas for crack initiation sites.

REFERENCES

AASHO. (1962). "The AASHO road test report 4 bridge research." Highway research board of the NAS-NRC division of engineering and industrial research, Special Report 61D, Washington, D. C.

ABAQUS reference manual; version 5.5. (1995). Hibbitt, Karlsson & Sorensen, Inc.

Abel, A., and Muir, H. (1973a). "The effect of cyclic loading on subsequent yielding." ACTA Metallurgica, Vol. 21, 93-97.

Abel, A., and Muir, H. (1973b). "The nature of microyielding." ACTA Metallurgica, Vol. 21, 99-105.

Abel, A., Donnell, M. J., and Spencer, W. (1986). "Fatigue of TEMPCORE reinforcing bars - the effect of galvanizing." 10th Australasian conference on the mechanics of structures and materials, University of Adelaide, Australia, 327-332.

ACI Committee 215 (1987). "Considerations for design of concrete structures subjected to fatigue loading," ACI Manual of Concrete Practice, part 1, materials and general properties of concrete, 215R-74 (revised 1986).

ACI Committee 439 (1973). "Uses and limitations of high strength steel reinforcement fy $\geq$ 60 ksi (42.2 kgf/mm^2)." ACI Journal, Vol. 70, 77-104.

ACI Committee 439 (1989). "Steel reinforcement - physical properties and US availability." ACI Material Journal, Vol. 86, 63-76.

Akinawa, Y., Tanaka, K., and Matsui, E. (1988). "Statistical characteristics of propagation of small cracks in smooth specimens of aluminium alloy 2024-T3." Mater. Sci. Engng., Vol. 104, 105-115.

Astiz, M. A (1986). "An incompatible singular elastic element for two- and three-dimensional crack problems." International Journal of Fracture, Vol. 31, 105-124.

ASTM. (1985). Metals Handbook, metallography and microstructures, 9th edition, Metals park.

ASTM. (1985a). "Standard specification for deformed and plain billet bars for concrete reinforcement." A615M-84a, Philadelphia, 517-522.

ASTM. (1985b). "Standard specification for rail-steel deformed and plain bars for concrete reinforcement." A616-84, Philadelphia, 523-527.

ASTM. (1985c). "Standard specification for axle-steel deformed and plain bars for concrete reinforcement." A617-84, Philadelphia, 529-533.

ASTM. (1985d). "Standard specification for low-alloy steel deformed bars for concrete reinforcement." A706-84a, Philadelphia, 656-661.

ASTM. (1990). "Standard methods for estimating the average grain size of metals." E 112-88, Philadelphia, 529-533.

ASTM. (1993). "Standard practice for conducting constant amplitude axial fatigue test of metallic materials." Designation: E466-82, Philadelphia, 540-543.

Australian standard (1991). Methods for tensile testing of metals, AS1391-1991.

Australian standard (1991). Steel reinforcing bars for concrete, AS1302-1991.

Babich, V. K., Kondratenko, V. M., Dementeva, Zh. A., and Yarmolenko, P. P. (1987). "Properties of reinforcing rod quenched and tempered in baths from rolling heat." Steel in the USSR, Vol. 17, March, 142-143.

Behan, J. E., and Warner, R. F. (1984). "Fatigue properties of TEMPCORE reinforcing bars." University of Adelaide Report, No. R63.

Belgian patent 790.867 (1972).

BHP (1982a). TEMPCORE (technical note).

BHP (1982b). TEMPCORE, Summarised technical information based on European TEMPCORE (technical note).

BHP (1982c). TEMPCORE technical information based on European TEMPCORE (technical note).

BHP (1993). TEMPCORE, steel rod and bar products division brochure.

Brame, D. R., and Evans, T. (1958). "Deformation of thin films on solid substrates." Philosophical Magazine, Series 8, 971-986.

Breen, D. H., and Wene, E. M. (1978). "Fatigue in machines and structures - ground vehicles." in Fatigue and microstructure, ASM material science seminar, St. Louis, Missouri, ASM metals park, Ohio 44073, 57-99.

Brentnall, W. D., and Rostoker, W. (1965). "Some observations on microyielding." ACTA Metallurgica, Vol. 13, 187-198.

Brown, C. W., and Hicks, M. A. (1983). "A study of short fatigue crack growth behavior in titanium alloy IMI 685." Fatigue Engng Mater. Struct., Vol. 6, 67-76.

Brown, C. W., King, J. E., and Hicks, M. A. (1984). "Effects of microstructure on long and short crack growth in Ni-base supperalloys." Metal Science, Vol. 18, 374-380.

Brown, N, and Ekvall, R. A. (1962). "Temperature dependence of the yield points in iron." ACTA Metallurgica, Vol. 10, 1101-1107.

Brown, N, and Lukens, K. F. (1961). "Microstrain in polycrystalline metals." ACTA Metallurgica, Vol. 9, 106-111.

Burton, K. T. (1965). "Fatigue tests of reinforcing bars." Journal of the PCA Research and Development Laboratories, September, 13-23.

Burton, K. T., and Hognestad, E. (1967). "Fatigue tests of reinforcing bars - tack welding of stirrups." ACI Journal, Vol. 64, 244-252.

Cahn, R. W., and Haasen, P. (1983). Physical metallurgy, Elsevier Science Publisher.

Carirns, J., and Abdullah, R. B. (1995). "Influence of rib geometry on strength of epoxy-coated reinforcement." ACI Structural Journal, Vol. 92, 23-27.

Centre for Advanced Structure Engineering. (1996). T 514 timber-concrete model testing, Department of Civil Engineering, the University of Sydney.

Chernenko, V. T., Filonov, O. V., Kazyrski, O. L., and Ivoditov, A. N. (1987). "In-line heat hardening of reinforcing bars in a rolling mill." Soviet Materials Science Reviews, No. 1, 41 - 42.

Chilton, J. M., and Kelly, P. M. (1968). " The strength of ferrous martensite." ACTA Metallurgica, Vol. 16, 673-656.

Cottrell, A. H. (1953). Dislocations and plastic flow in crystals, Clarendon press, Oxford.

Cowling, J. M. (1986). Fatigue cracking in nitrided steels, Parthenon Press.

Darwin, D. and Zavaregh, S. S. (1996). "Bond strength of grouted reinforcing bars." ACI Structural Journal, Vol. 93, 486-495.

Defourny, J., and Bragard, A. (1977). "TEMPCORE-process, the solution to rebar welding problems." Metallurgical Reports C. R. M., No. 50, 21-26.

Disney, L. A., and Reynolds, Chas. E. (1973). Reinforcement for concrete, Cement and Concrete Association, London.

Dolzhenkov, I. E., Chaikovskii, O. A., Khudik, Yu. T., and Ivchevko, A. U. (1987). "Influence of reheating on structure and properties of quenched and self tempered reinforcing steel." Steel in USSR, Vol. 17, June, 278 - 281.

Ebert, L. J. (1978). "The role of residual stresses in the mechanical performance of case carburized steels." Metallurgical Transactions, A, Vol. 9, 1537-1551.

Ebert, L. J., Hecker, S. S., and Hamilton, C. H. (1968). "The stress-strain behaviour of concentric composite cylinders." Journal of Composite Materials, Vol. 2, 458-477.

Ebert, L. J., Krotine, F. T., and Troiano, A. R. (1965). "A behavioural model for the fracture of surface hardened components." Journal of Basic Engineering, Transaction of ASME, Dec., 871-874.

Economopoulos, M. (1981). "The use of drastic and mild water cooling techniques for controlling bar and rod properties." Rod and Bar Production in the 1980's, Metal Society, London, 76-80.

Economopoulos, M., Respen, Y., Lessel, G., and Steffes, G. (1975). "Application of the TEMPCORE process to the fabrication of high yield strength concrete-reinforcing bars." Metallurgical Reports C. R. M., No. 45, 3-19.

Fletcher, A. J., Geary, W., and King, J. E. (1988). "Fatigue crack propagation and residual stress in a quenched and tempered C-Mn-B steel." in Analytical and Experimental Methods for Residual Stress Effects in Fatigue, ASM STP 1004, 82-96.

Forrest, P. G. (1962). Fatigue of metals, Pergamon press.

Gilman, J. J. (1955). "The role of thin surface films in the deformation of metal monocrystals." Symposium on basic effects of environment on the strength, scaling, and embattlement of metals at high temperature, ASTM STP 171, 3-13.

Goto, M. (1991). "Statistical investigation of the behaviour of microcracks in carbon steels." Fatigue Fract. Engng Mater. Struct., Vol. 14, pp 833-845.

Grönqvist, Nils-Ove. (1971). "Fatigue strength of reinforcing bars." in Concrete Bridge Design, Vol. 2, ACI SP26, 1011-1044.

Grapher version 1.02 (1992), Goden software, Inc.

Hahn, G. T. (1962). "A model for yielding with special reference to the yield-point phenomena of iron and related BCC metals." ACTA Metallurgica, Vol. 10, pp 727-738.

Hamad, B. S. (1995a). "Bond strength improvement of reinforcing bars with specially designed rib geometries." ACI Structural Journal, Vol. 92, 3-13 .

Hamad, B. S. (1995b). "Comparative bond strength of coated and uncoated bars with different rib geometries." ACI Materials Journal, Vol. 92, 579-90 .

Hanson, J. M., and Helgason T. (1971). "Discussion on Fatigue strength of hot-rolled deformed reinforcing bars", ACI Journal, Vol. 68, 725-726.

Hanson, J. M., Burton, K. T., and Hognestad, E. (1968). "Fatigue tests on reinforcing bars - effect of deformation pattern." Journal of the PCA Research and Development Laboratories, September, 2-13.

Hardeman, E. L. (1965). "Use of high strength reinforcing steel in bridges." ACI Journal, Vol. 62, 457-65.

Helgason, T., and Hanson, J. M. (1974). "Investigation of design factors affecting fatigue strength of reinforcing bars-statistical analysis." in Fatigue of Concrete, ACI SP 41, 107-138.

Helgason, T., Hanson, J. M., Somes, N. F., Corley, W. G., and Hognestad, E. (1976). "Fatigue strength of high-yield reinforcing bars, national cooperative highway research program report 164." Transportation Research Board National Research Council, Washington, D. C.

Hognestad, E. (1967). "Trends in consumer demands for new grades of reinforcing steel." Proceedings of concrete reinforcing steel institute, PCA Development Department Bulletin, D130, 22-32.

Honeycombe, R. W. K., and Bhadeshia, H. K. D. H. (1995). Steels : microstructure and properties, 2nd edition, Edward Arnold, London.

Honeycombe, R. W. K., and Hancook, P. (1981). Steels : microstructure and properties, Edward Arnold, London.

Hornbostel, C. (1991). Construction materials: types, uses, and applications, 2nd edition, John Wiley & Sons Inc., New York.

Howard E. B. (1984). Practical heat treating, American Society for Metals. Metals Park, OK 44073.

Ivashchenko, V. M., Golobochanskii, E. A., Prilepskii, Yu. V., Volovik, N. G., and Morozov, A. D. (1988). "Improving quality of medium grade hardened and tempered reinforcing steel by high frequency induction tempering." Steel in USSR, Vol. 18, April, 188 - 191.

Ivashchenko, V. M., Stychinskii, L. P., Borkovskii, Yu. Z, Erlikh, M. G., and Stavitskii, E. A. (1976). "Influence of interrupted cooling in quenching and tempering on the properties of 35GS reinforcing steel." Steel in USSR, April, 225 - 227.

Jhamb, I. C., and Mac Gregor, J. G. (1974a). "Effect of surface characteristics on the fatigue strength of reinforcing steel." in Fatigue of Concrete, ACI SP 41-7, 39-167.

Jhamb, I. C., and Mac Gregor, J. G. (1974b). "Stress concentration caused by reinforcing bar deformations." in Fatigue of Concrete ACI SP 41-8, 169-182.

Johnston, W. G., and Gilman, J. J. (1959). "Dislocation velocity, dislocation density, and plastic flow in lithium fluoride crystals." Journal of Applied Physics, Vol. 30, 129-147.

Kaar, P. H., and Hognestad, E. (1965). "High strength bars as concrete reinforcement, Part 7, control of cracking in T-beam flanges." Journal of the PCA Research and Development Laboratories, January, 42-53.

Kalmykov, V. V. (1987). "Selection and development of steels for in-line large-scale production of high-strength reinforcing bars." Soviet Materials Science Reviews, No. 1, 47 - 49.

Kalmykov, V. V., Pirogov, V. A., Yatsenko, R. V., and Galenko, G. V. (1989). "The effect of silicon on structure and properties of quenched and tempered low-alloy steel." Izvestiya Akademii Nauk SSSR. Metally, No. 5, 100-102.

Kang, K. J., Song, Ji. H., and Earmme, Y. Y. (1990). "Fatigue crack growth and closure behaviour through a compressive residual stress field." Fatigue Fract. Engng Mater. Struct., Vol. 13, 1-13.

Kerlins, V. (1987). "Models of fracture." Metals Hand Book, Vol. 12, ASM, Metals park, 12-71.

Killmore, C. R., and Barrett, J. F. (1984). "Vanadium microalloyed 'TEMPCORE' treated high strength concrete reinforcing bar steel." in High Strength Low Alloy Steels, Proceedings of an International Conference, Wollongong, Australia, South Coastal Printers, 265-270.

Killmore, C. R., Barrett, J. F., and Williams, J. G. (1985). "Mechanical properties of high strength reinforcing bar steels accelerated cooled by "TEMPCORE" process." in Accelerated Cooling of Steel, the Metallurgical Society, Inc., 541-558.

Kitagawa, H., and Takahashi, S. (1976). "Applicability of fracture mechanics to very small cracks or cracks in the early stage." Proceedings 2nd international conference on mechanical behaviour of metals, American Society of Metals, 627-631.

Klaus, F., and Vlad, C. M. (1985). "Mechanical and technological properties of TEMPRIMAR weldable high strength rebars." in HSLA steels, metallurgical and applications, Proceedings of an international conference on HSLA steels, Beijing, ASM, 901- 907.

Klesnil, M., and Lukas, P. (1967). " Fatigue softening and hardening of annealed low-carbon steel." Journal of the Iron and Steel Institute, July, 746-749.

Kokubu, M., and Okamura, H. (1968). "Fatigue behavior of high strength deformed bars in reinforced concrete bridges." Journal of the Faculty of Engineering, University of Tokyo, Vol. XXIX, No. 3, 181-198.

Kokubu, M., Tada, Y., Tachibana, I., and Matsumoto, Y. (1965). "Fatigue behaviour of reinforced concrete beams with high strength deformed bars." Transactions of the Japan Society of Civil Engineers, No. 122, 51-74 (in Japanese).

Kondratenko, V. M., Ivashchenko, V. M., Erlikh, M. G., Prileskii, Yu. V., Yarmolenko, P. P., and Osadchenko, A. V. (1989). "In-line quenching and tempering of 32 mm dia. Reinforcing steel." Steel in USSR, Vol. 19, June, 262 - 265.

Kossowsky, R., and Brown, N. (1966). "Microyielding in iron at low temperatures." ACTA Metallurgica, Vol. 14, 131-139.

Kugushin, A. A., Chernenko, V. T., Babchi, V. K., Gladshtein, L. I., Kazyrskii, O. L., Druzin, V. I., Odesskii, P. D., and Kudlai, A. S. (1986). "Improving strength and

subzero brittle fracture resistance in angle sections by quenching and self-tempering from rolling heat." Steel in USSR, Vol. 16, September, 442 - 446.

Kunio, T. , Shimizu, M., and Yamada, K. (1969) "Microstructural aspects of the fatigue behavior of rapid heat treated steel." Fracture 1969, proceedings of 2nd international conference, Brighton, England, Chapman and Hall Lit., 630-642.

Kurita, M., Yamamoto, M., Toyama, K., Komatsubara, N., and Kunifhige, K. (1997). "Effect of strengthening mechanism on fatigue properties of low carbon dual phase sheet steel." Advances in Fracture Research, ICF9, Sydney, Australia, Pergamon, 1533-1540.

Kurita, M., Yamamoto, M., Toyama, K., Normura, S., and Kunifhige, K. (1996). "Effect of strengthening mechanism on fatigue properties of ferrite-pearlite hot-rolled sheet steel." ISIJ International, The Iron and Steel Institute of Japan, Vol. 36, 481-486.

Laird, C. (1967). "The influence of metallurgical structure on the mechanisms of fatigue crack propagation." in Fatigue Crack Propagation, ASTM STP 415, 131-168.

Landgraf, R. W. (1978). "Control of fatigue resistance through microstructure - ferrite alloys." in Fatigue and Microstructure, ASM material science seminar, St. Louis, Missouri, ASM Metals park, Ohio 44073, 439-466.

Landgraf, R. W., and Richman, R. H. (1975). "Fatigue behaviour of carburized steel." in Fatigue of Composite Materials, ASTM STP 569, 130-144.

Lankford, J. (1982). "The growth of small fatigue cracks in 7075-T6 aluminium." Fatigue Engng Mtater. Struct., Vol. 9, 1-14.

Leis, B., Reemsnyder, H., cammett, J., Fuchs, H., Ricklefs, R., and Testin, B. (1997). "Effects of processing on fatigue performance." in SAE Fatigue Design Handbook, 3rd edition, Society of Automotive Engineers, Inc., Warredale, Pa., 67-113.

Mac Gregor, J. G., Jhamb, I. C., and Nuttall, N. (1971). "Fatigue strength of hot rolled deformed reinforcing bars." ACI Journal, March, 169-179.

Magnusson and Johannesson (1977). "Fatigue of case hardened low alloyed steel." Scandiavian Journal of Metallurgy, Vol. 6, 40-41.

Marsh, C. F. (1909). A concise treatise on reinforced concrete, a companion to the reinforced concrete manual, Constable & Company Lty., London.

Miller, K, J. (1991). "Metal fatigue-past, current and future." Journal of Mechanical Engineering Science, part C, Vol. 205, 291-304.

Miller, K. J. (1987a). "The behaviour of short fatigue cracks and their initiation, Part I - a review of two recent books." Fatigue Fract. Engng Mater. Struct., Vol. 10, 75-91.

Miller, K. J. (1987b). "The behaviour of short fatigue cracks and their initiation, Part II - a general summary." Fatigue Fract. Engng Mater. Struct., Vol. 10, 93-113.

Nakajima, K., Yokoe, M., and Miyata, T. (1997). "Effect of microstructure and prestrain on fatigue crack propagation of dual phase steel." Advances in Fracture Research, ICF9, Sydney, Australia, Pergamon, 1541-1548.

Nakayama, N. (1965). "Fatigue tests on T-shaped beams reinforced with various deformed bars." Transactions of the Japan Society of Civil Engineers, No. 122, 43-50 (in Japanese).

Nawy, E. G. (1985), Reinforced concrete : a fundamental approach, Prentice-Hall Inc. Englewood Cliffs, N.J.

Neves, C. I., Rodrigues, J. P. C., and Loureiro, A. de P. (1996). "Mechanical properties of reinforcing and prestressing steels after heating." Journal of Materials in Civil Engineering, November, 189-194.

Okamoto, A., and Nakamura, H. (1990). "The influence of residual stress on fatigue cracking." Journal of Pressure Vessel Technology, Transaction of ASME, Vol. 112, 199-203.

Parker, A. P. (1982). "Stress intensity factor, crack profiles, and fatigue crack growth rates in residual stress field." in Residual Stress Effects in Fatigue, ASTM STP 776, 13-31.

Paules, J. R., and Hansen, S. S. (1985). "Accelerated cooling of hot-rolled constructional plate steels." in Accelerated Cooling of Steel, the Metallurgical Society, Inc., 205-222.

Petit, J., Mendez, J., Berata, W., Legender, L., and Muller, C. (1992). "Influence of environment on the propagation of short fatigue cracks in titanium alloy." in Short Fatigue Cracks, Mechanical Publications, London, 235-250.

Pfister, J. F., and Hognestad, E. (1964). "High strength bars as concrete reinforcement, part 6, fatigue tests." Journal of the PCA Research and Development Laboratories, January, 65-84.

Plumbridge, W. J., and Knee, N. (1985). "Effect of tempering temperature on monotonic and cyclic properties of a high-strength low-alloy chain steel." Materials Science and Technology, Vol. 1, 577-582.

Polakowski, N. H. (1966). Residual stresses, strength and structure of engineering materials, Prentice-hall, Inc..

Pussegoda, L. N. (1984). "Comparison of two methods of cold work to increase strength of hot-rolled reinforcing bar." Metals Technology, Vol. 11, 208-300.

Qian, J., and Fatemi, A. (1995). "Cyclic deformation and fatigue behaviour of ion-nitrided steel." International Journal of Fatigue, Vol. 17, 15-24.

Ray, A., Mukerjee, D., Sen, S. K., Battacharya, A., Dhua, S. K., Prasad, M. S., Banerjee, N., Popli, A. M., and Sahu, A. K. (1997). "Microstructure and properties of thermomechnically strengthened reinforcement bars: a comparative assessment of plain-carbon and low alloy steel grades." Journal of Materials Engineering and Performance, Vol. 6, 335-343.

Rehm, G., and Russwurm, D. (1977). "Assessment of concrete reinforcing bars made by the TEMPCORE process." Metallurgical Reports C. R. M., No. 51, 3-16.

RILEM-FIP-CEB (1973). "Reinforcement for reinforced and presented concrete, tentative recommendations." Mater. Struct., Res. Testing (Pairs), 79-118.

Rios, E. R. de los, Navarro, A., and Hussain, K. (1992). "Microstructural variation in short fatigue crack propagation of a C-Mn steel." in Short Fatigue Cracks, ESIS 13, Mechanical Enginerring Publications, London, 115-132.

Rios, E. R. de los, Tang, Z., and Miller, K. J. (1984). "Short crack behaviour in a medium carbon steel." Fatigue Engng Mater. Struct., Vol. 7, 97-108.

Ritchie, R. O. (1986). " Fatigue crack growth: mechanistic aspects." in Encyclopaedia of Materials Science and Engineering, Vol. 3, Pergamon press, 1650-1666.

Roper, H., and Hetherington, G. B. (1980). "Fatigue of reinforced concrete in air, chloride solution and sea water." Research Report No. R 376, School of Civil and Mining Engineering, The University of Sydney.

Ruhl, J. A., and Walker, W. H. (1975). "Stress histroies for highway bridges subjected to traffic loading." Report UILU-ENG-75-2004, Department of Civil Engineering, University of Illinois, Urbana, Illinois.

Satskii, V. A., Khudik, Y. T., Kuzmenko, L. A., Zakharov, V. O., and Gvozdev, R. V. (1977). "Control of hardening and tempering of reinforcing steel in the mill line." Steel in USSR, January, 49 - 51.

Shibata, H., Tokaji, K., Ogawa, T., and Shiota, H. (1996). "Microstructure dependence of fatigue strength and fatigue crack propagation in titanuim aluminide." International Journal of Fatigue, Vol. 18, 119-125.

Shulaev, I. P., Parusov, V. V., Babich, V. K., Khotienko, Yu. P., Mulin, N. M., Filonov, O. V., and Rogatin, Yu. A. (1986). "Improvement of practice for heat treatment of coiled reinforcing rod from rolling heat." Steel in USSR, Vol. 16, July, 351 - 353.

Simon, P. (1990). "Optimization of TEMPCORE installations for rebars." Metallurgical Plant and Technology, No. 2, 61-69.

Simon, P., Economopoulos, M., and Nilles, P. (1984a). "TEMPCORE: a new process for the production of high quality reinforcing bars." Iron and Steel Engineer, March, 53-57.

Simon, P., Economopoulos, M., and Nilles, P. (1984b). "TEMPCORE, an economical process for the production of high quality rebars." Metallurgical Plant and Technology, No. 3, 80-93.

Solberg, J. (1988). "Fatigue crack initiation in quenched low carbon steel microstructures." Materials Science and Engineering, A, Vol. 101, 39-46.

Soretz, S. (1974). "Contribution to the fatigue strength of reinforced concrete." in Fatigue of Concrete, ACI SP-41, 35-58.

Spencer, W. (1985). "The fatigue properties of normal and galvanized TEMPCORE reinforcing bars." Thesis for Bachelor of Engineering (honours), the University of Sydney.

Stamm, H., Holzwarth, U. Boerman, D. J., Marques, F., Olchini, A., and Zausch, R. (1996). "Effect of laser surface treatment on high cycle fatigue of AISI 316L stainless steel." Fatigue Fract. Engng Mater. Struct., Vol. 19, 985-995.

Starker, P., Wohlfart, H., and Macherauch, E. (1979). "Subsurface crack initiation during fatigue as a result of residual stresses." Fatigue of Engineering Materials and Structures, Vol. 1, 319-327.

Stein, D. F., and Low, J. R. (1960). "Mobile of edge dislocations in silicon-iron crystals." Journal of Applied Physics, Vol. 31, 362-369.

Suits, J. C., and Chalmers, B. (1961). "Plastic microstrain in silicon-iron." ACTA Metallurgica, Vol. 9, 854-860.

Takahashi, T., and Nagumo, M. (1970). "Flow stress and work-hardening of pearlitic steel." Trans. Japan Institute of Metals, Vol. 11, 113-119.

Taylor, D. (1989). Fatigue thresholds, Butterworths.

Taylor, D., and Knott, J. F. (1981). "Fatigue propagation behaviour of short craks; the effect of microstructure." Fatigue Engng Mater. Struct., Vol. 4, 147-155.

Taylor, F. W., Thompson, S. E., and Smulski, E. (1925). Concrete: plain and reinforced, New York, John Wiley & Sons, Inc.

Thielen, P. N, and Fine, M. E. (1976). "Cyclic stress strain relations and strain-controlled fatigue of 4140 steel." ACTA Metallurgica, Vol. 24, 1-10.

Thomas, J., and Pasko, JR. (1973). "Fatigue of welded reinforcing steel." ACI Journal, Vol. 70, 757-758.

Tilly, G. P. (1979). "Fatigue of steel reinforcement bars in concrete: A review." Fatigue Engng Mater. Struct., Vol. 2, 251-268.

Tokaji, K., and Ogawa, T. (1992). "The growth behaviour of microstructural small fatigue cracks in metals." in Short Fatigue Cracks, ESIS 13, Mechanical Engineering Publications, London, 85-99.

Turnbull, A., and Rios, E. R. de los. (1995). "The effect of grain size on the fatigue commercially pure aluminium." Fatigue Fract. Engng Mater. Struct., Vol. 18, 1455-1467.

Uzlov, I. G., Chernenko, V. T., Sidorenko, O. G., Shinkarev, I. F., and Madatyan, S. A. (1987). "Low cost, weldable, thermomechanically treated reinforcing steel." Steel in USSR, Vol. 17 September, 427 - 429.

Vlad, C. M., (1985). "A comparison between the TEMPRIMAR and TEMPCORE processes for production of high strength rebars." in HSLA steels, metallurgical and applications, Proceedings of an international conference on HSLA steels, Beijing, ASM, 909 - 912.

Vlad, C. M., Klimpel, K., and Feldmann, U. (1983). "Microstructures and mechanical properties of sequential quenched and tempered HSLA wire rod and bar steels from rolling heat." HSLA steels technology & applications, Conference proceedings of international conference on technology and applications of HSLA steels, Philadelphia, Pennsylvania, ASM park, 1003-1015.

Vreeland, T., Wood, D. S., and Clark, D. S. (1953). "Preyield plastic and anelastic microstrain in low-carbon steel." ACTA, Metallurgica, Vol. 1, 414-421.

Warner, R. F., Rangan, B. V., and Hall, A. S. (1982). Reinforced concrete, 2nd edition, Pitman Australia, Carlton, Vic.

Wilson, D. V., and Mintz, B. (1972). "Effects of microstructureal instability on the fatigue behaviour of quenched and quench-aged steels." ACTA Metallurgica, Vol. 20, 985-995.

Worthington, P. J., and Smith, E. (1964). "The formation of slip band in polycrystalline 3% silicon iron in the pre-yield microstrain region." ACTA Metallurgica, Vol. 12, 1277-1281.

Yamada, K., Shimizu, M., Kunio, T., Nakamura, H., and Takahashi, H. (1968). "Microstructural approach of study on the fatigue behaviour of induction-hardened steel, report 1." Bulletin of JSME, Vol. 11, 771-777.

Yamada, K., Shimizu, M., Nakamura, H, and Kunio, T. (1968). "Microstructural approach of study on the fatigue behaviour of induction-hardened steel, report 2." Bulletin of JSME, Vol. 11, 778-784.

Yanopoulos, P. J. and Edwards, A. D. (1976). "Fatigue characteristic of hot-rolled deformed bars." Civil Engineering Report CSTR 76/1, Imperial College, London.

Ye, S., Liu, K, and Shi, Z. (1985). "The interrupted accelerated cooling process after hot rolling for deformed reinforcing bars." HSLA steels, metallurgical and applications, Proceedings of an international conference on HSLA steels, Beijing, ASM, 885-891.

Yu, M. T., Topper, T. H., and Wang, L. (1988). "The effect of microstructure on mechanical behavior of a low carbon, low alloy steel." International Journal of Fatigue, Vol. 10, 249-255.